DOT/FAA/AR-09/41

Air Traffic Organization
NextGen & Operations Planning
Office of Research and
Technology Development
Washington, DC 20591

Neck Injury Criteria for Side-Facing Aircraft Seats

July 2011

Final Report

This document is available to the U.S. public through the National Technical Information Services (NTIS), Springfield, Virginia 22161.

This document is also available from the Federal Aviation Administration William J. Hughes Technical Center at actlibrary.tc.faa.gov.

U.S. Department of Transportation
Federal Aviation Administration

NOTICE

This document is disseminated under the sponsorship of the U.S. Department of Transportation in the interest of information exchange. The United States Government assumes no liability for the contents or use thereof. The United States Government does not endorse products or manufacturers. Trade or manufacturer's names appear herein solely because they are considered essential to the objective of this report. The findings and conclusions in this report are those of the author(s) and do not necessarily represent the views of the funding agency. This document does not constitute FAA policy. Consult the FAA sponsoring organization listed on the Technical Documentation page as to its use.

This report is available at the Federal Aviation Administration William J. Hughes Technical Center's Full-Text Technical Reports page: actlibrary.tc.faa.gov in Adobe Acrobat portable document format (PDF).

Technical Report Documentation Page

1. Report No.	2. Government Accession No.	3. Recipient's Catalog No.
DOT/FAA/AR-09/41		

4. Title and Subtitle	5. Report Date
NECK INJURY CRITERIA FOR SIDE-FACING AIRCRAFT SEATS	July 2011
	6. Performing Organization Code
7. Author(s)	8. Performing Organization Report No.
Mat M.G.M. Philippens[1], Patrick A. Forbes[1], Jac S.H.M. Wismans[1] Rick DeWeese[2], and David Moorcroft[2]	
9. Performing Organization Name and Address	10. Work Unit No. (TRAIS)
TNO Industry & Science - Automotive[1] Steenovenweg 1, 5708 HN Helmond P.O.Box 756, 5700 AT Helmond Netherlands FAA CAMI AAM-630[2] P.O. Box 25082 Oklahoma City, OK 73125	11. Contract or Grant No. DTFA03-98-D-00008
12. Sponsoring Agency Name and Address	13. Type of Report and Period Covered
U.S. Department of Transportation Federal Aviation Administration Air Traffic Organization NextGen & Operations Planning Office of Research and Technology Development Washington, DC 20591	Final Report 14. Sponsoring Agency Code ANM-115

15. Supplementary Notes

The Federal Aviation Administration Airport and Aircraft Safety R&D Division COTR was Allan Abramowitz.

16. Abstract

This report documents research started in 2002 that identified the potential need for explicit neck injury criteria and tolerances for certification of side-facing seats in aircraft. Laboratory sled tests with full-body postmortem human subjects proved that there is a substantial risk for serious (potentially lethal) neck injuries under realistic crash load conditions, simulated by the 16-g, 180-ms crash pulse designated by Title 14 Code of Federal Regulations 25.562. Further research of the loading and injury mechanism were conducted using numerical simulations of advanced rigid-body models of the EuroSID-2 (ES-2) anthropomorphic side-impact crash dummy, which originated from automotive crash safety research. This research led to proposing an ES-2 upper-neck tension force injury assessment reference value of 2300 Newtons, corresponding to a 50% risk of an Abbreviated Injury Scale 3 neck injury, and a value at 1800 Newtons, corresponding to a 25% risk. Injuries to other body structures were documented and recommended for future research as they compromise the escape capabilities of the aircraft occupants, e.g., unconsciousness by head angular acceleration, immobilization by fractures to the upper leg, multiple rib fractures from belt loading, or carotid artery tears, which can lead to a fatal stroke months after the accident. The ES-2 was determined to have sufficient biofidelity for use in aircraft side-facing seat certification requirements. Issues with respect to the ES-2's neck durability and shoulder-belt interaction are noted.

17. Key Words	18. Distribution Statement
Side-facing seat, Neck injury criteria, Injury reference assessment values, EuroSID-2, Certification	This document is available to the U.S. public through the National Technical Information Service (NTIS), Springfield, Virginia 22161. This document is also available from the Federal Aviation Administration William J. Hughes Technical Center at actlibrary.tc.faa.gov.

19. Security Classif. (of this report)	20. Security Classif. (of this page)	21. No. of Pages	22. Price
Unclassified	Unclassified	142	

Form DOT F 1700.7 (8-72) Reproduction of completed page authorized

ACKNOWLEDGEMENTS

The authors acknowledge Gary Frings (retired) and Allan Abramowitz of the Federal Aviation Administration (FAA) William J. Hughes Technical Center for the project management on behalf of the FAA. Steve Soltis (retired Chief Scientific and Technical Advisor for Crash Dynamics, FAA) for supervising this research and keeping the focus of the project on the main goal: neck injury risk for aircraft passengers.

King Yang and Paul Begeman of the bioengineering department of Wayne State University for setting up the basic postmortem human subject test procedure used in the initial phase of this project. Narayan Yoganandan and Frank Pintar of the Medical College of Wisconsin for their willingness to discuss every hypothesis and design various test configurations and their test laboratory team who performed the PMHS-ES-2 tests at a high level of quality.

On behalf of TNO Industry and Science, the authors also want to acknowledge Rick DeWeese and David Moorcroft (Civil Aerospace Medical Institute) for their highly appreciated advice on typical aircraft seat certification and test procedures.

TABLE OF CONTENTS

		Page
EXECUTIVE SUMMARY		xiii
1.	INTRODUCTION	1
1.1	Objective	1
1.2	Problem Definition	1
1.3	Background	1
1.4	Approach	2
1.4.1	Phase 1: Literature Review	2
1.4.2	Phase 2: Tests	2
1.4.3	Phase 3: Injury Assessment Reference Values	2
1.4.4	Phase 4: Side-Impact Test Procedure Design	2
1.5	Report Outline	2
2.	LITERATURE REVIEW	3
2.1	Introduction	3
2.2	Abbreviated Injury Scale	3
2.3	Potential Injury Criteria	4
2.4	Literature Review Summary	7
3.	METHODOLOGY	8
3.1	Introduction	8
3.2	Test Setup and Test Matrix	9
3.2.1	Baseline Load Level	9
3.2.2	Test Configurations	10
3.3	Test Matrix	13
3.4	Subject Selection and Autopsy Procedure	14
3.4.1	The WSU Subject Pretest Screening Procedure	14
3.4.2	The MCW Subject Pretest Screening Procedure	14
3.4.3	The WSU Posttest Procedure	14
3.4.4	The MCW Posttest Procedure	15
3.4.5	The WSU Bone Quality Measurement Method	15
3.4.6	The MCW Bone Quality Measurement Method	16
3.5	Subject Characteristics	16

3.6 Data Acquisition and Processing 17

3.6.1 Instrumentation PMHS—WSU 17
3.6.2 Instrumentation PMHS—MCW 17
3.6.3 Instrumentation ES-2 18
3.6.4 Data Processing 19

4. TEST RESULTS 25

4.1 Introduction 25
4.2 Injuries 25

4.2.1 Summary 25
4.2.2 Neck Injuries 27
4.2.3 Other Body Area Injuries 27

4.3 PEAK VALUES 27

4.3.1 WSU—Rigid Seat, Side Wall 28
4.3.2 MCW—Rigid Seat, Full-Thorax Restraint 29
4.3.3 MCW—Aircraft Seat, Three-Point Belt With Retractor 31

4.4 Combined Loads 32
4.5 Analysis of Potential Injury Criteria 36

4.5.1 The PMHS 36
4.5.2 The ES-2 36

4.6 ES-2 Biofidelity 37
4.7 Discussion 41

5. NUMERICAL MODELING 42

5.1 Introduction and Objective 42
5.2 Methodology 42

5.2.1 Numerical ATD Model 42
5.2.2 Sled Test Model 43
5.2.3 Validation 45
5.2.4 Supporting Impact Simulations 46

5.3 RESULTS 48

5.3.1 Validation 48
5.3.2 Supporting Impact Simulations 56

6. INJURY PROBABILITY 61

6.1 Introduction 61
6.2 Probit Results 62
6.3 Discussion 64

7. STANDARD TEST PROCEDURE 65

7.1 Introduction 65
7.2 Anthropormorphic Test Dummies 65
7.3 Test Setup Considerations 66
7.4 Test Observations 68

7.4.1 Shoulder Belt Interaction 68
7.4.2 Neck Durability 69

7.5 Recommended Test Requirements 69

8. SUMMARY 69

8.1 Problem Definition 70
8.2 Test Results 70

9. CONCLUSIONS 72

10. RECOMMENDATIONS 73

11. BIBLIOGRAPHY 74

APPENDICES

A—Initial Literature Survey Details

B—Comparison of EuroSID-2 Response for Triangular- Versus Rectangular-Shaped Deceleration Pulses

C—Postmortem Human Subject and EuroSID-2 Response Time Histories for the Rigid-Seat Configuration

D—Postmortem Human Subject and EuroSID-2 Response Time Histories for the Aircraft Seat Configuration

LIST OF FIGURES

Figure		Page
1	The Heidelberg Setup for Lateral PMHS Tests	6
2	Setup for WSU Side-Facing PMHS and ES-2 Tests With a Three-Point, Nonleading Belt	11
3	Setup for MCW Rigid Seat With Lateral Arm Bracket	11
4	Aircraft Seat With Three-Point Belt	12
5	Diagram Showing Top View of Belt Configuration	12
6	Pretest X-Rays	14
7	Bone Mineral Density of the Femoral Region	15
8	Bone Mineral Density of the Trochanter Region	15
9	Example of BMD in Relation to the Full Population Average and Standard Deviation	16
10	Location of Linear Accelerometers for the Head, T1, T12, and Pelvis	17
11	Schematic of ES-2 Instrumentation	18
12	The TNO ATD NAP	19
13	Retro-Reflective Markers	19
14	Head Anatomical Coordinate System	20
15	The T1 Anatomical Coordinate System	21
16	Animated Reconstruction of the Kinematics Based on the Rigid-Body Kinematics	22
17	Position, Force, and Moment Vectors Used in the Inverse Dynamic Calculation	23
18	Maximum Upper-Neck (OC) Loads for Tension and Lateral Bending Moment	34
19	Maximum Lower-Neck (T1) Tension Force and Lateral Bending Moment	34
20	Maximum Upper-Neck (OC) Tension and Resultant Shear Force	35
21	Maximum Lower-Neck (T1) Tension and Resultant Shear Force	35
22	Spatial Flexion Angle of Head With Respect to T1, Aircraft Seat	38

23	Twist Angle of Head With Respect to T1, Aircraft Seat	38
24	Lateral T1 Linear Acceleration in Rigid-Restraint Thorax Configuration	39
25	Vertical T1 Linear Acceleration in Rigid-Restraint Thorax Configuration	39
26	Lateral Shear Force in the Upper Neck for the Rigid-Restraint Thorax Configuration	40
27	Lateral Bending Moment for the Aircraft Seat Configuration	41
28	The ES-2 Quality MADYMO Model	43
29	The MADYMO Sled Seat Environment Models	44
30	The ATD Settling Steps	45
31	Experimental and Simulation Acceleration Pulse	45
32	The ATD Model Neck Construction	48
33	Rigid Seat, ES-2 Head c.g. Linear Displacements Relative to the Sled	49
34	Rigid Seat, ES-2 Head c.g. Rotations Relative to the Sled	49
35	Rigid Seat, ES-2 T1 Linear Displacements Relative to the Sled	49
36	Rigid Seat, ES-2 T1 Rotations Relative to the Sled	50
37	Rigid Seat, ES-2 Upper-Neck Forces	50
38	Rigid Seat, ES-2 Upper-Neck Moments	51
39	Rigid Seat, Experimental and Simulated Kinematic Response	51
40	Aircraft Seat, ES-2 Head c.g. Linear Displacements Relative to the Sled	52
41	Aircraft Seat, ES-2 Head c.g. Rotations Relative to the Sled	52
42	Aircraft Seat, ES-2 T1 Linear Displacements Relative to the Sled	53
43	Aircraft Seat, ES-2 T1 Rotations Relative to the Sled	53
44	Aircraft Seat, ES-2 Upper-Neck Forces	53
45	Aircraft Seat, ES-2 Upper-Neck Moments	54
46	Aircraft Seat, Experimental and Simulated Kinematic Response	55
47	Triangular and Rectangular Pulses for 9- and 16-g Acceleration Conditions	56

48	The ES-2 Upper-Neck Loads for the Rectangular 7.2-g and Triangular 9-g Pulses	57
49	The ES-2 Upper-Neck Loads for the Rectangular 18.3-g and Triangular 16-g Pulses	57
50	Acceleration Pulses Used in Reducing Severity of Sled Impacts	58
51	Effect of the Acceleration Pulse on Upper-Neck Tension Forces in ES-2 Simulations	58
52	Comparison of Simulation and Experiment for 90% Sled Velocity	59
53	Comparison of Simulation and Experiment for 70% Sled Velocity	59
54	Effect of Locked Neck Joints on Upper-Neck Loads for 70% Sled Velocity	60
55	Upper-Neck Tension and Lateral Moment Response to Pulse Severity	60
56	Upper-Neck Loads for Additional Head Mass and Decreased Bending Stiffness	61
57	The AIS 3+ Probability for ES-2 Upper-Neck Force Fz	63
58	The AIS 3+ Probability for ES-2 Lower-Neck Force Fz	63
59	The AIS 3+ Probability for ES-2 Upper-Neck Resultant Shear Force Fxy	64
60	The AIS 3+ Probability for ES-2 Lower-Neck Resultant Shear Force Fxy	64
61	Horizontal Force (220 N) Applied to the Knees While ATD is Lowered Into the Seat	67
62	SAE AS8048 Two-Finger Belt-Tightening Procedure	67
63	String Holding Torso Upright	68
64	The PMHS Upper-Neck Tension and Lateral Bending Moment Grouped for AIS 0-2 vs AIS 3-6	71
65	The ES-2 Upper Neck Tension and Lateral Bending Moment Grouped for AIS 0-2 vs AIS 3-6	72

LIST OF TABLES

Table		Page
1	Abbreviated Injury Score Examples for the Spine	4
2	Potential Injury Criteria Prior to 2002—Literature Review	5
3	Injury Criteria and Tolerances From Studies After 2002	7
4	The 14 CFR 25.562 Longitudinal Impact Pulse	10
5	Test Matrix of Conducted PMHS and ES-2 Tests at WSU	13
6	Test Matrix of Conducted PMHS and ES-2 Tests at MCW	13
7	Main Characteristics of PMHS	16
8	Pathology and Injury Severity Scores for the PMHS Tests	26
9	Test Results With Potential Injury Criteria and Tolerances From Literature: WSU Tests 9 g ΔV at 8.5 m/s and 19 g ΔV at 12.1 m/s	29
10	Test Results With Potential Injury Criteria and Tolerances From Literature: MCW Results—Rigid Seat, Full-Thorax Restraint, 12.5 g at 12.5 m/s	30
11	Test Results With Potential Injury Criteria and Tolerances From Literature: MCW Results—Rigid Seat, Full-Thorax Restraint, 15.5 g at 18.0 m/s and 17 g at 18 m/s	30
12	Test Results With Potential Injury Criteria and Tolerances From Literature: MCW Results—Aircraft Seat, Three-Point Belt, 12.5 g at 12.5 m/s	31
13	Test Results With Potential Injury Criteria and Tolerances From Literature: MCW Results—Aircraft Seat, Three-Point Belt, 8.5 g at 8.7 ms and 10.5 g at 11.4 m/s	32
14	Upper and Lower Neck Resultant Shear and Moment	33
15	Acceleration Conditions for Simulating Pulse Shape Variation Study	47
16	Mean Value for 50% Risk, σ as a Percentage of the Mean 50% Risk Value	65

LIST OF SYMBOLS AND ACRONYMS

ΔV	Delta velocity
F	Force
Fxy	Shear force
Fz	Tension force
Mx	Bending moment
3-D	Three-dimensional
AIS	Abbreviated Injury Scale
ATD	Anthropomorphic test dummy
BMD	Bone mineral density
C	Cervical vertebra
CAMI	Civil Aerospace Medical Institute
CFR	Code of Federal Regulations
c.g.	Center of gravity
CL	Confidence limit
CT	Computed tomography
DEXA	Dual Energy X-Ray Absorptiometry
ES-2	EuroSID-2 (anthropomorphic test dummy)
FAA	Federal Aviation Administration
FNSC	FAA next sled cadaver
FNSD	FAA next sled dummy
fps	Frames per second
HIC	Head injury criteria
IARV	Injury Assessment Reference Value
km/h	kilometers per hour
MADYMO	Mathematic Dynamic Modeling
MCW	Medical College of Wisconsin
MRI	Magnetic Resonance Imaging
ms	Millisecond
N	Newton
NAP	Nine accelerometer package
NBDL	National Biodynamics Laboratory
N_{ij}	Neck injury criteria
Nm	Newton meter
OC	Occipital condyle or upper neck
PMHS	Postmortem human subject
rad/s	Radians per second
rad/s^2	Radians per second squared
SID	Side-impact dummy
T	Thoracal vertebra
TNO	TNO Industry and Science
WSU	Wayne State University

EXECUTIVE SUMMARY

The requirements of aircraft seats regarding occupant protection during emergency landing dynamic conditions are defined by the Federal Aviation Administration (FAA) in Title 14 Code of Federal Regulations (CFR) 25.562. The current regulations were designed for forward- and backward-facing seats but do not account for the inherent differences in occupant loading in side-facing aircraft seats. Therefore, specific certification requirements that provide an equivalent level of safety are needed for side-facing seats.

The objective of this study was to investigate neck injuries in side-facing aircraft seats and to develop neck injury criteria and injury tolerance levels. Using this information, an Injury Assessment Reference Value (IARV) will be determined for an anthropomorphic test dummy (ATD). This will be used as a basis for a performance standard for the certification of side-facing aircraft seats and corresponding protection systems.

In the first part of this study, a literature review was conducted on neck injuries, kinematics, and injury mechanisms on humans during lateral loading. From the literature review, potential injury criteria and corresponding tolerance levels in side-facing aircraft seats were proposed. On the basis of the literature review, a program consisting of ten postmortem human subject (PMHS) tests was conducted. These tests provided new and necessary information on neck injuries and injury criteria in side-impact loading. Computer simulations and ATD sled tests were performed to guide the definition of test conditions and to establish corresponding values for injury criteria and tolerance values for the ATD. The ATD used for this research was the EuroSID-2 (ES-2), which was designed for automotive side-impact applications. A rigid seat without cushions was initially used to minimize any influence of the seat on the results. A rigid seat with cushions (referred to as an aircraft seat) was used for the three-point tests. Due to the stiffness of in-service side-facing seats, the performance of the rigid seat with cushions was considered comparable. Since the kinematics of the occupant dominates the results (injury mechanisms), the affect of the seat (cushions) was not considered significant.

The first two PMHS tests and corresponding ES-2 tests were conducted at Wayne State University in Detroit, MI. A 9-g test and a 19-g test with a triangular pulse were conducted based on 14 CFR 25.562. The PMHSs were seated on a rigid seat, restrained with a fixed three-point belt and placed adjacent to a shoulder-height side wall. No gross neck injuries were detected in either test. However, serious rib fractures and shoulder injuries were found in these tests that may have reduced the severity of the head-neck loading.

The remaining tests were conducted at the Medical College of Wisconsin (MCW) in Milwaukee, WI. Since the MCW sled produces only rectangular-shaped pulses, it was necessary to substantiate the use of the MCW facility. Computer simulations were performed using Mathematic Dynamic Modeling and sled tests were conducted at the Civil Aerospace Medical Institute to investigate how the shape of the pulse affected the impact response. The results showed that ES-2 responses were very similar to those using the triangular pulse specified in 14 CFR 25.562.

A total of eight PMHS tests and corresponding ES-2 tests were conducted at MCW. Two test configurations were used to conduct these tests: (1) a rigid seat with the occupant's thorax and pelvis securely restrained to the seat and (2) an aircraft seat (including bottom, back panel, and armrest cushions) with the occupant restrained using a current in-service, three-point aircraft seat belt. Two pulse types were used for the rigid-seat configuration tests: (1) a 12.5-g sled deceleration with velocity change prescribed in 14 CFR 25.562 and (2) a 15.5-g sled deceleration with an increased velocity change of 44%, thereby doubling the kinetic energy. Similarly, two pulse types were used for the aircraft seat configuration tests: (1) a 12.5-g sled deceleration with velocity prescribed in 14 CFR 25.562 and (2) an 8.5-g sled deceleration with a velocity decrease of 30%.

Using the Abbreviated Injury Scale (AIS) for necks, minor neck injuries (AIS 1) were found in the 12.5-g rigid-seat tests (secured, well restrained). Major injuries (AIS 3 and greater (AIS 3+)) were found with the same impact severity using the aircraft seat and a three-point belt restraint system. The serious injuries were attributed to the kinematics of the occupant that occurred using the three-point belt restraint. Therefore, it was expected that serious injury to the neck can occur when using a standard three-point restraint system. The lower-severity (8.5 g) aircraft seat tests resulted in one AIS 3 and one AIS 0 score. The severe 15.5-g rigid-seat tests resulted in one PMHS with AIS 2 injuries and the other with AIS 3+ injuries.

With regard to other body parts, the PMHSs sustained rib fractures, femur shaft fractures due to flailing of the lower legs, and in one instance, a (life-threatening) carotid tear. Of deep concern was that head angular accelerations in the tests were high enough to induce unconsciousness. This would delay or prevent the occupant from exiting the airplane and could also delay or prevent adjacent occupants from exiting the aircraft.

This study focused on side-facing aircraft seats subjected to loading requirements specified in 14 CFR 25.562. However, the proposed injury criteria and tolerance values are sufficiently general so that they can be applied to other categories of aircraft as well.

From the analysis, it was concluded that the tension force is the most discriminating parameter for predicting AIS 3+ injuries to the neck. The probability analysis showed that a tension force of 2300 Newtons (N), corresponding to a 50% risk of an AIS 3 neck injury, and a value of 1800 N, corresponding to a 25% risk, in the upper neck of the ES-2 can be used as an appropriate IARV, when combined with a minimum shear force, bending, or torque precondition (indicates a bending position of the head-neck system). It should be noted that the number of data points available to allow for such a probability analysis of the tension forces was rather small. Explicit tolerance values for pure bending or shear loads would be helpful to complete the dataset. Additional tests would be necessary to establish the correlation of bending moment and injury with a strong degree of confidence. Additional tests are necessary to develop such criteria.

Kinematics of the ES-2 dummy and neck forces showed good biofidelity compared to the PMHS tests. This, however, excludes the early rebound observed in the dummy and the increased

stiffness of the dummy in vertical direction, resulting in lower thoracal 1 vertebra accelerations. Forces in the neck show the same trends; thus, the dummy forces can be used to reflect the PMHS neck forces, which are most significant in the injury mechanism.

The computer simulations showed realistic and repeatable responses in comparison to the ES-2 behavior in both the rigid and aircraft seat configurations. They were further helpful in supporting the selection of proper test conditions, indicating that a rectangular pulse could be used to replace a triangular pulse, as defined in the regulations. Additionally, the simulations were used in the selection of sled pulse severities that would induce specific injury severities. Finally, an investigation of supporting the neck through the use of a collar to increase the moment in neck was carried out. Results suggested that such an approach is valid and that further pulse severity increases could possibly cause moment-related injuries as opposed to tension-related injuries.

A first draft of a standardized test procedure was written, focusing on the appropriate seating procedure for the dummy. This was different from common automotive procedures used for side-impact tests. The tests performed in this effort suggested the use of the ES-2 was appropriate for these impact conditions but identified areas for future improvements. First, the durability of the ES-2 neck requires attention. Cracks were found in the neck after a few tests. Second, it was observed that the leading shoulder belt slips in the open space at the bottom of the neck and loads the lower part of the neck such that it could affect the lower-neck load cell reading. It is estimated, however, that this unwanted belt behavior simulates the observed shoulder depression in the PMHS and contributes to the biofidelic kinematics of the ES-2. Therefore, modification to the neck of the ES-2 to provide accurate lower load cell reading should also preserve its biofidelic kinematic behavior.

1. INTRODUCTION.

1.1 OBJECTIVE.

The objective of this study was to investigate neck injuries in side-facing aircraft seats and to develop neck injury criteria and injury tolerance levels. Using this information, an Injury Assessment Reference Value (IARV) will be determined for an anthropomorphic test dummy (ATD). This will be used as a basis for a performance standard for the certification of side-facing aircraft seats and corresponding protection systems. Data developed in this study was based on the existing and standardized acceleration pulse described in Title 14 Code of Federal Regulations (CFR) 25.562. The proposed injury criteria and tolerance values would also be applicable to other categories of aircraft.

1.2 PROBLEM DEFINITION.

The requirements of aircraft seats regarding occupant protection during emergency landing dynamic conditions are defined by the Federal Aviation Administration (FAA) in 14 CFR Parts 23.562, 25.562, 27.562, and 29.562. These CFRs apply for all occupied seats during takeoff and landing for their respective aircraft category. The current regulations were designed for forward- and backward-facing seats but do not account for the inherent differences in occupant loading in side-facing aircraft seats. In a crash, a sideways seated occupant is loaded in an entirely different manner than forward-aft facing occupants. Therefore, specific certification requirements for side-facing seats that provide an equivalent level of safety are needed.

1.3 BACKGROUND.

For forward-aft facing seats, injury criteria and tolerances have been adopted from automotive crash safety regulations; for example, head injuries are evaluated using the head injury criterion (HIC) and lower limb injuries are evaluated using femur axial loading. Although a similar approach to side-impact loading could be used, the current automotive regulations do not address injuries to the neck, an area identified from previous studies (Lankarani, et al., 1999, and Soltis, 2001) to be of significant importance for the loading scenarios considered in this study.

Shams, 1995, and Lankarani, et al., 1999, conducted full-scale, side-facing seat impact tests using ATDs and computer simulations to evaluate a number of potential occupant injury parameters. HIC and the pelvic injury criterion, both from the automotive side-impact regulations, were used to assess injury. Neck injury criteria (N_{ij}) proposed by Mertz and Patrick, 1967 and 1971, and Patrick and Chou, 1976, were used to assess neck injuries. The tests were conducted with the 16-g, 44-ft/s horizontal crash pulse for forward-aft facing seats specified in 14 CFR 25.562. The results of the studies showed fairly good agreement between the test and the simulations for a number of load and injury parameters. In both studies, the injury parameter that consistently exceeded the tolerance limit was neck loading. This was attributed to the high amplitude and long duration of the deceleration pulse. A study by Soltis, 2001, presented several potential neck criteria based purely on literature data, including a N_{ij}-type criterion, combining lateral neck-bending moment and tension force. However, it was concluded that data available

in the literature were not consistent or extensive enough to validate the choice of any of the potential criteria.

1.4 APPROACH.

The project was divided into the following four phases.

1.4.1 Phase 1: Literature Review.

A literature review was conducted on neck injuries, kinematics, and injury mechanisms in lateral-loading and existing neck injury criteria and tolerance levels. From the literature review, potential injury criteria and corresponding tolerance levels were proposed. On the basis of this study, an initial test setup was developed to conduct postmortem human subject (PMHS) tests and corresponding side-facing ATD tests to complement the literature-based biomechanical information.

1.4.2 Phase 2: Tests.

A series of PMHS and ATD tests were conducted to develop data on neck injuries and injury criteria in side-impact loading. The tests included simulated sled-based impact tests and computer simulations to guide and define test conditions. The primary objective was to establish corresponding IARV for the ATD. The IARV is the physical parameter measured in the ATD that predicts the injury risk for the human subject when exposed to the same loading conditions. Thus, the IARV is the ATD equivalent for the human specimen-related injury criteria and tolerance level. The EuroSID-2 (ES-2) ATD was selected for use in this study. The ES-2 was specifically designed to be used in studies to investigate automotive side impacts and was considered the best available match for this study.

1.4.3 Phase 3: Injury Assessment Reference Values.

Injury mechanisms, criteria, and tolerances were determined from the PMHS tests. IARVs for the ATD were developed in conjunction with the PMHS's injury criteria. The injury criteria and tolerance values were based on the PMHS test results and the information obtained in the literature review. The injury severity, as indicated by the injury criteria and IARV tolerance level, was chosen so as not to endanger the occupant's ability to escape the aircraft cabin after a crash. In general, this corresponds to a severity score of 2 or less on the Abbreviated Injury Scale (AIS) (AAAM, 1990).

1.4.4 Phase 4: Side-Impact Test Procedure Design.

A side-impact test procedure to be used for the certification of aircraft seats was developed in Phase 4. The test procedure was used by both participating test facilities.

1.5 REPORT OUTLINE.

This report is a detailed summary of the work conducted within the scope of the study. Additional reports have been written providing more detail for the particular tasks and tests

conducted within this study. The information included in those reports was, as much as possible, integrated and summarized here. The topics relevant to the development of the proposed IARVs were also reported here.

This report is organized in eight sections. Section 2 summarizes the results of the literature study (Phase 1) conducted in the initial phase of the project (2002/2003). Recent literature findings have been included as well.

Sections 3 and 4 describe the tests performed in Phase 2. In the test program, ten PMHS tests were conducted in conjunction with ATD tests. Two of these PMHS tests were performed at Wayne State University (WSU), Detroit, MI, and the other eight tests at the Medical College of Wisconsin (MCW), Milwaukee, WI. Section 3 describes the test methodology, test conditions, instrumentation used, and specifications of the PMHS's, while section 4 deals with the results of the test program.

Section 5 describes the computer modeling performed to support this study. Most of the simulation work was performed using ATD models; however, some simulation work was conducted with human body models. Unfortunately, due to the extreme loading conditions in this project, the human body models used, in general, were found not to be sufficiently realistic in comparison to the PMHS tests and were therefore not reported.

Section 6 describes the development of the ATD-specific IARVs related to occupant injury criteria and tolerance values (Phase 3). This was done using the Probit calculation method, for which a brief implementation description is provided.

In section 7, an initial setup for a standard side-impact test is presented (Phase 4). For this purpose, a large series of tests with various ATDs were performed at the FAA Civil Aerospace Medical Institute (CAMI) in Oklahoma City, OK. The results of these tests are included in this section.

Section 8 summarizes this research.

2. LITERATURE REVIEW.

2.1 INTRODUCTION.

This section provides background information and an overview of research pertaining to the impact of aircraft occupants in side-facing seats. An explanation of the injury severity scale used to qualify injuries is presented in section 2.2. Potential injury criteria based on the literature review are presented in section 2.3. Section 2.4 summarizes the most important findings.

2.2 ABBREVIATED INJURY SCALE.

Injury criteria are parameters that correlate to the severity of the sustained injury; consequently, an increasing value of the injury criteria usually indicates a more severe injury. These injury criteria can be single physical parameters or a composition of multiple parameters.

To address the severity of an injury, John D. States introduced the AIS for the Association for the Advancement of Automotive Medicine in 1969. It is an anatomical scoring system that provides a ranking of the injury severity using numbers from one to six where the severity score is related to the risk in terms of lethal consequences. The ranking system considers AIS 1 to be a minor injury, AIS 5 to be a severe injury, and AIS 6 to be a nonsurvivable injury. All remaining scores reside in between and have been summarized in table 1. Only injury definitions for the spine are presented (from AIS, 1990 revision and Pike, 1990); however, similar tables exist for all other body regions with classification of all potential injuries.

Table 1. Abbreviated Injury Score Examples for the Spine

AIS	Severity Code	Example for the Spine
0	No injury	-
1	Minor	Acute strain (no fracture or dislocation)
2	Moderate	Minor facture without any cord involvement
3	Serious	Ruptured disc with nerve root damage
4	Severe	Incomplete cord syndrome
5	Critical	Quadriplegia
6	Maximum (virtually nonsurvivable)	-

Neurological deficits cannot be diagnosed for a PMHS. Consequently, an objective AIS score for PMHS is limited to damage of anatomical structures. In this study, the neurological consequences were specified based on clinical experience by a board-certified neurosurgeon. This resulted in two AIS scores for each specimen, a pure anatomical-based AIS score and a clinically based score.

2.3 POTENTIAL INJURY CRITERIA.

To provide quantitative descriptions of responses that cause injuries, several methods were used to correlate the measurable response of a PMHS to the severity of the sustained injuries. These correlations are used to predict human body tolerances to different types of impact. Studies by Lankarani, et al., 1999, and Soltis, 2001, showed that there are differences between the lateral impact due to an emergency scenario in airplanes and a side-impact car crash. It was found that accelerations in a survivable aircraft accident are lower and have a longer duration than those in side-impact car crashes. Additionally, contact of the occupant with the interior, especially of the head, is the main source of severe injuries in a side-impact car crash; however, the most common injuries observed in aircraft accidents occur within the neck as a result of inertial loading and without head-to-interior contact. Therefore, the automotive side-impact literature provides only limited application to research on aircraft accident injury.

A literature review performed in 2002 at the start this project, in addition to an earlier study done by Soltis, 2001, disclosed only a limited number of studies on neck injuries under lateral loading conditions. The details on this literature survey are presented in appendix A. The criteria and tolerances listed in table 2 are the result of this literature review.

Table 2. Potential Injury Criteria Prior to 2002—Literature Review

Criteria	Tolerance Range for the Neck		Criteria
	AIS 1	AIS 2	
Impact velocity (km/h)	0-40	30-60	Input
Impact acceleration (g)	5-10	10-14.7	
Head angle (°)	50-70	57-75	Kinematic
Head angular velocity (rad/s)	8-30	32-39	
Head angular acceleration (rad/s^2)	680-1460	1588-2601	
Head linear acceleration (g)	13-32	12.5-18	
Lateral bending moment (Nm)	22.6-40.7	40.7-60	Load
Upper-neck tension (N)	N/A	4170	
Upper-neck compression (N)	N/A	4000	
Upper-neck shear force (N)	240	>900	

From this analysis, it was observed that only AIS scores less than 3 were reported in cases where only inertial loading was found (i.e., those that are applicable for aircraft crashes).

Note that the injury criteria and their subsequent tolerance values include input criteria, as used for the experiment, as well as kinematic and load criteria. The listed criteria address injuries for the neck under lateral loading conditions. Therefore, all criteria are measured in lateral direction. Due to the eventual redirection of the head and neck from a vertical orientation into a lateral orientation during loading, the head linear acceleration is the resultant for both the lateral and the vertical directions. Furthermore, forces and moments are measured in the occipital condyle (OC), i.e., upper neck. The tolerance values occasionally show overlapping values for AIS 1 and AIS 2 scores. These thresholds result from different studies, where test conditions can vary significantly.

More recent research neck injury studies have been extensively reviewed by McIntosh, et al., 2007. An overview of publications on lateral impacts of volunteers and PMHS was performed, including recent studies like Kettler, et al., 2006; Lund, 2003; and Frechede, et al., 2005. McIntosh, et al., 2007, performed an evaluation of 15 PMHS lateral sled tests conducted at the University of Heidelberg, which was never published. In these Heidelberg tests, a bench seat with an instrumented side panel was mounted on the sled with the bench parallel to the direction of sled motion (figure 1). The test object slid along the bench and impacted its left side against the side panel. The motions of the sliding body stopped by the wall may be different from the restrained aircraft passenger; however, the loading level was in the same range.

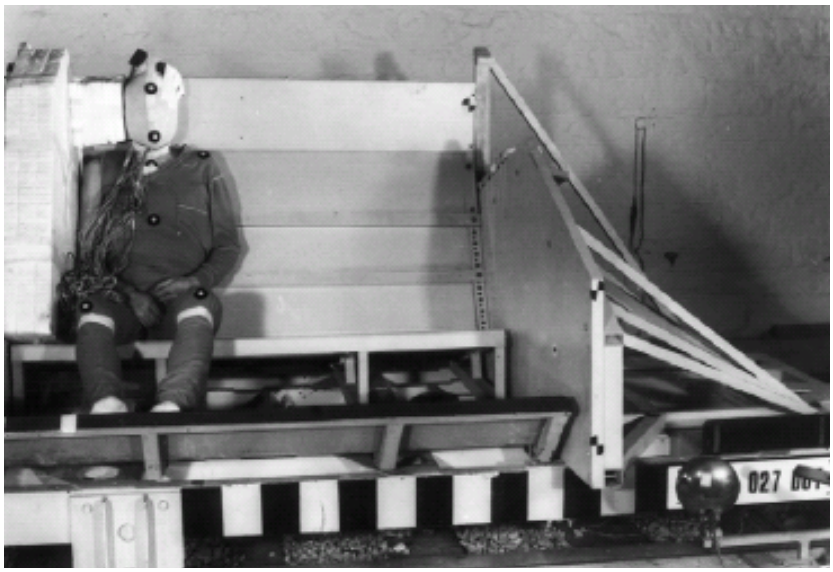

Figure 1. The Heidelberg Setup for Lateral PMHS Tests

The 15 Heidelberg tests showed mainly hemorrhages of the disc distributed at all cervical levels. More severe injuries, i.e., ruptures of the intervertebral disc or ligamentum flavum, were only found in the lower cervical spine (C4 to T1), and no vertebral fractures were observed. This compares well with other reports Bourhis, 1996, and Hartwig, et al., 2004. Kallieris, et al., 1991, had stated that severe injuries associated with severe impacts are mainly found at the lower cervical spine, while less severe injuries are found more in the middle cervical spine. Resultant head acceleration and neck force showed a statistical significant relationship with neck injury severity. The average resultant head acceleration for AIS 2 neck injuries was 112 g's, while the resultant neck force was 4925 N, and the upper-neck moment was 241 Nm.

McIntosh, et al., 2007, compared published test results with his findings (similar loading conditions, i.e., no head impact). Noninjury sled tests with volunteers (Patrick and Chou, 1976; Ewing, et al., 1977, 1978; Wismans and Spenny, 1983; Wismans, et al., 1986) and tests with cadavers/PMHS (Kallieris, et al., 1981, 1991, 2001; Bendjellal, et al., 1987) at injurious levels were included. The values for the measured biomechanical parameters in the McIntosh study were generally larger than those reported in the other studies. However, as expected, the magnitude of the averaged neck force, neck moment, and head acceleration maxima increased with increasing injury severity. The minimum shear force-inducing injury, 829 N in the McIntosh study, is close to the maximum shear reported for volunteers, 794 N. The averaged upper-neck lateral shear force maxima reported by McIntosh, 1693 N, is slightly less than the 2050 N reported for earlier cadaver tests inducing AIS 1 neck injuries. Injury criteria and tolerances, as published by McIntosh, et al., 2007, are listed in table 3.

Table 3. Injury Criteria and Tolerances From Studies After 2002

Injury Response	AIS 1	AIS 2
Impact velocity (km/h)	28.7	34.0
Impact acceleration (g)	14.4	16.9
Head angle (°)	N/A	N/A
Head angular velocity (rad/s)	N/A	N/A
Head lateral angular acceleration (rad/s^2)	4878	6173
Head lateral linear acceleration (g)	40.8	63.4
Head resultant linear acceleration (g)	58	112
Lateral bending moment (Nm)	132	180
Resultant bending moment (Nm)	178	241
Upper-neck tension (N)	1084	1892
Upper-neck compression (N)	N/A	N/A
Upper-neck lateral shear force (N)	1693	2797
Upper-neck resultant force	2419	4925

The order of magnitude of impact velocity and acceleration tolerances reported by McIntosh, et al., 2007, is consistent with previous values. The difference between 14.4 and 16.9 (g) for AIS 1 and AIS 2 appears not to be significant as intersubject variations of 30% are considered realistic.

McIntosh's study did not include ATD tests; thus, correlation with ATD responses related to the injury assessment tolerances could not be derived. McIntosh suggested that, based on Lund's study (Lund, 2003), which used a side-impact dummy (SID) II female ATD, resultant force and moment may be useful in setting initial IARVs. Lund found a lateral upper-neck flexion moment of 67 Nm, lower-neck lateral flexion moment of 134 Nm, and an axial (torsion) moment of 39 Nm in the SID II female, corresponding with AIS 0-1 injury severity in the PMHS. The shear force tolerance was also increased compared to the value reported previously; 2800 N for AIS 2 in contrast with the >900 N found in pre-2002 publications.

2.4 LITERATURE REVIEW SUMMARY.

For some of the potential neck injury criteria, significant differences could be observed between the earlier literature review and the later study by McIntosh. The earlier tolerance for pure single tension, 4170 N (as specified in the N_{ij} criteria), appears to be almost double the value found by McIntosh for AIS 2 injuries in lateral-loading conditions. The earlier lateral bending moment (60 Nm), as suggested earlier by Soltis, 2001, is significantly lower than the number concluded by McIntosh (180 Nm) for AIS 2 injuries. The lateral shear force tolerance for AIS 2 was reported earlier to be >900 N. The recent research efforts provide a more specific tolerance of 3000 N for AIS 2 injuries. However, it is unlikely that the tolerances for bending and shear are resulting from pure single load conditions. The neck loads are induced by inertia of the head, which automatically implies a combined tension, bending, and shear load in the neck.

3. METHODOLOGY.

3.1 INTRODUCTION.

Establishing injury risks for the neck in aircraft side-facing seating configurations were studied by subjecting full-body PMHSs to acceleration levels close to the crash pulse specified in 14 CFR 25.562. An ES-2 was subjected to exactly the same loading conditions and test configurations to facilitate the development of dummy-related IARV and corresponding tolerances. The test configurations and measurement setup are presented in more detail in section 3.2. The selection of the worst-case seating configuration was based on the results of a series of sled tests conducted at CAMI and is included in appendix B.

PMHSs were selected to be as close as possible to the 50% male, 78-kg body weight, 1.72-m standing height. A bone mineral density (BMD) test was performed to ensure no abnormal weakness in bone strength. This also allowed older subjects to be used for testing and avoided age-specific injuries. A list of the main subject characteristics is presented in section 3.4.

PMHSs were evaluated pretest by x-rays and a clinical evaluation. This was repeated posttest. A full-body pathological autopsy was conducted immediately after the test. The neck was conserved and a detailed inspection of the neck using a cryomicrotome was performed. The head was separated from the neck since there is no established method to apply inverse dynamics taking into account a neck mass. The mass of the neck cannot be considered a rigid body, and therefore, its moment of inertia would be problematic to obtain. The detected injuries were rated according to the AIS (AAAM, 1990) using two methods: (1) the pathological findings and (2) a clinical interpretation by an experienced neurosurgeon, as functional deficits are not evident in nonliving subjects.

Cross-sectional loads in the PMHS head-neck junction, OC level, and at the base of the cervical spine were calculated through inverse dynamics. A procedure to allow this calculation was developed:

- Segment coordinate systems for head and thoracal (T) vertebra T1 were defined by anatomical landmarks.
- Three-dimensional (3-D) position and orientation of instrumentation with regard to the anatomical segment coordinate systems were determined posttest after the autopsy using the dissected head and T1.
- Mass and moments of head inertia were determined.
- Relevant anthropometrical data were recorded.
- Linear and angular accelerations at the head center of gravity (c.g.) were calculated using an array of nine accelerometers fixed to the skull. The linear acceleration of T1 was recorded.

- 3-D dynamic kinematics of the head and T1 were determined by a high-speed infrared photogrammetric system.

Loads in the ES-2 upper and lower neck, and linear accelerations of the head and base of the neck were recorded using the standard ES-2 instrumentation. Custom instrumentation was used to capture head angular acceleration and velocity. Kinematics of the dummy was determined using the same high-speed infrared photogrammetric system used for the PMHS. Documentation of the instrumentation and data processing is presented in section 3.6.

Kinematic trajectories of the PMHS and ES-2 were compared by displacement of the head c.g. with respect to the T1 anatomical coordinate system. Angular motions were compared by using spatial flexion-twist angles. Definition and examples of the kinematic parameters are presented in section 3.6.

Numerical simulations were used throughout the project to support the design of the test configurations to establish loading conditions and to get an estimate of the expected response. Estimates of ATD responses were made in relation to seating configuration, belt system, and sled pulse characteristics. One example was the decision to modify the sled pulse in an effort to reduce the neck tension force to 1500-1750 N. A second example was a numerical study performed to investigate increasing the bending moment in the neck by using a neck brace or by increasing the moments of inertia of the head through mass added to the outside of the skull.

3.2 TEST SETUP AND TEST MATRIX.

3.2.1 Baseline Load Level.

The load level for the project was the Emergency Landing Condition defined in 14 CFR 25.562 for longitudinal tests of aircraft seats, shown in table 4.

The sled pulse of the first two PMHS test series performed at WSU were triangular in shape but differed from the 14 CFR Part 25 pulse in magnitude, duration, and velocity change. The first test was conducted at a 9-g peak value, and the second test at a 19-g peak value.

The sled pulses for the baseline tests performed at MCW had a similar velocity change as the 14 CFR Part 25 pulse, but were rectangular in shape, with a 12.5-g level, 100 ms duration, and a velocity change of 12.5 m/s. The impact with rebound sled system used for these tests only produced rectangular pulses. Computer simulations, described in section 5, showed that the results with a rectangular wave of this magnitude would be at least as severe as the triangular pulse with the same velocity change. Sled tests conducted at CAMI, which are described in appendix B, verified that the response of the ES-2 was similar for the triangular 14 CFR Part 25 pulse as for the baseline rectangular-shaped pulse. Additional tests were performed with velocity changes of 70% and 144% of the baseline 12.25 m/s.

Table 4. The 14 CFR 25.562 Longitudinal Impact Pulse

Minimum ΔV	13.41 m/s (44 ft/s)
Maximum t_1	0.09 s
Minimum G	16

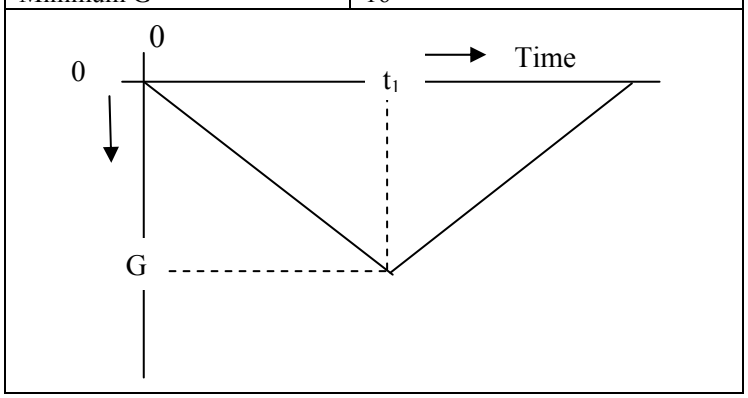

ΔV = Change in velocity t = Time G = Acceleration

3.2.2 Test Configurations.

Three test configurations were used throughout this study. At WSU, an unpadded rigid seat with a rigid support wall and a fixed three-point restraint was used to minimize the influence of the seat and restraint system on the results. At MCW an unpadded rigid seat with lateral rigid torso supports and multiple strap restraints was used to minimize torso movement with the goal of maximizing the head and neck response. When it was found that this configuration did not produce significant injuries at the initial energy levels, a second configuration was used that consisted of a rigid seat with seat cushions, a padded armrest, and a three-point belt with retractor. Analysis of typical side-facing seat configurations conducted at CAMI (DeWeese, et al., 2007) concluded that this configuration produced the largest combined neck loading.

- WSU—Rigid Seat, Side Wall

Seat:	Rigid side-facing seat (figure 2)
Sled system:	Standard 12-inch HYGE
Restraint system:	Fixed three-point belt with shoulder belt at nonleading shoulder. Wall located at the right-hand side of the subject at armpit height. Two layers of plastic sheeting were under the subject to reduce sliding friction. Additional sliding chest strap attached to the top bar was applied to the PMHS to help maintain an upright posture.
Sled pulse:	1. 9-g, 160-ms triangular pulse, ΔV 8.5 m/s 2. 19-g, 130-ms triangular pulse, ΔV 12.1 m/s

Figure 2. Setup for WSU Side-Facing PMHS and ES-2 Tests With a Three-Point, Nonleading Belt

- MCW—Configuration 1: Rigid Seat, Full-Thorax Restraint

Seat:	Rigid side-facing seat (figure 3)
Sled system:	Rebound sled
Restraint system:	Five-point belt with additional straps. Bracket laterally supporting the upper arm and shoulder only. Extra straps around the thorax and a cast on the ribs. An adjustable support bracket extending the top of the seat back allows pulling back and restraining the specimen without disturbing the natural thoracic kyphoses.
Sled pulse:	1. 12.5-g, 100-ms rectangular pulse ΔV 12.5 m/s 2. 15.5-g, 85-ms rectangular pulse ΔV 18.0 m/s, (144% ΔV, 200% kinetic energy) 3. 17-g, 95-ms rectangular pulse ΔV 18 m/s

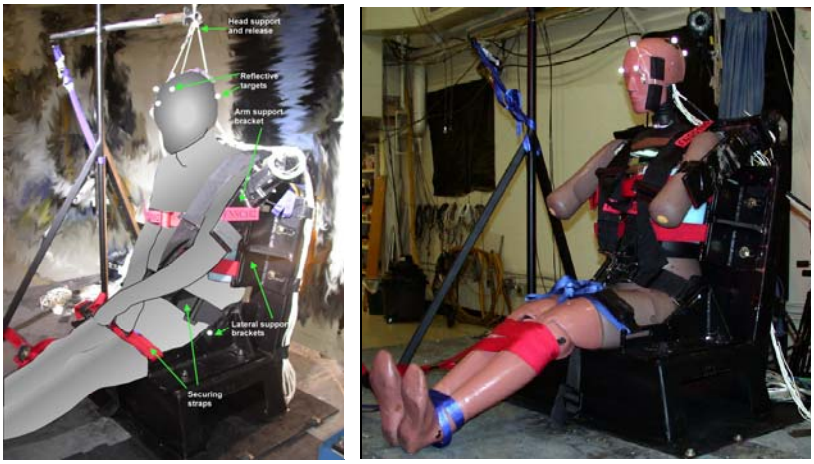

Figure 3. Setup for MCW Rigid Seat With Lateral Arm Bracket

- MCW—Configuration 2: Aircraft Seat, Three-Point Belt With Retractor

Seat:	Aircraft seat with cushions (figure 4)
Sled system:	Rebound sled
Restraint system:	Three-point belt with retractor. Sling-type lap belt with rear central anchorage and lateral anchorage at trailing side of specimen, see figures 4 and 5.
Sled pulse:	1. 12.5-g, 100-ms rectangular pulse, ΔV 12. 5 m/s 2. 10.5-g, 90-ms rectangular pulse, ΔV 11.4 m/s (90% ΔV, 80% kinetic energy) 3. 8.5-g, 95-ms rectangular pulse, ΔV 8.7 m/s (70% ΔV, 50% kinetic energy)

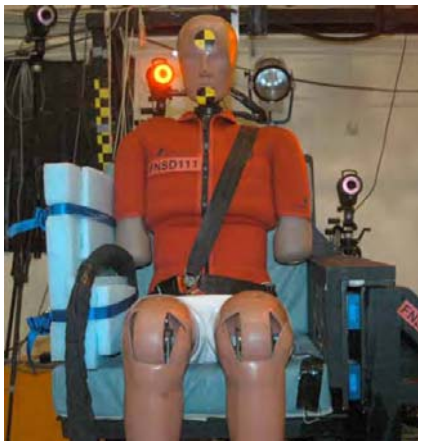

Figure 4. Aircraft Seat With Three-Point Belt

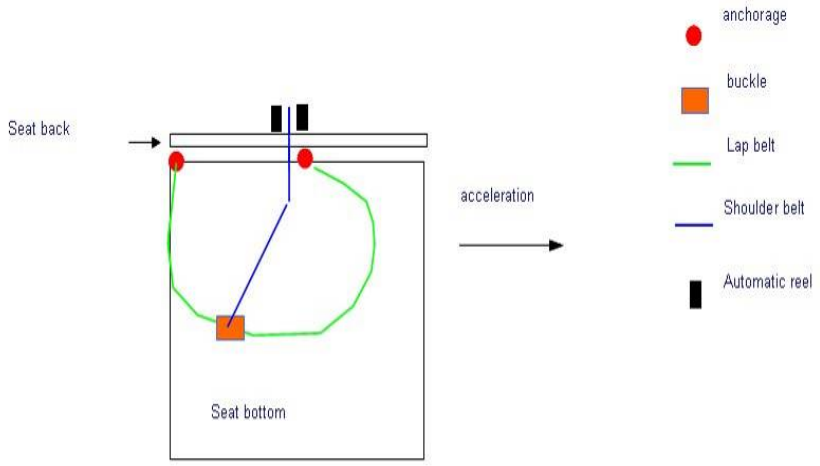

Figure 5. Diagram Showing Top View of Belt Configuration

3.3 TEST MATRIX.

The test matrix used in the analysis is presented in tables 5 and 6. Gray-shaded test numbers are ES-2 tests. All MCW tests are specified by the FAA next sled cadaver (FNSC) or FAA next sled dummy (FNSD) code, where the C represents a cadaver (PMHS) and the D represents an ATD. Note that FNSD 113 has no equivalent PMHS test, as this test was used to verify the dummy loads estimated from numerical simulations.

Table 5. Test Matrix of Conducted PMHS and ES-2 Tests at WSU

Test No.	Pulse WSU Triangular	Configuration	Seat	Restraint
FAA-22	9 g, 180 ms	Side wall up to shoulder	Rigid	Three-point, nonleading shoulder belt
FAA-23	9 g, 180 ms			
FAA-25	19 g, 125 ms	Side wall up to shoulder	Rigid	Three-point, nonleading shoulder belt
FAA-26	19 g, 125 ms			

Note: Gray-shaded test numbers are ES-2 tests.

Table 6. Test Matrix of Conducted PMHS and ES-2 Tests at MCW

Test No.	Pulse MCW Rectangular	Configuration	Seat	Restraint
FNSC 102	12.5 g, 100 ms	Side wall up to shoulder	Rigid	Rigid
FNSD 103				
FNSC 104	12.5 g, 100 ms	Side wall up to shoulder	Rigid	Rigid
FNSD 105				
FNSC 109	12.5 g, 100 ms	Aircraft seat with armrest	Aircraft seat with cushions	Three-point retractor
FNSC 110	12.5 g, 100 ms	Aircraft seat with armrest	Aircraft seat with cushions	Three-point retractor
FNSD 111				
FNSD 113	10.5 g, 90 ms (90% ΔV)	Aircraft seat with armrest	Aircraft seat with cushions	Three-point retractor
FNSC 115	8.5 g, 95 ms (70% ΔV)	Aircraft seat with armrest	Aircraft seat with cushions	Three-point retractor
FNSD 114				
FNSC 116	8.5 g, 95 ms (70% ΔV)	Aircraft seat with armrest	Aircraft seat with cushions	Three-point retractor
FNSC 118	15.5 g, 85 ms (144% ΔV)	Side wall up to shoulder	Rigid	Rigid
FNSC 126	15.5 g, 85 ms (144% ΔV)	Side wall up to shoulder	Rigid	Rigid
FNSD 129	17 g, 95 ms (144% ΔV)	Side wall up to shoulder	Rigid	Rigid

Note: Gray-shaded test numbers are ES-2 tests. C denotes cadaver and D denotes ATD in test number.

3.4 SUBJECT SELECTION AND AUTOPSY PROCEDURE.

3.4.1 The WSU Subject Pretest Screening Procedure.

Anthropomorphic measurements were obtained and evaluated to comply with the 50th percentile male anthropometry (mass 78 kg and standing height 1.72 m). Unembalmed PMHSs were procured and screened for HIV and Hepatitis A, B, and C. Pretest x-rays were then taken and evaluated for any pre-existing conditions that may have compromised the validity of the tests. The quality of the bone was quantified by the bone mineral content of the bone using the Dual Energy X-Ray Absorptiometry (DEXA) method. Each specimen was dressed in tight-fitting leotards and a mask was used to cover head and facial structures prior to the tests.

3.4.2 The MCW Subject Pretest Screening Procedure.

A preselection of available subjects was made based on body weight and anthropometry to fulfill criteria for a 50th percentile male (mass 78 kg and standing height 1.72 m). Unembalmed PMHSs were procured and screened for HIV and Hepatitis A, B, and C. Anthropomorphic data were then obtained. Pretest radiographs were obtained to identify various body and musculoskeletal components. This included the head, neck, chest, thorax, upper and lower extremities, and pelvis. Spinal radiographs were evaluated by a board-certified neurosurgeon for potential abnormalities, using only specimens suitable for the test. Figure 6 shows representative views of the head and cervical spine structures. Each specimen was dressed in tight-fitting leotards and a mask was used to cover head and facial structures prior to the tests.

(a) Lateral-Mid (b) Lateral-Flexion (c) Lateral-Extension (d) Frontal-Mid

Figure 6. Pretest X-Rays

3.4.3 The WSU Posttest Procedure.

A series of posttest x-rays was taken to verify the instrumentation mounting locations and to record the photograph instrumentation targets that were added prior to the test. Computed tomography (CT) scans with a 0.62-mm slice width were made of the neck (cervical (C) vertebra C1 to T2) at Henry Ford Hospital. Magnetic Resonance Imaging (MRI) scans with a 2-mm slice width were made from C1 to T2 at the WSU 1.5 Tesla Facility. A radiologist examined the CT and MRI scans in detail. After the CT and MRI scans, a board-certified pathologist conducted an autopsy with emphasis on the neck and torso.

3.4.4 The MCW Posttest Procedure.

Immediately following the test, a neurosurgeon performed a clinical examination. X-rays were taken prior to an autopsy that was conducted by a board-certified pathologist, carefully isolating the head and neck structures. Isolation was achieved with radiographic assistance, dissecting the craniocervical junction and preserving the entire ligamentous column. Functional radiographs and close-up CT images were obtained to identify neck pathology. All pre- and posttest evaluations were conducted by the same neurosurgeon to maintain consistency. Inertial properties of the head were obtained using a torsion pendulum and were eventually used to compute forces and moments at the head-neck junction. The cervical spinal column was then subjected to quantitative CT measurements for bone quality.

3.4.5 The WSU Bone Quality Measurement Method.

As described in section 3.4.1, WSU evaluated the bone quality of the tested subjects prior to the test using the DEXA method. This procedure produces a score related to the area of cross-sections obtained from the femoral neck and trochantor and intertrochantor regions, expressed in mg/cm^2. The subsequent score is therefore an average of the cortical and trabecular parts of the bone. For demonstrative purposes, figures 7 and 8 show BMD measurements taken from U.S. male and female subjects 45 years and older. These measurements were taken from both the femoral and trochantor regions of the bone.

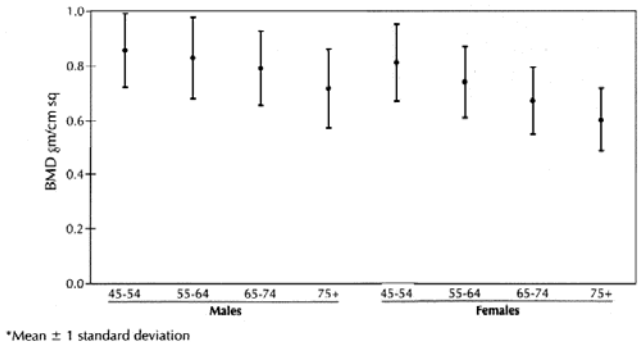

Figure 7. Bone Mineral Density of the Femoral Region

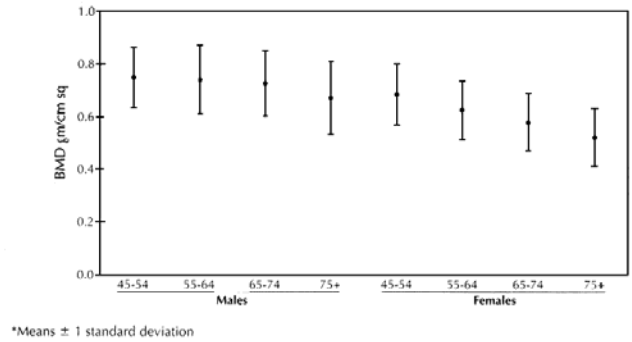

Figure 8. Bone Mineral Density of the Trochanter Region

3.4.6 The MCW Bone Quality Measurement Method.

As described in section 3.4.2, MCW evaluated the posttest bone quality using a quantitative CT method that uses several solid stage phantoms for calibration and mineral assay (Mindways, Inc., San Francisco, CA). This method required dissected bone samples and was performed following the impact test. The resultant measurement provided a density measure in mg/cm^3 for the typical population, shown in figure 9.

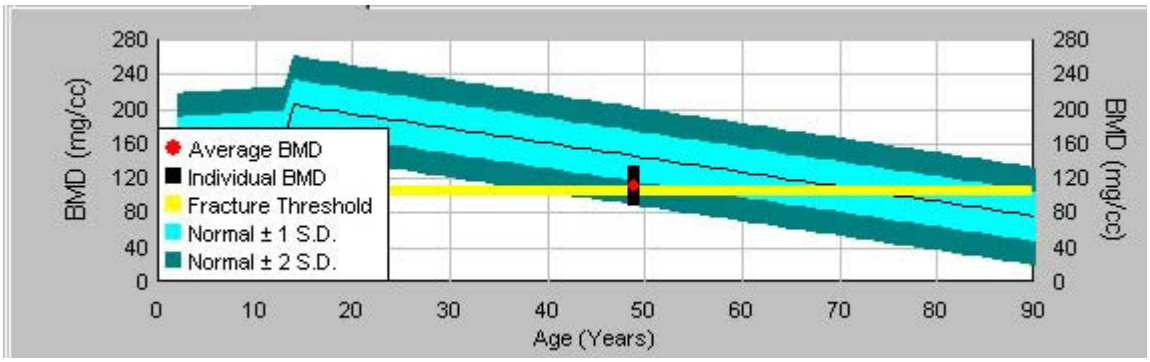

Figure 9. Example of BMD in Relation to the Full Population Average and Standard Deviation

3.5 SUBJECT CHARACTERISTICS.

Primary specimen anthropometrics are listed in table 7. Relative to the 50th percentile male, the specimens varied no more than -15 and +9.5 kg in mass and -0.07 and ±0.16 m in standing height. The bone quality scores from both the WSU and MCW subjects were within the boundaries described by their age.

Table 7. Main Characteristics of PMHS

Specimen	Age (years)	Body Weight (kg)	Standing Height (m)	BMD
FAA-23	63	87.5	1.77	1.7-0.6 mg/cm^2
FAA-26	57	74	1.82	0.665-0.461 mg/cm^2
FNSC 102	55	86	1.88	127 mg/cc
FNSC 104	49	69.9	1.85	110 mg/cc
FNSC 109	59	64.4	1.68	49.3 mg/cc
FNSC 110	55	76.2	1.84	113.2 mg/cc
FNSC 115	57	81.3	1.82	108 mg/cc
FNSC 116	47	74.5	1.75	172 mg/cc
FNSC 118	63	63	1.65	74 mg/cc
FNSC 126	61	67	1.86	122 mg/cc

3.6 DATA ACQUISITION AND PROCESSING.

3.6.1 Instrumentation PMHS—WSU.

Instrumentation used at WSU is similar to the instrumentation at MCW (see section 3.6.2). Noteable differences were the type of nine accelerometer package (NAP) used, and the video photogrammetric system and data processing. The NAP at WSU is aligned by eye with the head anatomical coordinate system. WSU developed a 3-D video photogrammetric system in-house based on regular high-speed video cameras using visible light images. The rigid-body reconstruction from the video recordings was custom-developed for this project.

3.6.2 Instrumentation PMHS—MCW.

The sled was instrumented with a single accelerometer to obtain the change in velocity throughout the test. Each PMHS subject was fitted with triaxial accelerometers fixed to the head, upper spine (T1 region), lower spine (T12 region), and pelvis (see figure 10). In addition, a pyramid-shaped NAP was rigidly fixed to the skull. The 3-2-2-2 design was comprised of three sets of biaxial accelerometers mounted to the triangular base of the pyramid and one triaxial accelerometer mounted at its vertex. The positions and orientations of the accelerometers were determined using a 3-D coordinate measuring machine. All sensor data was collected at 12,500 Hz. Retro-reflective photographic markers were placed on the head, spinous process of T1, and at salient locations on the sled and seat, all of which were used to obtain kinematic information. Each location required a minimum of three individual markers positioned in a noncollinear pattern to describe 3-D motions during impact. Marker movements were captured using a system of nine cameras at 1000 frames per second (fps).

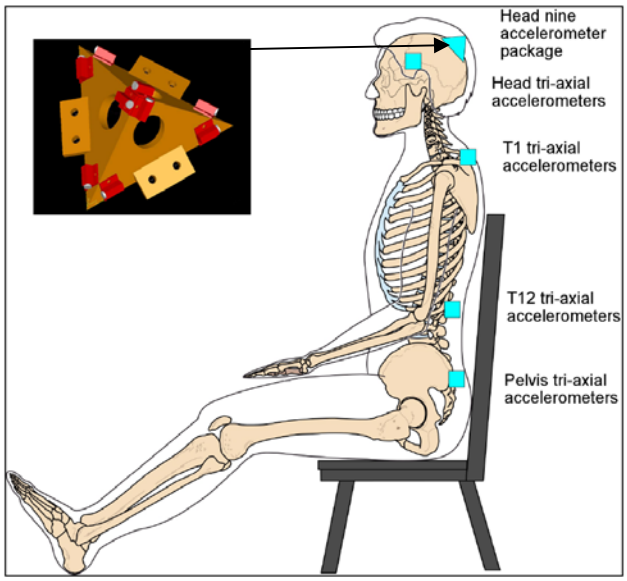

Figure 10. Location of Linear Accelerometers for the Head, T1, T12, and Pelvis

3.6.3 Instrumentation ES-2.

Instrumentation equivalent to that used in the PMHS tests was used during all ES-2 tests, see figure 11. Linear accelerations were measured at the head c.g. using a NAP provided by TNO Industry and Science (TNO) mounted inside the ATD skull (see figure 12). In the last test series, angular rate sensors were also included. Additional accelerometers were placed at the equivalent T1, T12, and pelvic locations. The upper- and lower-neck forces and moments were measured through integrated load cells. All sensor data were collected at 12,500 Hz. Retro-reflective photographic markers were placed on the head (see figure 13), T1, T12, sacrum, and at salient locations on the sled and seat, all of which were used to obtain kinematic information. Each location required a minimum of three individual markers positioned in a noncollinear pattern to describe 3-D motions during impact. Marker movements were captured using a system of nine cameras at 1000 fps.

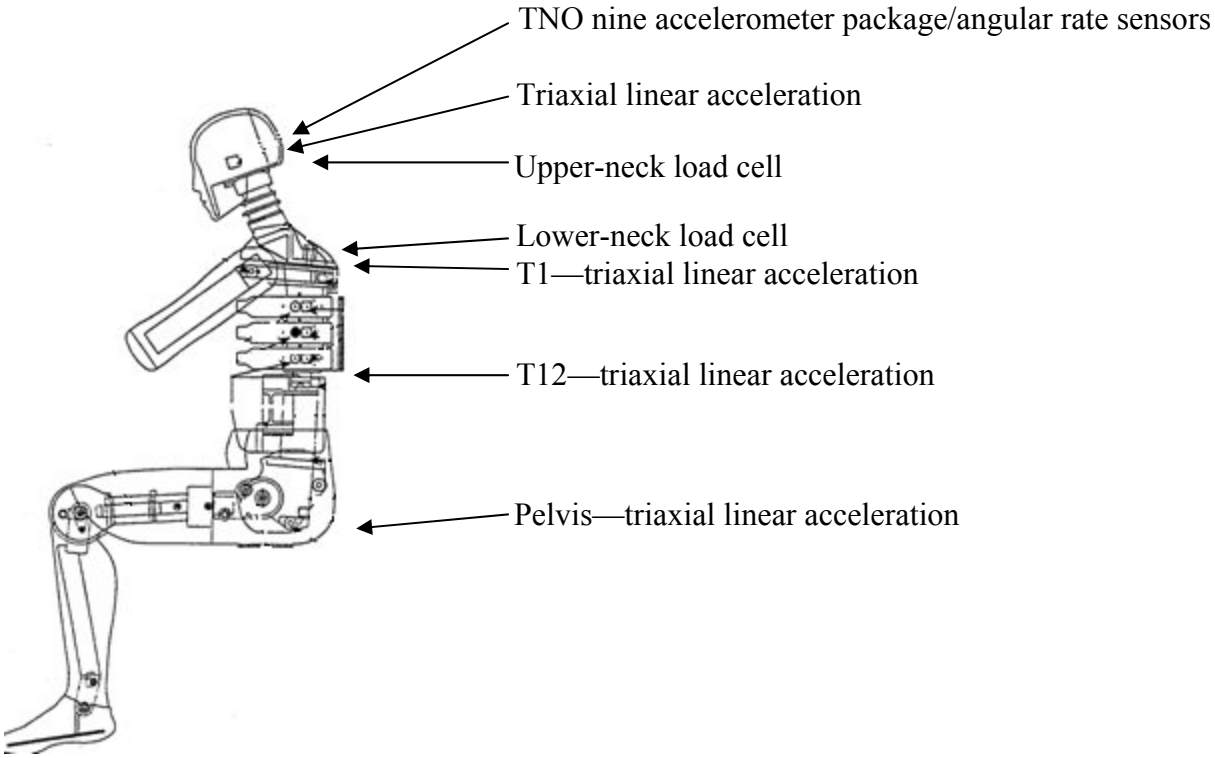

Figure 11. Schematic of ES-2 Instrumentation

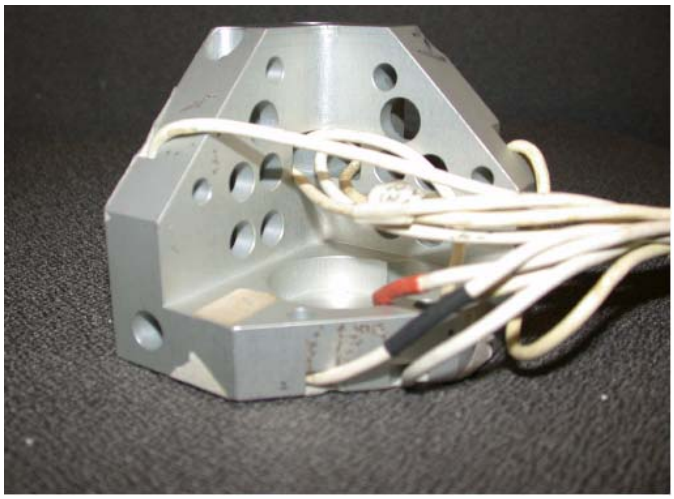

Figure 12. The TNO ATD NAP

Figure 13. Retro-Reflective Markers

3.6.4 Data Processing.

Raw data obtained from the experiments were used in combination with geometric measurements to calculate additional impact responses. This section details the information and methodologies used to define these responses.

3.6.4.1 Anatomical Coordinate Systems.

The sensor data and kinematics were linked to either body-coupled coordinate systems or a sled laboratory-coupled coordinate system. The anatomical coordinate systems were defined using anatomical landmarks on the head and T1.

The head anatomical coordinate system (figure 14) was defined as follows:

- Origin—Measured head c.g.
- X axis—Parallel to Frankfort plane from midpoint of left and right porion to midpoint of left and right infraorbital notches
- Y axis—Parallel to Frankfort plane from left porion to the right porion
- Z axis—Perpendicular to Frankfort plane superior to inferior

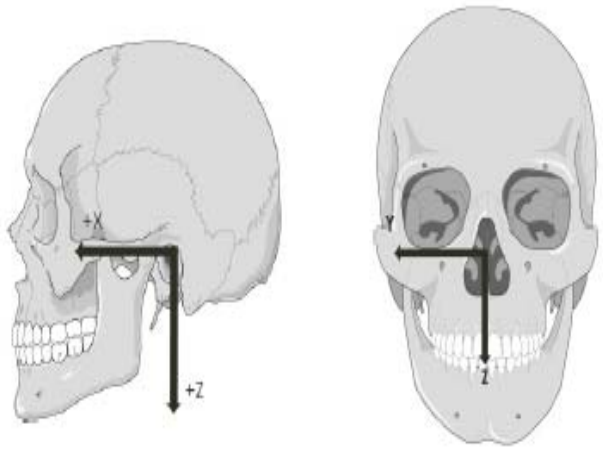

Figure 14. Head Anatomical Coordinate System

The T1 anatomical coordinate system (figure 15) was defined as follows:

- Origin—Posterior tip of the T1 spinous process
- X axis—The cross-product of Y axis and normal vector from midsuperior-anterior aspect (Point A) of T1 to inferior-anterior aspect of T1 (Point B)
- Y axis—The normal vector from left lateral superior (Point C) aspect of T1 to right lateral superior aspect of T1 (Point D)
- Z axis—The cross-product of the X and Y axes

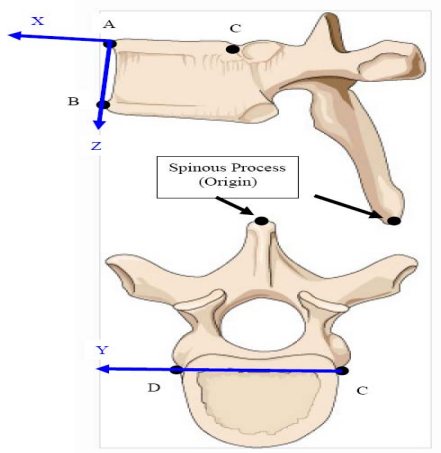

Figure 15. The T1 Anatomical Coordinate System

3.6.4.2 Accelerations and Velocities.

Additional acceleration and velocity responses were calculated for points away from the original sensor locations. Transformation matrices relating the sensor, anatomical, and video coordinate systems to one another were developed to facilitate the calculation. The following parameters were calculated from the head NAP using geometric data and principles of rigid-body kinematics:

- Linear acceleration time histories at head c.g.
- Head angular acceleration time histories
- Head angular velocity time histories

3.6.4.3 Rigid-Body Motions.

Three dimensional kinematic data were collected at 1000 fps using the nine-camera motion analysis system (Vicon Systems, Lake Forest, CA) for the following responses:

- Head
  - Position of head c.g. with regard to the sled coordinate system
  - Orientation of head with regard to sled coordinate system (An animated reconstruction of the head motion is presented in figure 16.)
  - Angular data calculated by reducing the 3 x 3 orientation matrix to spatial flexion twist angles
  - Position of head c.g. with regard to T1 coordinate system
  - Orientation of head with regard to T1 coordinate system

- T1
  - Position of head c.g. with regard to T1 coordinate system
  - Orientation of head with regard to T1 coordinate system
  - Angular data were calculated by reducing the 3 x 3 orientation matrix to spatial flexion twist angles

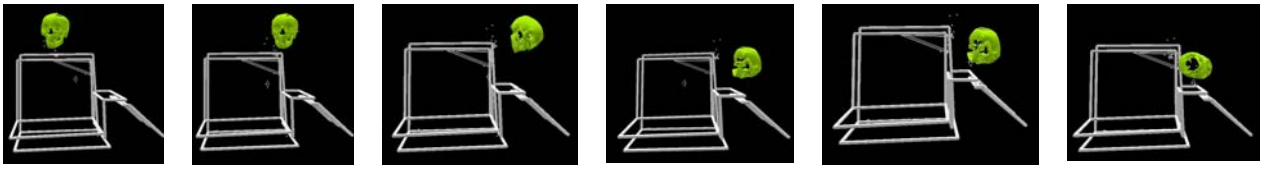

Figure 16. Animated Reconstruction of the Kinematics Based on the Rigid-Body Kinematics

3.6.4.4 Upper-Neck Forces and Moments.

The generalized forces and moments at the occipital condyles were calculated using the following information:

- Specimen geometric measurements
- Specimen inertial measurements
- Head angular acceleration measurements
- Head c.g. linear acceleration measurements

Under the assumption that the principle moments of inertia axes are coincident with the head anatomic axes, this data was combined in the following equations to calculate the upper-neck forces and moments.

$$\overline{F}_{OC} = m \bullet \overline{a}_{CG} \tag{1}$$

$$\overline{M}_{OC} = \overline{I}_{head-anatomical} \bullet \dot{\overline{\omega}}_{head} - \overline{r}_{OC} \times \overline{F}_{OC} \tag{2}$$

where the following axes and vector definitions were used:

- $+F_{OCx}$ = Head rearward, neck forward
- $+F_{OCy}$ = Head leftward, neck rightward
- $+F_{OCz}$ = Head upward, neck downward
- $+M_{OCx}$ = Left ear toward left shoulder
- $+M_{OCy}$ = Chin to chest
- $+M_{OCz}$ = Chin towards left shoulder
- $+r_{OC}$ = Position vector of occipital condyles with regard to head c.g.

It is noted, however, that this data was calculated and delivered by MCW following their preliminary analysis of the test results.

3.6.4.5 Lower-Neck Forces and Moments.

The lower-neck forces and moments where calculated in a method similar to the upper neck and under the assumption that the neck inertia could be neglected. The following equations describe the method of calculations:

$$\overline{F}_{T1} = T_{head \to T1} \circ m \bullet \overline{a}_{CG} \tag{3}$$

$$\overline{M}_{T1} = T_{head \to T1} \circ \overline{I}_{head-anatomical} \bullet \overline{\dot{\omega}}_{head} - \overline{r}_{T1} \times \overline{F}_{T1} \tag{4}$$

where the vectors used therein are shown in figure 17, and the following direction and geometric parameters were used:

- $+F_{T1x}$ = Head rearward, neck forward
- $+F_{T1y}$ = Head leftward, neck rightward
- $+F_{T1z}$ = Head upward, neck downward
- $+M_{T1x}$ = Left ear toward left shoulder
- $+M_{T1y}$ = Chin to chest
- $+M_{T1z}$ = Chin towards left shoulder
- r_{T1} = Head c.g.—T1 anatomical origin vector T1 coordinates
- $T_{head\text{->}T1}$ = Transformation matrix from head to T1 anatomical coordinate system

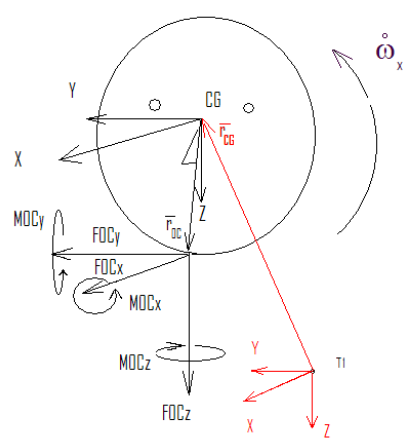

Figure 17. Position, Force, and Moment Vectors Used in the Inverse Dynamic Calculation

Since upper-neck (OC) forces and moments were supplied by MCW, the equations were modified to make use of this data. The following variables were those supplied by MCW.

- $\bar{r}_{CG_{T1}}$: position vector of T1 with regard to head c.g. in T1 coordinate orientation
- $\bar{r}_{oc_{head}}$: position of OC in head anatomical coordinate system
- $\overline{M}_{OC_{head}}$: Moments at OC in head coordinate system
- $\overline{F}_{oc_{head}}$: Forces at OC in head coordinate system
- $R_{head<-T1}$: Rotation matrix: T1 anatomical to head anatomical coordinate system

Modification of the equations first required the definition of the upper-neck x, y, and z moments in the head anatomical coordinate system, defined with the following equations:

$$Mcg_x = Moc_x - r_{OCz_{head}} * Foc_y + r_{OCy_{head}} * Foc_z \tag{5}$$

$$Mcg_y = Moc_y - r_{OCx_{head}} * Foc_z + r_{OCz_{head}} * Foc_x \tag{6}$$

$$Mcg_z = Moc_z - r_{OCy_{head}} * Foc_x + r_{OCx_{head}} * Foc_y \tag{7}$$

where the general equation could be defined as:

$$\bar{M}cg_{head} = \bar{M}oc_{head} - (\bar{r}_{OC_{head}} \times \bar{F}oc_{head}) \tag{8}$$

With the above relationships, the moments and forces at T1 were then defined as:

$$\overline{F}_{T1_{T1}} = R^{inv}_{head \leftarrow T1} * \overline{F}oc_{head} \tag{9}$$

$$\bar{M}_{T1_{T1}} = R^{inv}_{head \leftarrow T1} * \bar{M}cg_{head} - (\bar{r}_{CG_{T1}} \times \bar{F}_{T1_{T1}}) \tag{10}$$

where the moment expressed with regard to the moment and forces supplied by MCW can be expressed as:

$$\bar{M}_{T1_{T1}} = R^{inv}_{head \leftarrow T1} * \bar{M}oc_{head} - R^{inv}_{head \leftarrow T1} * (\bar{r}_{OC_{head}} \times \bar{F}_{OC_{head}}) - \bar{r}_{CG_{T1}} \times (R^{inv}_{head \leftarrow T1} * \bar{F}oc_{head}) \tag{11}$$

Note that the inverse dynamics used to calculate the upper- and lower-neck loads for the PMHS are only valid for the phase where the head was not in contact with any surrounding structure or body part, except the neck. Contact times were determined by visual inspection of the high-speed video and specific response patterns in the measured accelerometer sensor data. Use of copper foil contact switches in the last two PMHS tests confirmed this procedure.

3.6.4.6 Filtering.

PMHS and ES-2 sensor data were filtered using an SAE/J211 Channel Frequency Class 180, 300-Hz filter. However, local peaks with frequencies over 300 Hz due to artifacts were found in the PMHS tests.

4. TEST RESULTS.

4.1 INTRODUCTION.

The final goal of this research was to develop data to support a certification procedure for side-facing aircraft seats, monitoring the injury risk to the neck. Therefore, the analysis of the tests performed was intended to develop potential IARVs for application with the ES-2. These were thought to be best described by peak ATD response parameters; thus, the test results presented here were focused on the PMHS and ATD responses, as described by the potential injury criteria listed in tables 2 and 3.

The injuries found in the PMHS under the tested loading conditions are presented in section 4.2, with a description of the injury and specification of the injury severity. Peak values of the selected parameters for the PMHS and ATD responses were determined for the phase prior to head contact with any surrounding structure or body part and are presented in section 4.3. Time histories for these response parameters are presented in appendices D and E of this report, and parts of the PMHS test results were already published by Yoganandan, et al., 2006 and 2008.

The combinations of various neck load parameters are presented in section 4.4. The effect of combined loading was thought to increase the injury risk in the neck and therefore was chosen as a focus point in the analysis. Combinations of peak values for neck tension-lateral bending, tension-shear, and shear-bending were examined. The results from the first eight PMHS tests were presented at the Triennial International Aircraft Fire and Cabin Safety Research Conference (Philippens, et al., 2007).

An analysis of the peak responses as viable injury criteria in relation to the test type (i.e., PMHS versus ES-2) is presented in section 4.5.

The ES-2 biofidelity with regard to kinematics and dynamics observed in the ATD test is discussed in section 4.6. Comparison of the responses was made against PMHS tests with comparable loading conditions. This entire section is concluded by a discussion in section 4.7.

4.2 INJURIES.

4.2.1 Summary.

A summary of the injuries and the AIS severity score of all tests is listed in table 8. The WSU tests, FAA-23 and FAA-26, were evaluated only by an autopsy and CT scan. No cryomicrotome was available at the time. All MCW tests were evaluated by a pathologist (familiar with PMHS) and an experienced board-certified neurosurgeon. The severity qualification of the neck injuries by the pathologist is listed as “Anatomical” and the severity qualification of the surgeon is listed

as "Clinical." The clinical qualification includes an estimate of the neurological consequences that cannot be directly diagnosed from PMHS tests. The tests with similar test conditions are grouped. The first two are the WSU tests with the rigid-wall configuration. The next four consist of the MCW rigid-restraint thorax setup and the last four consist of the MCW aircraft seat configuration.

Table 8. Pathology and Injury Severity Scores for the PMHS Tests

Test Type	Test No.	Pathology	AIS		
			Anatomical Neck	Clinical Neck	Other Body Area
WSU: Rigid Wall	FAA-23	None	0	N/A	0
	FAA-26	Bilateral multiple rib fractures	1	N/A	4/5
MCW: Rigid Restraint	FNSC 102	C4-T1 diastasis (widening)	0	1	0
	FNSC 104	C2-3 antreolisthesis (subluxation) C3-4 joint laxity, C6-7 ligament thinning	0	1	0
	FNSC 118	T1 avulsion fracture costo-vertebral junction, potential dislocation	2	2	N/A
	FNSC 126	Anterior longitudinal ligament disruption at C5-6, and complete disruption at C6-7.	3	5	N/A
MCW: Aircraft Seat	FNSC 109	C2 fx/dislocation, C6-7 joint dislocation, carotid artery intimal tear, rib fractures, femur fracture	3	5	4
	FNSC 110	T1-2 fx/dislocation, clavicle fx, rib fractures, left shoulder dislocation, left distal femur fx	3	5	4
	FNSC 115	Anterior longitudinal ligament, disc C5-6, C4-5 subluxation	2	3	N/A
	FNSC 116	None	0	N/A	N/A

fx = fracture
N/A = Not applicable

4.2.2 Neck Injuries.

No neck injuries were found in the WSU tests (FAA-23 and FAA-26) rigid wall tests.

Injuries during the MCW tests were assumed to occur at some peak load level. Video documentation showed that the head strike was relatively "soft" (e.g., head hitting the shoulder). Therefore, it is unlikely that the injuries sustained in specimens experiencing head strikes were due to the head strike. No skull fractures were reported for any of the tests.

Minor (AIS <3) and major (AIS 3 and greater (AIS 3+)) neck injuries were found in the MCW rigid-seat tests. The two tests performed with the 100% pulse (FNSC 102 and 104) and one of the tests performed with the 144% pulse (FNSC 118) produced minor injuries. The second 144% pulse test (FNSC 126), however, produced major neck injuries.

Similarly, minor and major neck injuries were found in the MCW aircraft seat setup. One of the tests performed with the 70% pulse (FNSC 116) produced minor injuries. However, the two tests performed with the 100% pulse (FNSC 109 and 110) and the second test performed with the 70% pulse (FNSC 115) produced major injuries. Interestingly, a C2 fx/dislocation was observed in test FNSC 109, an atypical injury for this type of loading condition. In all other tests, injury occurred primarily in the lower neck. Overall, the aircraft seat setup was found to produce higher severity injuries, even at a reduced pulse severity.

4.2.3 Other Body Area Injuries.

Multiple rib fractures were induced by the shoulder belt and lateral compression of the ribcage into the rigid wall during the WSU tests. However, no other injuries were found.

No injuries other than neck injuries were found within the MCW rigidly restrained condition. However, multiple rib fractures were found in the MCW aircraft seat tests 109 and 110. These were attributed to shoulder belt load at the frontal region of the ribcage that also resulted in a clavicle fracture of the PMHS in test 110. Additionally, a carotid artery intimal tear was found in test 109; an injury that cannot be diagnosed clinically but can lead to a stroke within the first 3 to 6 months after the injury is sustained. This injury was probably caused by depression of the shoulder by the shoulder belt and simultaneous stretching of the neck. No vertebral body fractures were reported, which is consistent with the literature results. Femur fractures were also observed in MCW tests 109 and 110; caused by the flailing of the lower legs generating high-axial torques in the femur shaft.

4.3 PEAK VALUES.

The most important results of the tests are presented in sections 4.3.1 to 4.3.3. The peak values of the impact response measures, as discussed in section 2, are presented along with the injury tolerance values obtained from the literature. The AIS values (anatomical as well as clinical) from the PMHS tests are also included. Detailed time histories for the various parameters are included in appendices C and D.

The results are presented in a table format for the three groups:

- WSU—rigid-seat, side wall test, section 4.3.1.
- MCW—rigid-seat, full restraint upper torso series, section 4.3.2.
- MCW—aircraft seat, three-point belt with retractor, section 4.3.3.

The test identification and object type, i.e., PMHS or ES-2, are specified in the first two rows of the tables. The injury severity (anatomical and clinical) for each specimen is listed in the third row below the PMHS test identification. The tolerances developed from phase 1 of this study are listed in columns two through four. The new tolerance values obtained from McIntosh, et al., 2007, are presented in column five. Cells with the N/A designation indicate a response that could not be obtained from the results.

The cells are color-coded according to their relationship to the various tolerance values. Cells that are shaded green, orange, or red indicate their severity relative to the tolerances developed from phase 1 as follows:

- Green AIS 0-1
- Orange AIS 2
- Red AIS >2

Cells that have boxes colored green or red indicate their severity relative to the tolerances as reported by McIntosh, et al., as follows:

- Green AIS <2
- Red AIS 2+

Comparison of color shading and boxing provided by the actual AIS scores (clinical and anatomical) and that predicted by the individual response peaks indicates to what extent the injury criteria and their related tolerances predict the injuries. For example, in table 9, the scored severities for both tests were below AIS 2 and were colored green. Therefore, all parameters with a green-shaded cell or green-boxed peak value predict the injury severity correctly.

4.3.1 WSU—Rigid Seat, Side Wall.

WSU tests were not documented extensively due to missing data, a malfunction of the data acquisition system, and problems with calculating the inverse dynamics. Therefore, only maximum values of upper-neck forces were used as results for the WSU tests, as shown in table 9. Head contact times were not recorded in the WSU tests.

Table 9. Test Results With Potential Injury Criteria and Tolerances From Literature: WSU Tests 9 g ΔV at 8.5 m/s and 19 g ΔV at 12.1 m/s

Test Identification					FAA-23	FAA-22	FAA-26	FAA-25
					PMHS	ES-2	PMHS	ES-2
	AIS—Anatomical/Clinical				0/?	N/A	1/?	N/A
	Head Contact Time (ms)				---	---	---	---
	Tolerance Range for		Soltis	McIntosh				
Injury severity criteria	AIS 1	AIS 2	AIS 2+	AIS 2				
Impact velocity (km/hr)	<40	30-60		34	30.6	31.0	44.0	43.0
Impact acceleation (g)	5-10	10-14.7		16.9	9.0	9..2	18.6	18.7
Head rotation angle (degree)	50-70	57-75	60		84	74	97	N/A
Head angular velocity (rad/s)	8-30	32-39			29	29	21.8	N/A
Head angular acceleration (rad/s^2)	680-1460	1588-2601	2600	6173	1638	1000	2833	N/A
Head linear acceleration (g)	13-32	12.5-18	36	63	25	10	35.7	15
Upper-Neck Loads								
Moment Mx (Nm)	22.6-40.7	40.7-60	60	180	N/A	30	70	76
Tension Fz (N)	?	4170	4170	1892	104	570	1600	2000
Compression Fz (N)	?	4000	4000		N/A	N/A	N/A	N/A
Shear Fy (N)	240	>900		2797	315	450	1270	-600

ΔV = Delta velocity N/A = Not applicable

4.3.2 MCW—Rigid-Seat, Full-Thorax Restraint.

The results for the MCW tests using a rigid seat and full-thorax restraint are listed in tables 10 and 11. The calculated upper-neck loads in the PMHS are only valid for the initial phase where the head has not made contact with any surrounding structure, e.g., seat, bulkhead, or shoulder. The maximum values were determined for the phase prior to head contact.

The ATD has a load cell at the upper neck and, consequently, no inverse dynamics were required to obtain the cross-sectional neck loads.

Table 10. Test Results With Potential Injury Criteria and Tolerances From Literature: MCW Results—Rigid Seat, Full-Thorax Restraint, 12.5 g at 12.5 m/s

Test Identification					FNSC 102	FNSD 103	FNSC 104	FNSD 105
					PMHS	ES-2	PMHS	ES-2
	AIS—Anatomical/Clinical				1/0	N/A	1/0	N/A
	Head Contact Time (ms)				62	---	65	---
	Tolerance Range for		Soltis	McIntosh				
Injury severity criteria	AIS 1	AIS 2	AIS 2+	AIS 2				
Impact velocity (km/hr)	<40	30-60		34	44.0	44.0	45.0	45.0
Impact acceleration (g)	5-10	10-14.7		16.9	12.5	12.5	12.5	12.5
Head rotation angle (deg) with regard to sled (S), T1	50-70	57-75	60		68 (S) 50 (T1)	77 (S) 73 (T1)	68 (S) 50 (T1)	86 (S) 82 (T1)
Angular velocity (rad/s)	8-30	32-39			43	---	47	44
Angular acceleration (rad/s^2)	680-1460	1588-2601	2600	6173	3242	---	2027	2815
Head linear acceleration (g)	13-32	12.5-18	36	63	y 17.1	y 14.1	y 11.9	y 10.2
Upper-Neck Loads								
Moment Mx (Nm)	22.6-40.7	40.7-60	60	180	62	42	61	43
Tension Fz (N)	?	4170	4170	1892	1262	831	1360	916
Compression Fz (N)	?	4000	4000		---	---	---	---
Shear Fy (N)	240	>900		2797	726	592	452	602

N/A = Not applicable

Table 11. Test Results With Potential Injury Criteria and Tolerances From Literature: MCW Results—Rigid Seat, Full-Thorax Restraint, 15.5 g at 18.0 m/s and 17 g at 18 m/s

Test Identification					FNSC 118	FNSC 126	FNSD 129
					PMHS	PMHS	ES-2
	AIS—Anatomical/Clinical				2-2	3-5	N/A
	Head Contact Time (ms)				52	56	---
	Tolerance Range for		Soltis	McIntosh			
Injury severity criteria	AIS 1	AIS 2	AIS 2+	AIS 2			
Impact velocity (km/hr)	<40	30-60		34	64.0	65.0	64.0
Impact acceleration (g)	5-10	10-14.7		16.9	15.6	17.3	15.6
Head rotation angle (degree) with regard to sled (S), T1	50-70	57-75	60		84 (S) 57 (T1)	94 (S) 77 (T1)	116 (S) 112 (T1)
Angular velocity (rad/s)	8-30	32-39			53	56	60
Angular acceleration (rad/s^2)	680-1460	1588-2601	2600	6173	3591	3860	4382
Head linear acceleration (g)	13-32	12.5-18	36	63	y 19.4	y 16.1	y 13.7
Upper-Neck Loads							
Moment Mx (Nm)	22.6-40.7	40.7-60	60	180	44	56	43
Tension Fz (N)	?	4170	4170	1892	1748	2187	1981
Compression Fz (N)	?	4000	4000		---	---	---
Shear Fy (N)	240	>900		2797	678	639	649

N/A = Not applicable

4.3.3 MCW—Aircraft Seat, Three-Point Belt With Retractor.

The results for the MCW tests using an aircraft seat and a three-point belt with retractor are listed in tables 12 and 13. Similar to section 4.3.2, the maximum upper-neck load values were determined for the phase prior to head contact.

Table 12. Test Results With Potential Injury Criteria and Tolerances From Literature: MCW Results—Aircraft Seat, Three-Point Belt, 12.5 g at 12.5 m/s

Test Identification					FNSC 109	FNSC 110	FNSD 111
					PMHS	PMHS	ES-2
	AIS—Anatomical/Clinical				3-5	3-5	N/A
	Head Contact Time (ms)				104	102	---
	Tolerance Range for		Soltis	McIntosh			
Injury severity criteria	AIS 1	AIS 2	AIS 2+	AIS 2			
Impact velocity (km/hr)	<40	30-60		34	45.0	45.0	45.0
Impact acceleration (g)	5-10	10-14.7		16.9	12.1	12.7	12.3
Head rotation angle (degree) with regard to sled (S), T1	50-70	57-75	60		75 (S) 51(T1)	82(S) 31(T1)	118(S) 93(T1)
Angular velocity (rad/s)	8-30	32-39			-47	-44	-94
Angular acceleration (rad/s^2)	680-1460	1588-2601	2600	6173	-2652	-2596	-5850
Head linear acceleration (g)	13-32	12.5-18	36	63	10	5.3	15.8
Upper-Neck Loads							
Moment Mx (Nm)	22.6-40.7	40.7-60	60	180	40	15	72
Tension Fz (N)	?	4170	4170	1892	2246	2249	2900
Compression Fz (N)	?	4000	4000		---	---	---
Shear Fy (N)	240	>900		2797	407	222	881

N/A = Not applicable

Table 13. Test Results With Potential Injury Criteria and Tolerances From Literature: MCW Results—Aircraft Seat, Three-Point Belt, 8.5 g at 8.7 ms and 10.5 g at 11.4 m/s

Test Identification					FNSC 115	FNSC 116	FNSD 114	FNSD 113
					PMHS	PMHS	ES-2	ES-2
	AIS—Anatomical/Clinical				2-3	0-0	N/A	N/A
	Head Contact Time (ms)				112	113	---	---
	Tolerance Range for		Soltis	McIntosh				
Injury severity criteria	AIS 1	AIS 2	AIS 2+	AIS 2				
Impact velocity (km/hr)	<40	30-60		34	31.9	31.4	31.0	41.0
Impact acceleration (g)	5-10	10-14.7		16.9	8.7	9.0	8.9	10.6
Head rotation angle (degree) with regard to sled (S), T1	50-70	57-75	60		97 (S)	90 (S)	125(S)	125 (S)
					47 (T1)	42 (T1)	91(T1)	89 (T1)
Angular velocity (rad/s)	8-30	32-39			43	40	64	78
Angular acceleration (rad/s^2)	680-1460	1588-2601	2600	6173	1669	1642	4562	5041
Head linear acceleration (g)	13-32	12.5-18	36	63	y 6.0	y 5.5	8.25	11.8
Upper-Neck Loads								
Moment Mx (Nm)	22.6-40.7	40.7-60	60	180	10	9	57	68
Tension Fz (N)	?	4170	4170	1892	1583	1174	1707	2480
Compression Fz (N)	?	4000	4000		---	---	---	---
Shear Fy (N)	240	>900		2797	276	204	657	723

N/A = Not applicable

4.4 COMBINED LOADS.

Combined loads are known to potentially increase the injury risk. For example, a combination of tension force and bending moment for flexion-extension is adopted in automotive safety in the N_{ij} criterion. As such, this section presents the combination of load responses to evaluate injury risk. Table 14 lists the upper and lower neck resultant shear (Fx + Fy) forces. The shear forces are computed using the maximum values recorded for Fx and Fy. If the shear forces were computed using the paired values for Fx and Fy, the results would range between 1% and 19% less than using the peak values. Given the limited number of tests, using the peak values gives a conservative estimate of expected shear values.

Table 14. Upper and Lower Neck Resultant Shear and Moment

Test	Restraint	Anatomical-Clinical	Upper Neck		Lower Neck	
			Mx (Nm)	Fx+Fy (N)	Mx (Nm)	Fx+Fy (N)
FNSC 102	Rigid	0-1	62	895	85	930
FNSC 104	Rigid	0-1	61	574	86	1097
ES-2-103	Rigid	----	42	755	201	1312
ES-2-105	Rigid	----	43	782	213	1285
FNSC 118	Rigid	2-2	44	835	60	1569
FNSC 126	Rigid	3-5	56	851	62	1996
ES-2-129	Rigid	----	43	835	287	2357
FNSC 109	Three point	3-5	40	1150	46	1585
FNSC 110	Three point	3-5	15	892	13	590
ES-2-111	Three point	----	72	971	328	2886
FNSC 115	Three point	2-3	10	436	6	554
FNSC 116	Three point	0-0	9	632	17	754
ES-2-114	Three point	----	57	717	N/A	1688
ES-2-113	Three point	----	68	812	288	2480

Peak values were calculated prior to head contact and occur at times independent from one another. Data points with the same test configurations are indicated by text boxes and directing arrows with the following color scheme:

- Green—rigid seat with rigidly restrained thorax
- Blue—aircraft seat with three-point belt
- Orange—rigid seat with side wall

Additional color and shape schemes identify the following information:

- Solid red markers—PMHS tests with AIS 3+ injuries
- Circular markers—ES-2 tests

The yellow marker on the tension axes indicates the Fz tension tolerance defined in the N_{ij} criterion, while the dotted lines separate PMHS data points with and without AIS 3+ injuries.

The following response combinations were plotted for both the upper and lower neck as calculated and obtained for both the PMHS and ES-2 test results, respectively:

- Neck tension versus neck lateral bending moment (figures 18 and 19)
- Neck tension versus neck resultant shear (figures 20 and 21)

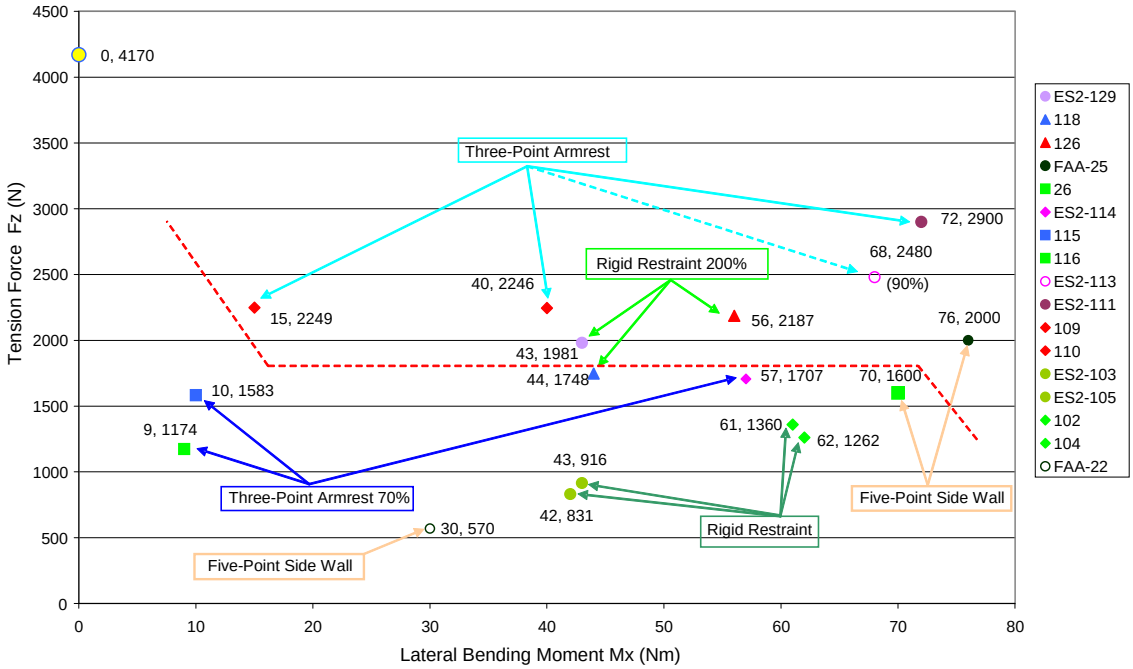

Figure 18. Maximum Upper-Neck (OC) Loads for Tension and Lateral Bending Moment

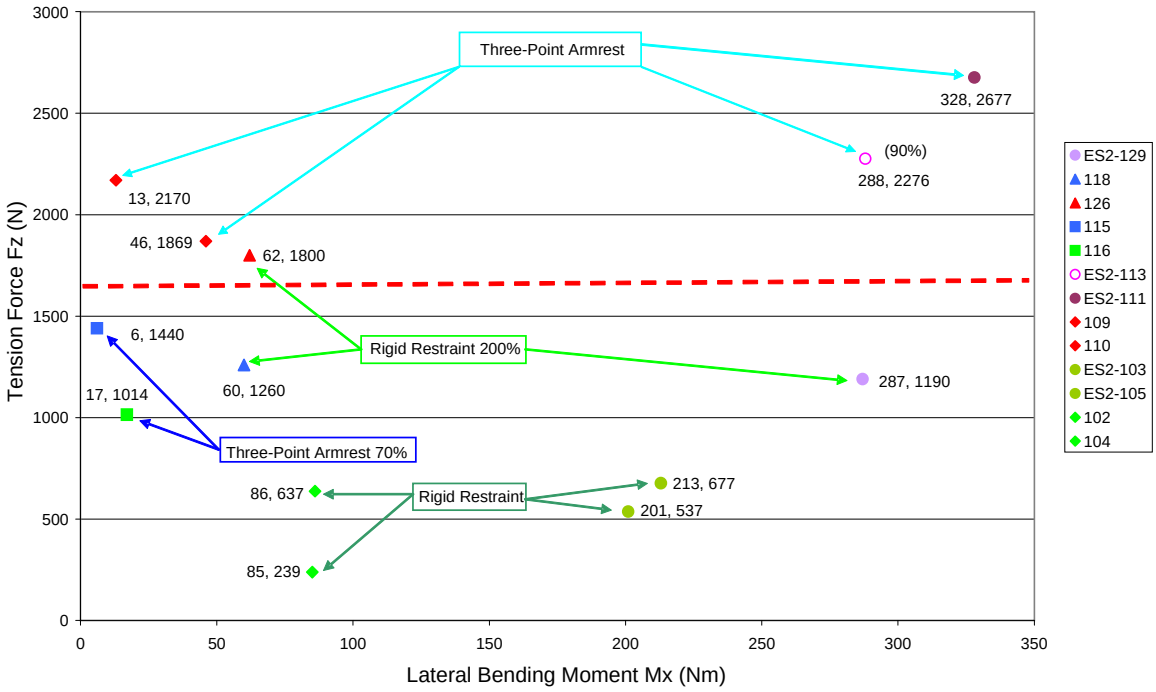

Figure 19. Maximum Lower-Neck (T1) Tension Force and Lateral Bending Moment

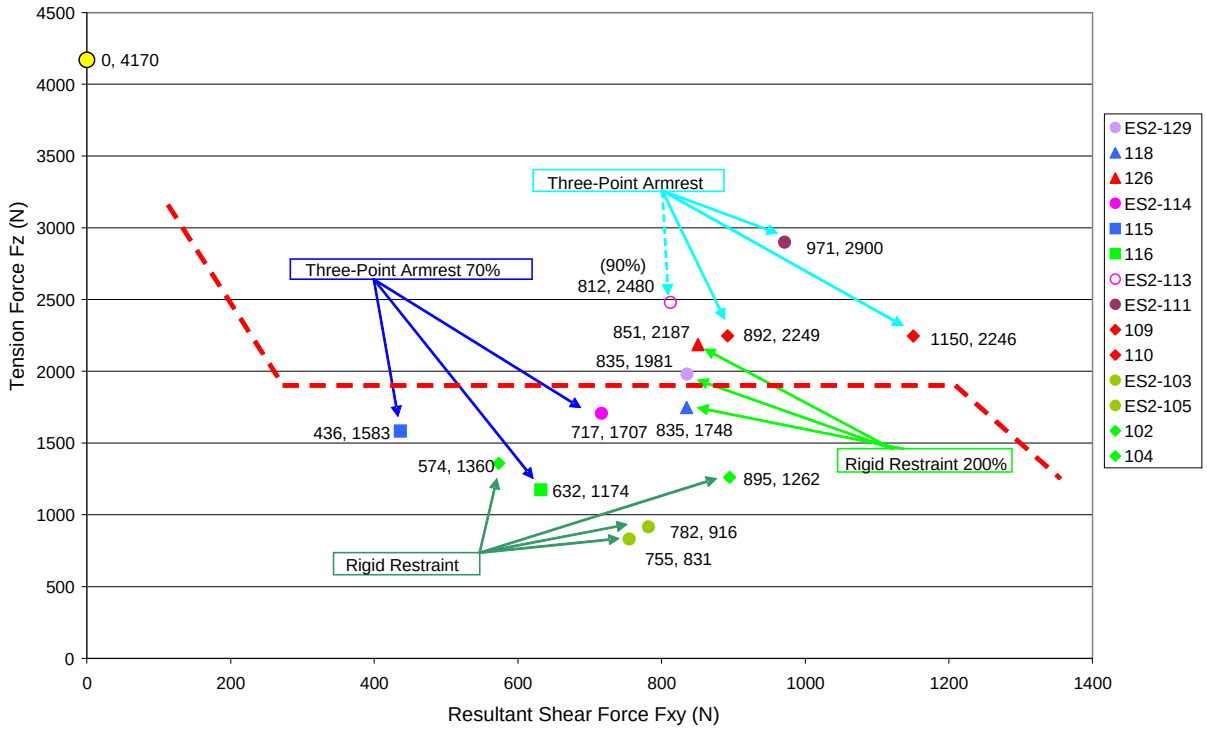

Figure 20. Maximum Upper-Neck (OC) Tension and Resultant Shear Force

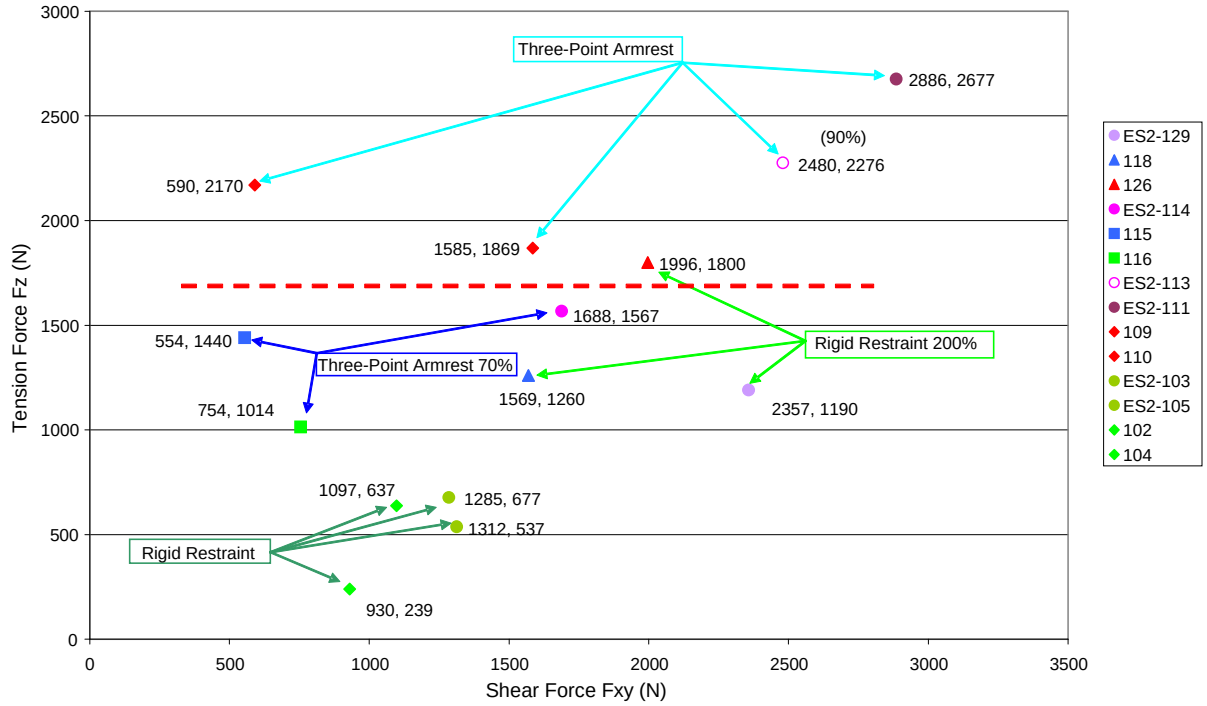

Figure 21. Maximum Lower-Neck (T1) Tension and Resultant Shear Force

4.5 ANALYSIS OF POTENTIAL INJURY CRITERIA.

Several general observations can first be made relating the different response criteria to one another as a result of impact kinematics. Tension force in the upper neck occurred as a result of the neck bending into the direction of the acceleration field. This transferred part of the load into shear forces in the lower neck. Tension and shear forces in the upper neck significantly contributed to the lateral bending moment in the lower neck. The tension and shear force contributions to the lower-neck bending moment is higher than the contribution to the upper-neck bending moment due to the distance between the OC and T1, which creates a lever arm approximately 140-150 mm.

4.5.1 The PMHS.

The upper-neck bending moments in the PMHS tests were scattered between 15 and 70 Nm, with no visually obvious relationship to injury or injury severity, as shown in figure 18. A similar observation was made for the lower-neck bending moment, which showed a slightly larger range between 6 and 86 Nm, as shown in figure 19.

The upper-neck shear does not correlate with the injury severity. The lowest, 436 N, for test FNSC 115 resulted in an AIS 2, whereas resultant shear forces of 895 and 574 N for tests FNSC 102 and 104 resulted in an AIS 0 score. Maximum shear forces range from 851 to 1150 N for injury severities of AIS 3 and higher. For AIS scores less than 3, the shear forces vary between 436 and 895 N.

Injuries were observed in tests where the upper-neck tension forces exceeded 1583 N for AIS 2 and 2186 for AIS 3+ severity. AIS 1 or lower injuries were observed for tension forces less than 1600 N. This is consistent with the 1892 N tension tolerance of McIntosh, et al., 2007. A similar trend was observed in the lower-neck tension force; however, smaller tolerance values were defined as 1260 N for AIS 2 and 1800 N for AIS 3 severity.

Both the shear and tension responses were observed to be sensitive to the loading condition, whereas the rigid-seat configuration provided a slightly increasing offset from the aircraft seat configuration.

4.5.2 The ES-2.

The ES-2 MCW aircraft seat tests showed an almost linear relation of upper-neck tension versus upper-neck moment for the various load severities considered (i.e., 70% FNSD 114, 90% FNSD 113, and 100% FNSD 111). A similar, although less prominent, relationship existed for the lower-neck tension and moments. This same trend was exhibited for the MCW rigid seat and WSU side wall seat configurations; however, neither could be confirmed nor denied due to a lack of sufficient data points. Consistent PMHS moment response was not observed, therefore, ATD moment tolerance could not predict the occurrence of serious injuries.

Similarly, the ATD tests showed a linear relationship between tension and resultant shear when varying the impact severity in the same conditions (aircraft seat) for both the upper- and lower-neck responses. All ES-2 tests with corresponding serious PMHS injuries resulted in tension forces above 1981 N and shear forces above 835 N.

Lower-neck lateral bending moments in the ATD are distinctively higher than in the PMHS, and the values are consistent for the duplicated tests. As with the upper neck, Fz seems to correlate with injury severity.

Lower neck ES-2 values for AIS 3+ are larger than 2357 N for resultant shear.

4.6 ES-2 BIOFIDELITY.

Responses of the ES-2 and PMHS tests were analyzed and compared. In figures 22 to 27, the ES-2 responses are represented by thin lines while their equivalent PMHS test responses, with regard to impact conditions, are represented by thick lines of the same color. Complete time histories for ES-2 kinematics, dynamics, and neck loads are included in appendices C and D of this report.

Comparison of the overall ES-2 kinematics with the PMHS suggested comparable biofidelity of the ES-2. This is evident by closely following the head-neck motions of the PMHS throughout the loading phase. Figures 22 and 23 show the spatial flexion and head axial twist with regard to T1 when loaded in the aircraft seat configuration. Discrepancies in response, however, are evident in the larger flexion angle peak and the early kinematic rebound of these signals. Both were attributed primarily to the stiffer internal characteristics and reduced damping of the ES-2 compared to the PMHS. It is noted here that these measurements are different from the more traditional Euler angles used in previous intermediate reports. More detailed information regarding the definition and calculation of these measurements can be found in Philippens, et al., 2004.

The lateral acceleration response of the ES-2 was remarkably similar to the PMHS response. Figure 24 shows the T1 lateral acceleration of both impact surrogates (ES-2 and PMHS) in the rigid-restraint configuration. The vertical ES-2 acceleration response, however, showed poor correlation to the PMHS response, particularly in the rigid-seat configuration, as shown in figure 25.

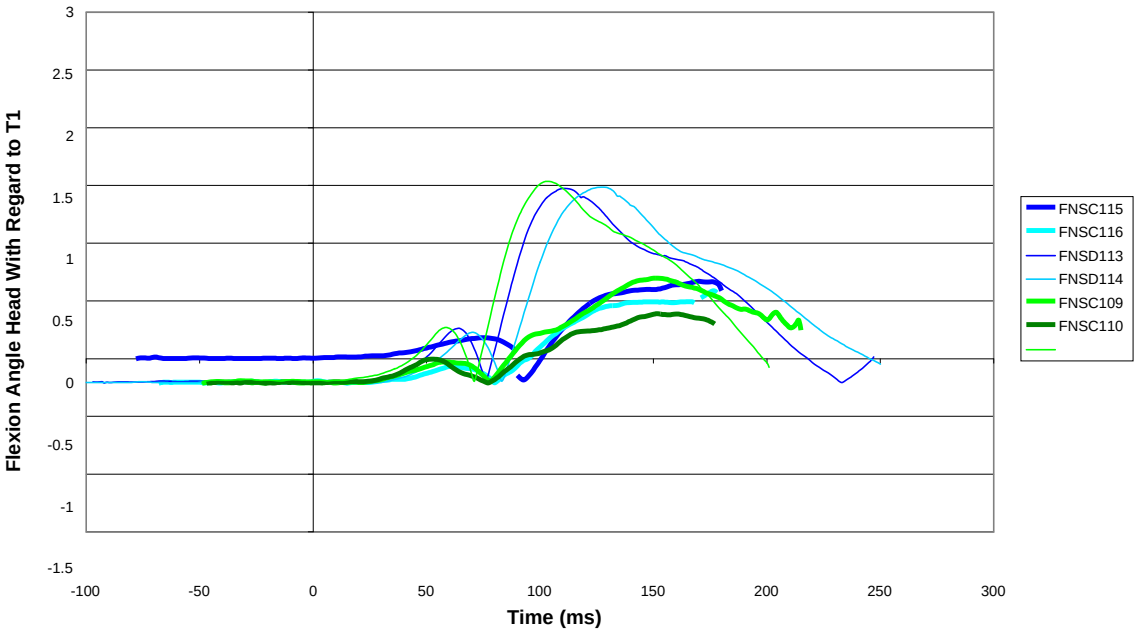

Figure 22. Spatial Flexion Angle of Head With Respect to T1, Aircraft Seat

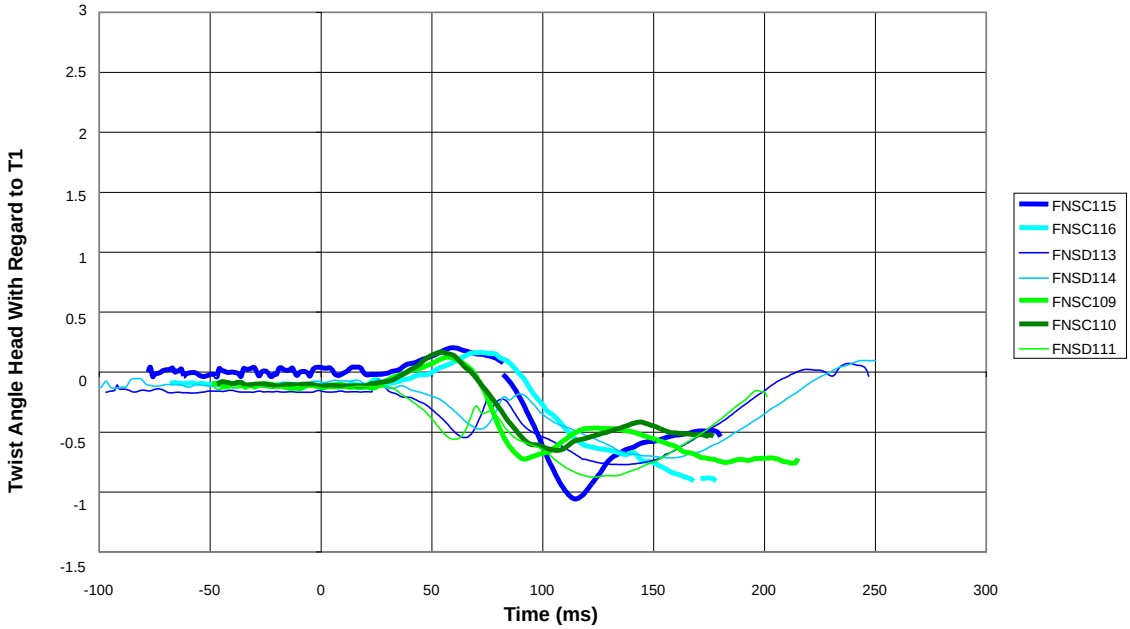

Figure 23. Twist Angle of Head With Respect to T1, Aircraft Seat

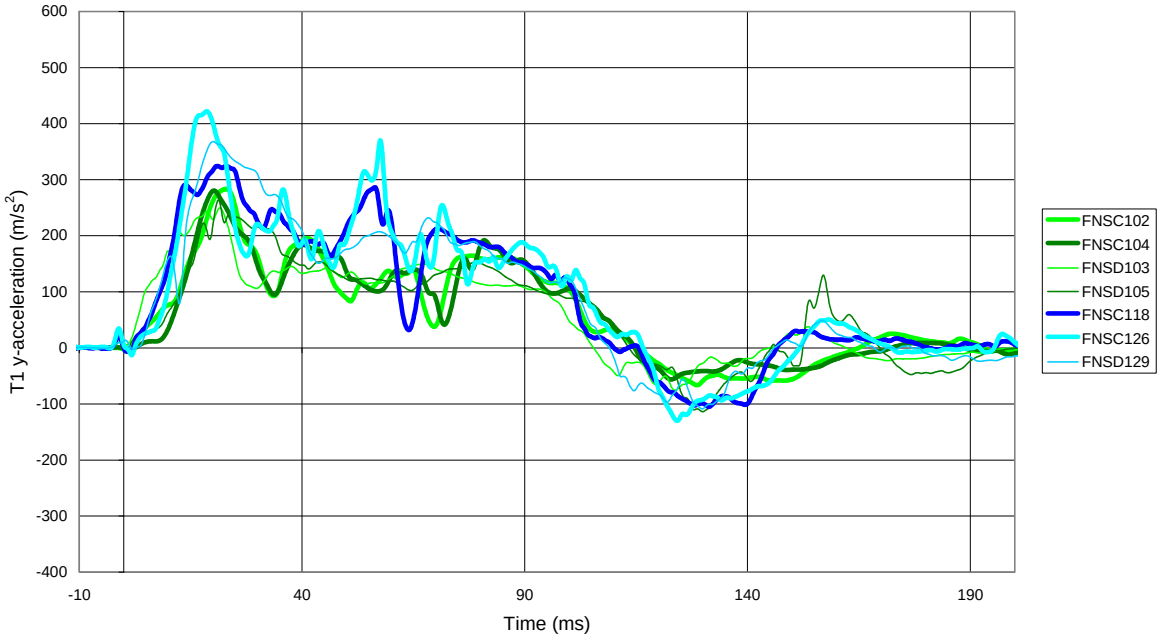

Figure 24. Lateral T1 Linear Acceleration in Rigid-Restraint Thorax Configuration

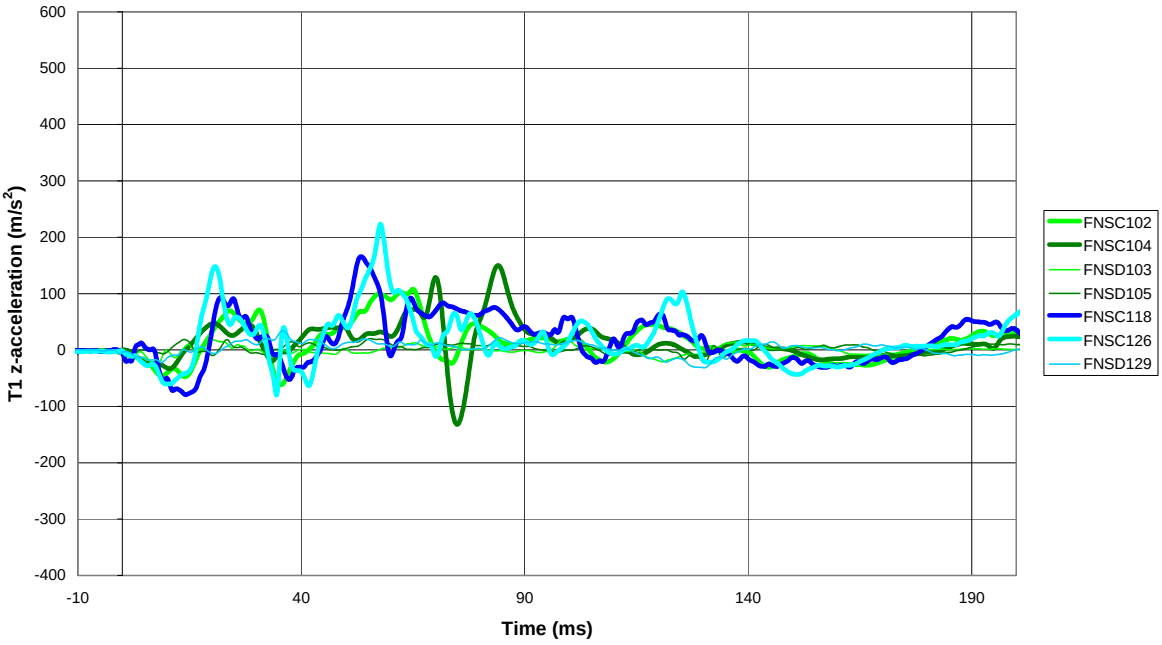

Figure 25. Vertical T1 Linear Acceleration in Rigid-Restraint Thorax Configuration

Forces in the neck showed similar trends to the PMHS for most impact conditions. This was similar to the linear accelerations and was inevitable since these values are directly linked to one another in their calculation. The ES-2 follows the PMHS response for the upper-neck lateral shear force up to the point of head contact with the shoulder or seat component, as shown in figure 26, after which the PMHS responses become inaccurate.

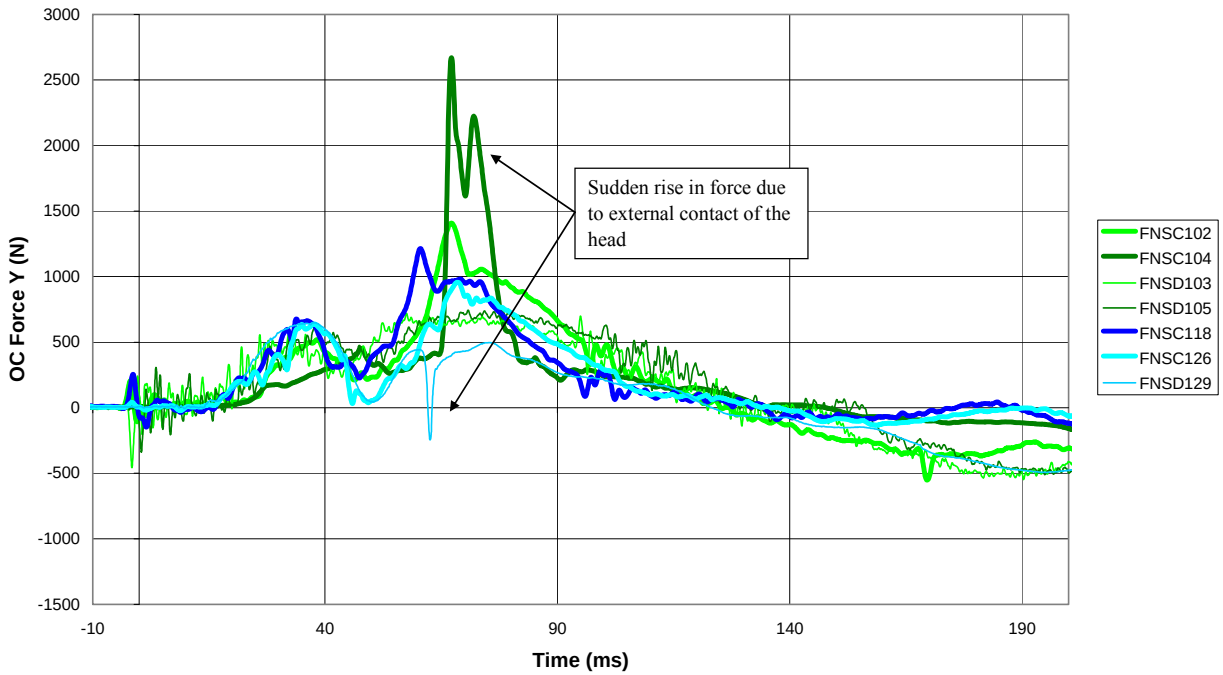

Figure 26. Lateral Shear Force in the Upper Neck for the Rigid-Restraint Thorax Configuration

Moments recorded in the ES-2 showed differing characteristics compared to the PMHS. Figure 27 highlights the smoother ES-2 bending moment time history compared to the PMHS in the aircraft seat configuration. During the first phase of the impact where the initial loading occurred, the ES-2 moment amplitude is higher and the duration is longer than the PMHS. Additionally, the bending moment in the ES-2 was proportional to the loading level, as discussed in section 4.5, while the maximum bending moment for the PMHS tests were scattered. These differences are attributed to their biomechanical design and operation of the ES-2. Due to the solid beam structure of the ES-2, the coupling of forces and moments are more prominent than in the explicitly segmented human neck. In addition, the ES-2 allows only a first and second bending mode, whereas the human neck can facilitate much more complex bending modes.

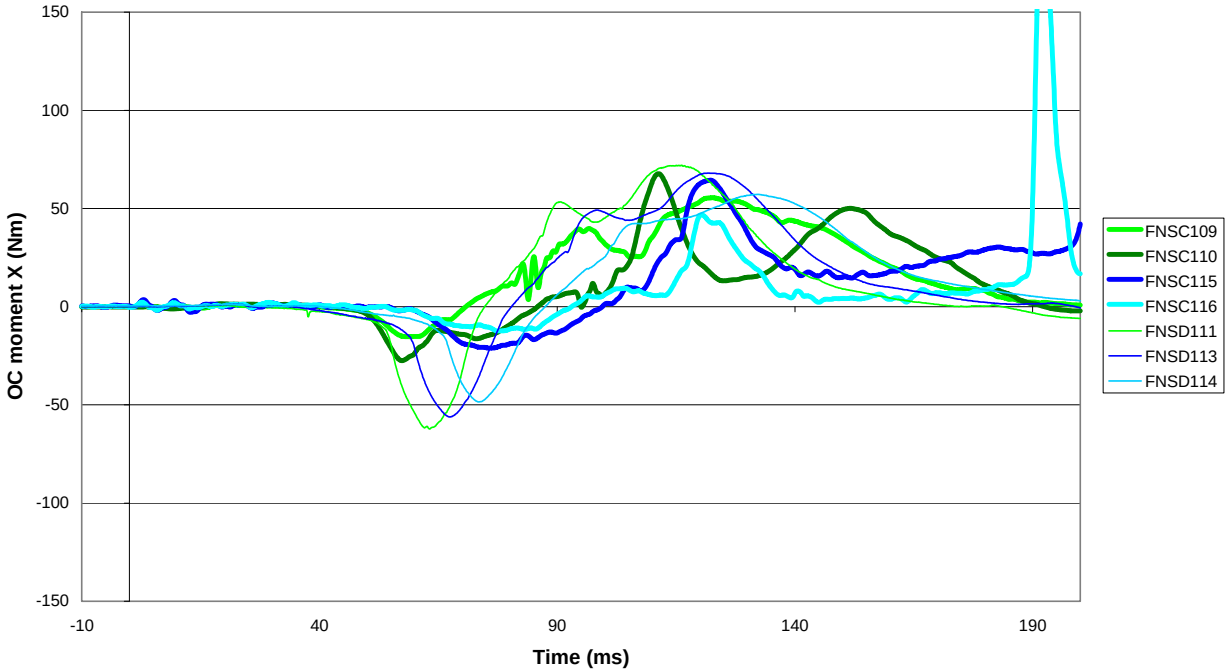

Note: The large spike occurring at approximately 195 ms in FNSC 116 is due to head strike.

Figure 27. Lateral Bending Moment for the Aircraft Seat Configuration

4.7 DISCUSSION.

From the results above, it can be concluded that the tension force is the most discriminating parameter for predicting AIS 3+ injuries to the PMHS neck, while the lateral bending moment lacks correlation to either loading or injury severity. A tension tolerance between 2000 and 2500 N seems appropriate for these loading conditions. It is noted however that such a tolerance level on its own does not match those reported for pure neck tension tests, which exceed 4000 N. It is believed that the injury mechanism requires a certain minimal lateral bending precondition combined with the tension load (for example, over 1500 N) to generate AIS 2+ injuries. The resultant shear force is not dominant in discriminating injury severities.

In defining an IARV to be used in ATD tests such as this, it is often preferred to use sensor-based response parameters. The ATD sensors, accelerometers, and load cells can be measured directly from the dummy and evaluated immediately following the test. Parameters that need video recording, posttest processing, and analysis require significant time to come to a conclusion. Therefore, the neck loads in the ES-2 are most likely to be accepted as a basis for IARVs. Linear head acceleration could be an alternative for defining internal loads (forces and moments) provided no contact with external structures occurs. However, a shoulder belt airbag for aircraft restraints is available as a promising injury mitigating tool, which supports the head throughout impact and invalidates the F=m*a relation between head acceleration and neck forces.

The kinematics and neck forces of the ES-2 show good biofidelity throughout the impact. In particular, forces capture the same trends observed in the PMHS when varying impact

conditions. Thus, the ATD forces can be used to reflect the PMHS neck forces almost one-to-one. Moments recorded from the ATDs, on the other hand, have differing characteristics compared to the PMHS. Due to the solid beam structure of the ES-2, the coupling of forces and moments is more prominent than in the explicitly segmented human neck. The ES-2 allows only a first and second bending mode, while the human neck can facilitate much more complex bending modes. Because of this, the ES-2 bending moment shows a proportional relation to loading severity, which is directly related to the head flexion angle.

It should also be noted that a lateral flexion of the human head consists of frontal flexion in the lower cervical spine, combined with axial torsion in the upper cervical spine (mainly C2-C1). This is a completely different deformation pattern compared to the deformation of the ES-2, which is almost pure lateral bending with a slight portion of axial torsion.

The ES-2 showed two major artifacts:

- The neck failed after a limited number of tests. However, a review of the test data showed no degradation of test results prior to the neck failing.

- The leading shoulder belt slips in the open space at the bottom of the neck and loads the lower part of the neck so that it could affect the lower-neck load cell reading.

5. NUMERICAL MODELING.

5.1 INTRODUCTION AND OBJECTIVE.

Numerical modeling plays an important role in today's automotive engineering and, more specifically, in automotive safety developments. Simulated automotive crash environments can be created to replicate the conditions observed in real-life impact scenarios. Numerical ATD models help reduce the number of complicated and expensive tests required in the design cycle of a typical safety system. In the performance of this study, a numerical ES-2 was used to simulate test conditions to investigate the ES-2 and PMHS side-impact tests. The results have facilitated the development of the experimental setups used throughout this project, providing insight into injuries induced in these impact conditions. This section details more recent work involving an advanced numerical ES-2 model, performed in an effort to replicate the MCW ES-2 sled tests and to continue answering questions regarding side-impact conditions. The methods used and the validation results are provided, followed by implementation of the models in supporting simulation scenarios. Additionally, this section summarizes the previous numerical efforts made throughout the project, covering the primary conclusions derived.

5.2 METHODOLOGY.

5.2.1 Numerical ATD Model.

The ES-2 Quality ATD model was used for the simulations performed in the final phase of the research. This model was a replacement to that used in the early phases of this research. The term quality represents a significant attempt by the model developer to ensure the accurate

response of the model compared to the physical ATD. All geometry is represented by facet surfaces and is based on technical drawings of the ES-2 (revised) ATD and/or 3-D laser scans of molded parts of the ES-2 hardware. In general, an element size of approximately 10 mm was used. All facet parts have contact compliance included in their material characteristics, capturing the local deformation properties of the ATD. Masses, c.g.'s, and moments of inertia are determined on the basis of hardware component mass measurements and geometric representation of the components in 3-D computer-aided drawings. Subassemblies, such as entire legs, arms, and neck, were modeled using different parts; screws that connect these subassemblies were modeled as rigid joints.

The model has been validated for side-impact loading using segment pendulum impact tests of the head, neck, arms, ribs, abdomen, pelvis, legs, and lumbar spine, as well as full-scale ES-2 sled impacts. In full-scale side impacts, the model is well validated for velocities up to 9.67 m/s. More detailed information regarding the model construction and validation can be found in the Mathematic Dynamic Modeling (MADYMO) Manual. Figure 28 shows the ES-2 Quality model seated in its reference position.

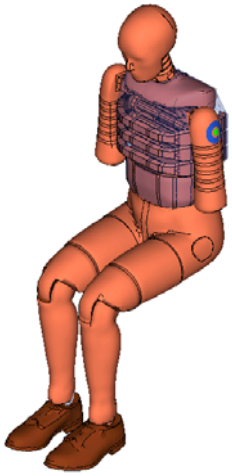

Figure 28. The ES-2 Quality MADYMO Model

5.2.2 Sled Test Model.

Two test setups were considered for the evaluation of the numerical simulation during side-impact scenarios, both of which mimicked the MCW configurations: (1) rigid seat, full-thorax restraint and (2) aircraft seat with cushions, three-point belt with retractor. The dimensions for the rigid-seat setup were obtained from 3-D geometric measurements taken during the tests and schematic drawings of the seat setup provided by MCW. With this information, a finite element mesh of both seat setups was created, as shown in figure 29.

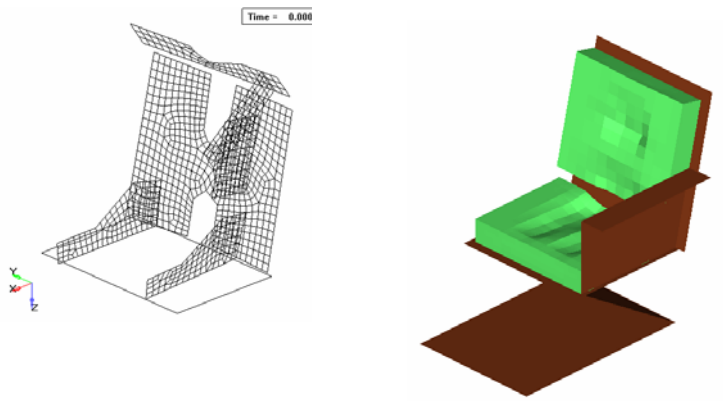

(a) Rigid Seat (b) Aircraft Seat Right

Figure 29. The MADYMO Sled Seat Environment Models

For the rigid-seat model, only shell element surfaces were created and were assumed rigid throughout the simulation. Under this assumption, contact between the ES-2 and the seat was implemented so that the ES-2 properties governed the response. For the aircraft seat model, the same rigid surfaces were implemented for the seat pan, foot rest, and arm rest. The soft cushions used on the seat bottom and back were modeled as solid elements with a shelled-element outer layer representing the inner soft foam and leather casing, respectively. Material properties were implemented to represent the DAX47 foam and the outer leather cover.

Implementation of the ES-2 model in the seat and restraint systems was done through a series of presimulations. The model was first positioned immediately above and in front of the seat and was subjected to gravity. For the aircraft seat, an additional settling presimulation was performed, where the knees were pushed backwards with a force of 222 N. Once settled, the presimulation applied the restraint system as specified by the experiment. For the rigid seat, a five-point restraint system (shoulders, pelvis, and crotch belts) was used with additional torso belts at the armpit and fifth-rib height. For the aircraft seat, a three-point belt was used, consisting of two separate lap belts and a single shoulder belt. A buckle connected all three in the center of the ATD. All restraints were modeled using a combination of finite element and multibody belt elements. The finite element belts were used where contact with the occupant was expected, while the multibody belts were used to anchor to the surroundings and connect finite element belt sections to one another (i.e., belt buckle). The finite element belts were shaped around the model throughout the presimulation. The process used to generate the models is shown in figure 30.

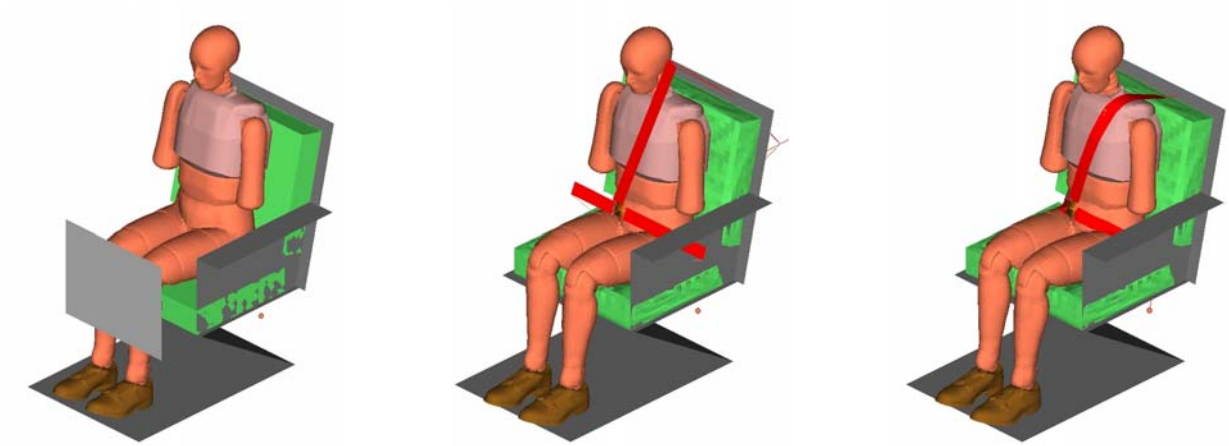

(a) Gravity and Knee Plate (b) Belt Alignment (c) Belt Tightening

Figure 30. The ATD Settling Steps

The model was loaded according to the acceleration signal obtained from the experiment. The acceleration signal was applied to the occupant model while the sled was kept stationary. This allowed an easy comparison of simulation and experiment responses, all of which were noted to be relative to the sled. The acceleration pulse used is shown in figure 31. A constant acceleration of 1 g downward was implemented throughout the simulation, representing gravity.

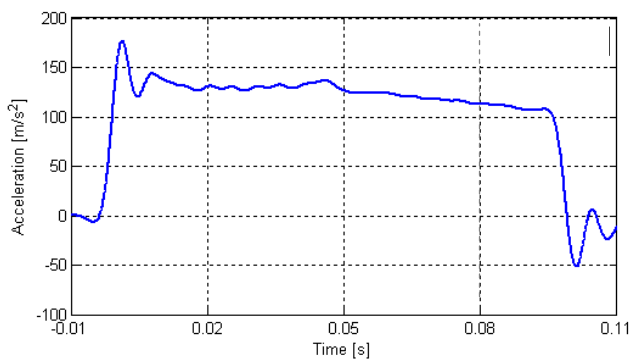

Figure 31. Experimental and Simulation Acceleration Pulse

5.2.3 Validation.

Validation of the model was performed using two methods: (1) quantitatively, where simulated ATD response signals were compared to experiments in the time domain, and (2) qualitatively, where simulation impact kinematics were compared against the experiments using screen shots.

From the work performed using the PMHS tests results, it was identified that bending moment and tension are the most important injury criteria inducing neck injuries due to lateral loading. Therefore, the quantitative validation of the ATD model was focused on generating the appropriate responses to predict neck loads. Accurate head and neck kinematics were also

identified as important responses for generating an accurate impact simulation. Therefore, the following parameters were used for evaluating the validity of the models:

- Linear and angular displacements of the head c.g.
- Linear and angular displacements of T1
- Upper-neck forces
- Upper-neck moments

The qualitative analysis compared simulated screen shots against those obtained from the experiments. The following impact events were chosen for this analysis, encompassing key points throughout the impact:

- Initial position
- Start of head lateral rotation
- Maximum lateral head rotation

5.2.4 Supporting Impact Simulations.

Throughout this project, the ATD-sled models described above and their development predecessors have been used to simulate unexplored impact conditions experimentally. The models were used to verify design choices made when defining the sled pulse, as well as to identify impact conditions that could excite particular responses—for example, severe upper-neck bending. The objective of such work was to define experimental conditions that could be used for both ATD and PMHS experiments, selecting the appropriate test to be performed without the expense and complications associated with numerous trial experiments. Four key experimental uncertainties were investigated in defining the various experimental approaches used throughout this project.

5.2.4.1 Investigation 1: Triangular Versus Rectangular Sled Pulse.

Throughout the project two different sled pulses were used in performing the side-impact sled tests. The first was a triangular shape specified by 14 CFR 25.562 and performed by WSU. Due to complications in test protocol and a lack of PMHS availability, MCW was selected as the replacement test facility. However, the MCW sled produced only rectangular pulses. As a result, numerical ES-2 simulations were performed to investigate how the shape of the pulse affected the impact response. Table 15 lists the impact conditions considered at the time of this study. It is noted here that these do not reflect the final pulses chosen within this study, and represent a first attempt at implementing a rectangular pulse shape. The final pulse was chosen following the ES-2 sled tests at CAMI; however, the details of these tests were not included in this section. The model used for this part of the study was the previous ES-2 numerical model. More detailed information regarding these experiments can be found in appendix B.

Table 15. Acceleration Conditions for Simulating Pulse Shape Variation Study

Delta Velocity (m/s)	Triangular Pulse		Rectangular Pulse	
	Acceleration Peak (g)	Duration (msec)	Acceleration (g)	Duration (msec)
7.2	9	160	7.2	100
14.4	16	180	18.3	80

5.2.4.2 Investigation 2: Variations in Sled Pulse Severity.

Results obtained from the first PMHS tests identified the conditions that could induce specific injury severities (AIS 3+). In an effort to investigate what impact conditions could induce alternative injury severities, ES-2 impact simulations were performed using the validated ES-2 sled model. The ΔV of the original sled pulse was reduced in increments of 10% to a minimum of 50%, and the tension in the upper-neck joint was recorded throughout the simulations. New PMHS test conditions were defined in which neck tension was used to identify test conditions that identified both AIS 1 and AIS 2 injuries in the rigid-seat configuration.

5.2.4.3 Investigation 3: Supporting the Neck to Increased Neck Moments.

Continued results from PMHS tests suggested that the combined effect of tension and moment was the driving factor in inducing injuries in side-impact inertial loading. The low tension values (compared to the biomechanical limits) recorded in conditions where AIS 3+ injuries occurred suggested that the combined lateral moment lowered the injury-inducing tension limit. It was approximated that OC tension forces close to and over 1500 N led to AIS 3+ injury risks if combined with a minimum moment of 54 Nm. Therefore, it was decided to perform tests that induced high moment and low tension values in an effort to see if a higher OC moment reduced the allowable tension force. Although difficult to implement, it was thought that a poorly designed neck support (collar) might help to induce such load characteristics. By supporting the neck just below the OC joint in the rigid-seat conditions (fully restrained), the head and neck would be less likely to rotate into the direction of the acceleration pulse and instead induce high OC moments.

This was investigated using the ATD model and progressively locking the five ATD neck joints (see figure 32) to simulate different neck collar heights. At the same time, the severity of the sled pulse was increased in two conditions, supported and unsupported, to see how far the moment could be increased without exceeding the 1500 N tension limit.

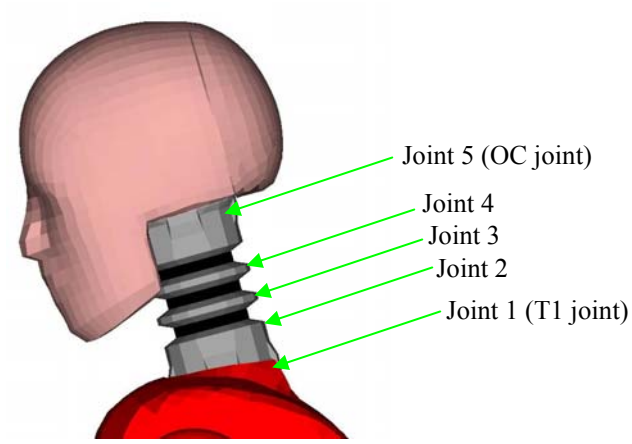

Figure 32. The ATD Model Neck Construction

5.2.4.4 Investigation 4: Increasing Head Mass to Increase Neck Moments.

Another method to induce the high-moment, low-tension responses desired for the PMHS tests was to add extra mass to the top of the head. It was believed that the added inertia, combined with the vertical distance away from the OC joint, would induce higher moments during loading. This was investigated by performing ATD impact simulations in the rigid-restraint condition with an extra mass (1 kg) added to the top of the head. However, given the high flexibility (i.e., an increased number of deformation modes) of the PMHS neck and its tendency to buckle under the influence of gravity, it was argued that the ATD simulation results would not appropriately represent a PMHS with an extra mass. To approximate such conditions, the ATD neck stiffness was reduced in increments of 10%, 25%, and 50%. Moment and tension were recorded to assess the impact response.

5.3 RESULTS.

5.3.1 Validation.

5.3.1.1 Rigid Seat.

The results of the rigid-seat simulation are presented in figures 33 to 38. Figures 33 and 34 show the results of the linear displacements and rotations of the head c.g., measured with regard to the sled. The simulated displacements possessed similar shape in time compared to the experimental data, although a slight delay in the simulated data can be seen. Furthermore, overestimated peak values are observed in the y and z peak responses. However, these results suggest a slight delay in the simulation, where the linear displacements and rotations begin slightly after the experiment. The same phenomenon was described by the linear and rotational displacements of T1, as shown in figures 35 and 36. Here, the simulated T1 y-displacement almost doubles the experimental results. However, displacement overestimations of only 3 cm were thought to be of minimal concern.

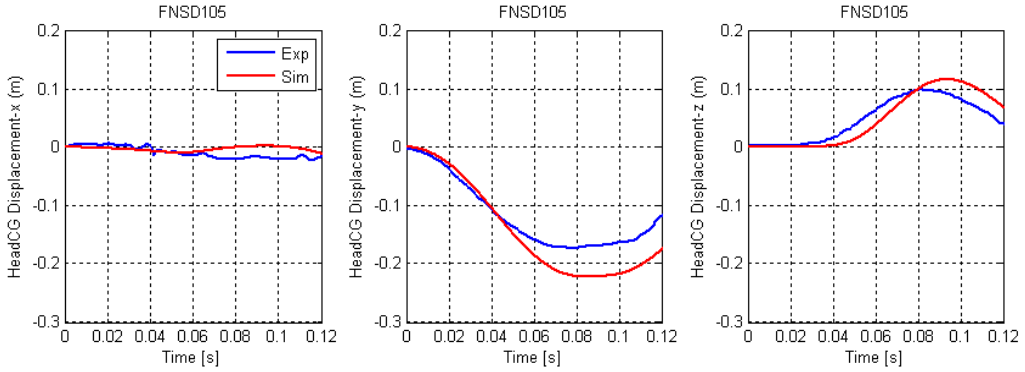

Figure 33. Rigid Seat, ES-2 Head c.g. Linear Displacements Relative to the Sled

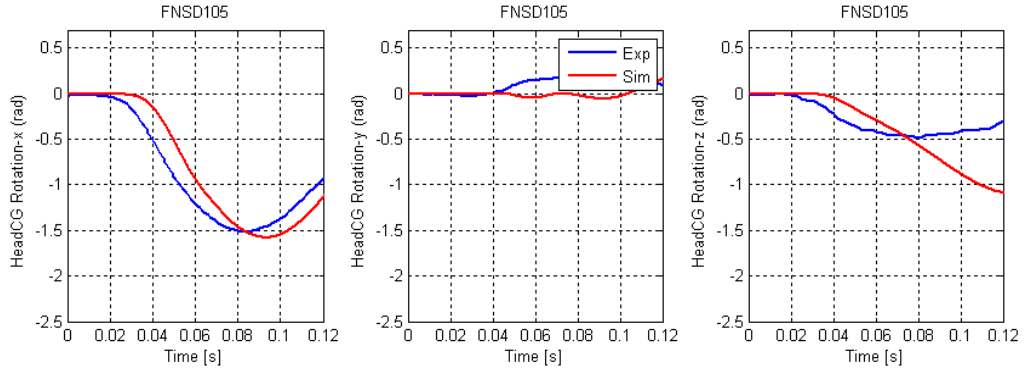

Figure 34. Rigid Seat, ES-2 Head c.g. Rotations Relative to the Sled

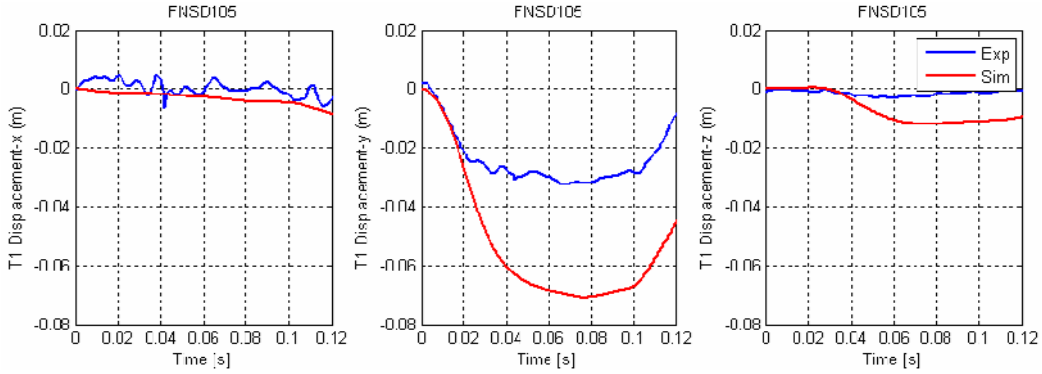

Figure 35. Rigid Seat, ES-2 T1 Linear Displacements Relative to the Sled

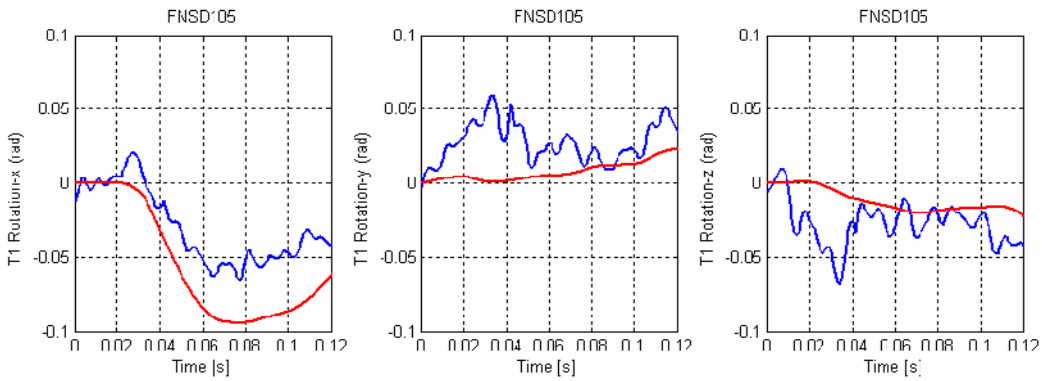

Figure 36. Rigid Seat, ES-2 T1 Rotations Relative to the Sled

In figure 37, the upper-neck forces show some differences between the simulation and experiment, particularly in the x and y directions. However, the close agreement of the neck axial tension, which was thought to be one of the key measurements for predicting neck injuries, overshadows the discrepancies found in the other directions. Delays noted in the kinematic measurements were also observed in force responses.

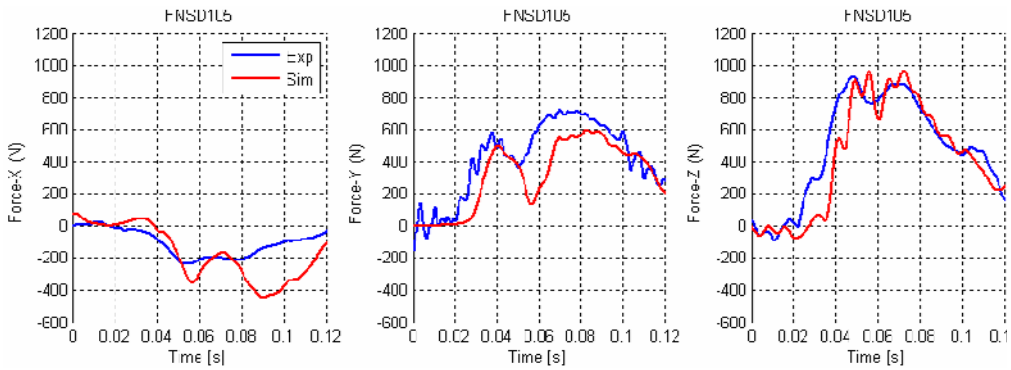

Figure 37. Rigid Seat, ES-2 Upper-Neck Forces

The most important moment, the lateral flexion moment, shows consistent shape and peak values for the simulation compared to the ATD test (see figure 38). Similar shape responses were observed in the flexion-extension (y) and twist (z) moments; however, their peak values vary significantly from the experiments. Similar differences were observed in the original development of the model where the simulated flexion-extension overpredicts the component validation results used. No validation of the model in the twist direction was ever performed. However, the M_z observed is lower in comparison to the moment observed in the x axis and for the purposes of injury investigation considered negligible.

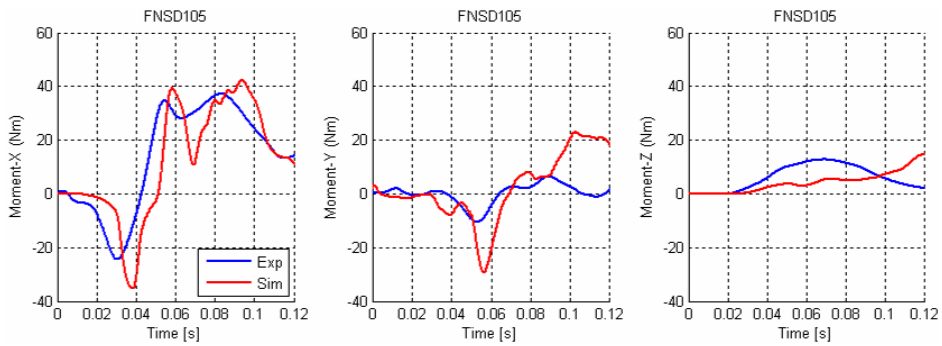

Figure 38. Rigid Seat, ES-2 Upper-Neck Moments

Figure 39 shows the kinematic response of the simulation compared to the experiment. The delay observed in the signals is evident in comparing the time when particular events (i.e., start of and maximum lateral bending) take place. However, this delay does not significantly influence the kinematics or neck loads; so it was concluded that the MADYMO ES-2 simulations were suitable for further study of the rigid-seat condition.

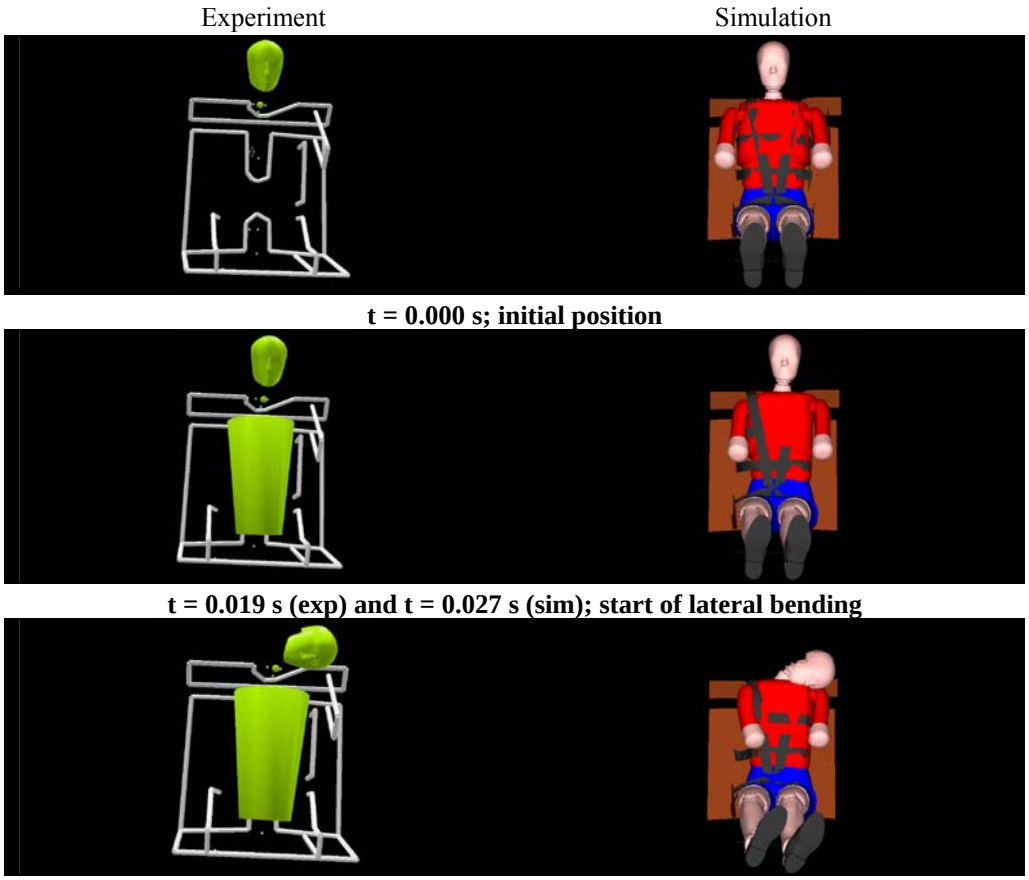

Figure 39. Rigid Seat, Experimental and Simulated Kinematic Response

5.3.1.2 Aircraft Seat.

The results of the aircraft seat simulation are presented in figures 40 to 46. Figures 40 and 41 show the results of the linear displacements and rotations of the head c.g., measured with regard to the sled. The simulated linear head c.g. displacements show similar shape and peak response throughout the impact while rotations in the z and y directions vary from the experiments in the later stages. The simulated T1 linear and rotational displacements, as shown in figures 42 and 43, match the shape of the experiments. However, the peak responses of the x and z rotations underestimate the experiments by approximately 19% and 55%, respectively. The overestimated T1 lateral y-displacement was thought to be due to a potentially unrealistic belt-to-shoulder interaction, resulting in high belt penetrations into the shoulder. The ES-2 (both physically and numerically) was designed to simulate occupant response in side impacts where the shoulder does not undergo the severe belt loading that was observed in the FAA side sled tests. The numerical model further lacks the shoulder stiffness properties present in the physical dummy, even though these properties were not designed for such belt interactions.

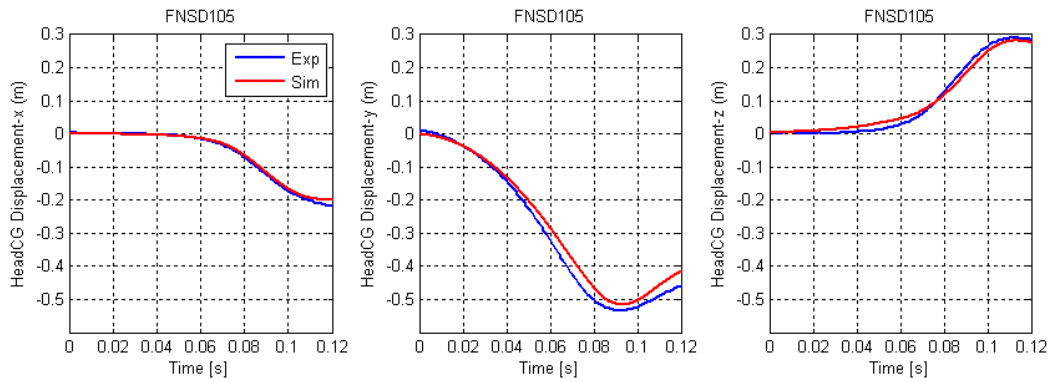

Figure 40. Aircraft Seat, ES-2 Head c.g. Linear Displacements Relative to the Sled

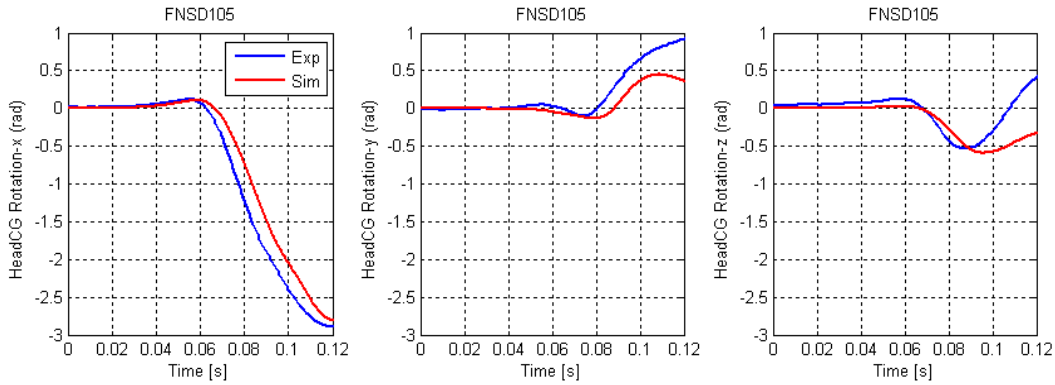

Figure 41. Aircraft Seat, ES-2 Head c.g. Rotations Relative to the Sled

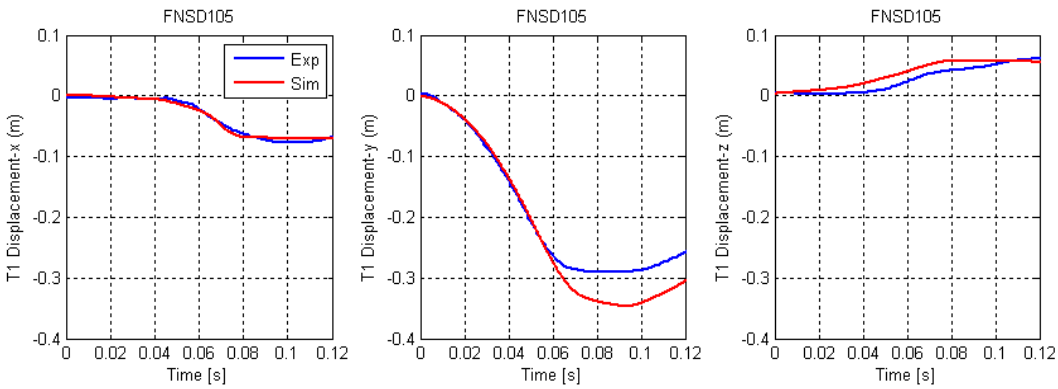

Figure 42. Aircraft Seat, ES-2 T1 Linear Displacements Relative to the Sled

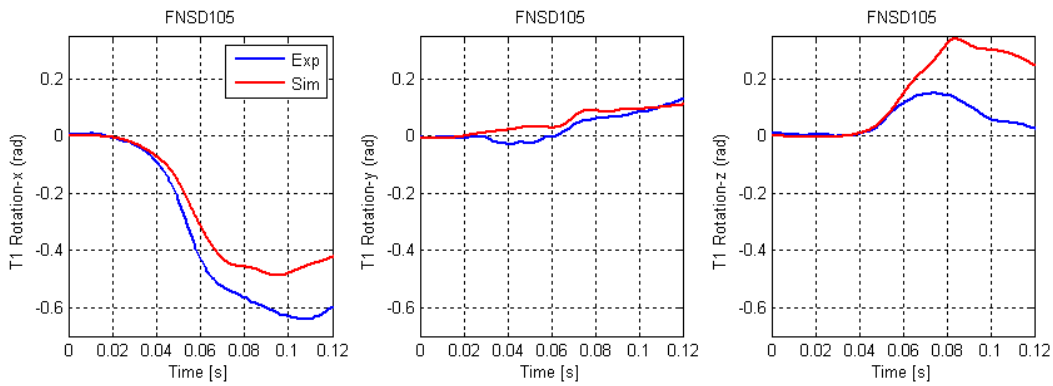

Figure 43. Aircraft Seat, ES-2 T1 Rotations Relative to the Sled

For upper-neck forces (see figure 44), differences between the simulation and the experiment were observed. The x and y forces in the later stages of the impact produced an unexpected peak after 0.1 sec. However, the observed similarity of the simulated and experimental neck axial tension shape and peak responses (z-force) along with its primary importance in the impact response, suggest the results were sufficient in predicting this scenario.

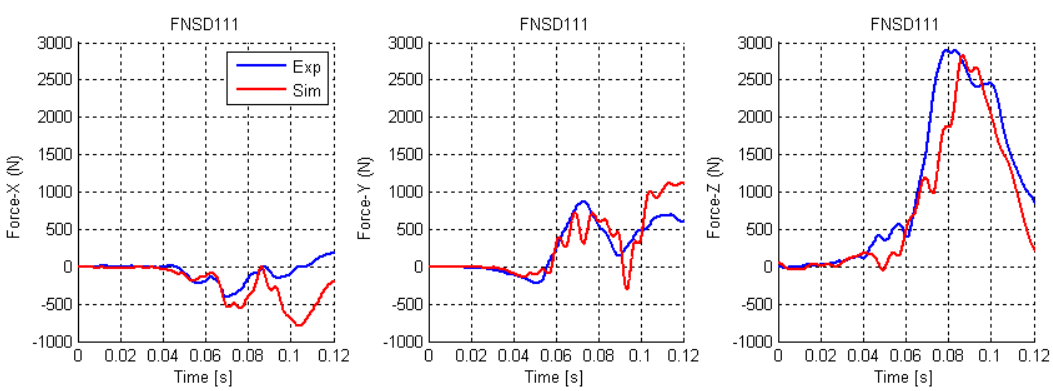

Figure 44. Aircraft Seat, ES-2 Upper-Neck Forces

In this seat configuration, the most important moment (lateral x-moment) once again produces similar peak and shape characteristics throughout the impact, as shown in figure 45. The flexion-extension y-moment produces similar characteristics (shape and timing) throughout most of the impact, but varies significantly in the later stages. A similar discrepancy is observed in the twist z-moment of the neck, but given the occurrence of these signals' differences so late in the impact, they were thought to be of minimal concern. Additionally, the severity of these moments was much lower than the lateral moment.

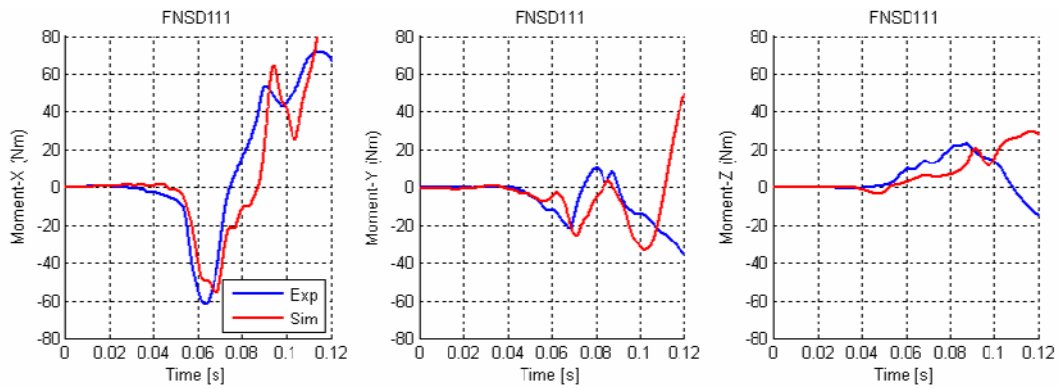

Figure 45. Aircraft Seat, ES-2 Upper-Neck Moments

Figure 46 shows the kinematic response of the simulation compared to the experiment. Almost no delay is evident in the timing of the primary events. At maximum neck bending, only a difference of 4 msec could be observed. Differences do, however, appear in the twist of the head, apparent in the response, as plotted in figure 45. Once again, this was believed to be due to the lack of validation provided in the neck torsion response during development. However, such discrepancies were considered minimal, and it was concluded that the MADYMO ATD simulations were suitable for further study of the rigid-seat condition.

Experiment Simulation

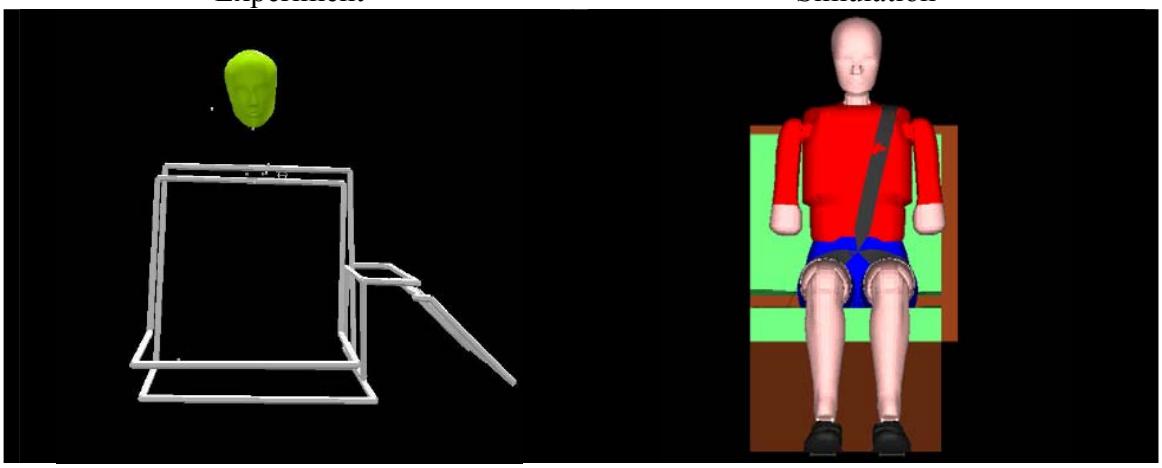

t = 0.000 s (experiment and simulation); initial position

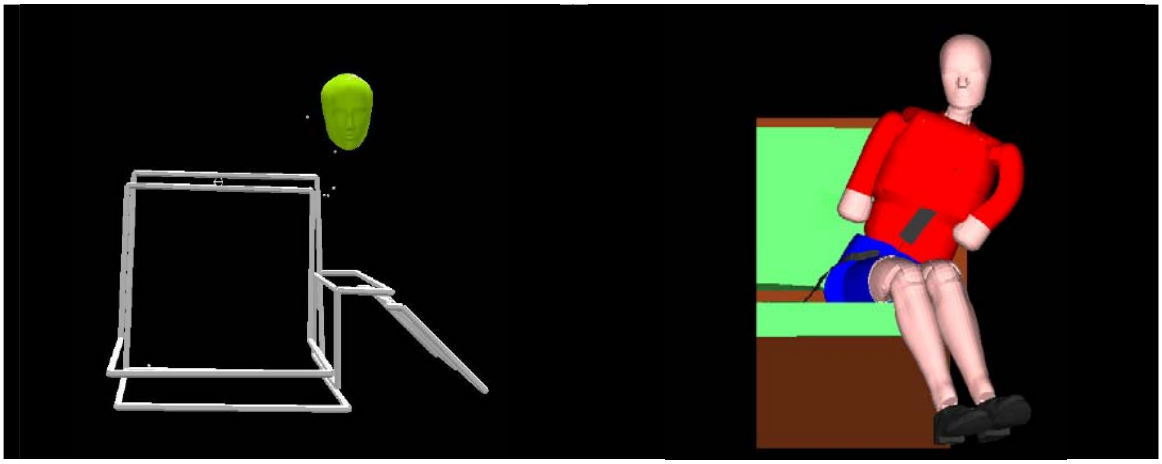

t = 0.060 s (experiment) and t = 0.061 s (simulation) start of head lateral rotation

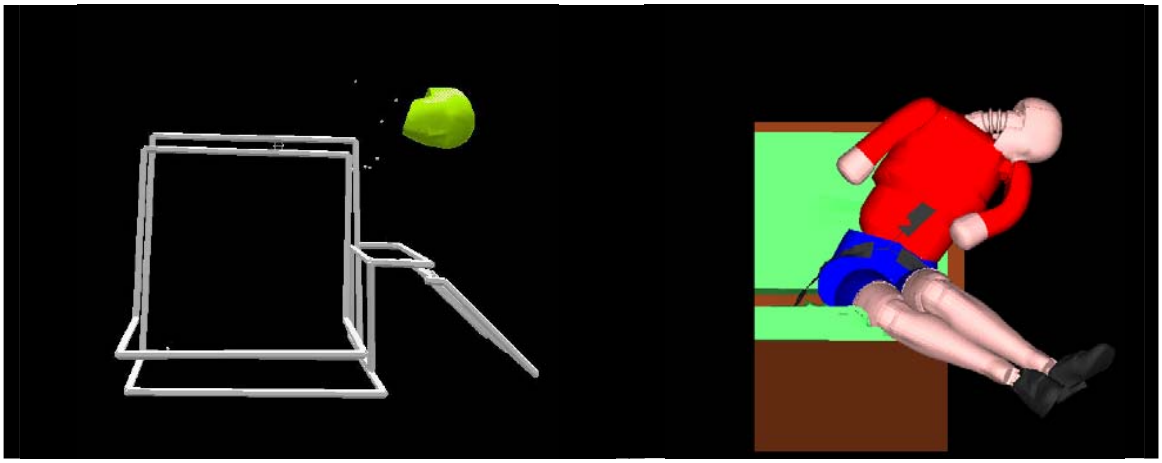

t = 0.087 s (experiment) and t = 0.091 s (simulation); maximum neck bending

Figure 46. Aircraft Seat, Experimental and Simulated Kinematic Response

5.3.2 Supporting Impact Simulations.

5.3.2.1 Investigation 1: Triangular Versus Rectangular Sled Pulse.

Figure 47 shows the pulses used to investigate the effect of using a rectangular-shaped pulse as a replacement for a triangular pulse for both the 9- and 16-g conditions. The deceleration displacement constraints of the sled were taken into account, and the same ΔV was used for the rectangular pulse (9 g ΔV = 7 m/s and 16 g ΔV = 14.4 m/s). Results obtained from the simulation of the triangular and rectangular pulse conditions are shown in figures 48 and 49. It was concluded that the MCW sled performed well for the lower impact cases (~10 g). However, for an impact with the same ΔV as the 14 CFR 25.562 pulse (13.4 m/s), significantly higher neck loads and, consequently, a higher injury risk could be expected.

At the time, it was believed that a modification of the 18.3-g rectangular pulse duration and peak might produce an impact response closer to the triangular pulses. This was investigated by CAMI using ES-2 sled tests, and the results indicated that a 12.5-g pulse lasting 100 ms (ΔV = 12.5 m/s) produced comparable responses. More detailed information regarding these experiments can be found in appendix B.

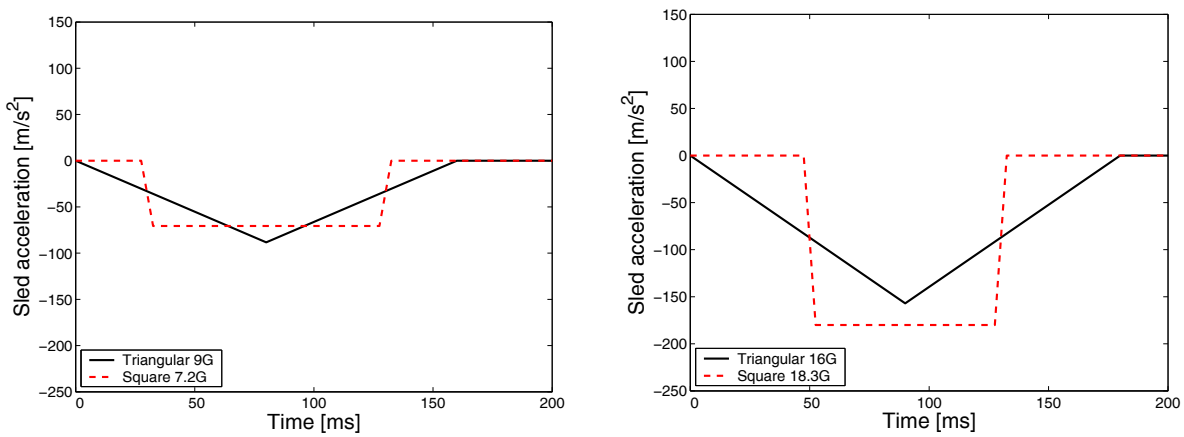

(a) 9 g (b)16 g

Figure 47. Triangular and Rectangular Pulses for 9- and 16-g Acceleration Conditions

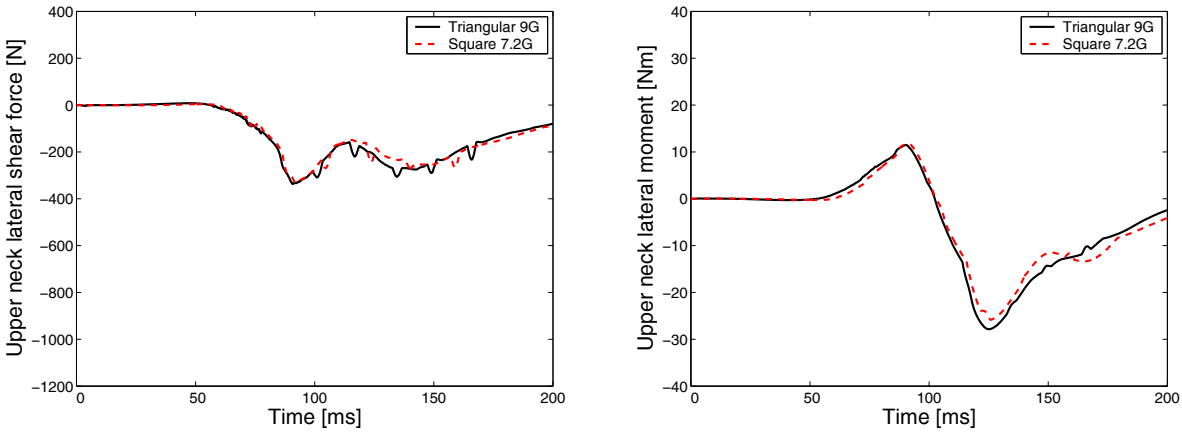

(a) Shear (b) Lateral Bending Moment

Figure 48. The ES-2 Upper-Neck Loads for the Rectangular 7.2-g and Triangular 9-g Pulses

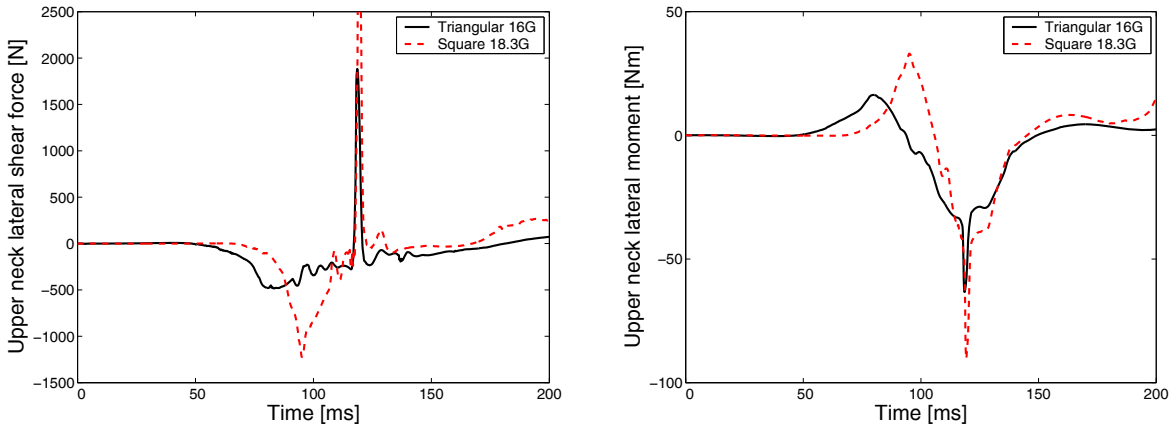

(a) Shear (b) Lateral Bending Moment

Figure 49. The ES-2 Upper-Neck Loads for the Rectangular 18.3-g and Triangular 16-g Pulses

5.3.2.2 Investigation 2: Variation in Sled Pulse Severity.

The pulses used to produce a reduced impact severity are shown in figure 50, where the curves were y-scaled in increments of 10%. The results of these simulations were used by plotting the upper-neck tension against the pulse severity, as shown in figure 51. AIS 1 and AIS 2 limits were additionally specified to identify the pulse severity that will generate the appropriate neck tension responses. It is noted here that the AIS limits applied to the ES-2 were transformed from the PMHS biomechanical limits, using data obtained from previous tests performed in this study and assuming a linear relationship regardless of impact severity.

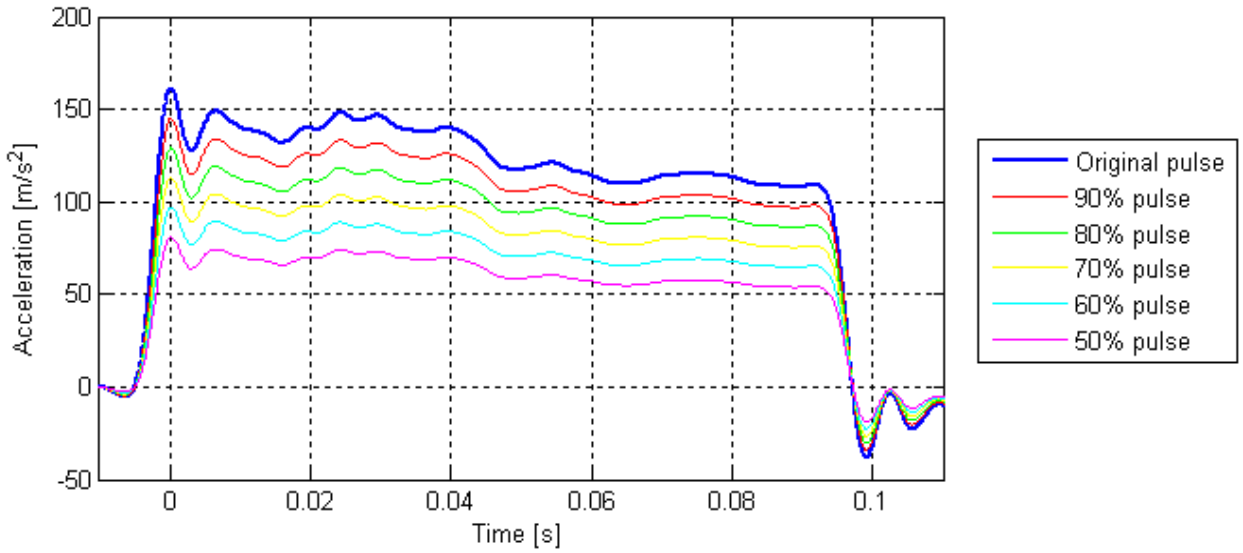

Figure 50. Acceleration Pulses Used in Reducing Severity of Sled Impacts

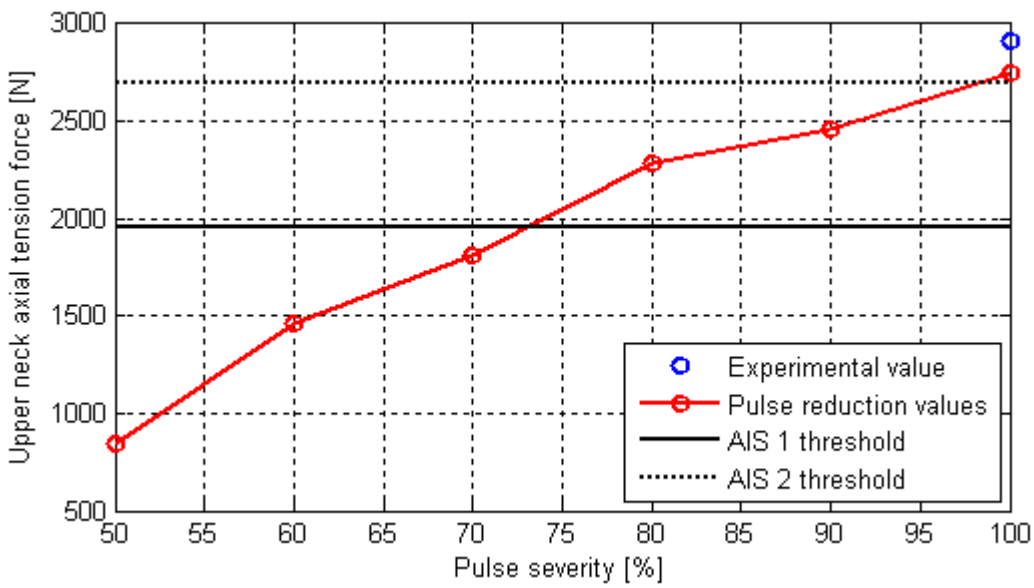

Figure 51. Effect of the Acceleration Pulse on Upper-Neck Tension Forces in ES-2 Simulations

From these results, it was found that an acceleration pulse, which was lowered to 90% of the original pulse velocity, was just under the AIS 2 limit, and an acceleration pulse, which was lowered to 70% of the original pulse velocity, was just under the AIS 1 limit. Corresponding experimental tests were performed implementing these pulses, eventually confirming the results of the simulations, as shown in the responses plotted in figures 52 and 53. Upper-neck tension and moment both correspond to the results obtained from the experiments. These conditions were eventually used for PMHS tests, as described in section 4.

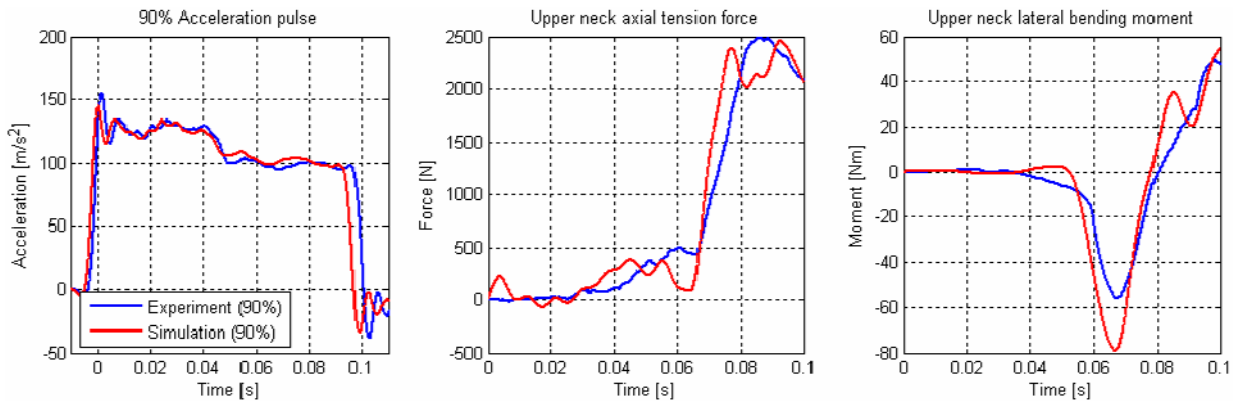

Figure 52. Comparison of Simulation and Experiment for 90% Sled Velocity

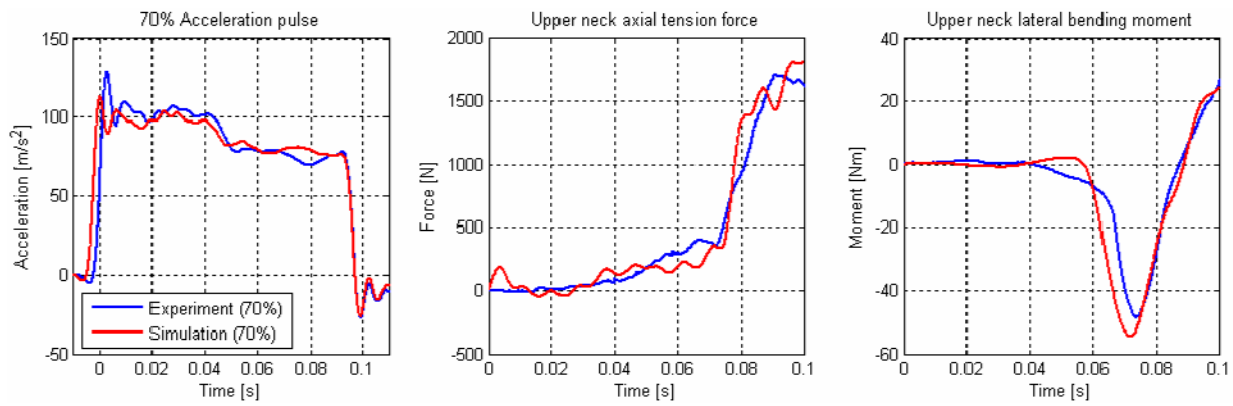

Figure 53. Comparison of Simulation and Experiment for 70% Sled Velocity

5.3.2.3 Investigation 3: Supporting the Neck to Increase Neck Moments.

Figure 54 shows the results of the progressively locked neck joint simulations, comparing the upper-neck tension against the upper-neck moment. As expected, the simulations showed an increasing upper-neck lateral moment with a decreasing neck tension when progressively locking the joints.

The additional simulations performed considering the above results involved increasing the pulse severity in an effort to drive the moment further upwards. The ΔV was increased by 11.8%, 22.5%, and 41.4%, generating an increase in the impact energy by 25%, 50%, and 100%. These values were calculated according to the limitations of the sled where a consistent sled displacement was used. The "3-joints locked" condition was used as the best approximation to replicate the supporting conditions proposed for the PMHS tests. Additionally, the "free"-neck scenario was simulated under these same pulses to gauge the effect caused by the supported neck. Figure 55 plots the tension and moment loads of the upper neck for both the free- and supported-(half-lock joints) neck conditions. The results for both conditions show an increase in tension and moment as expected, as well as the ability to maintain a significantly lower-neck tension when using the supported condition. A 144% ΔV impact condition was eventually used as a test condition for conducting both ES-2 and PMHS experiments, as detailed in section 4.2.2.

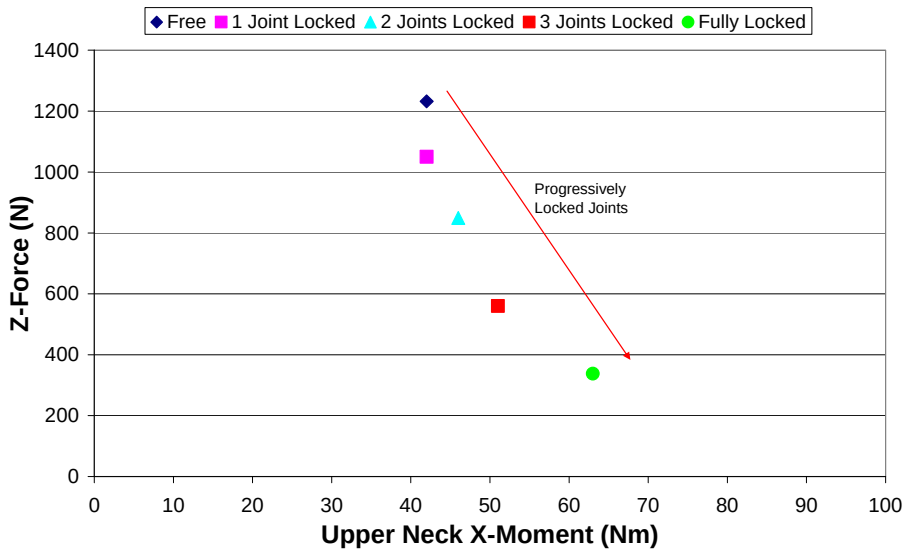

Figure 54. Effect of Locked Neck Joints on Upper-Neck Loads for 70% Sled Velocity

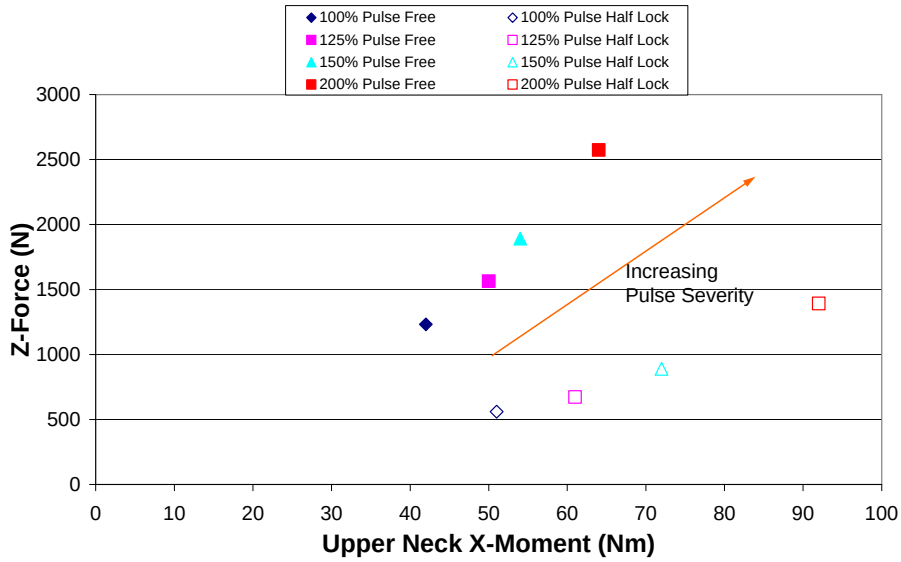

Figure 55. Upper-Neck Tension and Lateral Moment Response to Pulse Severity

5.3.2.4 Investigation 4: Increasing Head Mass to Increase Neck Moments.

Figure 56 shows the ES-2 responses in the rigid-restraint condition where the bending stiffness of the neck was lowered to 10%, 25%, and 50% of the original value and were simulated both with and without the extra 1-kg mass conditions. Several conclusions can be drawn from these responses. First, by adding mass to the head, an increase in neck tension was generated for all simulation cases. Second, by adding mass to the standard ES-2 (100% neck stiffness), an increase in moment was found, as theorized. The added mass increased the neck inertia and significantly increased the moment load in the neck. Third, when the neck stiffness was decreased, the resultant moment decreased, as expected. And fourth, when the mass was added

to the low-stiffness cases (i.e., the PMHS representation), the neck moment increased to a lesser degree and, in two cases, was even lower. The neck was able to rotate significantly before generating significant moment and was instead stopped by the interaction of the head with the shoulder. It was believed that this same phenomenon will occur throughout any PMHS tests, and using an added mass as a method for increasing neck moment was not recommended.

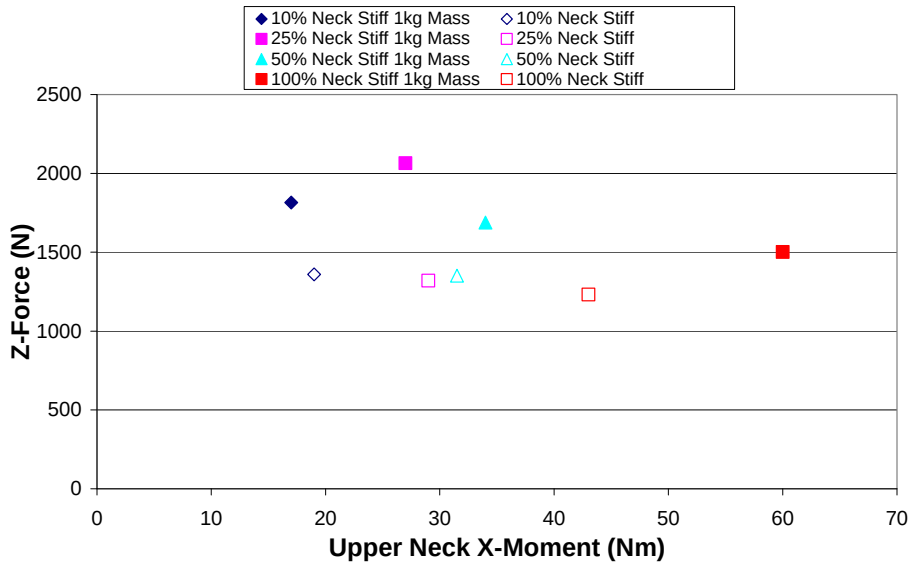

Figure 56. Upper-Neck Loads for Additional Head Mass and Decreased Bending Stiffness

6. INJURY PROBABILITY.

6.1 INTRODUCTION.

The Probit calculation method (Caceci and Cacheris, 1984) was used to define the 50% injury risk curves. The procedure consists of fitting a cumulative normal curve (Probit) through the AIS 3+ criteria data. All data points are plotted on a probability plot, where a test representing an injury less than AIS 3 is considered 0% probable and a test representing an injury AIS 3 or higher is considered 100% probable. These data points are then fitted with a cumulative normal curve using a simplex algorithm (Caceci and Cacheris, 1984) with a 90% confidence level. From the fit, the average (50% risk) and the standard deviation (sigma-σ) are described, which define the shape of the curve. Generally speaking, this algorithm uses the maximum likelihood estimation to fit a complex nonlinear mathematical function to a set of multivariable data points.

The peak values for the ATD neck load responses were analyzed using the Probit method to derive a potential injury assessment reference value. The presence of an injury was defined by the corresponding PMHS sled tests. The actual PMHS response peak values are not analyzed here because the final target of this research is a proposal for one or more ATD IARVs. It is additionally noted that statistically significant results require a minimum of data points with a significant consistency between peak value and occurrence of injury. Since the number of data points and the injury/noninjury distribution for AIS 1 or AIS 2 did not sufficiently achieve this minimum number, an adequate fit to a normal distribution with a 90% confidence level could not

be achieved. On the other hand, an AIS 3-based Probit analysis could be made for upper- and lower-neck tension and shear forces. The neck bending peak values were not sufficiently consistent in their injury/noninjury distribution to allow for such an analysis.

6.2 PROBIT RESULTS.

The results of the Probit analysis are listed in figures 57 to 60 for the signals upper neck tension, lower neck tension, upper neck shear, lower neck shear, respectively. The peak values of the neck loads are represented by the blue diamond data points in the graphs. A data marker at the "0" line represents an injury severity less than AIS 3, a data marker at the "1" represents a severity of AIS 3 or higher. These data points are input to the Probit algorithm. The confidence level for the Probit analysis is 90%, as represented by the normal distribution fit.

The contents of the graphs and parameters listed in the tables beside the graphs are explained by using figure 57 as an example. This shows the analysis of the ES-2 upper neck tensile response detailing the average of the probability fit, "Fit Prob," and the upper and lower limits (CL upper and CL lower) for a probability with a 90% confidence level. The following parameters are included in the tables beside the graphs.

- OC Fz 50: the average Fz (tension force) for 50% AIS 3+ risk.
- Sigma: The calculated standard deviation for the fitted Cumulative Normal distribution.
- Fit error: The error between the fitted curve and the experimental data. The error is expressed as the root mean square value of the difference between the experimental data and the fitted curve.
- OC Fz 50 max: maximum value of Fz – CL upper for 0.5 AIS 3+ probability.
- OC Fz 50 min: minimum value of Fz – CL lower for 0.5 AIS 3+ probability.

Therefore, the peak value for 50% probability AIS 3+ risk is with 90% confidence in the range (OC Fz 50 max: OC Fz 50 min) with OC Fz 50 as an average.

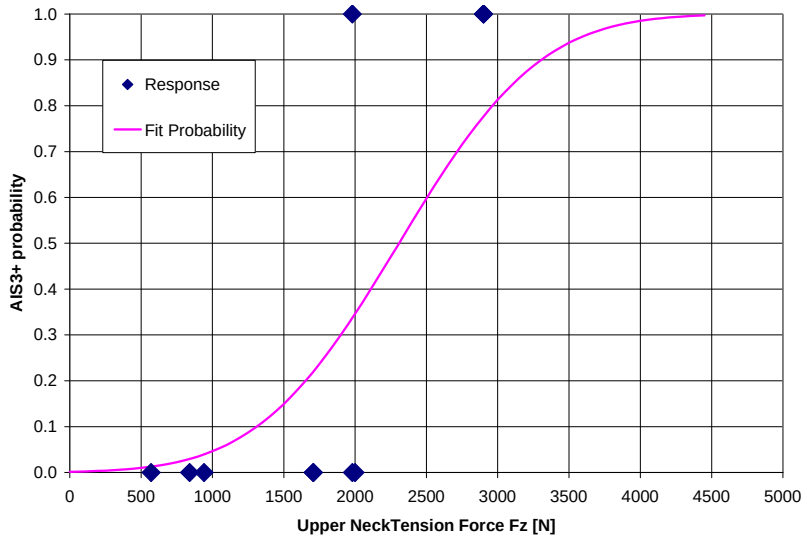

OC Fz 50	2308.02
Sigma	778.47
Fit error	0.09
OC Fz 50 max	2861.20
OC Fz 50 min	1754.84

Figure 57. The AIS 3+ Probability for ES-2 Upper-Neck Force Fz

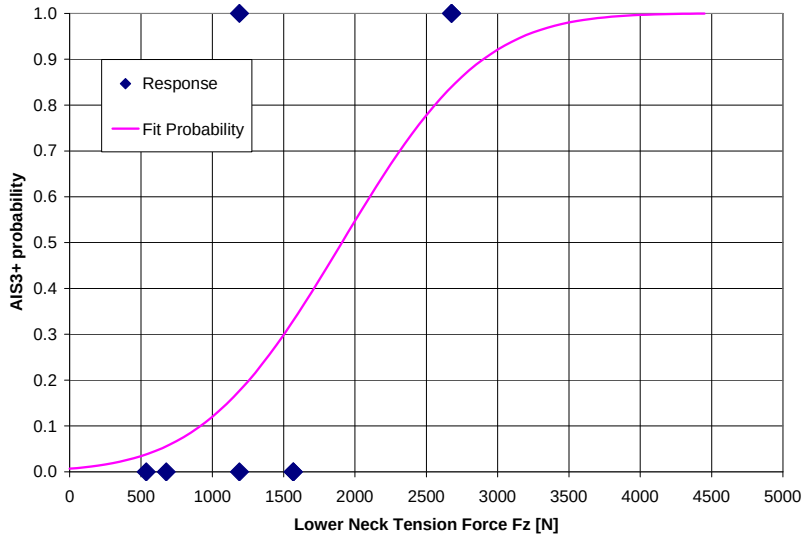

T1 Fz 50	1908.31
Sigma	773.5
Fit error	0.12
T1 Fz 50 max	2561.77
T1 Fz 50 min	1254.85

Figure 58. The AIS 3+ Probability for ES-2 Lower-Neck Force Fz

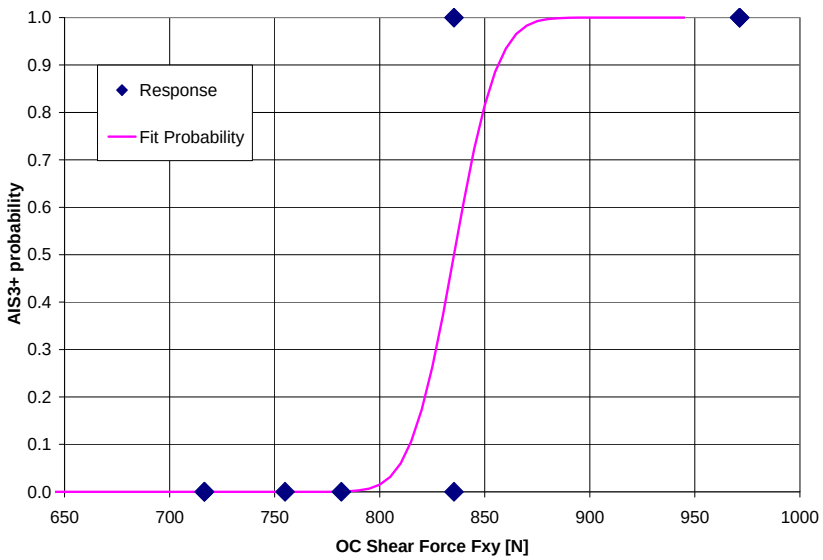

OC Fxy 50	835.37
Sigma	16.31
Fit error	0.06
OC Fxy 50 max	849.15
OC Fxy 50 min	821.60

Figure 59. The AIS 3+ Probability for ES-2 Upper-Neck Resultant Shear Force Fxy

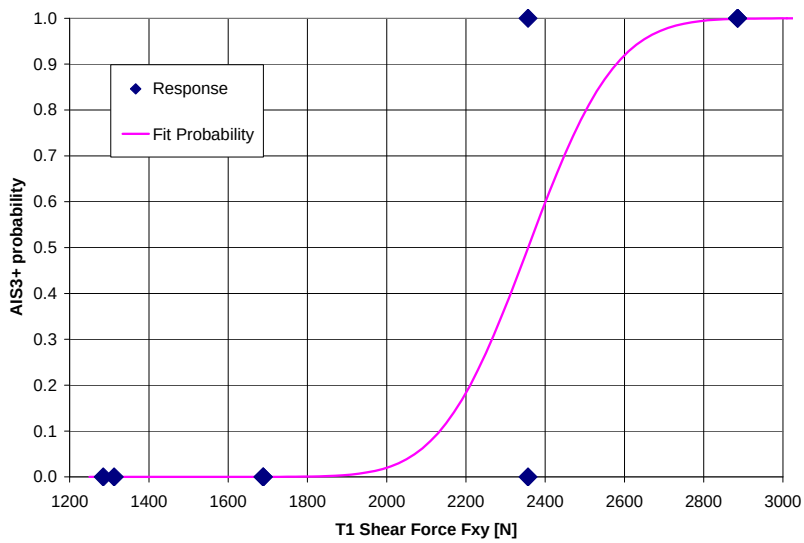

T1 Fxy 50	2356.83
Sigma	173.64
Fit error	0.06
T1 Fxy 50 max	2503.52
T1 Fxy 50 min	2210.13

Figure 60. The AIS 3+ Probability for ES-2 Lower-Neck Resultant Shear Force Fxy

6.3 DISCUSSION.

The number of data points and injury severity distribution was minimally sufficient for performing the Probit analysis with a 90% confidence for the AIS 3+ injury severity. However, the small number of data points was reflected by the relatively large standard deviations (σ) for the fitted normal distributions, as summarized in table 16. The severity of these significant measures was seen by dividing the standard deviations by the respective means, which vary between 2% and 34%.

Table 16. Mean Value for 50% Risk, σ as a Percentage of the Mean 50% Risk Value

Criteria	50% Risk	σ	σ/mean_50 *100%
Upper-neck Fz	2308	778	34
Lower-neck Fz	1908	773	41
Upper-neck shear Fxy	835	16	2
Lower-neck shear Fxy	2357	174	7

While table 16 reflects the values for a 50% risk of injury, the values for other risk levels may be derived from the risk curves (figures 57-60) in a similar fashion. For example, in figure 57, an upper neck tension force of about 1800 N corresponds to a 25% probablity of an AIS 3 injury.

7. STANDARD TEST PROCEDURE.

7.1 INTRODUCTION.

Detailed guidance currently exists for conducting certification tests with forward- and aft-facing seats (e.g., Advisory Circular 25.562-1B and SAE AS8049B). However, standard procedures for side-facing seats have not been established. Phase 4 of this research project was to identify the unique requirements necessary for conducting certification tests with side-facing seats. It was anticipated that proper evaluation of side-facing seats would require different test dummies and setup procedures than those called for in the current standards. This section summarizes the development of a new side-facing seat procedure including detailed test setup procedures, observations for quality implementation of the procedure, and recommendations for future use.

These efforts were facilitated through tests conducted at CAMI to assess the injury potential of current side-facing aircraft seat configurations using the ES-2, proposed for use in the Federal Motor Vehicle Safety Standards. Impact sled tests were conducted using a similar aircraft seating configuration as the PMHS tests described in section 3. Further analysis of the results obtained from these tests is included in appendix B.

7.2 ANTHROPORMORPHIC TEST DUMMIES.

The ATDs currently cited in aircraft seat certification procedures are designed to primarily assess injuries in the forward and vertical directions. However, for injury assessment in the lateral direction, a specialized ATD is required. The ES-2 was chosen for this project because it is specified in automotive regulations, has available injury criteria, and has a fully instrumented head and neck. The specific version used for this research differs somewhat from the ES-2re cited in the automotive regulations in that it does not have rib extensions (re). The primary purpose of the rib extension modification to the ES-2 is to prevent unrealistic interaction between heavily contoured seat cushions, found in typical automobile applications, and the back plate of the ATD when subjected to oblique acceleration vectors. Since aircraft side-facing couches are not typically contoured and the tests would be conducted without yaw, it was determined that the E2.AI version of the ES-2 (which was available for this project) would provide sufficiently equivalent results for the purposes of this research. However, the ATD

recommended for use in side-facing seat tests is the standard ES-2re version, as specified in 49 CFR Part 572, Subpart U.

7.3 TEST SETUP CONSIDERATIONS.

The current procedures for seating ATDs in forward-facing seats do not provide a specific rearward preload. This has not caused excessive variability in ATD initial position because of the relatively thin seat backs found on typical forward-facing passenger seats. When the same procedure is applied to seating an ES-2 in a side-facing couch, however, it was found that excessive variation in the initial fore/aft position of the ATD's pelvis, torso angle, and head position can result. This is apparently due to the interaction between the ES-2's protruding back plate and the thick, soft seat back cushions typical of aircraft side-facing couches.

The special ATD installation procedures outlined below were developed to achieve a consistent initial position.

a. Lower the ATD vertically into the seat, aligning the midsagittal plane with the seat centerline while applying a 50-lb (220-N) force to the knees of the ATD, as shown in figure 61. This compresses the seat back cushion in the same manner that an occupant would when being seated.

b. Tighten the lap belt per SAE AS8049B. This procedure calls for the belt to be tightened until only two fingers can be placed between the belt and the ATD pelvis, as shown in figure 62.

c. Push the ATD upper torso backward with a nominal amount of force to bring it upright and then secure it in place with 32-lb (142-N) (total all strands) breaking force string, as shown in figure 63. This rearward preload is necessary to overcome the tendency for the interaction of the back plate and the seat back cushion to push the torso forward into an unnatural posture.

d. Align the head and torso midsagittal planes. This is necessary because the design of the ES-2 neck permits a significant amount of free head rotation about the Z axis.

e. Place both of the arms at 40° with regard to the ATD torso. This was necessary to avoid interaction with the ribs, which can lead to inconsistent test results.

Figure 61. Horizontal Force (220 N) Applied to the Knees While ATD is Lowered Into the Seat

Figure 62. SAE AS8048 Two-Finger Belt-Tightening Procedure

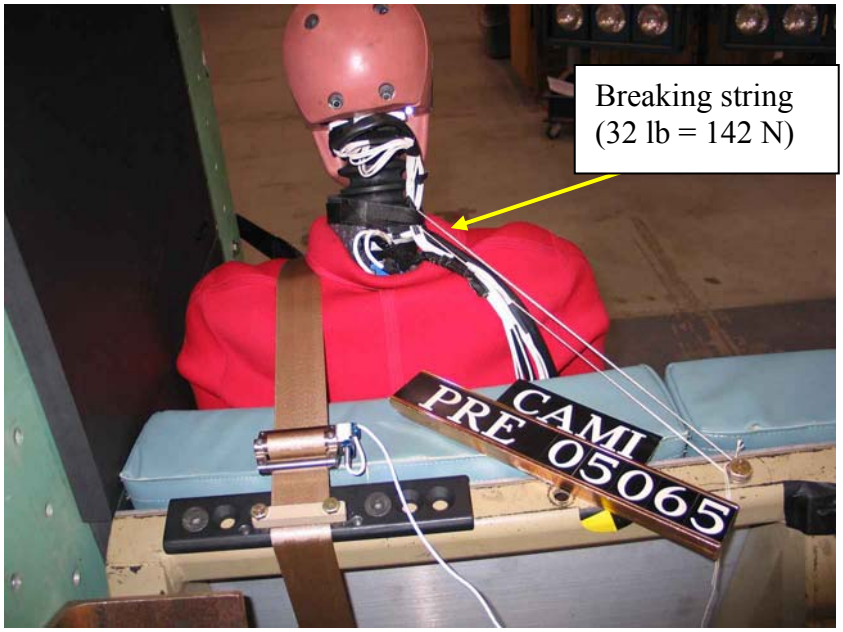

Figure 63. String Holding Torso Upright

This seating procedure resulted in a very consistent pelvis location (±2.5 mm laterally and ±7.5 mm fore/aft) and a somewhat consistent head c.g. location (±5.0 mm laterally and ±25.4 mm fore/aft). When this same procedure was used with the FAA Hybrid-III ATD, it resulted in a more reclined posture, with the head c.g. 48 mm further back than achieved with the ES-2. This difference is primarily due to the protruding, anthropometrically incorrect back plate of the ES-2. Further development is needed to adapt the procedure for use with the ES-2re and to produce an initially reclined angle that is not just consistent but also more representative of a human occupant.

7.4 TEST OBSERVATIONS.

Overall, the ES-2 functioned in a satisfactory manner in these types of tests. However, several issues were noted, as summarized below.

7.4.1 Shoulder Belt Interaction.

The ES-2 (like most side-facing test ATDs) was designed to primarily assess injuries caused by direct contact with adjacent interior structure (i.e., the car door). Because of this, biofidelic interaction with belt systems was not a priority during their development. This is evident in the construction of the ES-2's shoulder, which has a very soft foam top surface and no structure that simulates the human clavicle. This allows the shoulder belt to penetrate significantly into the top of the shoulder and the front of the torso at relatively low loads. This response would not be expected with human occupants, who have bony support structures in these areas, and certainly not with frontal test dummies that have very stiff structures in these areas. This unrealistic interaction with the top of the shoulder also allows the belt to apply forces to the upper torso below the level of the lower-neck load cell. This means that belt forces that would be applied to the lower neck of a human occupant would not be measured at all with the ATD. Lack of

support structure in the ES-2 shoulder increases the lateral flail envelope compared to the FAA Hybrid-III. While the kinematic biofidelity when restrained by belts during a side impact has not been validated for either of these ATDs, it was observed that the head lateral excursion of the ES-2 was similar to PMHS for the configurations tested in this research project. While certainly an area for potential improvement, this unique interaction with the shoulder belt does not prevent measurement of critical injury parameters and therefore does not preclude use of the ES-2 for side-facing seat tests.

7.4.2 Neck Durability.

The ES-2's neck is very flexible, which is one factor in providing its superior biofidelity. The tensile strength of the design is apparently much less than on typical forward-facing ATDs. Accordingly, the ES-2 cannot be lifted by its head unlike other test dummies since the repeated loading could damage the neck. Loads encountered during some test scenarios were sufficient to damage the neck's rubber center section. As a result, a thorough inspection of the neck for damage is necessary after tests that result in high tension or bending loads.

7.5 RECOMMENDED TEST REQUIREMENTS.

Using ES-2re, as specified in 49 CFR Part 572, Subpart U, in side-facing seat certification tests would provide a means of assessing the potential for injury using a state-of-the-art understanding of injury mechanisms and criteria related to lateral loading. ES-2re can also measure current aviation injury criteria, such as HIC and shoulder belt tension, as well as potential aircraft-specific criteria for limits on neck loading, femur torsion, and body-to-body contact. Improvements in the ES-2re shoulder's biofidelity would allow better assessment of the potential for injury caused by belt contact forces on the neck.

Current seat certification test procedures for fore/aft-facing seats can generally be applied to side-facing seat tests; however, the specialized ES-2 installation procedures that are necessary to achieve the appropriate initial position should be added.

These recommended test requirements were developed for seats that are installed in the aircraft, side facing with little or no yaw. Further development is required to determine the appropriate ATD(s), injury criteria, and test procedures for certification of seats installed in the aircraft at a significantly oblique angle.

8. SUMMARY.

The objective of this study was to investigate neck injuries in side-facing aircraft seats and to develop neck injury criteria and injury tolerance levels. Using this information, an IARV will be determined for an ATD. This will be used as a basis for a performance standard for the certification of side-facing aircraft seats and corresponding protection systems. Data developed in this study was based on the existing and standardized acceleration pulse described in 14 CFR 25.562. The proposed injury criteria and tolerance values would also be applicable to other categories of aircraft.

8.1 PROBLEM DEFINITION.

A literature review was conducted at the start of the project and was supplemented by a literature update at the end of the project (section 2). From this update, new information on injuries and neck-loading levels was found. The tolerance for single tension (4170 N, as specified in the criterion) N_{ij} appears to be almost double the value found in recent literature for AIS 2 injuries in lateral loading conditions. The lateral bending moment, as suggested by Soltis, 2001, (60 Nm) is significantly lower than the recent values reported by McIntosh, et al., 2007, (180 Nm) for AIS 2. The lateral shear force tolerance for AIS 2 was reported earlier to be >900 N; however, recent research specifies a much higher value of almost 3000 N as an AIS 2 tolerance. Furthermore, the use of any tolerance value for application with ATDs and the definition of IARVs could not be accommodated without additional and appropriate analysis. The PMHS research performed in this study attempted to fill these informational voids.

8.2 TEST RESULTS.

Two PMHS tests and corresponding ES-2 ATD tests were conducted at WSU. The first test was conducted at 9-g loading and the second at 19 g using a triangular pulse based on 14 CFR 25.562. The PMHSs and ES-2s were seated on a rigid seat and restrained with a three-point belt restraint as well as a side wall up to shoulder height. In both tests, no gross neck injuries were detected. However, serious rib fractures and shoulder injuries were sustained by the PMHSs. These injuries may have reduced the severity of the loading experienced by the head-neck system.

The remaining tests were performed at MCW. Since the MCW sled produces only rectangular-shaped pulses, it was necessary to substantiate the use of the MCW facility. Computer simulations were performed (see section 5) and sled tests were conducted (see appendix B) to investigate how the shape of the pulse affected the impact response of the ES-2. Based on these investigations, it was concluded that a 12.5-g test with a rectangular pulse would have a similar severity on the subjects as the triangular pulse specified in 14 CFR 25.562.

Eight PMHS tests and supporting ES-2 tests were conducted at MCW. Four tests were performed on a rigid seat (without cushions) with the PMHS/ES-2 rigidly restrained to the seat using a five-point belt system to minimize displacements of the seat occupants relative to the sled. The other four tests were performed with the PMHS/ES-2 positioned on a rigid seat with cushions and armrests (referred to as an aircraft seat), and restrained by a three-point belt with retractor. This test condition allowed significant motion of the PMHS relative to the sled.

In the rigid-seat tests, two test severities were used: (1) a 12.5-g test with a similar severity as the 14 CFR 25.562 tests and (2) a much more severe 15.5-g test (ΔV: +44%). Using the AIS for necks in these conditions, only minor neck injuries were found (AIS 1). In the aircraft seat tests, two PMHS tests with the same 12.5-g pulse were performed and two PMHS tests with a significantly lower 8.5-g pulse (ΔV: -30%) were performed. In this seating and restraint configuration, the test with an acceleration load equivalent to the rigid-restraint configuration (i.e., 12.5 g) produced major injuries (AIS 3+). The serious injuries were attributed to the kinematics of the occupant that occurred using the three-point belt restraint. In the lower-

severity (8.5 g) aircraft seat tests, one test showed AIS 3 injuries, while in the other, no injuries were found. In one of the 15.5-g rigid-seat tests, AIS 2 injuries were sustained, while in the other, AIS 3+ injuries were sustained. Of the injuries in other body regions, rib fractures and a carotid tear were noted to be life-threatening. Femur fractures, caused by lower-limb flailing, and potential passenger unconsciousness, caused by high head angular accelerations, although less serious, can prevent passengers from exiting the aircraft. For each test, first the anatomical, then the clinical AIS injury scores are listed. For FAA-26, only the anatomical data were available.

The results for the PMHS tests were best illustrated by plotting one neck response measure against another. Figure 64 shows the combination of upper-neck tension force versus lateral bending moment. Data points are ordered in two groups, red markers for tests with an anatomical injury score of AIS 3 or higher and green markers for AIS scores of 2 or lower. The yellow marker on the tension axes indicates the Fz tension tolerance defined in the N_{ij} criterion. The red-dotted line indicates the boundary between AIS 3+ injuries and AIS 0-2 severity scores. Analysis of these responses concluded tension force to be the most discriminating parameter for predicting AIS 3+ injuries to the neck. Results indicated that there was better agreement between upper-neck loads and moments than lower-neck loads and moments.

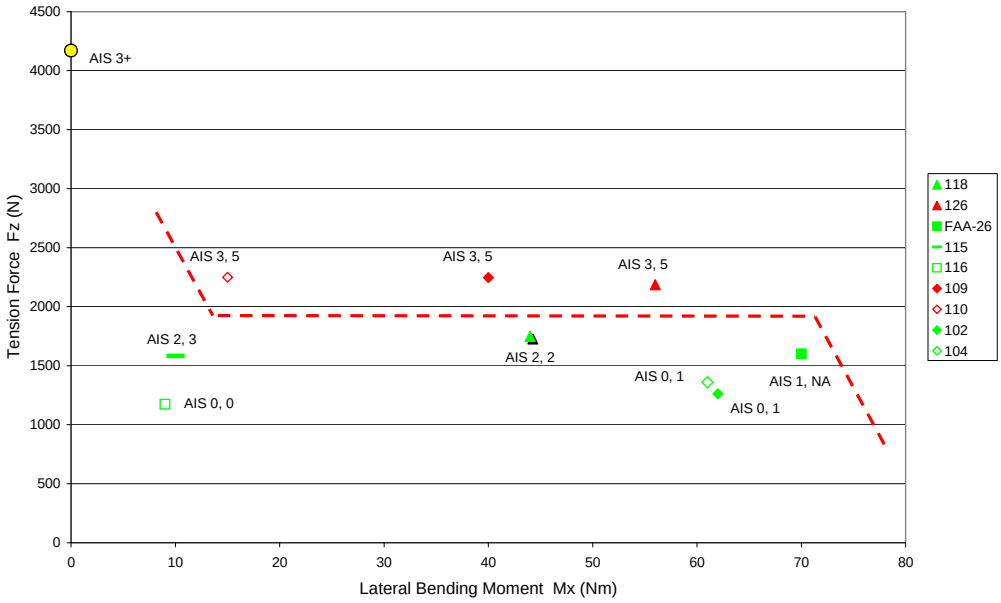

Figure 64. The PMHS Upper-Neck Tension and Lateral Bending Moment Grouped for AIS 0-2 vs AIS 3-6

The maximum values for tension and lateral bending for each ES-2 test and the corresponding PMHS AIS injury scores are shown in figure 65. For tests FAA-22 and FAA-25, only anatomical data were available. A red marker indicates an anatomical injury score of AIS 3 or higher, and a green marker indicates an AIS injury score of 2 or lower. The red-dotted line indicates the boundary between AIS 3+ injury scores and AIS 0-2 injury scores. The yellow marker on the tension axes indicates the F_z tension tolerance defined in the N_{ij} criterion.

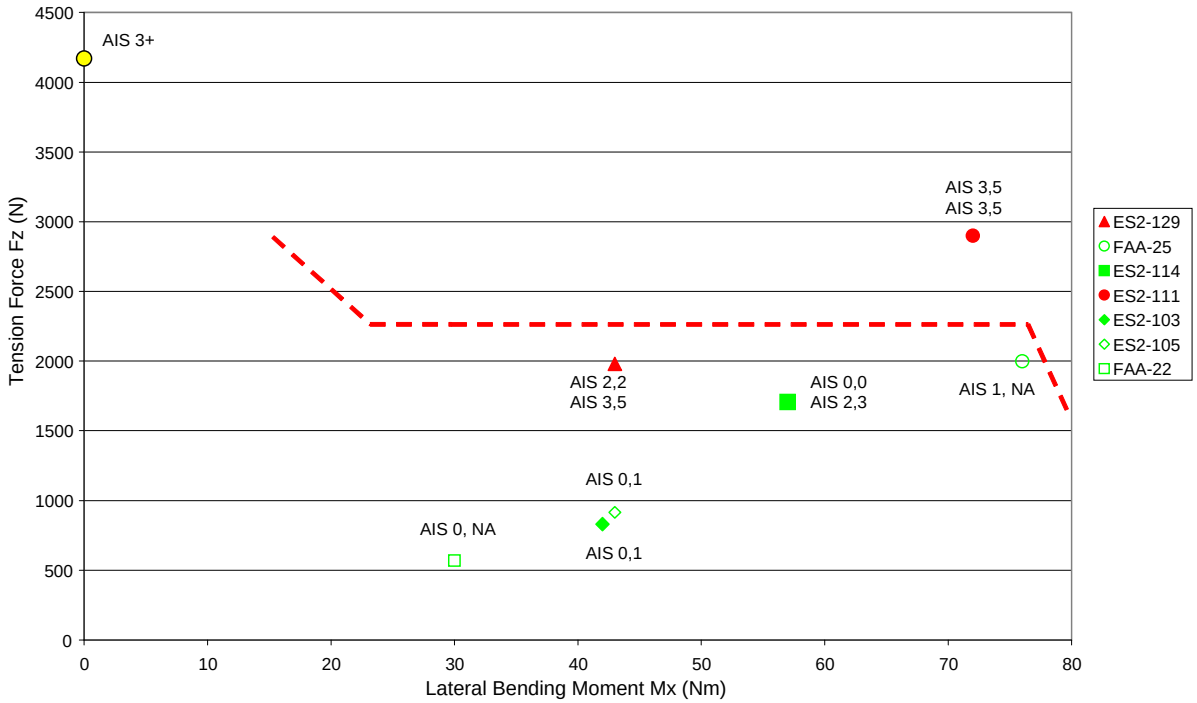

Note: Data points are labeled with AIS scores for the matching PMHS tests.

Figure 65. The ES-2 Upper Neck Tension and Lateral Bending Moment Grouped for AIS 0-2 vs AIS 3-6

9. CONCLUSIONS.

Kinematics of the EuroSID-2 (ES-2) (anthropomorphic test dummy) and measured neck forces showed generally good biofidelity compared to the postmortem human subject (PMHS) tests, with the exception that a slightly earlier rebound was observed in the ES-2. Additionally, the ES-2 was slightly stiffer in the vertical direction, resulting in lower thoracal 1 accelerations. Forces in the neck showed the same trend; thus, the ES-2 forces can be used to reflect the PMHS neck forces, most likely without further corrections. Moments recorded in the ES-2 showed a different response for the ES-2 compared to the PMHS, where the ES-2 showed an increasing bending moment with increasing sled pulse-loading condition and the PMHS was far less consistent.

The following can be concluded from the computer simulation work performed as part of this study:

- The simulation work was able to show comparable results to the ES-2 response for the aircraft seats with cushions and the rigid-seat configurations.

- The simulation work was helpful in supporting the selection of the proper test conditions and, in particular, the selection of sled severities that would induce specific injury severities. ES-2 and PMHS results matched the simulation predictions well.

- The simulations evaluated the use of a collar that supported the neck, thereby increasing the lateral moment in the neck during the sled test. Results suggested that such an approach is valid and that further pulse severity increases could possibly cause moment-related injuries as opposed to tension-related injuries.

A seating procedure for the ES-2 was developed, achieving satisfactory repeatability and reproducibility. However, a "break" strap was needed to keep the ES-2 in a stable upright position during setup. This was due to the fact that the ES-2 was originally designed for a 25° backward tilted automotive seat while the typical aircraft seat has a 13° tilted back panel. Further development is needed to adapt the procedure for use with the ES-2re and to produce an initially reclined angle that is not just consistent but also more representative of a human occupant.

Some issues with the ES-2 ATD were observed during tests. The durability of the ES-2, when used in these test configurations, requires further attention. The rubber ES-2 neck was found to sustain damage in the form of cracking after a few tests. Furthermore, it was observed that the leading shoulder belt slips into the open space at the bottom of the neck and loads the lower part of the neck such that it could affect the lower neck load cell reading.

This study focused on the use of side-facing seats in 14 CFR 25.562 aircraft. However, the proposed injury criteria and tolerance values are thought to be sufficiently general such that they can be applied to other categories of aircrafts. Additionally, the results obtained could be transferred to other applications (i.e., automotive safety), where similar long-duration loading, such as far-seated occupants in side impacts and specific rollover test conditions, can be observed.

10. RECOMMENDATIONS.

Based on the Probit analysis, the risk of serious neck injury for occupants of side facing seats can be limited to a 50% probability if the value of upper neck tension measured in an ES-2 ATD during seat qualification tests is ≤2300 N. This limit assumes that a shear, bending, or torque precondition exists.

Additional data concerning high lateral moments and low tension, and high shear forces and low tension are necessary to complete the dataset.

The rationale for this recommendation is that the probability analysis showed that 2300 N tension in the upper neck of the ES-2 can be used as an appropriate IARV for a 50% risk of serious injury, when combined with a minimum shear force or bending torque precondition (indicates a bending position of the head-neck system). It is improbable if not almost impossible that the neck in side impact conditions would be subjected to only pure tension loading; therefore, a precondition is assumed to exist. To provide the overall level of safety desired, an IARV representing a lower risk of injury is sometimes needed. For instance, the Probit analysis indicates that an upper neck tension IARV of ≤1800 N will limit the risk of a serious neck injury to 25% or less. The number of data points available to perform the probability analysis was noted as being minimally acceptable.

11. BIBLIOGRAPHY.

Association for the Advancement of Automotive Medicine, Committee on Injury Scaling (1990), *The Abbreviated Injury Scale*, 1990 Revision (AIS-90), Des Plains, Illinois, Association for the Advancement of Automotive Medicine.

Bendjellal, F., C. Tarriere, D. Gillet, P. Mack, and F. Guillon, 1987, "Head and Neck Responses Under High G-Level Lateral Deceleration," *Proceedings of the 31st Stapp Car Crash Conference*, Paper 872196, pp. 29-47.

Bourhis, S., 1996, "Traumatismes du Rachis Cervical," Nanterre, France, LAB—PSA Peugeot Citro¨en/RENAULT.

Caceci, M.SS. and W.P. Cacheris, 1984, "Fitting Curves to Data: The Simplex Algorithm is the Answer," *BYTE*.

DeWeese, R., D. Moorcroft, T. Green, and M. Philippens, 2007, "Assesment of Injury Potential in Aircraft Side-Facing Seats Using the ES-2 Anthropometric Test Dummy," Office of Aerospace Medicine, DOT/FAA/AM-07/13, Washington, DC 20591.

Ewing, C., D. Thomas, L. Lustick, W. Muzzy III, G. Willems, and P. Majewski, 1977, "Dynamic Response of the Human Head and Neck to +Gy Impact Acceleration," *21st Stapp Car Crash Conference*, Paper 770928, pp. 549-586.

Ewing, C., D. Thomas, L. Lustick, W. Muzzy III, G. Willems, and P. Majewski, 1978, "Effect of Initial Position on the Human Head and Neck Response to +Y Impact Acceleration," *Proceedings of the 22nd Stapp Car Crash Conference*, Paper 780888, pp. 103-138.

Fréchède, B., N. Bertholon, J-Y Le Cos, F. Lavaste, and W. Skalli, 2005, "Finite Element Model of the Human Neck During Omni-Directional Impacts," *Biomechanics of Impact*, pp. 463-485.

Hartwig, E., A. Kettler, M. Schultheiss, L. Kinzl, L. Claes, and H.J. Wilke, 2004, "In Vitro Low-Speed Side Collisions Cause Injury to the Lower Cervical Spine but do not Damage Alar Ligaments," *European Spine Journal*, Vol. 13 (7), pp. 590-597.

Kallieris, D., R. Mattern, E. Miltner, G. Schmidt, and K. Stein, 1991, "Considerations for a Neck Injury Criterion," *35th Stapp Car Crash Conference*, SAE Technical Paper 912916, pp. 401-417.

Kallieris, D., R. Mattern, G. Schmidt, and R.H. Eppinger, 1981, "Quantification of Side Impact Responses and Injuries," *Proceedings of the 25th Stapp Car Crash Conference*, Paper 811009, pp. 329-368.

Kallieris, D., A. Rizzetti, R. Matten, J. Thunnissen, and M. Philippens, 2001, "Cervical Human Spine Loads During Traumatomechanical Investigations," *Proceedings of the IRCOBI Conference*, Bron, France, pp. 89-106.

Kettler A., K. Fruth, L. Claes, and H.-J. Wilke, 2006, "Influence of the Crash Pulse Shape on the Peak Loading and the Injury Tolerance Levels of the Neck in Vitro Low-Speed Side-Collisions," *Journal of Biomechanics*, Vol. 39, pp.323-329.

Lankarani, H.M., P. Kishore, A. Murthy, V. Gowdy, and R. DeWeese, 1999, "Compliance Criteria for Side Facing Aircraft Seats," SAE Paper 1999-01-1598.

Lund, A.K., 2003, "Recommended Procedures for Evaluating Occupant Injury Risk From Deploying Side Airbags," Side Airbag Out-of-Position Injury Technical Working Group.

McIntosh, A.S., D. Kallieris, and B. Fréchède, 2007, "Neck Injury Tolerance Under Inertial Loads in Side Impacts," *Accident Analysis and Prevention*, Vol. 39, pp. 326-333.

Mettz, H.J. and L.M. Patrick, 1967, *Investigation of the Kinematics and Kinetics of Whiplash*, SAE International, Warrendale, Pennsylvania, SAE Paper 67019.

Mertz, H.J. and L.M. Patrick, 1971, "Strength and Response of the Human Neck," SAE Paper 710855.

Patrick, L.M. and C.C. Chou, 1976, "Response of the Human Neck in Flexion, Extension and Lateral Flexion," VRI-7.3, Society of Automotive Engineers, Warrendale, PA.

Philippens, M., H. Cappon, and M. Van Ratingen, 2004, TNO Automotive Safety Netherlands, "Human Volunteer Head-T1 Response for Oblique Impact Conditions," *Proceedings of the International IRCOBI Conference on the Biomechanics of Impact*, GRAZ (Austria).

Philippens, M., J. Mordaka, J. Wismans, N. Yoganandan, F. Pintar, S. Soltis, and R. DeWeese, 2007, "Side-Impact Neck Injury Criteria and Tolerances for Occupants of Sideward Facing Aircraft Seats," *Triennial International Aircraft Fire and Cabin Safety Research Conference*, Atlantic City, New Jersey.

Pike, J.A., 1990, *Automotive Safety*, Society of Automotive Engineers, Inc., 400 Commonwealth Drive, Warrendale, Pennsylvania 15096-0001.

SAE International, 2005, Performance Standard for Seats in Civil Rotorcraft, Transport Aircraft, and General Aviation Aircraft, Warrendale, Pennsylvania, SAE International, AS8049B.

SAE International, 2003, *Instrumentation for Impact Test—Part 1—Electronic Instrumentation*, Warrendale, Pennsylvania, SAE International, Surface Vehicle Recommended Practice No. J211-1.

SAE International, 1994, *Sign Convention for Vehicle Crash Testing*, Warrendale, Pennsylvania, SAE International, SAE Surface Vehicle Information Report No. J1733.

Shams, T., Y.M. Zhao, and N. Rangarajan, 1995, "Safety of Side-Facing Seats in General Aviation Aircraft," SAE Paper 951164.

Soltis, S.J., 2001, "An Overview of Existing and Needed Neck Impact Injury Criteria for Sideward-Facing Aircraft Seats," *The Third Triennial International Aircraft Fire and Cabin Safety Research Conference*.

Wismans, J., and C. Spenny, 1983, "Performance Requirements for Mechanical Necks in Lateral Flexion," *Proceedings of the 27th Stapp Car Crash Conference*, Paper 831613, pp. 137-149.

Wismans, J., E. Van Oorschot, and J.H. Woltring, 1986, "Omni-Directional Human Head-Neck Response," *Proceedings of the 30th Stapp Car Crash Conference*, Paper 861893, pp. 313-332.

Yoganandan, N, F.A. Pintar, D.J. Maiman, M. Philippens, and J. Wismans, 2006, "Head Linear and Rotational and Craniocervical Loads in Lateral Impact," *IRCOBI*, Madrid, Spain, pp. 127-142.

Yoganandan, N, F.A. Pintar, B.D. Stemper, J.Z. Zhang, and M. Philippens, 2008, "Upper Neck Forces and Moments and Cranial Angular Accelerations in Lateral Impact," *Annals of Biomedical Engineering*, Vol. 36, pp. 406-414.

APPENDIX A—INITIAL LITERATURE SURVEY DETAILS

Relevant studies are summarized in this appendix.

Zaborowski, 1964, performed 50 lateral sled tests with 37 male National Biodynamics Laboratory (NBDL) volunteers aged 20-40 years. They were restrained by a lap belt only. The peak sled acceleration was 3.25-9.02 g and acceleration duration was 100-300 ms. Fifty percent of the subjects had minor complaints attributed to muscular strain and stiffness for loading levels over 6.25 g. The volunteers were able to stay in an upright position until 6 g. At a higher acceleration, the body started to rotate significantly. At 10 g, it was practically impossible to stay in an upright position. One subject passed out.

In a later study, Zaborowski, 1966, performed 87 lateral sled tests with 52 male volunteers aged 20-43 years. They were restrained by a 4-point belt (a lap belt connected to two shoulder belts. The sled acceleration was 4.47-11.59 g and the duration was 90-220 ms. Sixty percent of the subjects had physiological complaints attributed to muscular strain and stiffness for loading levels over 8.86 g. One subject passed out 40 seconds after the test, which might be attributed to a slowing of the heart rate.

Gadd, et al., 1971, performed static head lateral bending tests on postmortem human subjects (PMHS) and dissected necks. The PMHSs were all older than 66 years. The head rotation was measured with regard to the torso and the bending moments were measured at approximately the cervical (C)5-C6 level. The difference in bending stiffness at the second time loading was used as an indication of strain injury. Minor injuries to the neck in lateral bending appeared at 60°. The lateral bending moment was 200 in-lb (22.6 Nm). The overall resisting moment and injury threshold were similar under dynamic loading.

Horsch, et al., 1979, simulated far-side lateral impacts on a sled using PMHSs and an anthropomorphic test dummy (ATD). They were seated on a bench seat restrained by either a two-point or three-point belt, which was inboard- (impact side) or outboard-anchored. The sled acceleration was 10 g, and the velocity change was 35 km/h. Tears in the dura, vertebral artery lesions, transsection, and softening of the cord at C6 were found. Torn longitudinal, interspinal and dorsal ligaments were found at C6 in four cases. Complete and/or partial separations of the C5-C6 and C6-C7 discs were found in five cases. Vertebral fractures were found at C2 and C6. Also, fractures of the C5 and C6 transverse processes and C5 arch and spinous process were found. Further, intradiscal clefts were found in C3-C4, C4-C5 and most frequently in C5-C6 and C6-C7 discs. Only a 23-year-old PMHS with an inboard belt did not sustained injuries. The other PMHSs were aged 56 years or older. Intradiscal clefts were also found in the PMHS control group, which was not subjected to lateral loading. This indicates that intradiscal clefts are more likely to be age-induced. In addition, it was also mentioned that PMHSs are more vulnerable to impact than volunteers.

Bendjellal, et al., 1987, performed 11 lateral sled tests on PMHSs. The PMHS was restrained by a lap belt. The subject's torso was secured by shoulder straps and a nylon belt around the chest. Four tests were performed at a peak sled acceleration of 6.6-9.2 g and a delta velocity (ΔV) of 5.9-6.3 m/s, which was comparable to the NBDL volunteers. The NBDL volunteer lateral

impact tests have been published by Wismans and Spenny, 1983 (this study is described later in this section). Seven tests were performed at a peak sled acceleration of 12.2-14.7 g and a ΔV of 6.08-8.61 m/s. One PMHS in the high-g level tests sustained cervical fractures. Unfortunately, the locations and types of the cervical fractures were not mentioned in this paper.

Kallieris, et al., 1987, performed 31 lateral car-to-car crashes in which PMHSs were far-sided. The PMHSs were 19-65 years old and were restrained by three-point belts. The striking car reached velocities of 40, 45, 50, or 60 km/h. Hemorrhages were used as indication for strains that were classified as AIS 1 injuries (AAAM, 1990). Five subjects did not sustain any injuries, 15 sustained AIS 1 injuries, 9 AIS 2, 1 AIS 3, and 1 AIS 5. Strains and lacerations were found in longitudinal ligaments, ligamentum flavum, intervertebral discs, interspinal muscle, and joints of the vertebral arc. Also, a complete separation between C4 and C5 was found in one case. Sometimes, lacerations in intervertebral discs and fractures in vertebrae were found. Most affected were the C0-C6 segments, especially the C6 segment.

Kallieris, et al., 1990 and 1991, performed side-impact car crashes in which PMHS were far-sided. In the tests, three male and five female PMHSs aged 24-74 years were used. The subjects were restrained by inboard, upper-anchored shoulder belts. The impact velocities of the striking car were 30, 35, and 50 km/h. The peak head angular velocity took place about 80 ms after the crash. Belt-induced, minor injuries at the skin on the neck, neck muscles, and cervical spine were observed with AIS 1. Laceration of the muscles was also noticed in the left neck region (far side), which may be explained by tensile strain during lateral head bending. Further, hemorrhages in the intervertebral discs C2-C3 and C4-C5 were found. The most common region for injuries sustained was C2-C6. The AIS level was 2 or less for all cases, except in two cases where the AIS were 3 and 5. The only uninjured subject was impacted at 50 km/h, for which the maximum lateral head rotation was 27º, the angular velocity 8 rad/s, the angular acceleration 560 rad/s^2, and linear acceleration 27 g. The AIS 1-injured subjects sustained a maximum lateral head rotation of 54°-58º, an angular velocity of 16-31 rad/s, an angular acceleration of 680-1460 rad/s^2, and linear acceleration of 13-26 g. The AIS 2 or higher injured subjects sustained a maximum lateral head rotation of 57°-80º, an angular velocity of 32-39 rad/s, an angular acceleration of 1610-2601 rad/s^2, and linear acceleration of 14-18 g. For PMHS, that were restrained by a three-point inboard, upper-anchored belt, a lateral displacement of the head with regard to the torso was observed. Head lateral bending towards the impact side occurred 80-100 ms after the crash started.

Schmidt, 1973, performed PMHS lateral bending and axial translation tests. Vertebral artery lesions were found at lateral bending over 60º. Robbins and Roberts, 1972, found a tolerance level of 40°-57º for lateral bending.

Myers, et al., 1997, noted from experiments that shear load results in Odontoid fracture and transverse ligament rupture. Lateral bending can result in nerve root avulsion and peripheral nerve injury.

The National Transportation Safety Board accident databases were searched for neck injuries in lateral impact. Unfortunately, no relevant information was recorded.

Kinematics and injuries are not always specified adequately to allow a meaningful comparison in terms of translations, rotations, and AIS qualifications. An overview of the studies described above in which the kinematics and injuries were described adequately is shown in table A-1.

Table A-1. Overview of Lateral Neck Kinematics and Neck Injuries From Literature

Reference	Lateral Kinematic Peak Values	Subject	Age (years)	Restraint	No Pain/ Injury	Pain/ AIS 1	AIS 2	AIS 3	AIS 4	AIS 5
Gadd, et al.	Quasi-static Head 60º	PMHS 4 M	>66	no	0	4	0	0	0	0
Zaborowski (1964)	Sled 2.93-3.50 g, Head 2.33-6.20 g	Vol. 39 M	20-40	Lap	12	0	0	0	0	0
	Sled 5.48-9.95 g, Head 6.59-31.61 g				17	18	0	0	0	0
Zaborowski (1966)	Sled 3.69-8.41 g, Head 5-61º, 5.51-21.16 g	Vol. 52 M	20-43	4-point	39	0	0	0	0	0
	Sled 7.70-11.74 g, Head 15-66º, 9.55-45.41 g				18	26	0	0	0	0
Horsch, et al. (1979)	Sled 10 g, 34-38 km/h Head ±30 g	PMHS 10 M+F	23, >56	2- and 3-point	1	0	3	4	2	0
Bendjellal, et al. (1987)	Sled 6.6-9.2 g, Head 57º, ±18 g	PMHS 11 M	51-66		4	0	0	0	0	0
	Sled 12.2-14.7 g, Head 50-75º, 1588-2526 rad/s^2, 12.5-17.2 g,				6	0	1	0	0	0
Kallieris, et al. (1987)	Car 40, 45, 50, 60 km/h Head 70-90º	PMHS 31 M+F	19-60	3-point	5	15	9	1	0	1
Kallieris, et al. (1990, 1991)	Car 30, 35 km/h, Head 57-80º, 32-39 rad/s, 1610-2601 rad/s^2, 14-18 g	PMHS,3 M 5 F	24-74	3-point	0	0	1	0	1	1
	Car 50 km/h, Head: 27-58º, 8-31 rad/s, 560-1460 rad/s^2, 13-26 g				1	4	0	0	0	0

M = male; F = female

APPENDIX B—COMPARISON OF EuroSID-2 RESPONSE FOR TRIANGULAR- VERSUS RECTANGULAR-SHAPED DECCELERATION PULSES

B.1 INTRODUCTION.

The initial series of sled tests were conducted using a triangular-shaped pulse with a 19 g peak, 130-ms duration and a 44-km/hr velocity change. The facility at the Medical College of Wisconsin (MCW) is an impact-with-rebound sled that produces rectangular-shaped deceleration pulses. Computer simulations of the rigid-seat configuration used in the initial tests were conducted with rectangular pulses at 7.2 and 18.2 g and produced results that bracketed the predicted 16-g triangular pulse response. To emulate the 16-g inertial loading during the first rigid-seat series at MCW, a 100-ms duration rectangular pulse was chosen that had approximately the same velocity change (45 km/hr) as the initial test pulse and an average acceleration of 12.5 g.

The second series of tests planned at MCW were intended to emulate the tests described in the Civil Aerospace Medical Institute (CAMI) EuroSID (ES-2) report (DeWeese, et al., 2007). Some of these test configurations produced much higher neck loads than had been observed during the first series at MCW. The CAMI tests used the triangular deceleration pulse defined by the Federal Aviation Administration (FAA) in Title 14 Code of Federal Regulations (CFR) 25.562. The test pulse proposed for use in this second test series at MCW was the same 12.5-g pulse that had been used for the first series. An evaluation was necessary to determine if tests using this rectangular pulse would produce similar results to the triangular pulse tests.

B.2 COMPARISON TEST DESCRIPTION.

The CAMI sled test facility has the capability to produce rectangular and triangular pulses. Therefore, tests were conducted at CAMI to quantify the effect of pulse shape on the response of an ES-2 side-facing anthropomorphic test dummy (ATD). The test configuration chosen for comparison was the armrest configuration, as described in the CAMI ES-2 report that had been selected for the next series of tests at MCW. The series of tests described in that report were conducted using deceleration pulses meeting the 16-g, 48.3-km/hr, 180-ms duration triangular pulse specified in 14 CFR 25.562. The rectangular pulse chosen for comparison was the 12.5-g, 45-km/hr, 100-ms duration used by MCW for tests FAA next sled cadaver (FNSC) 102 through FAA next sled dummy (FNSD) 105. Two tests that were virtually identical in setup were used for the comparison. CAMI sled test A05-075 was conducted using the triangular pulse, and test A06-003 was conducted with the rectangular pulse. Figure B-1 shows the test configuration used.

Figure B-1. Sled Setup for Rectangular and Triangular Pulse Response Evaluations

B.3 TEST RESULTS.

B.3.1 DATA ACQUISITION AND PROCESSING.

Test data was gathered and processed as outlined in the CAMI ES-2 report. Head angular velocity and acceleration were derived using a Nine Accelerometer Package. Occupant position data was derived using a two-dimensional (2-D) planar photometric technique per SAE J211/2 rather than the three-dimensional (3-D) method used for the MCW tests. The absolute accuracy of the position data derived by the 2-D method is limited since this technique cannot compensate for scaling factor changes as the head rotates out of the initial plane of motion. Also, since one of the two targets required to calculate head angle was obscured during portions of each test, the values for head angle derived during those periods should be considered only an estimate.

B.3.2 DATA SUMMARY.

Table B-1 provides the same selected measured parameters and calculated injury criteria for the compared tests as those provided for the tests cited in the CAMI ES-2 report. Table B-2 provides a summary of the same calculated potential injury criteria for the compared tests as those used for PMHS and ATD evaluation. Comparison graphs of selected parameters are provided in figures B-2 through B-18. Initial examination of the data revealed that a consistent phase shift was present in all signals. To facilitate comparison, the data from test A05075 was time shifted (27 ms) to match the phase between the two tests in figures B-3 through B-18.

Table B-1. Selected Measured Parameters and Calculated Injury Criteria

Test Parameter	Criteria Limit	Test Number		% Difference
		A05075	A06003	
Pulse shape		Triangle	Square	
Impact velocity (km/hr)		49.4	45.6	-7.8
Impact acceleration (g)		-17.1	-13.3	-22.2
HIC after contact	1000	294	115	-60.8
HIC15	700	735	424	-42.4
TTI (g)	85	38	36	-5.1
V*C (m/s)	1.0	0.0	0.0	0.0
Pelvis Ay (g)	130	26	35	35.9
Upper rib deflection (mm)	35 - 44	0	0	0.0
Middle rib deflection (mm)	35 - 44	0	0	0.0
Lower rib deflection (mm)	35 - 44	4	2	-54.7
T12 Ay (g)	82	32	33	4.6
Front abdominal Fy (N)	2400-2800 total	449	423	-5.8
Mid abdominal Fy (N)	2400-2800 total	588	437	-25.7
Rear abdominal Fy (N)	2400-2800 total	421	344	-18.3
Pubic Fy (N)	6000	1770	-	-
T1 Ay (g)		48.3	44.7	-7.6
N_{ij} (preliminary lateral)	1.0	1.47	1.37	-6.8
Upper-neck shear Fy (N)		920	776	-15.6
Upper-neck tension Fz (N)	4170	3508	2709	-22.8
Upper-neck moment Mx (N-m)		75	68	-9.8
Lower-neck shear Fy (N)		2992	2554	-14.6
Lower-neck tension Fz (N)		3470	2802	-19.3
Lower-neck moment Mx (N-m)		277	257	-7.3

Table B-1. Selected Measured Parameters and Calculated Injury Criteria (Continued)

Test Parameter	Criteria Limit	Test Number		% Difference
		A05075	A06003	
Head excursion (mm)		636	639	0.4
Head lateral angle with regard to T1 (degree)		-122	-108	-11.4
T1 lateral angle (degree)		-46	-43	-7.2
Upper-shoulder belt tension (N)	7785	6801	5988	-12.0
Lower-shoulder belt tension (N)		4427	3835	-13.4
Shoulder belt payout (mm)		22.9	15.2	-33.3
Right lap belt tension (N)		6232	6407	2.8
Left lap belt tension (N)		-	-	-
Femur Mz (N-m)		-	5536	-
Back plate Fy (N)		3217	2083	-35.2
Arm rest Fy (N)		12124	10266	-15.3
Arm rest Fz (N)		3772	3456	-8.4

Ay =Acceleration in y direction
T1 = Thoracal vertebra 1
HIC = Head injury criteria
Fz = Tension force
TTI = Thoracic trauma index
N = Newton
Mx = Bending moment
Fy = Force in y direction
V*C = Viscous criterion

Table B-2. Potential Injury Criteria

Test Parameter/Injury Criteria	Test Number		% Difference
	A05075	A06003	
Pulse shape	Triangle	Square	
Restraint	Standard	Standard	
Velocity change (Km/hr)	-51.1	-48.0	-6.0
Impact acceleration (peak or plateau) (g)	-17.1	-13.3	-22.2
Relative energy $(m/s)^2$	100.9	89.1	-11.7
Head rotation angle with regard to T1 (deg)	-121.9	-108.0	-11.4
Angular velocity (rad/s)	-82.5	-83.0	0.6
Angular acceleration (rad/s^2)	-4420.0	-4110.0	-7.0
Head linear acceleration (g)	80	63	-21.4
Upper-neck moment Mx (Nm)	75	68	-9.8
Upper-neck tension Fz (N)	3508	2709	-22.8
Upper-neck shear Fy (N)	920	776	-15.6

Fz = Tension force
N = Newton
Mx = Bending moment
V*C = Viscous criterion
Fy = Force in y direction

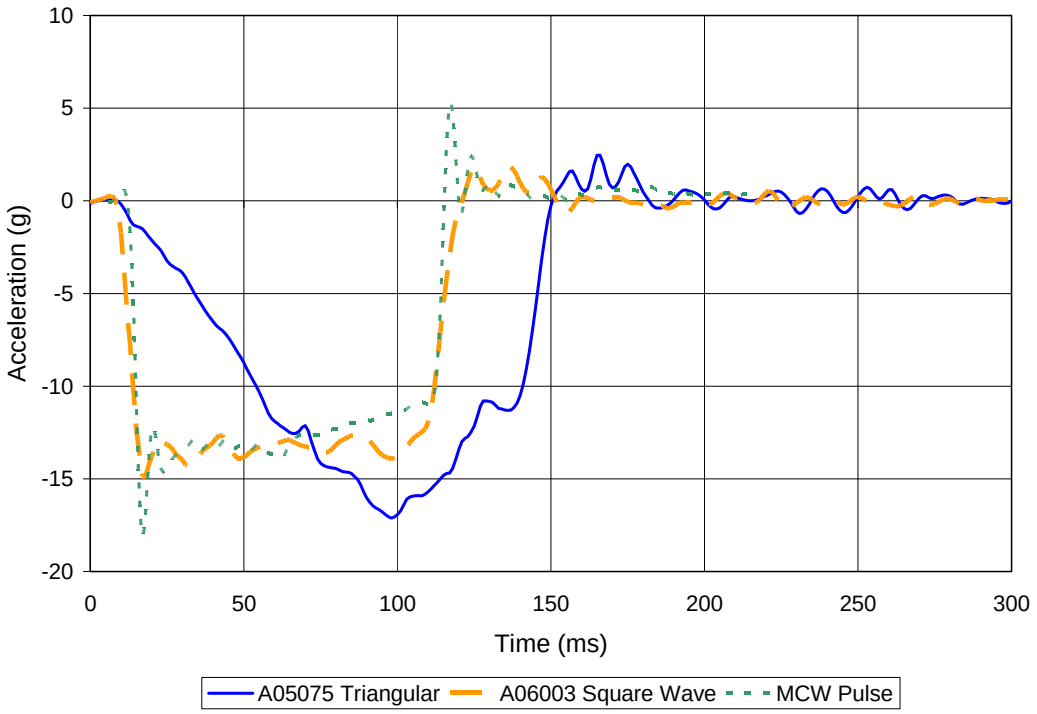

Figure B-2. Sled Acceleration (Ax)

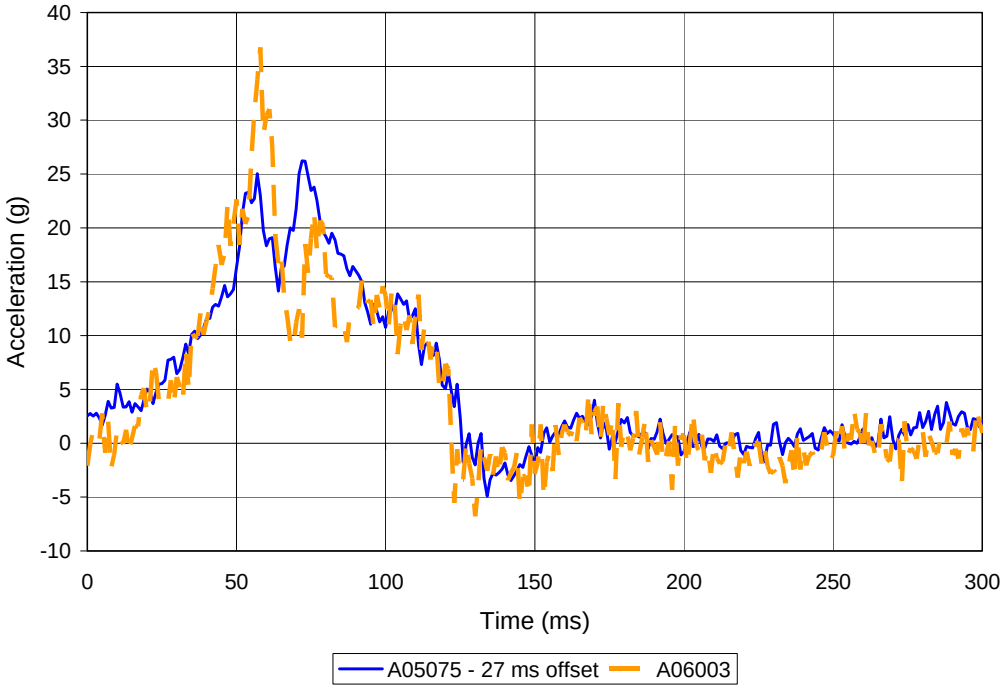

Figure B-3. Pelvis Acceleration (Ay)

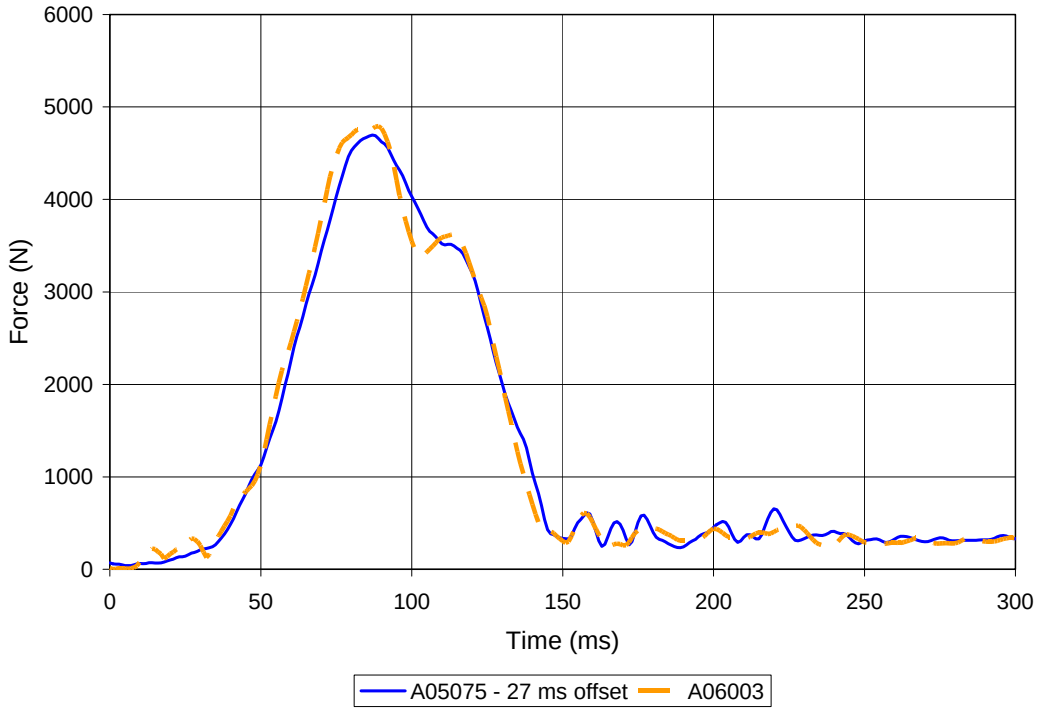

Figure B-4. Lap Belt Force

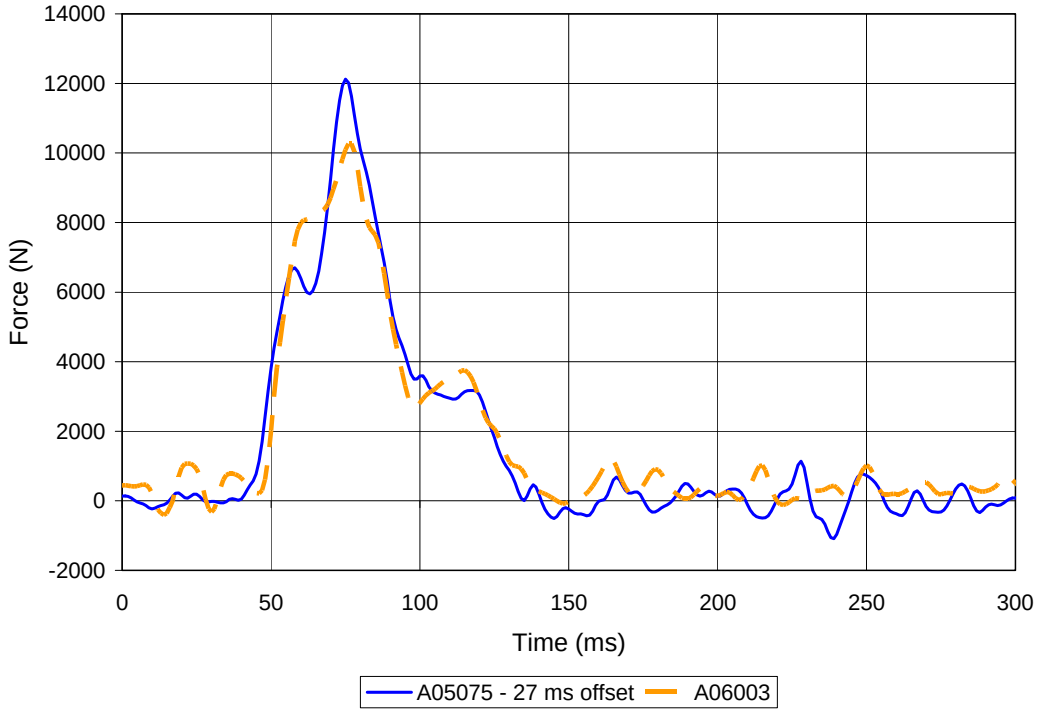

Figure B-5. Arm Rest Lateral Force

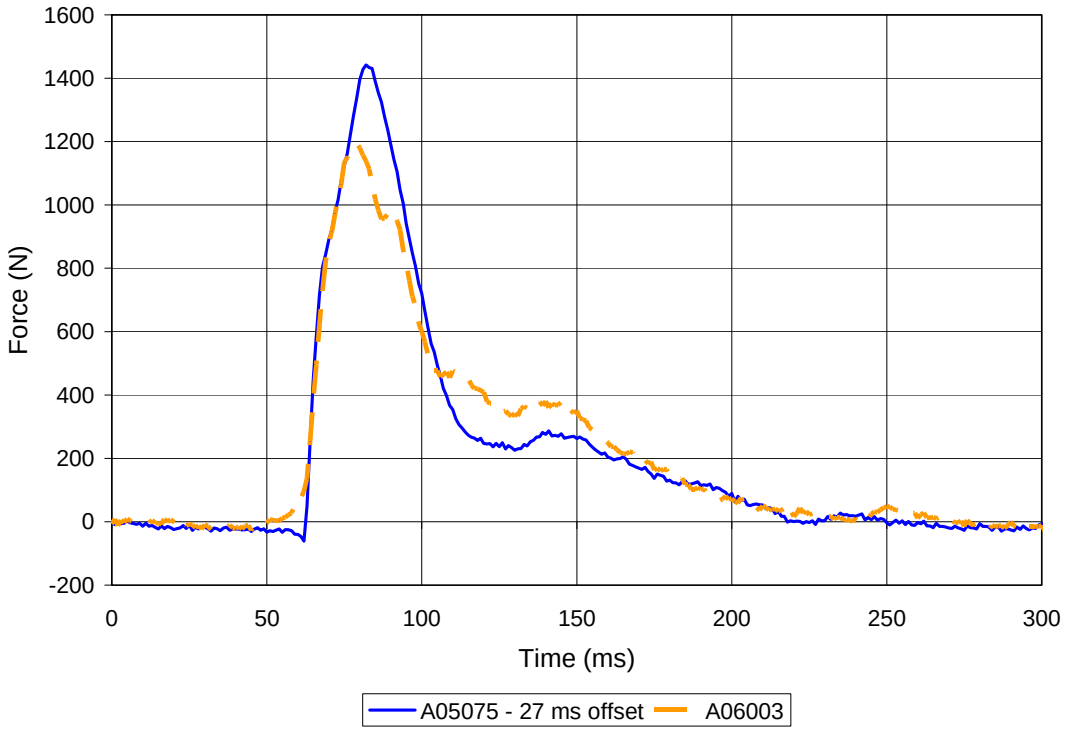

Figure B-6. Abdominal Force Sum

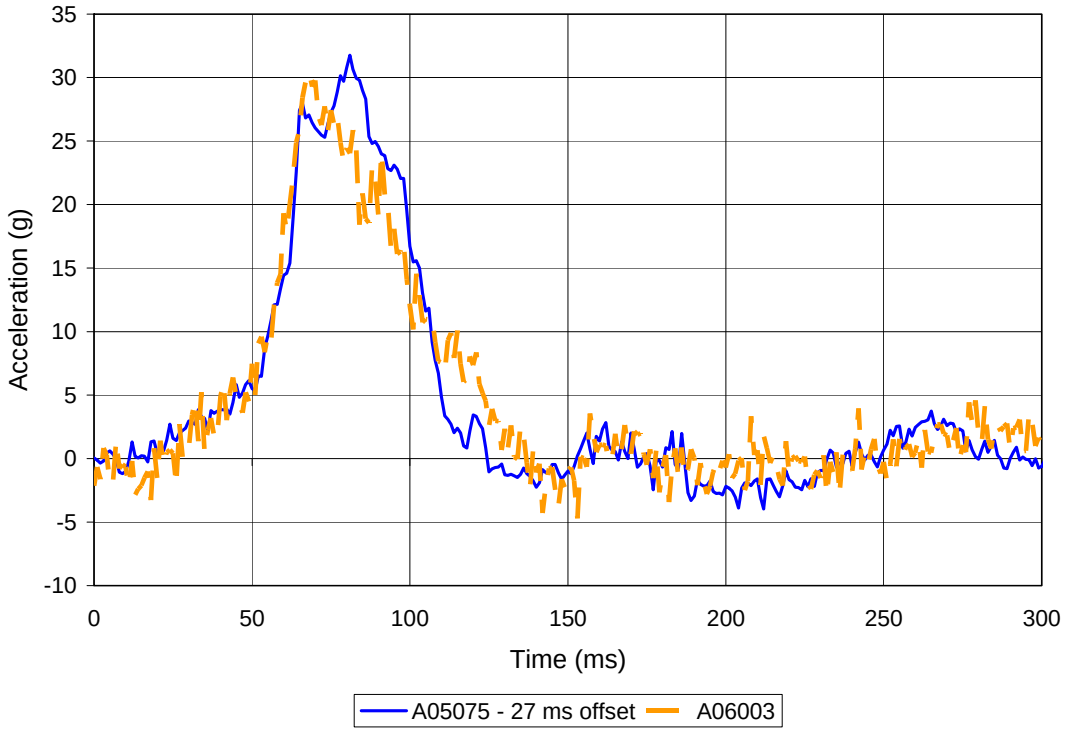

Figure B-7. Thoracic T12 Acceleration (Ay)

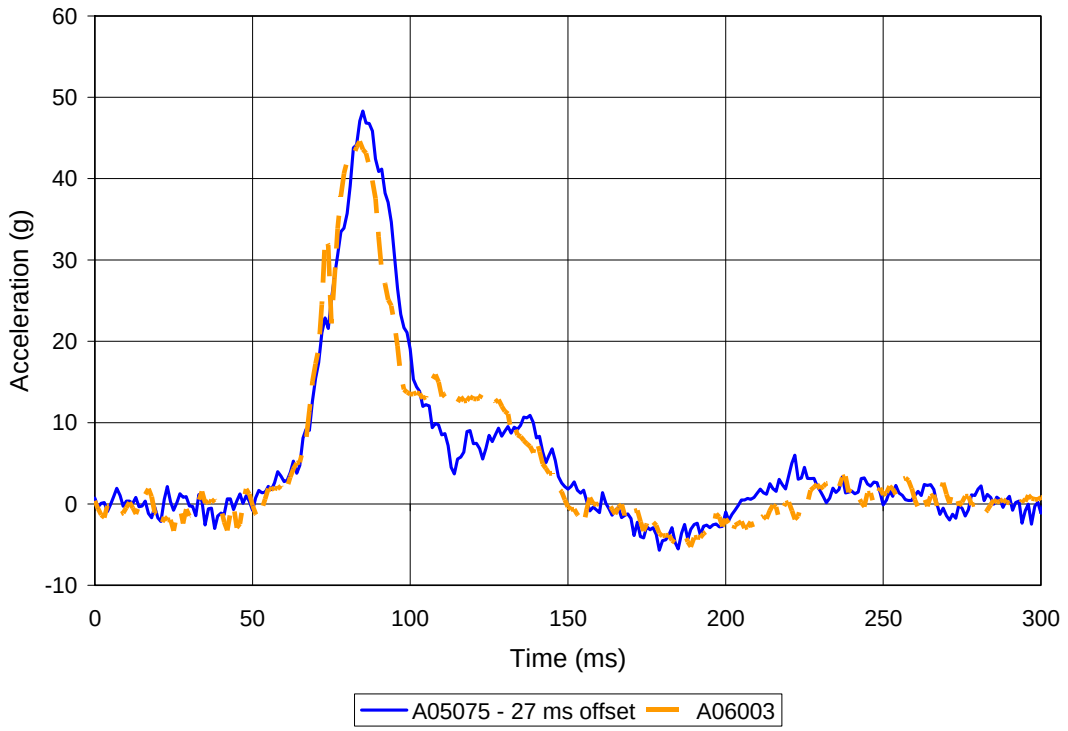

Figure B-8. Thoracic T1 Acceleration (Ay)

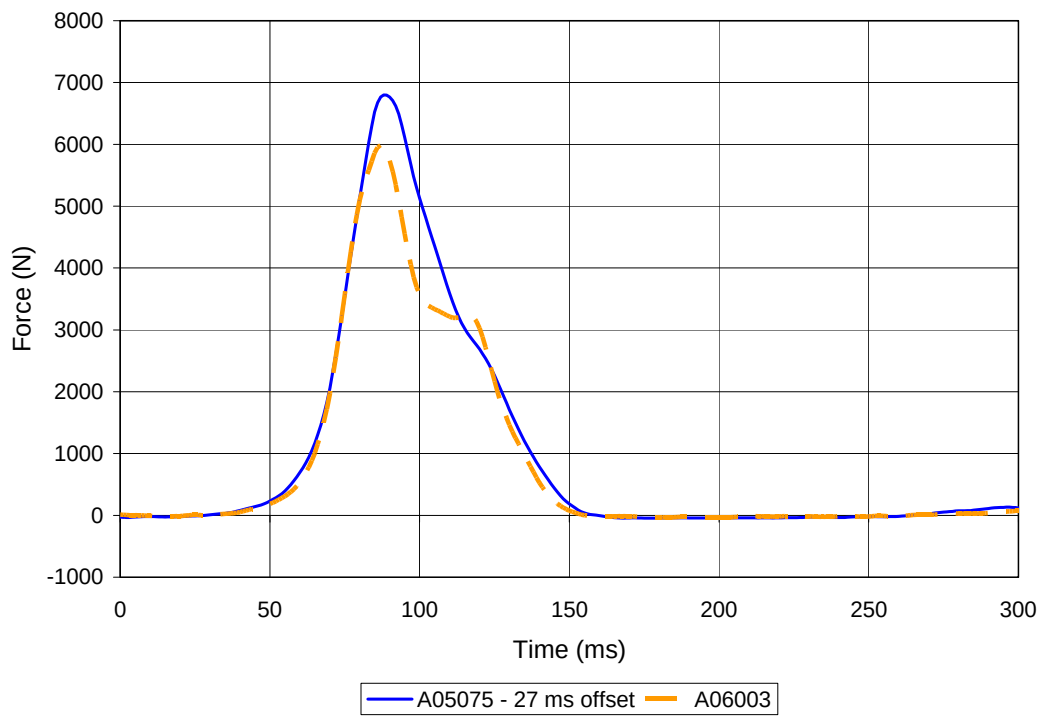

Figure B-9. Upper-Shoulder Belt Tension

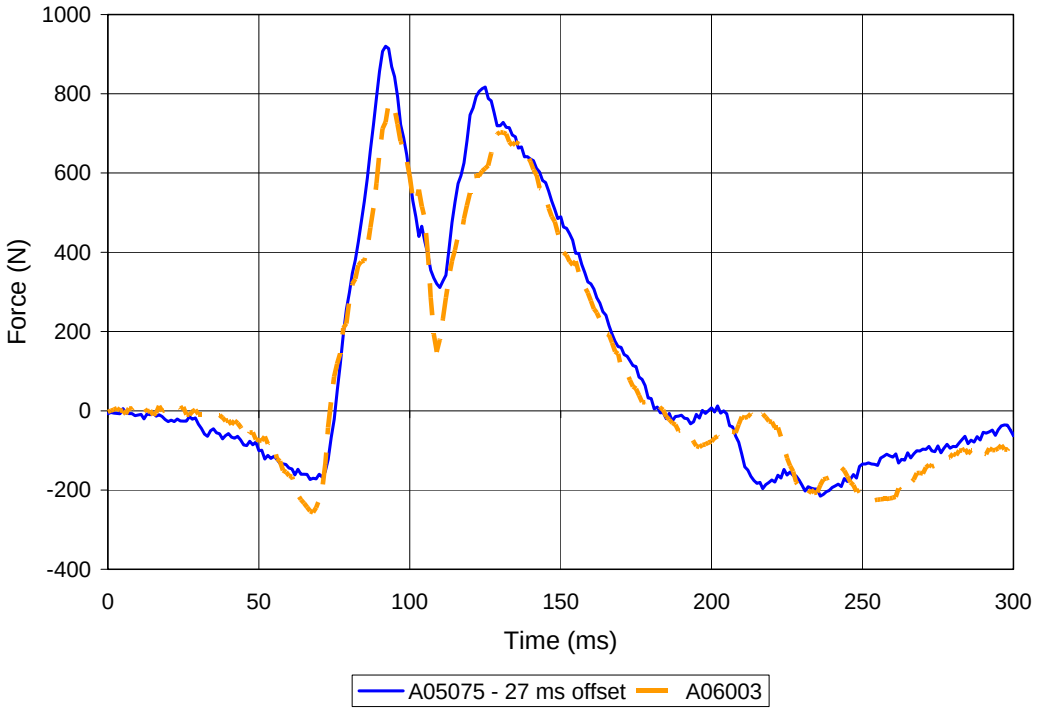

Figure B-10. Upper-Neck Force (Fy)

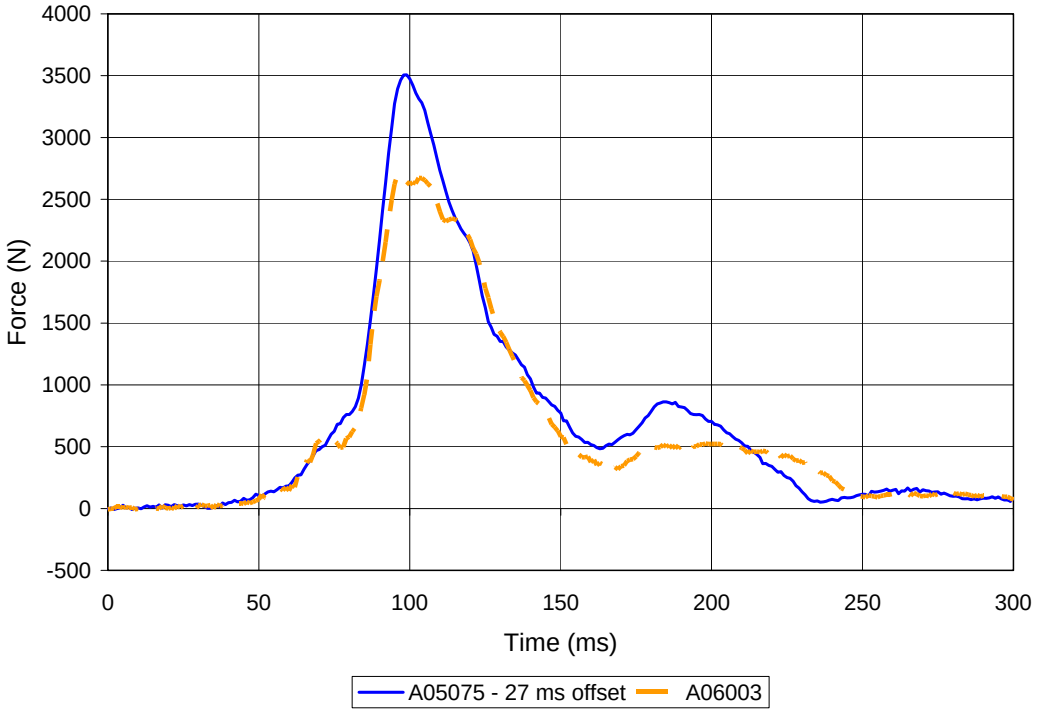

Figure B-11. Upper-Neck Force (Fz)

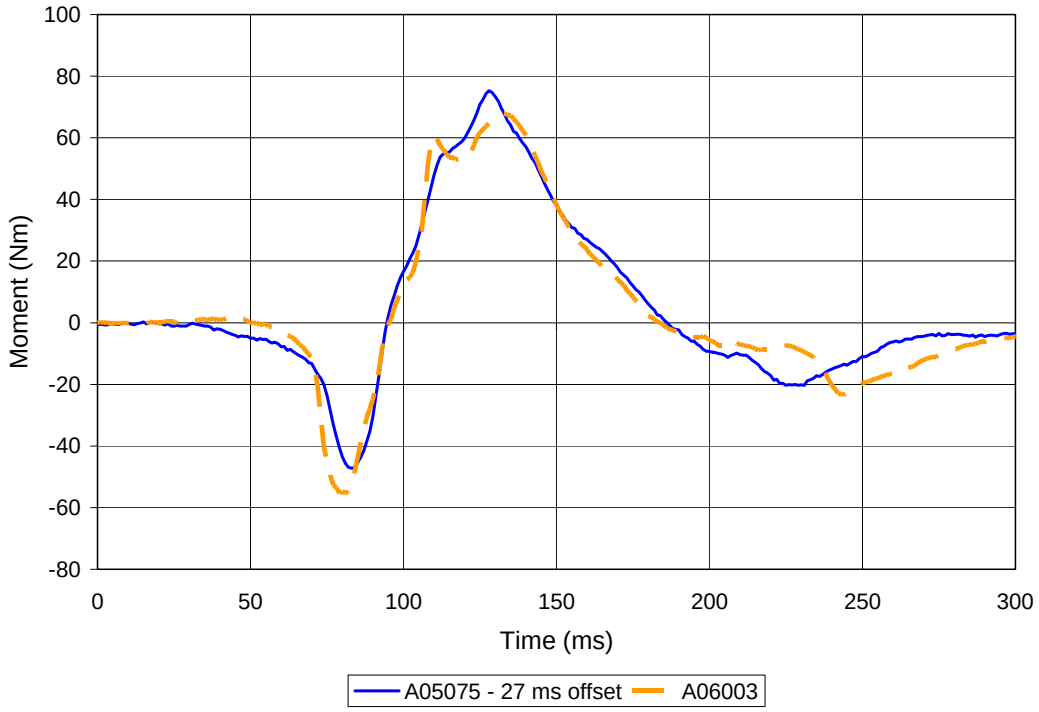

Figure B-12. Upper-Neck Moment (Mx)

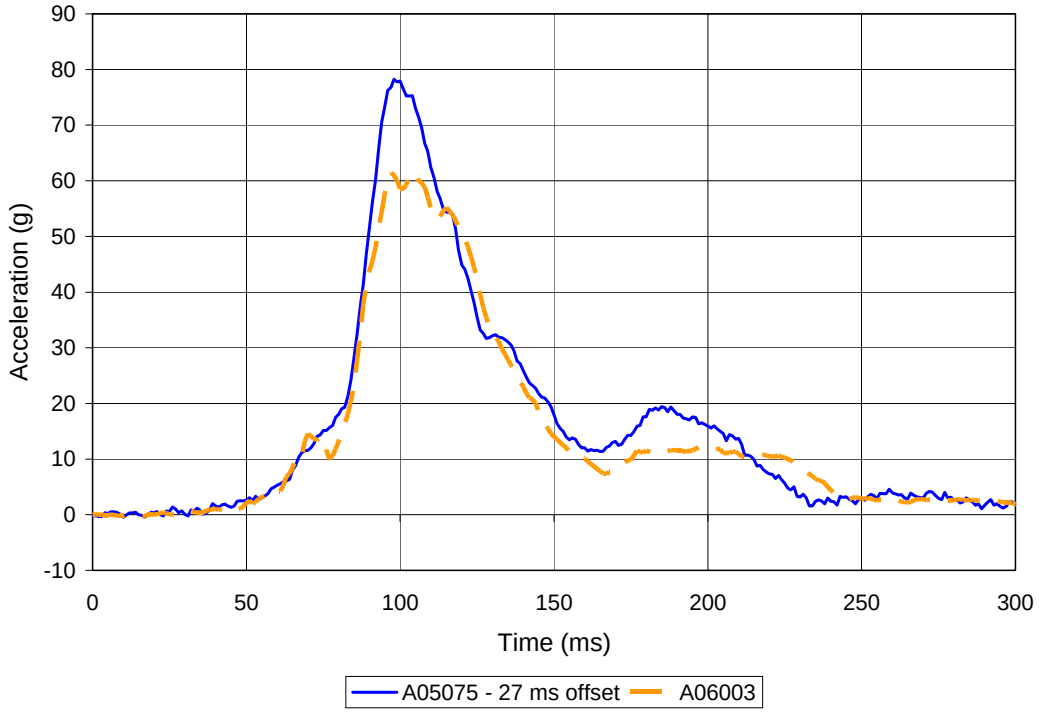

Figure B-13. Head Acceleration (Az0)

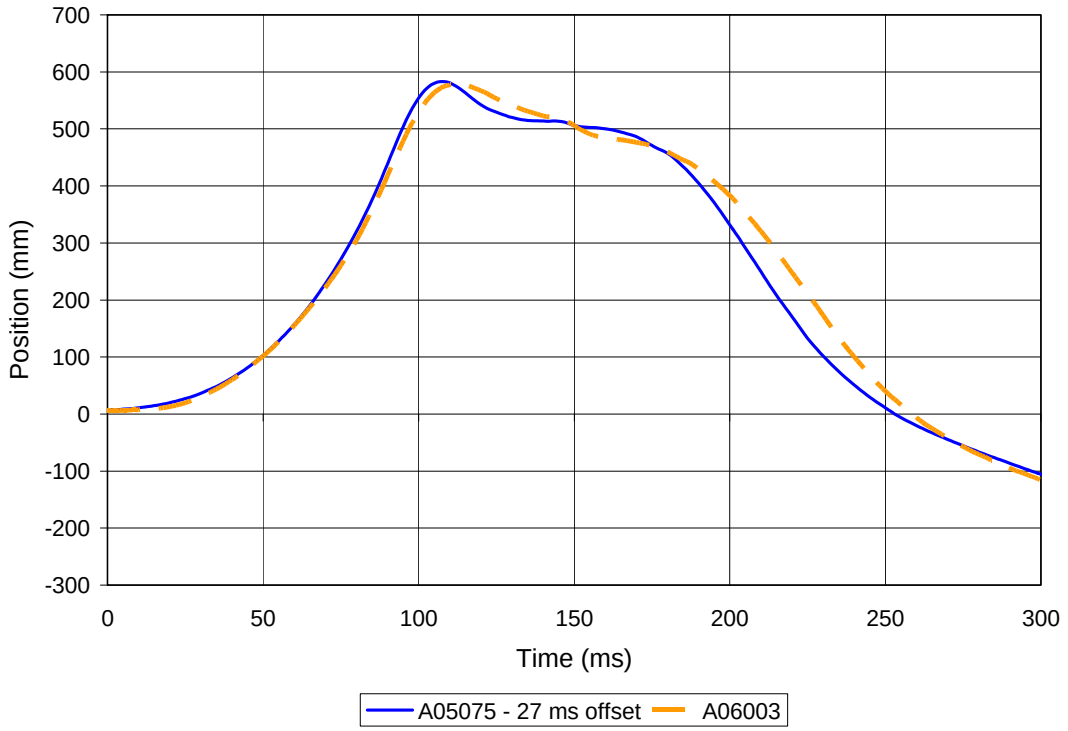

Figure B-14. Head X Position

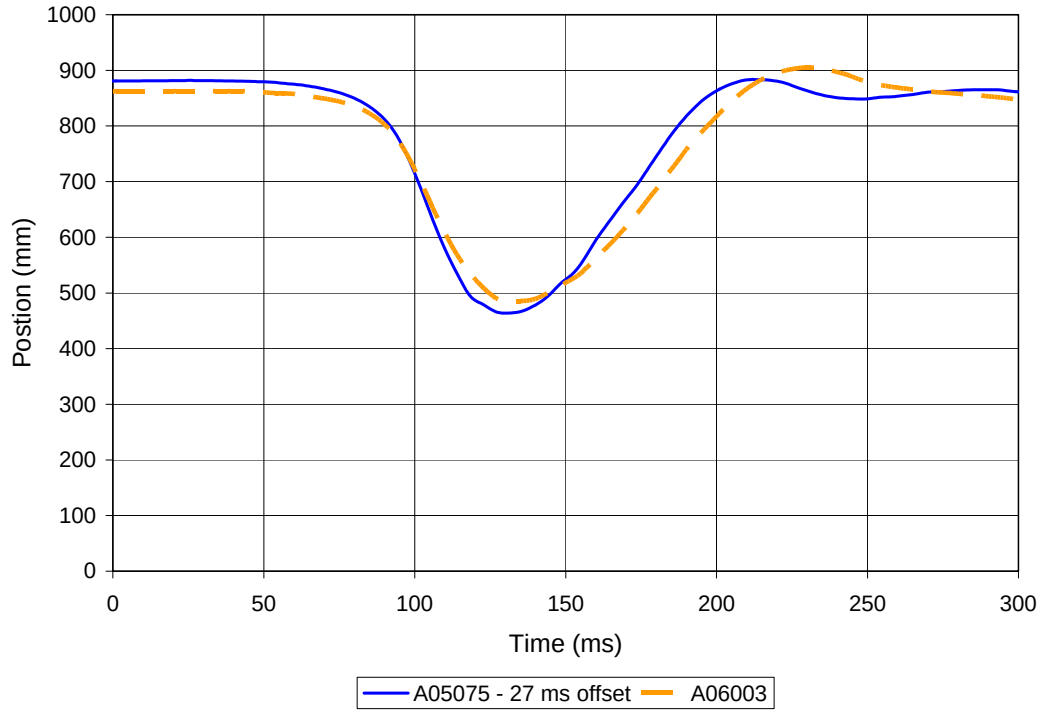

Figure B-15. Head Z Position

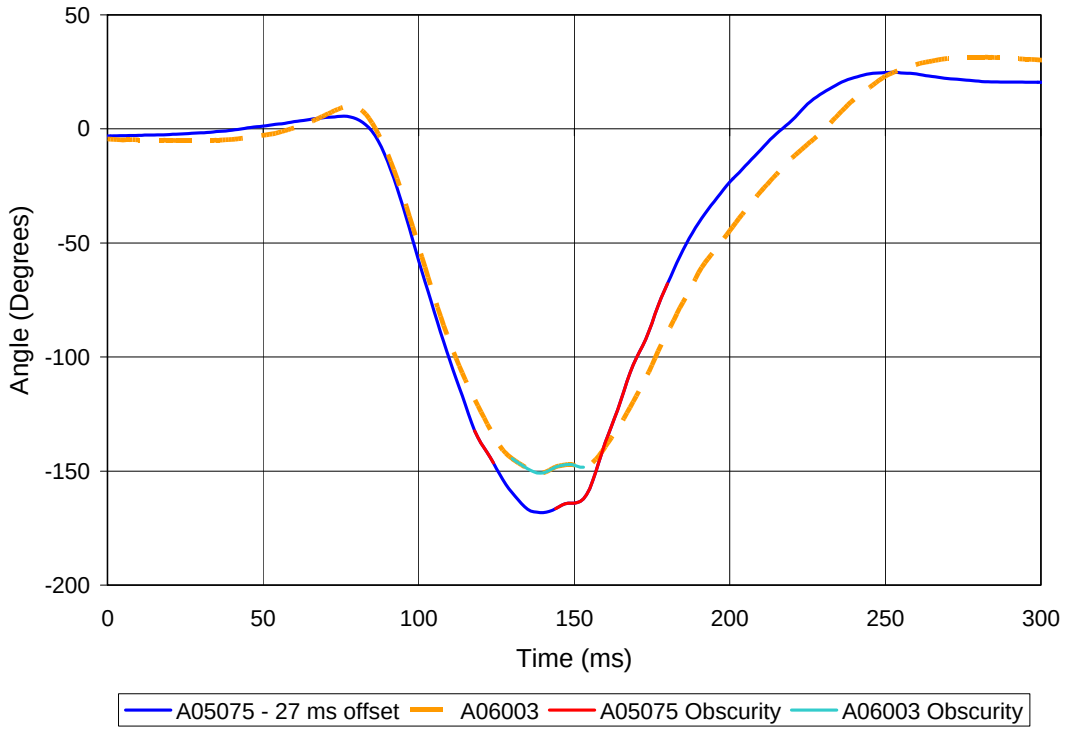

Figure B-16. Head Absolute Lateral Flexion Angle in Sled X-Z Plane

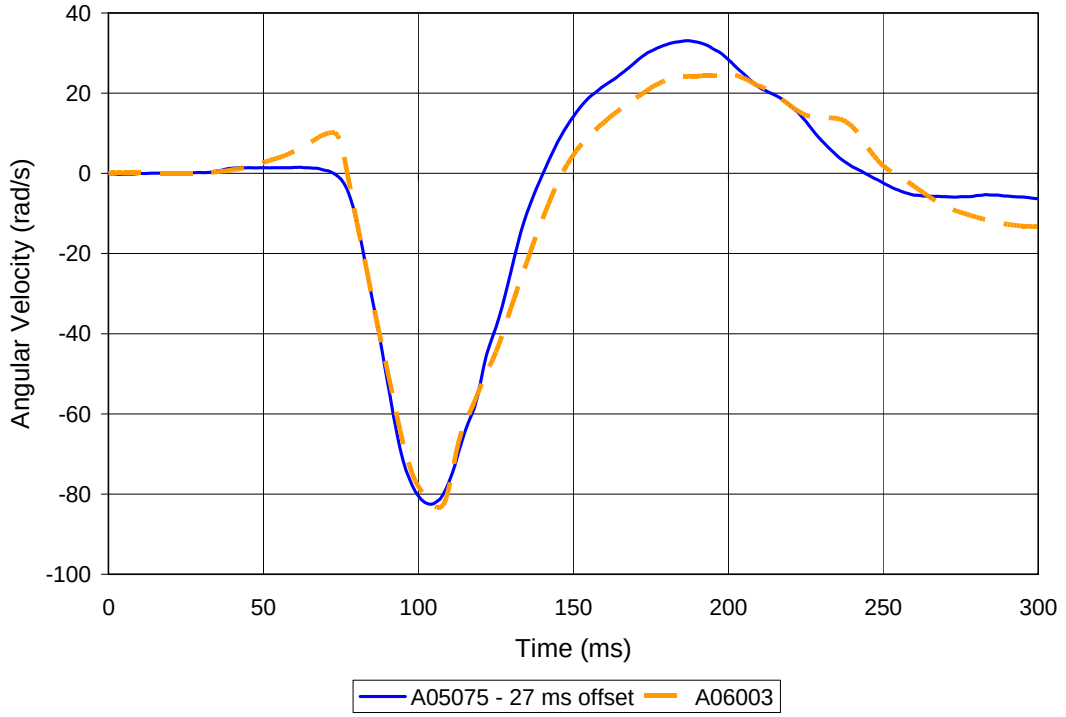

Figure B-17. Head Angular Velocity About Head X Axis

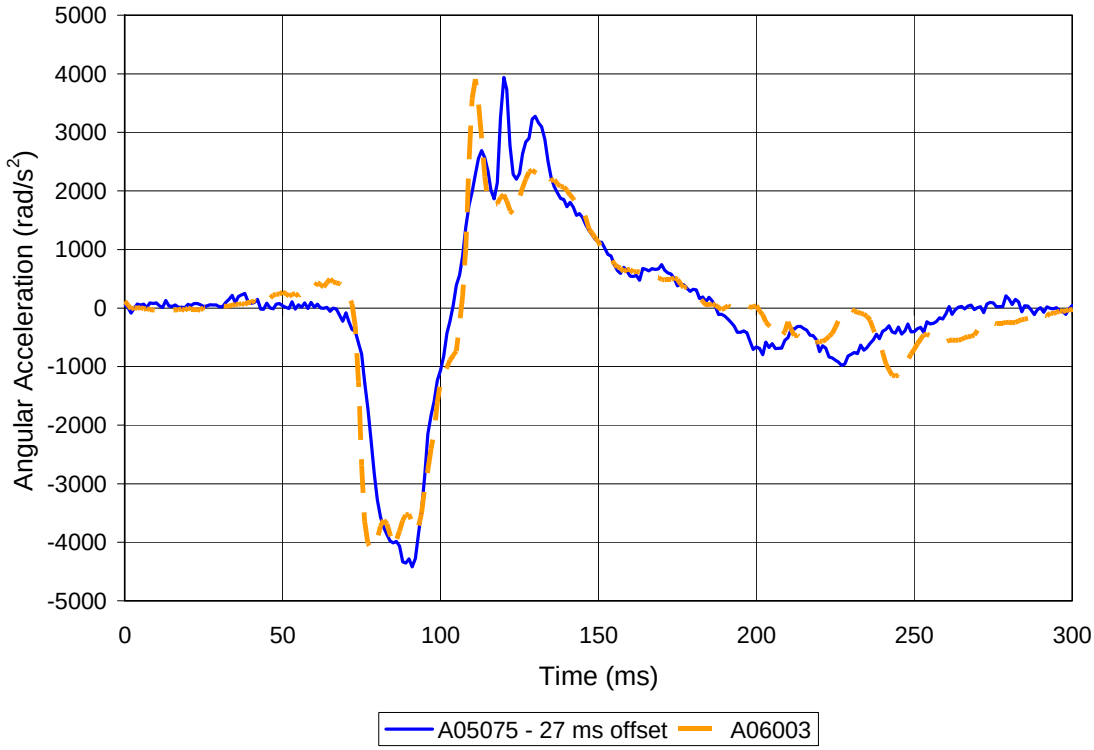

Figure B-18. Head Angular Acceleration About Head X Axis

B.3.3 Observations.

- As shown in figure B-2, the rectangular pulse produced at CAMI is similar to the MCW pulse.

- The impact velocity of the two test conditions was not identical; the triangular pulse was 6 km/hr faster. This represents a 12% difference in energy, which could account for some of the differences in the results.

- The phase response of all ATD signals in the rectangular pulse test led the response of the triangular pulse signals by 27 milliseconds. This was consistent for all locations in the ATD regardless of the degree of coupling to the sled. This suggests the existence of a generalized transfer function between rectangular and triangular pulse tests.

- In general, the ATD accelerations, velocities, and kinematics agreed well between the two tests. A significant exception was the head vertical acceleration, which was less in the rectangular pulse test. The magnitude in this case was related to the peak sled deceleration difference and occurred when the head Z axis was aligned with the sled deceleration vector. Another exception was the pelvis acceleration, which had a higher initial peak in the rectangular pulse test. This result is converse to the trend noted in the other signals and is likely caused by an increase in the velocity of pelvis contact with the arm rest during in the rectangular pulse test. Of note was that upper-neck lateral bending

moment and the head lateral angle with respect to thoracal vertebra 1 (T1) were both about 10% less in the rectangular pulse test. The consistent difference of these two responses should be expected since the bending moment is a function of the neck bending stiffness.

- Almost all measured forces were between 12% and 23% lower for the rectangular pulse test compared to the triangular pulse test. Previous research has shown that ATD peak loads are related to peak sled deceleration. That relationship for each instrument location is dependent on the alignment of the load cell, and the degree of coupling to the sled. In general, most of the differences in measured forces between these tests can be attributed to the peak sled deceleration difference of 22%. One force measurement that did not follow this trend was the right lap belt load, which was in good agreement between the two tests. The tested lap belt configuration provides good coupling between the pelvis and the sled because the left belt wraps around the left side of the occupant and anchors at the seat centerline. Typically, items of mass that are well coupled to the sled produce reaction forces proportional to the sled deceleration. It is not clear why this force did not follow the change in sled deceleration, as the other force signals did. One possibility is that the increase in pelvis lateral velocity that resulted in higher pelvis acceleration could cause higher belt loading as well.

B.4 CONCLUSIONS.

When comparing the measured parameters that have the greatest affect on lateral neck response, (thoracic 1 acceleration, upper-neck forces and moments, head linear and rotational acceleration, and head excursion), the results of the two tests were either similar or the difference could be clearly related to the difference in sled acceleration magnitude. Therefore, for the purposes of neck injury research using this test configuration (i.e., EuroSID-2 test dummy occupying a side-facing couch with armrest end closure and a three-point, body-centered restraint system), sled tests with a 16-g, triangular-shaped deceleration pulse can be emulated by tests with a rectangular pulse having a 12.5-g plateau and a similar velocity change.

B.5 BIBLIOGRAPHY.

DeWeese, R., D. Moorcroft, T. Green, and M. Philippens, 2007, “Assesment of Injury Potential in Aircraft Side-Facing Seats Using the ES-2 Anthropometric Test Dummy,” Office of Aerospace Medicine, DOT/FAA/AM-07/13, Washington, DC 20591.

APPENDIX C—POSTMORTEM HUMAN SUBJECT AND EuroSID-2 RESPONSE TIME HISTORIES FOR THE RIGID-SEAT CONFIGURATION

This appendix presents the response of the postmortem human subject (PMHS) and EuroSID-2 (ES-2) in the sled tests performed at the Medical College of Wisconsin. Time histories of various parameters are presented in figures C-1 to C-33. Note that the load parameters for the PMHS are only valid for the initial phase where the head has no contact with any surrounding structure. The contact times are listed in table C-1.

Table C-1. The PMHS Head Contact Times for the Rigid-Seat Test Configuration

Test	FNSC 102	FNSC 104	FNSC 118	FNSC 126
Contact Time (ms)	62	65	52	56

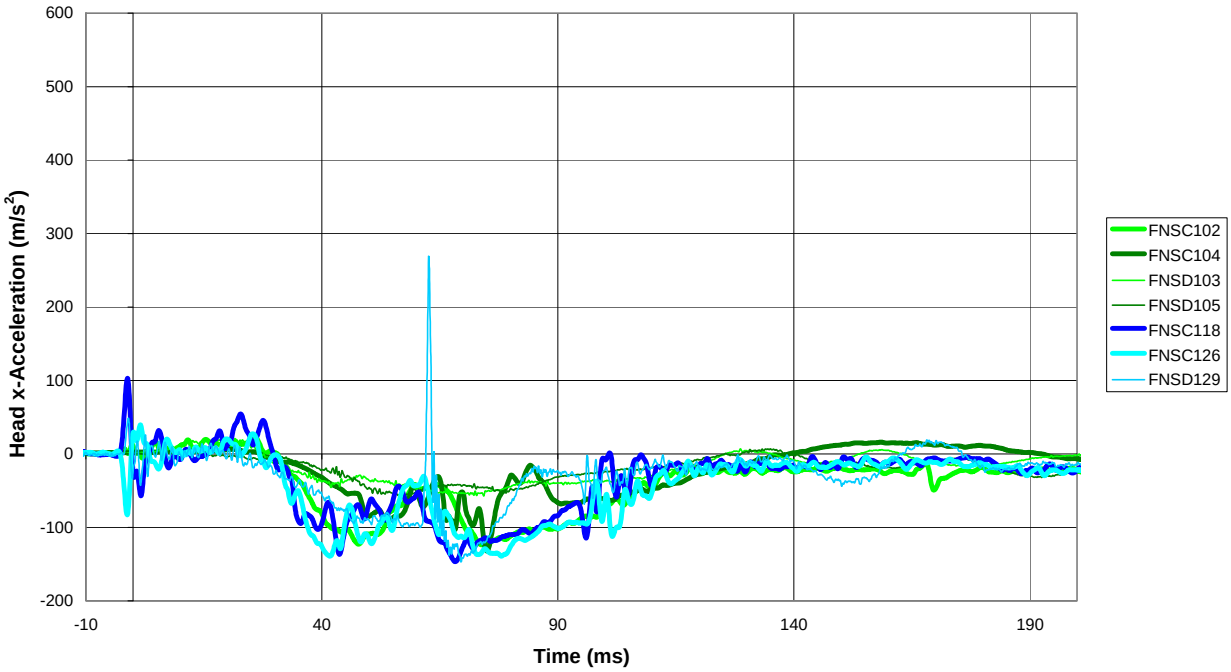

Figure C-1. Head Linear x-Acceleration

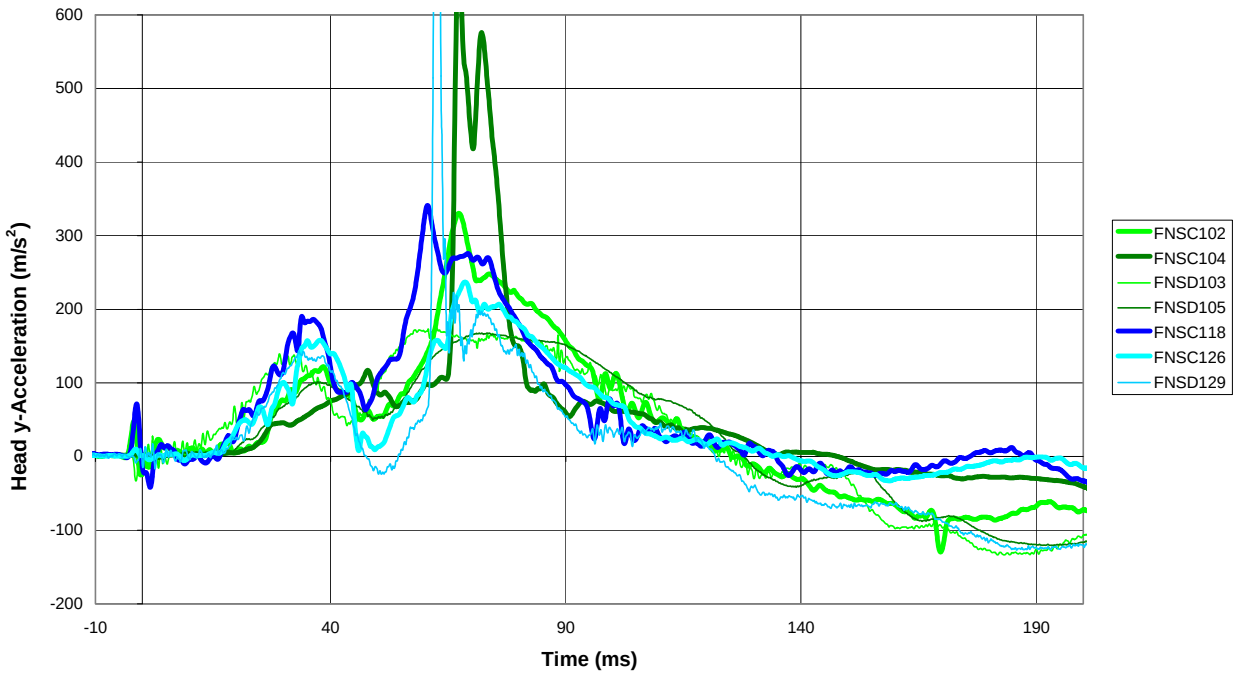

Figure C-2. Head Linear y-Acceleration

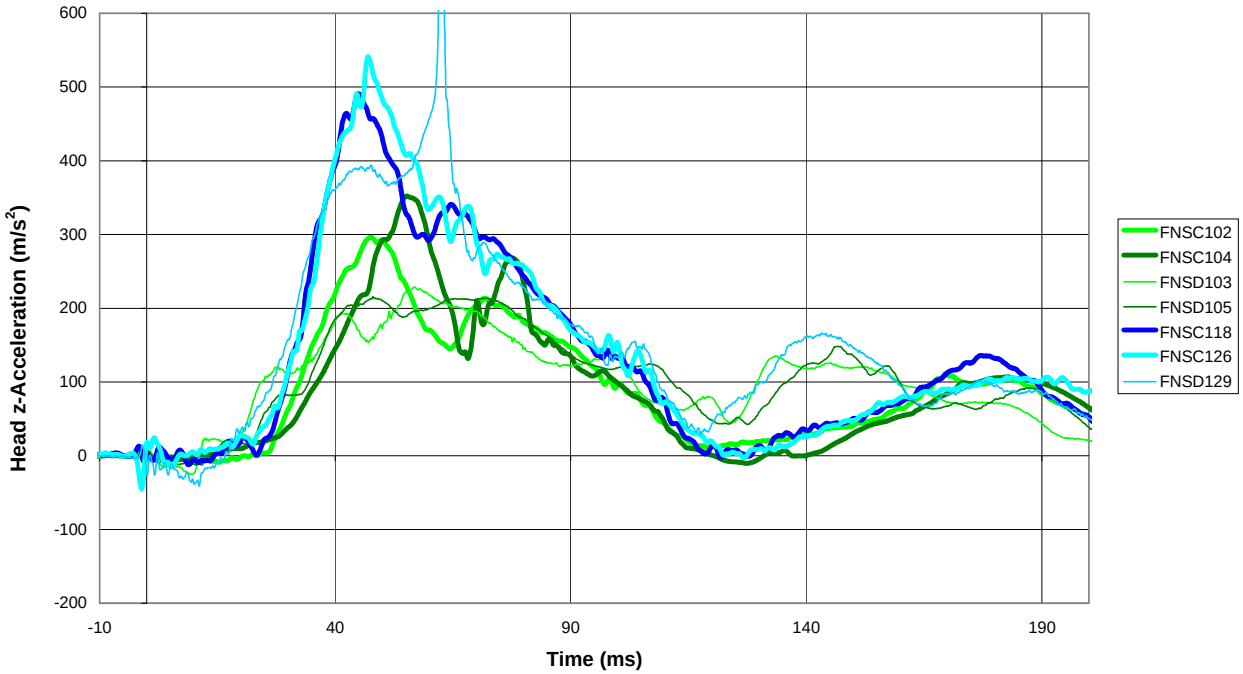

Figure C-3. Head Linear z-Acceleration

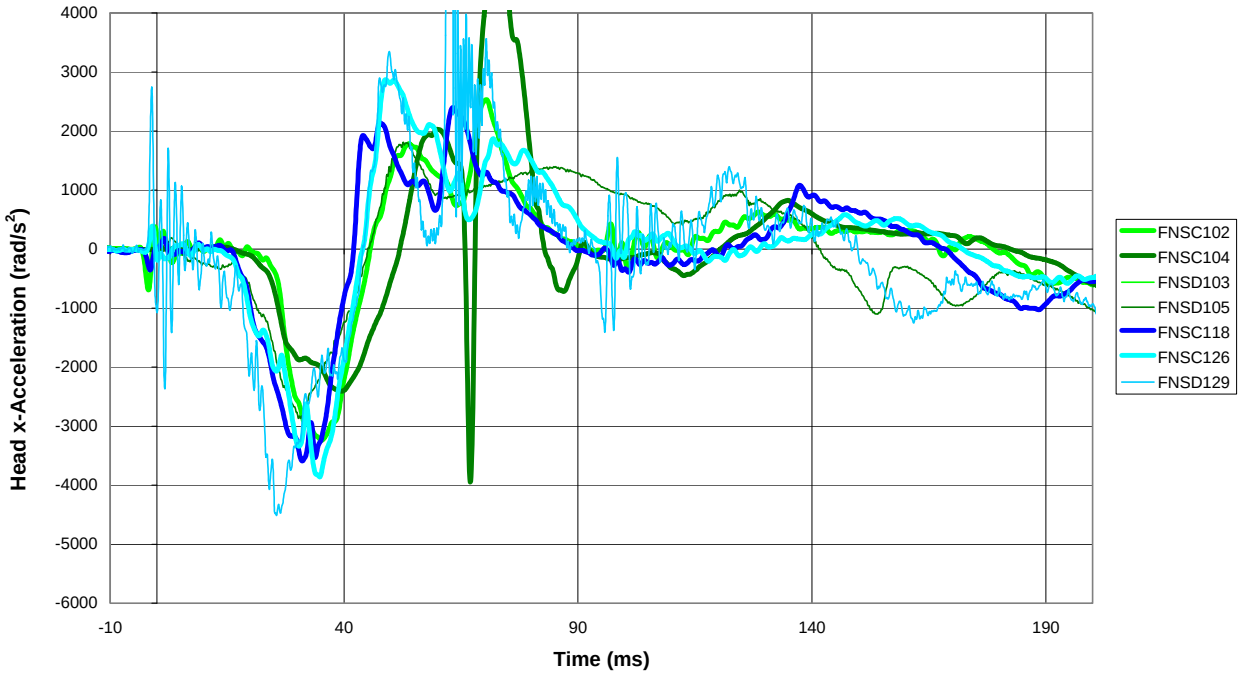

Figure C-4. Head Angular x-Acceleration

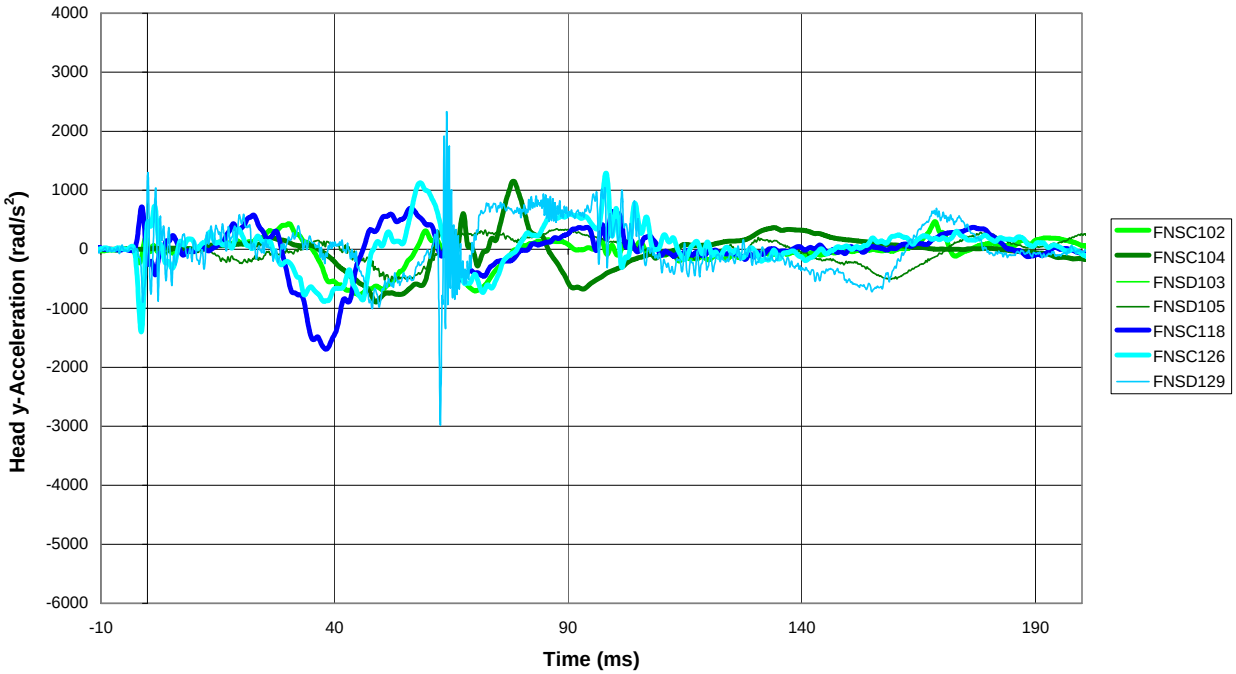

Figure C-5. Head Angular y-Acceleration

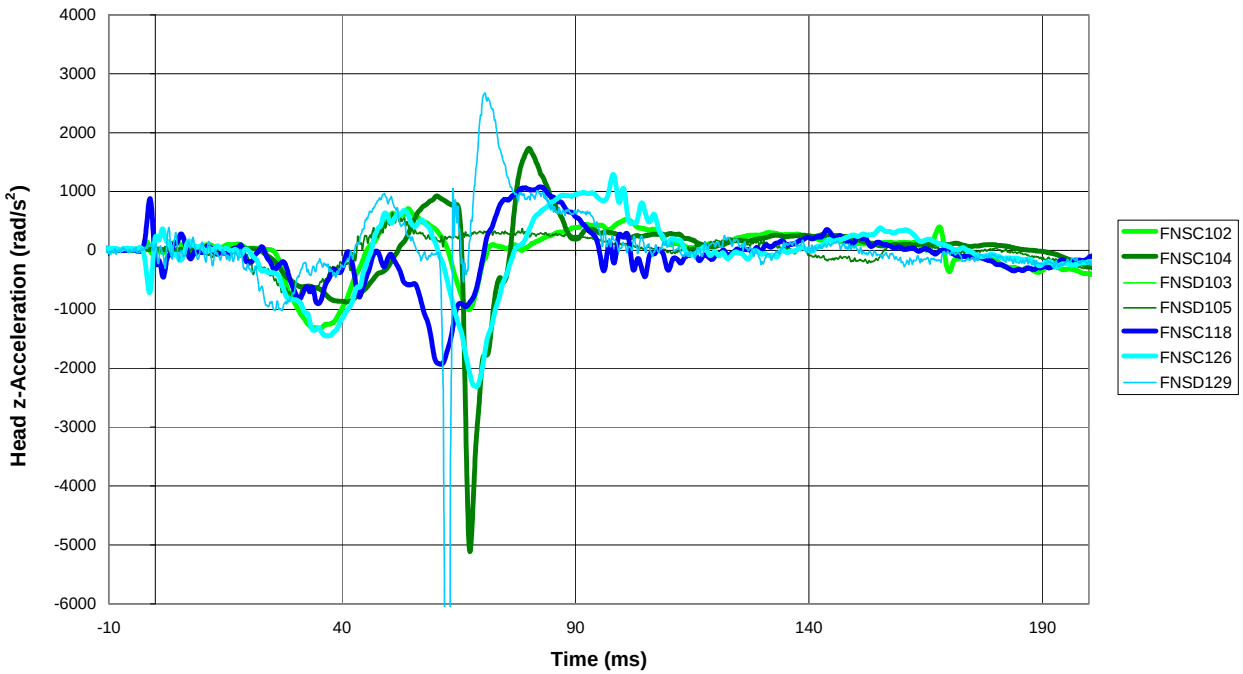

Figure C-6. Head Angular z-Acceleration

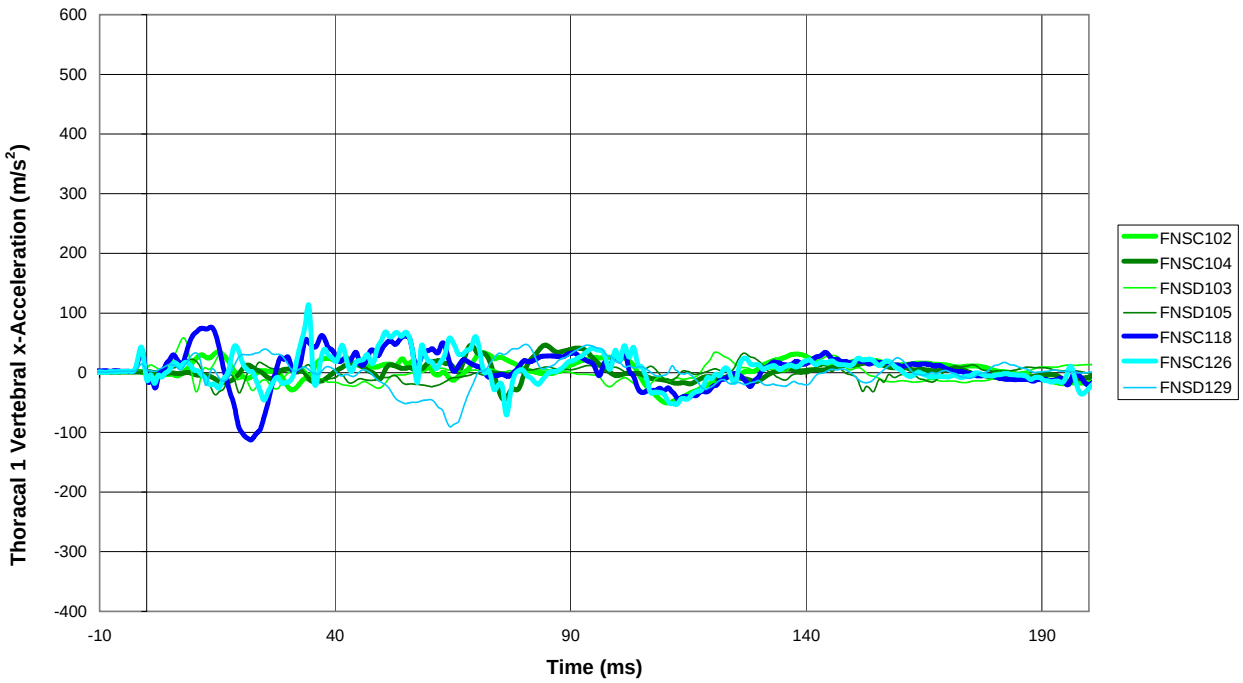

Figure C-7. The Thoracal 1 Linear x-Acceleration

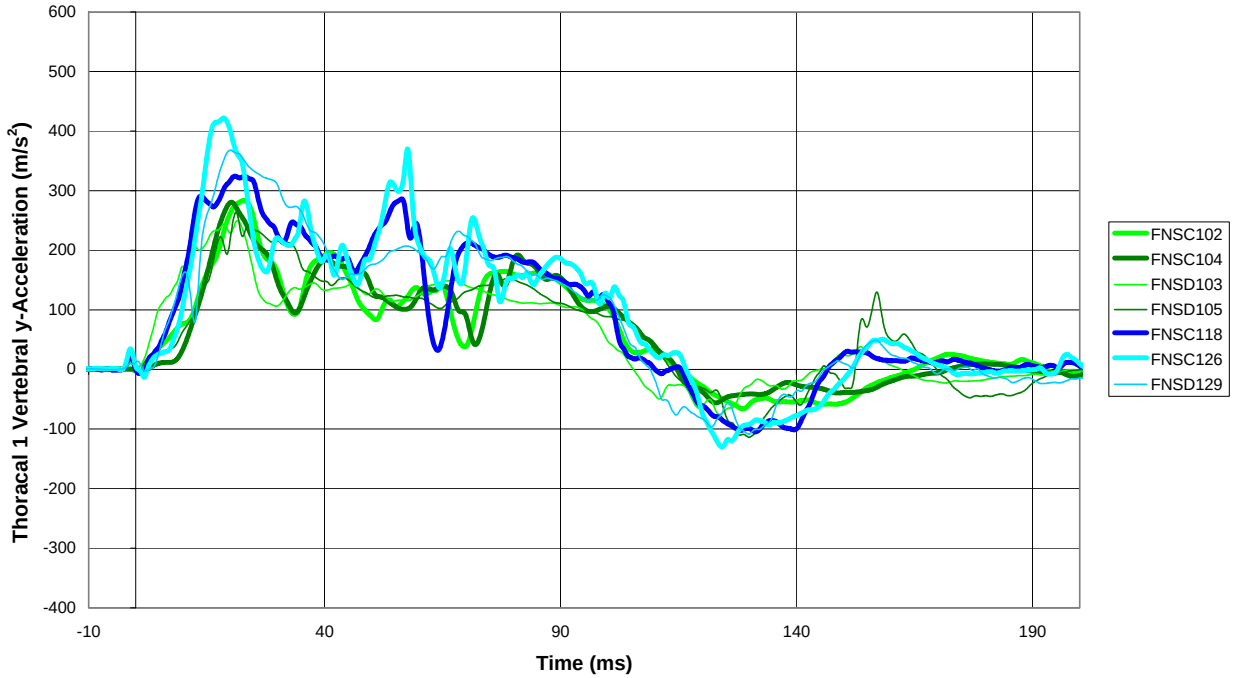

Figure C-8. The Thoracal 1 Vertebrae Linear y-Acceleration

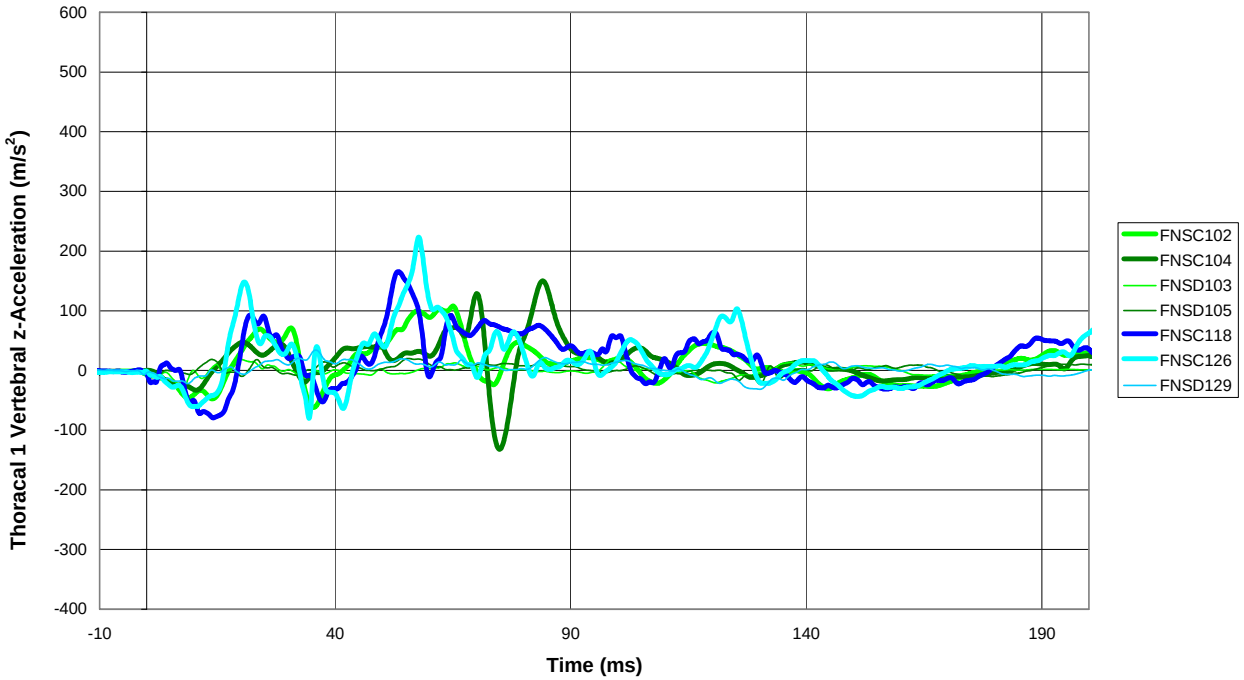

Figure C-9. The Thoracal 1 Vertebrae Linear z-Acceleration

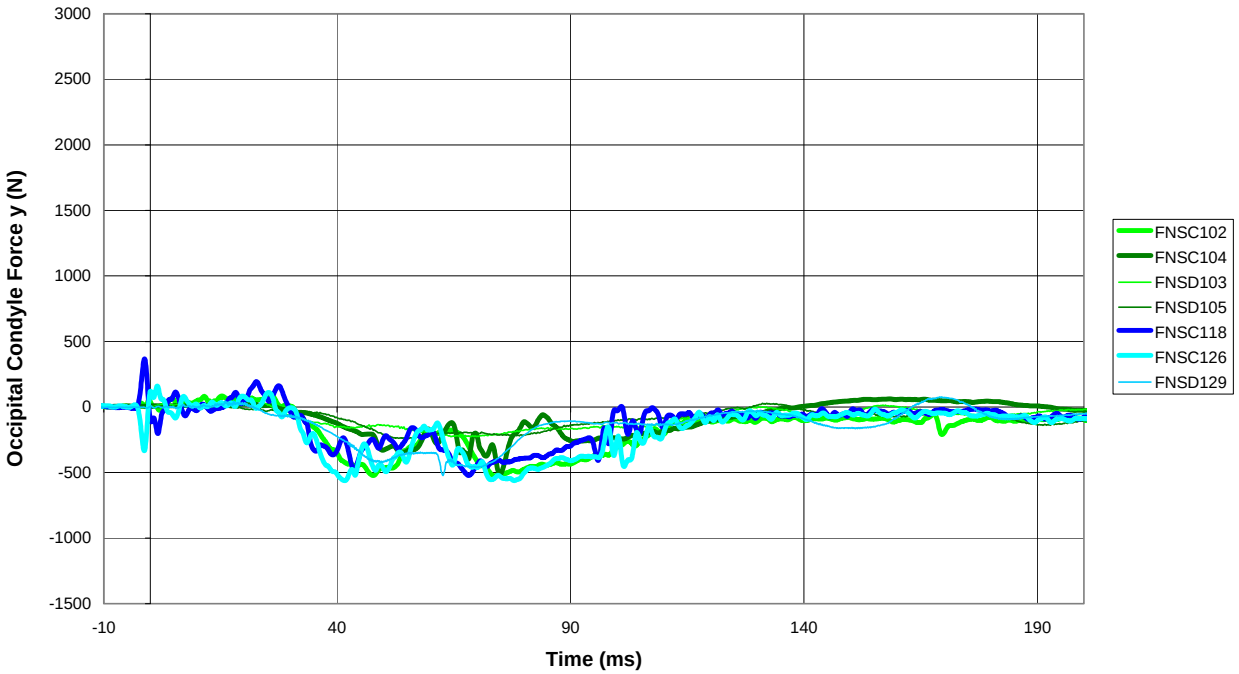

Figure C-10. The Occipital Condyle x-Force

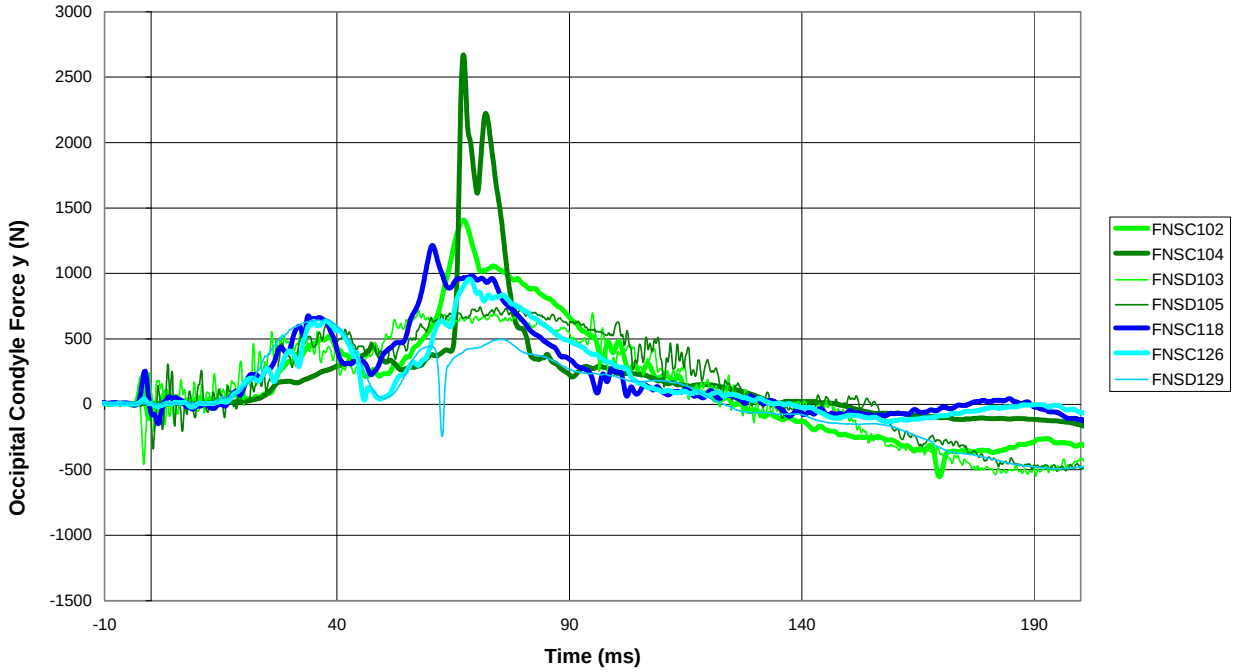

Figure C-11. The Occipital Condyle y-Force

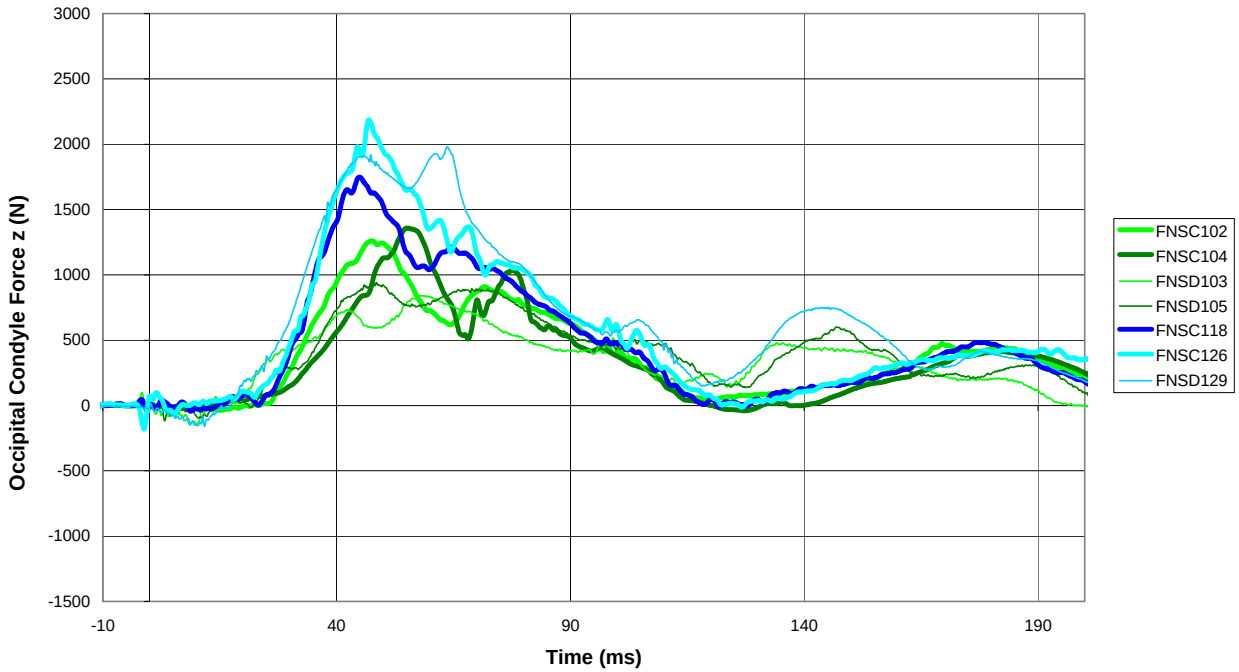

Figure C-12. The Occipital Condyle z-Force

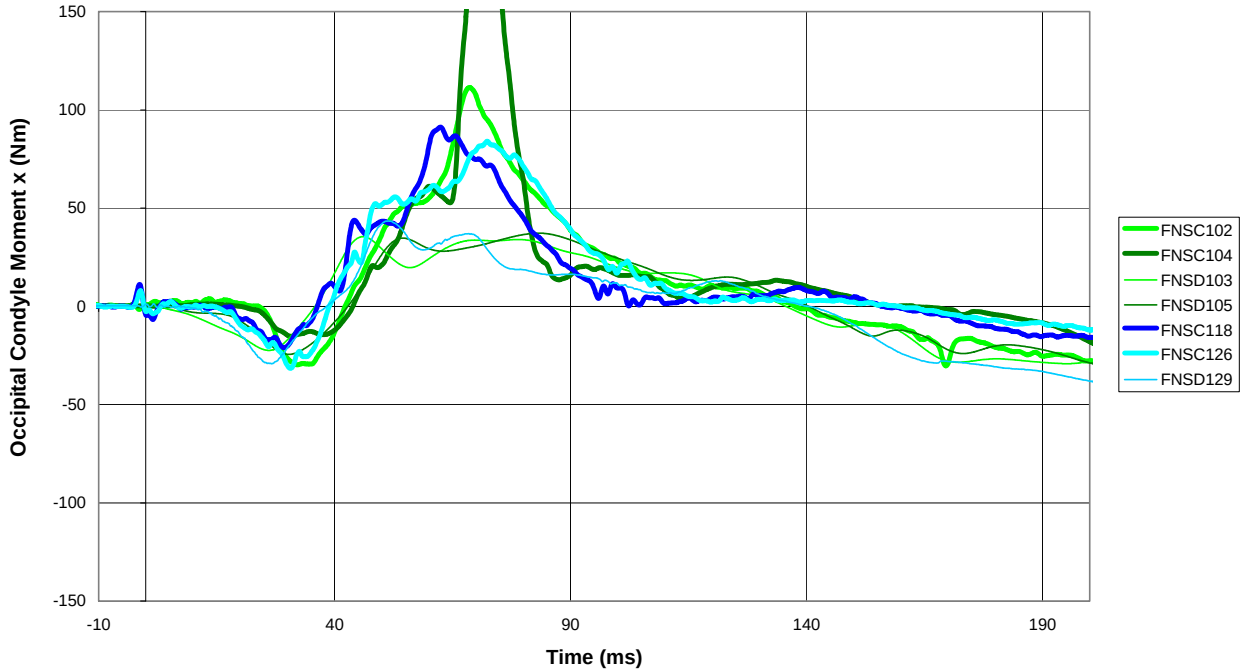

Figure C-13. The Occipital Condyle x-Moment

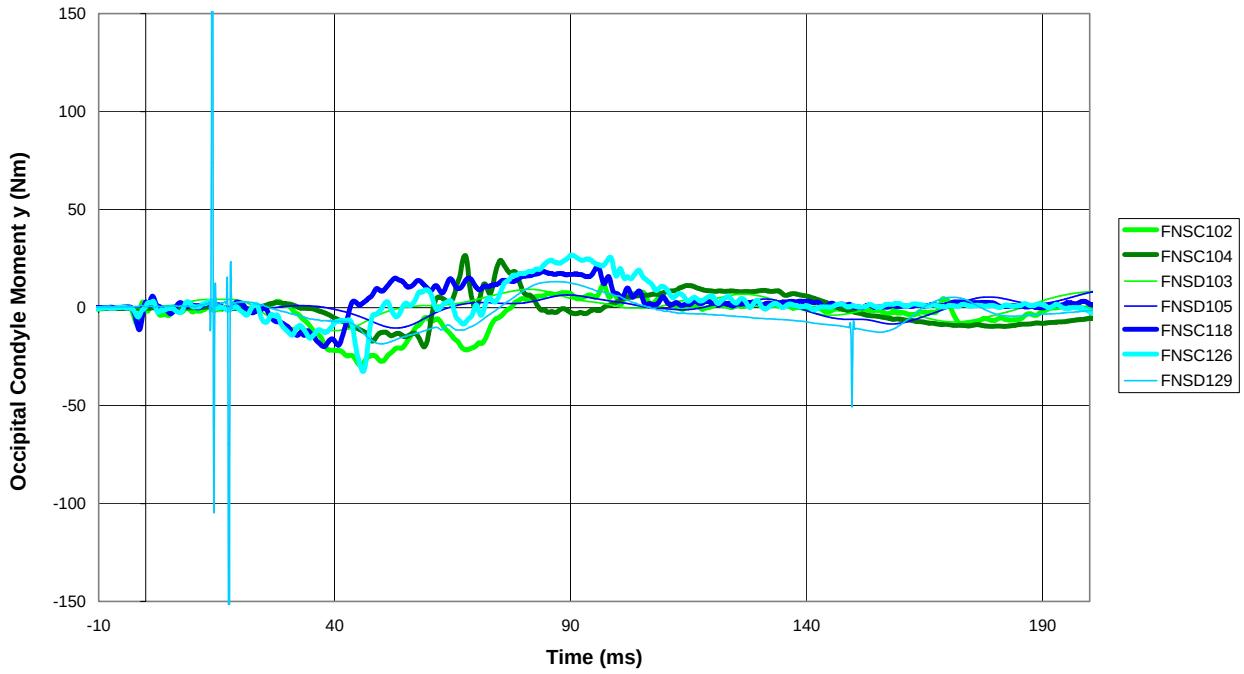

Figure C-14. The Occipital Condyle y-Moment

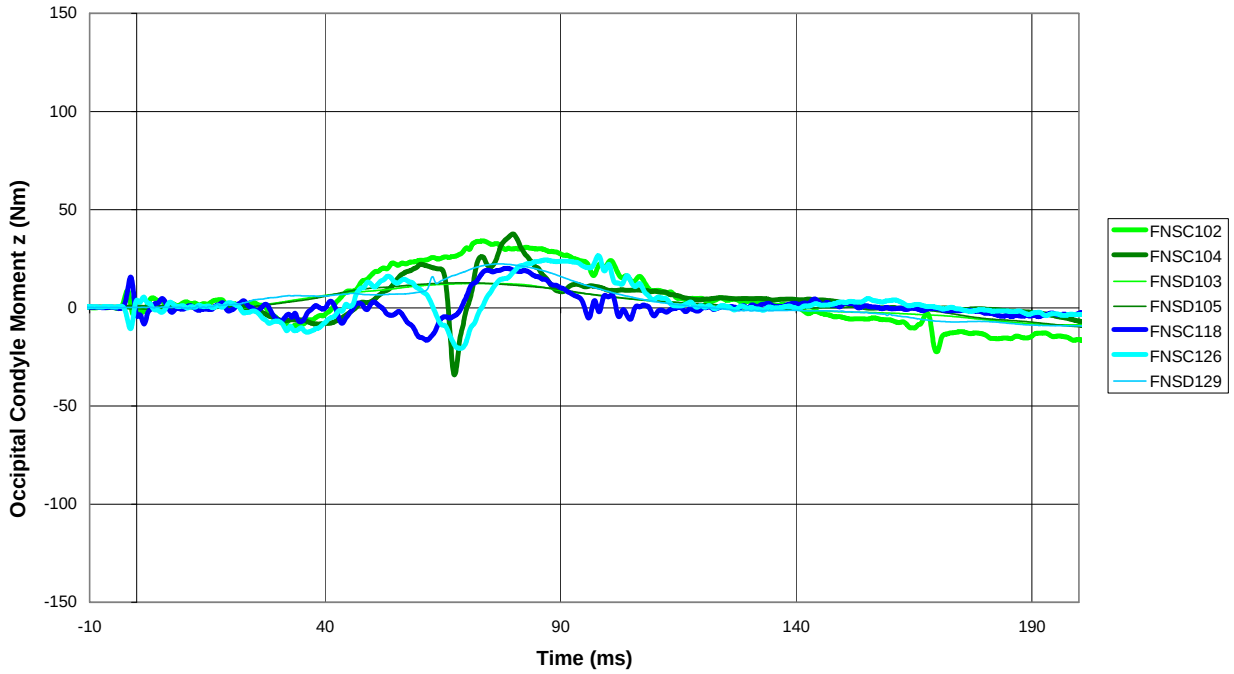

Figure C-15. The Occipital Condyle z-Moment

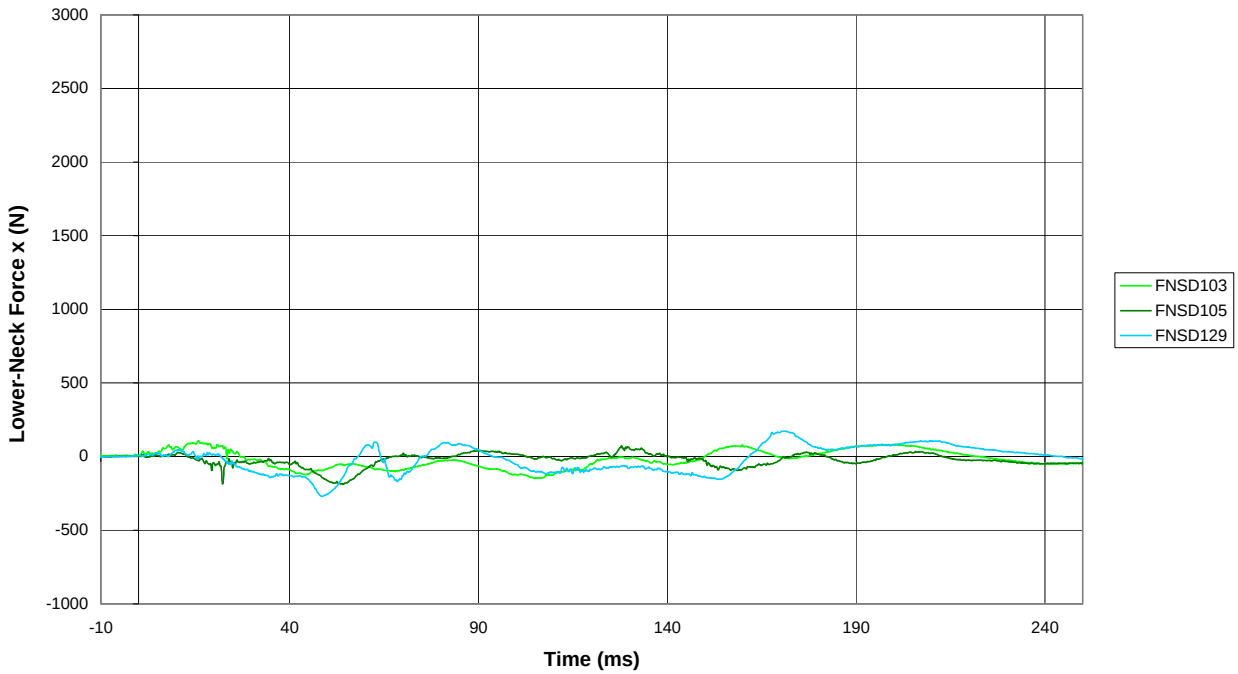

Figure C-16. Lower-Neck x-Force

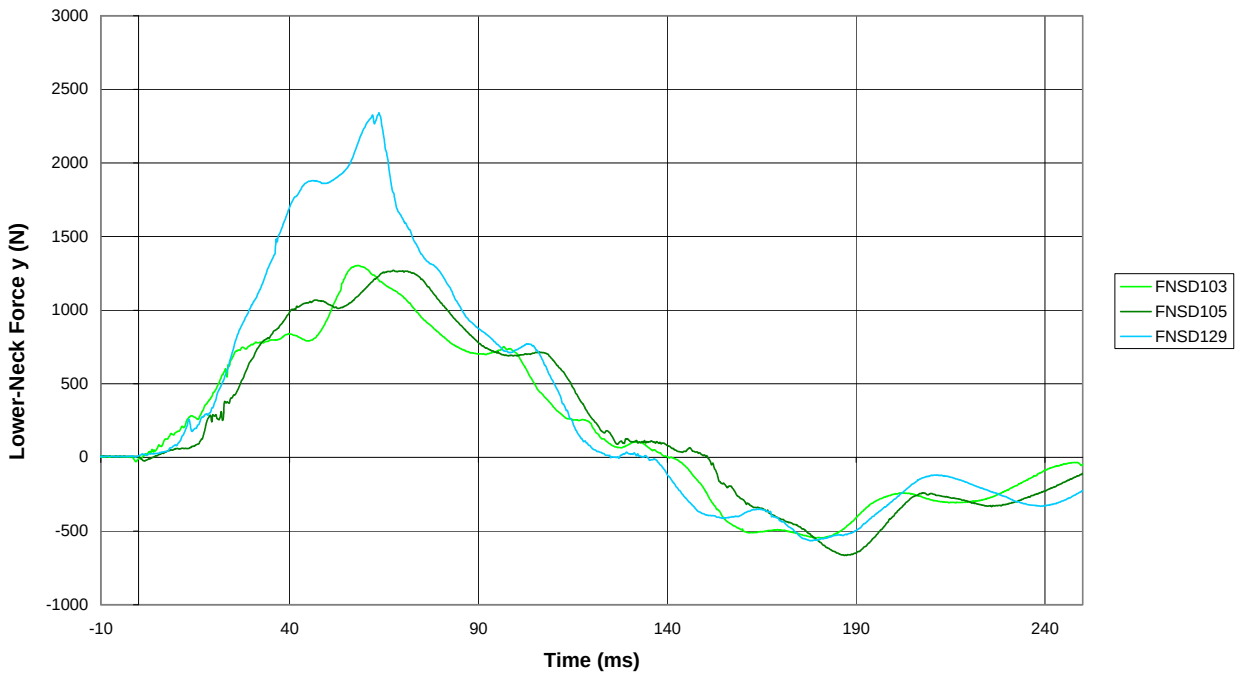

Figure C-17. Lower-Neck y-Force

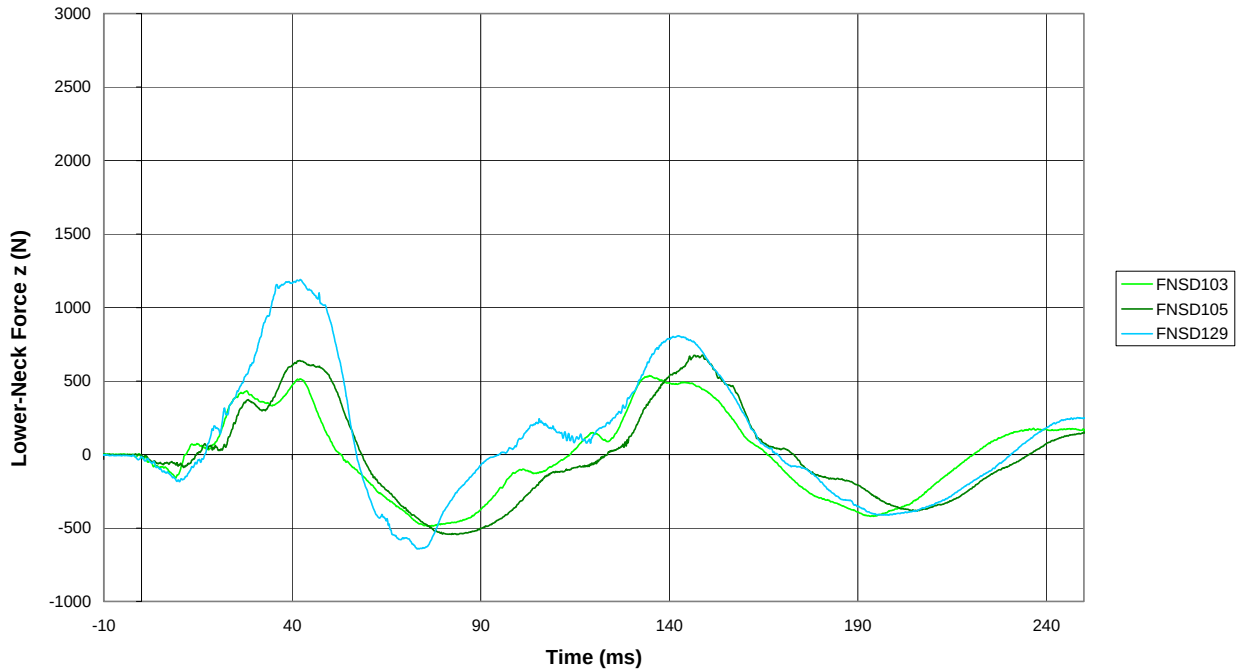

Figure C-18. Lower-Neck z-Force

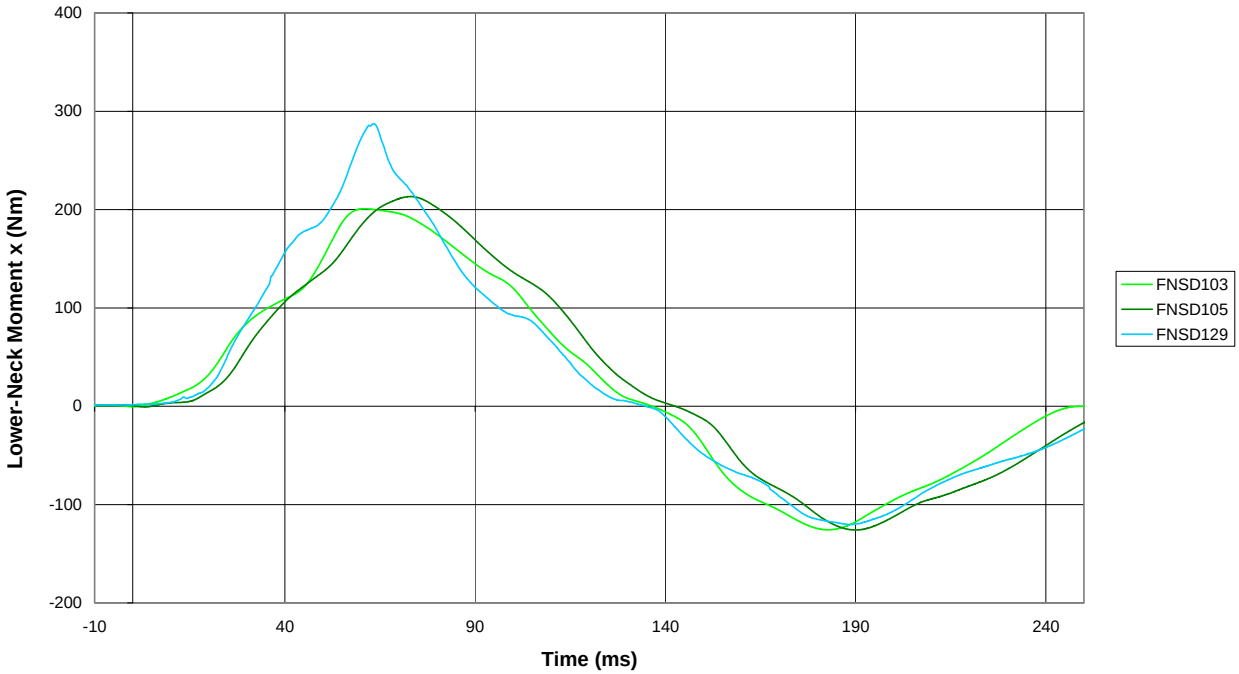

Figure C-19. Lower-Neck x-Moment

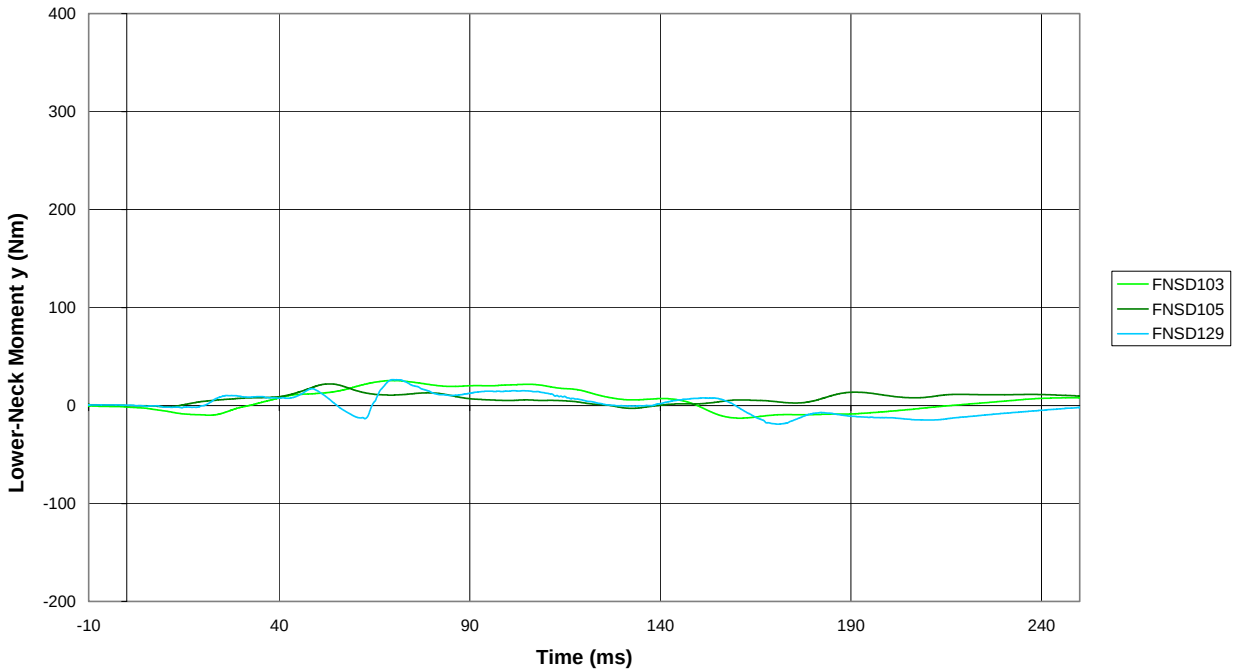

Figure C-20. Lower-Neck y-Moment

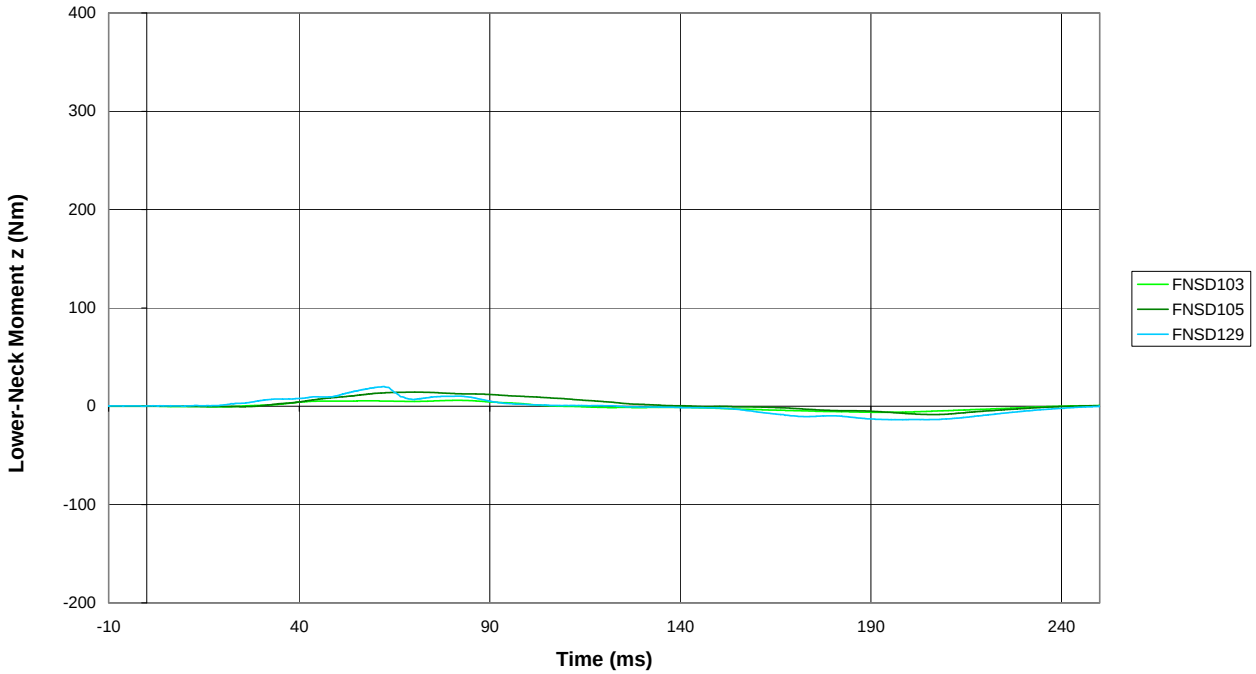

Figure C-21. Lower-Neck z-Moment

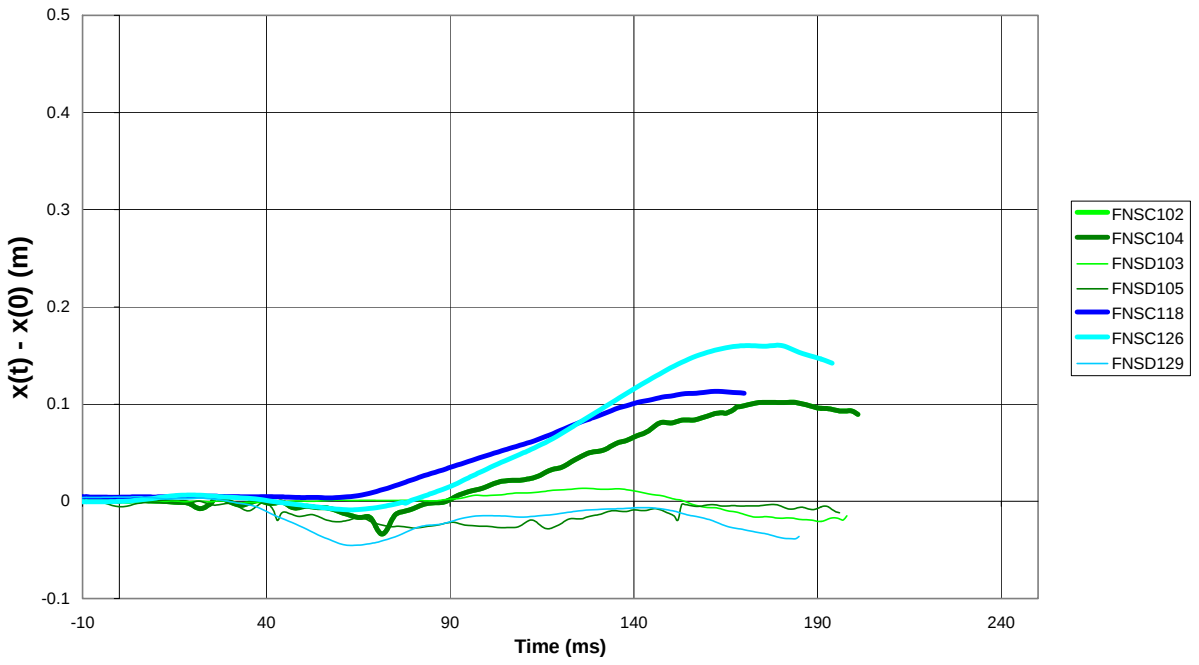

Figure C-22. Head c.g. x With Regard to Sled

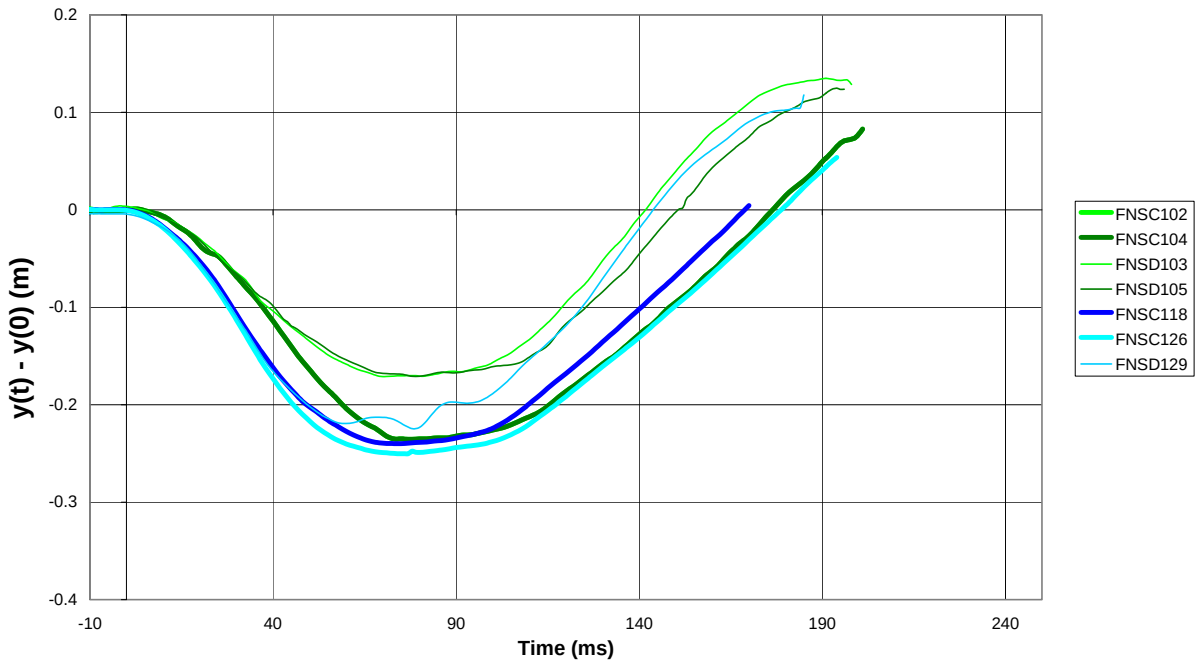

Figure C-23. Head c.g. y With Regard to Sled

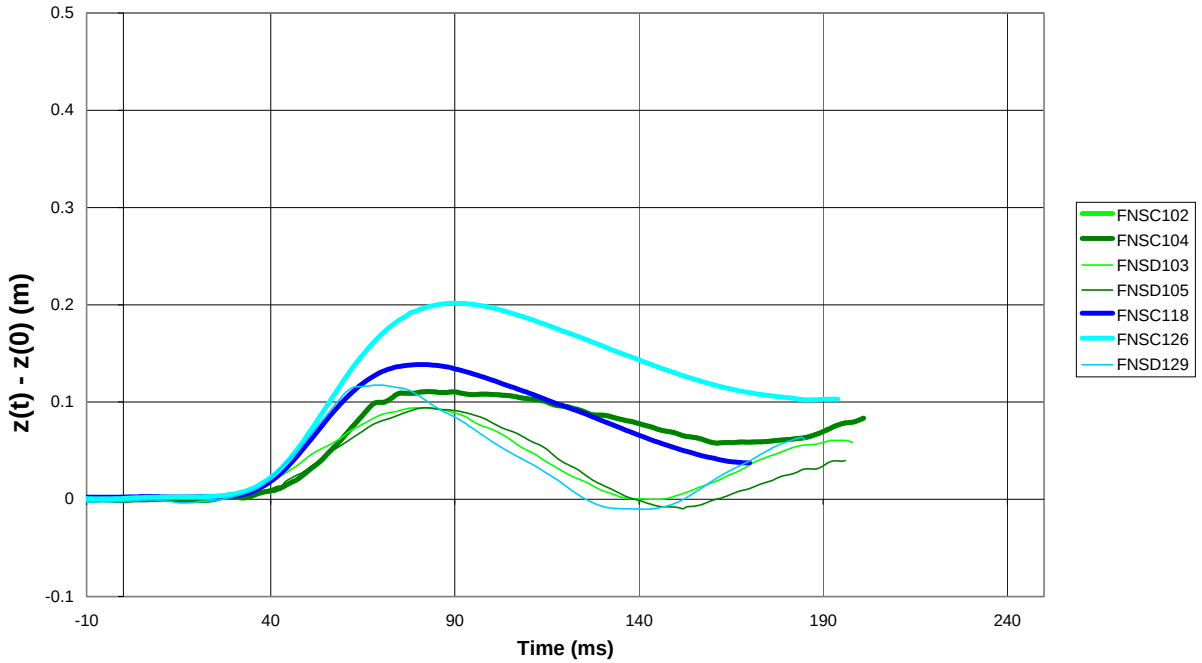

Figure C-24. Head c.g. z With Regard to Sled

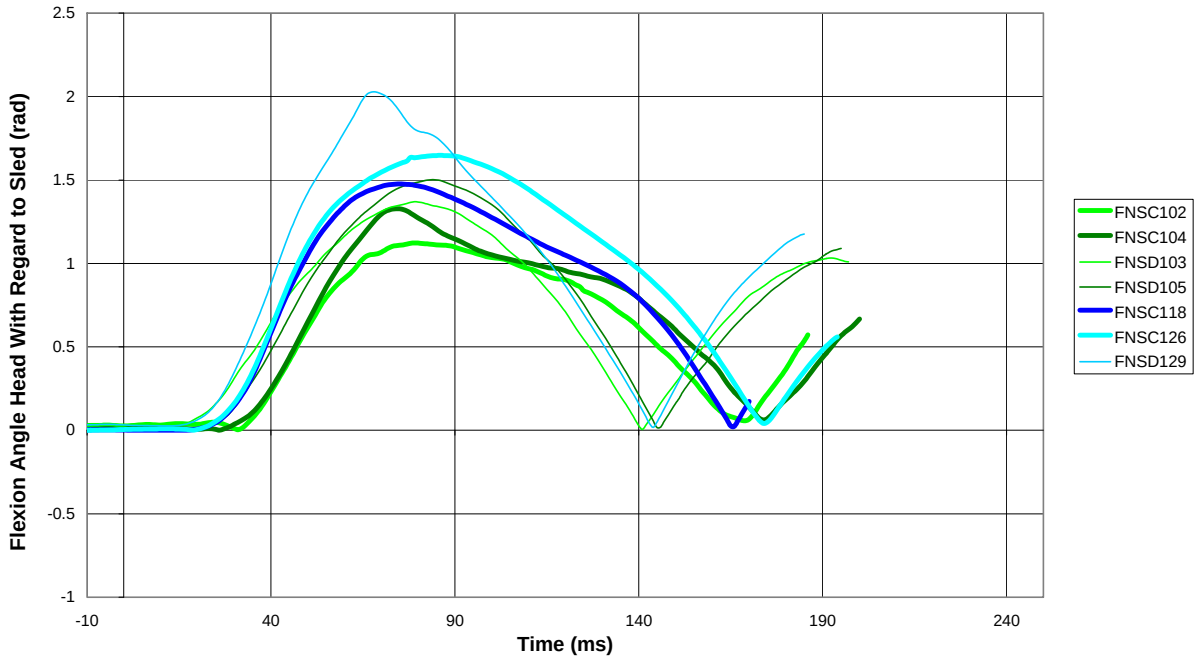

Figure C-25. Head Flexion Angle With Regard to Sled

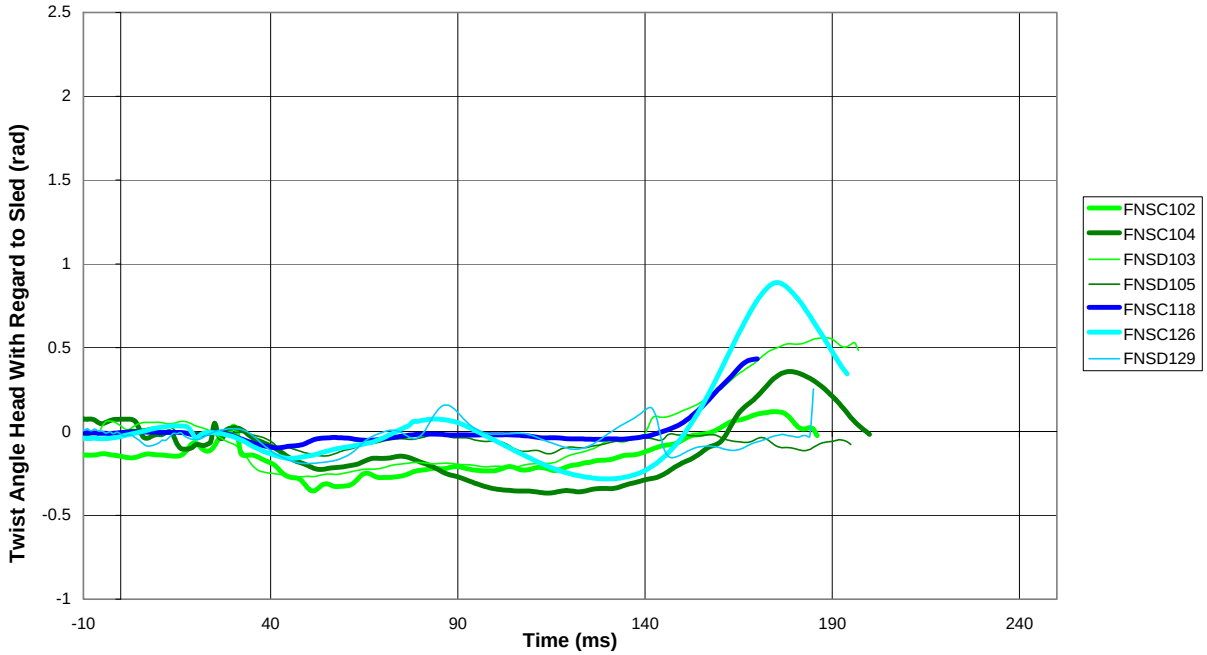

Figure C-26. Head Twist Angle With Regard to Sled

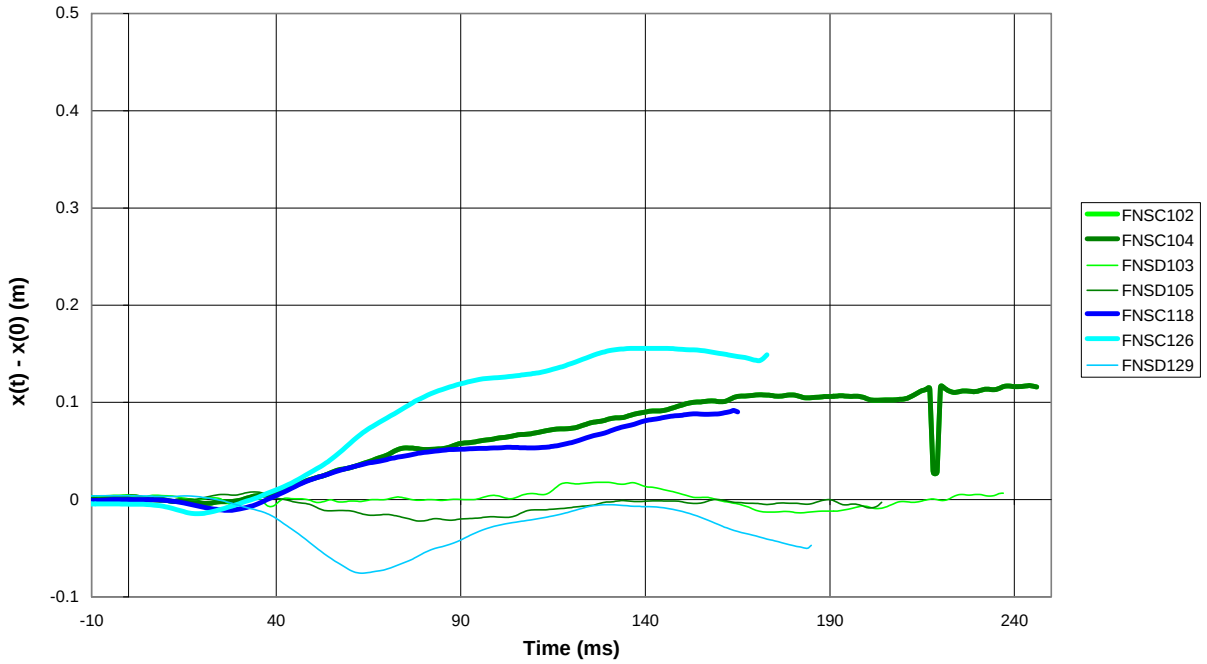

Figure C-27. Head c.g. x With Regard to the Thoracal 1 Vertebrae

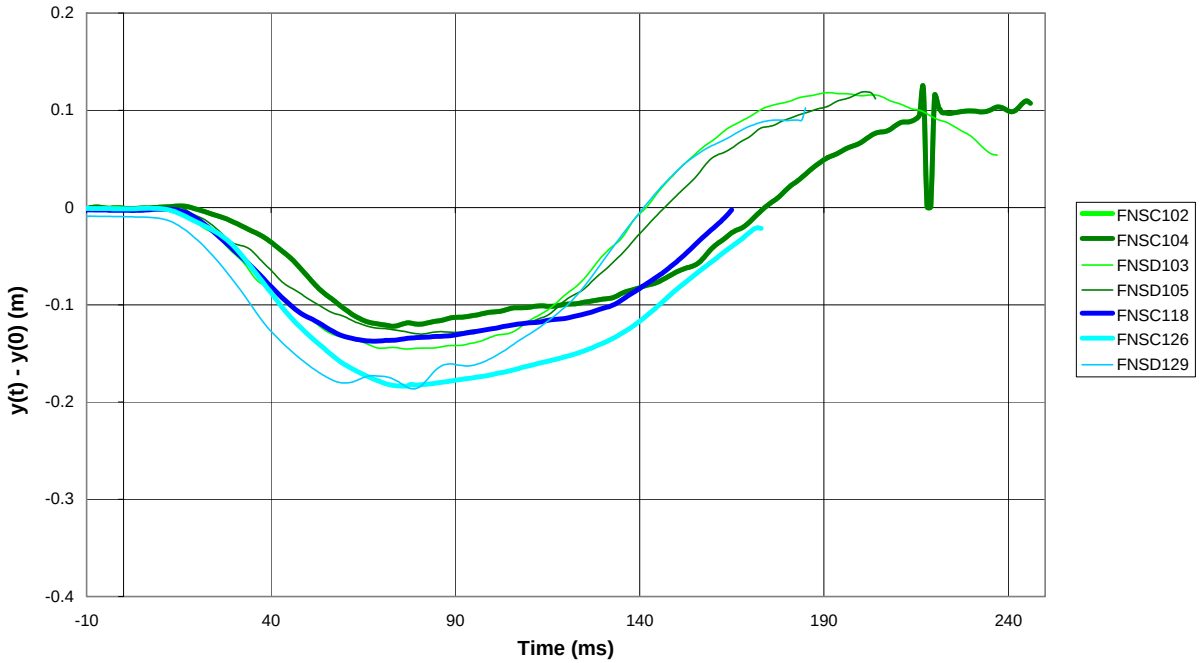

Figure C-28. Head c.g. y With Regard to Thoracal 1 Vertebrae

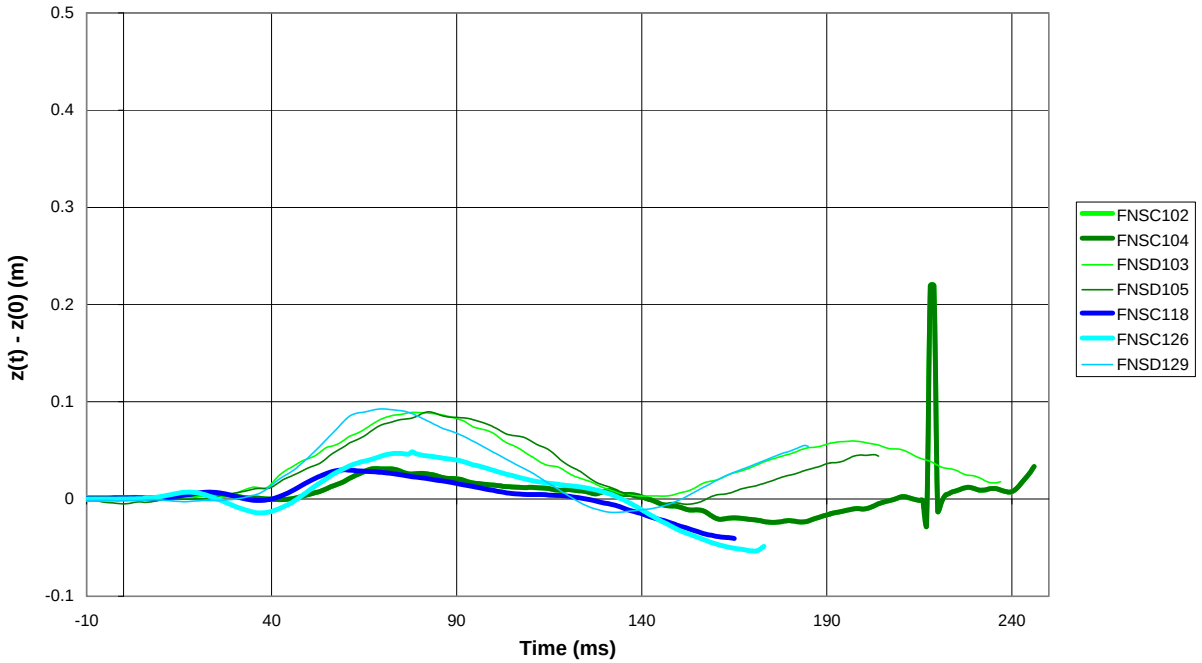

Figure C-29. Head c.g. z With Regard to Thoracal 1 Vertebrae

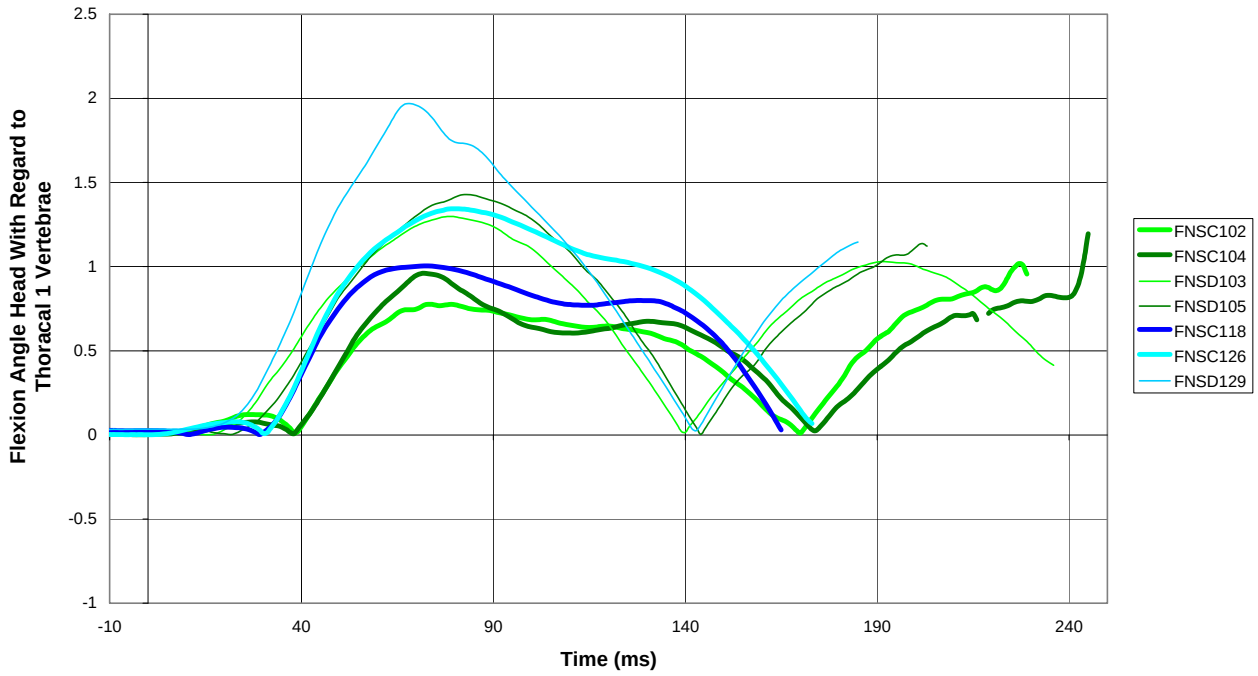

Figure C-30. Head Flexion With Regard to Thoracal 1 Vertebrae

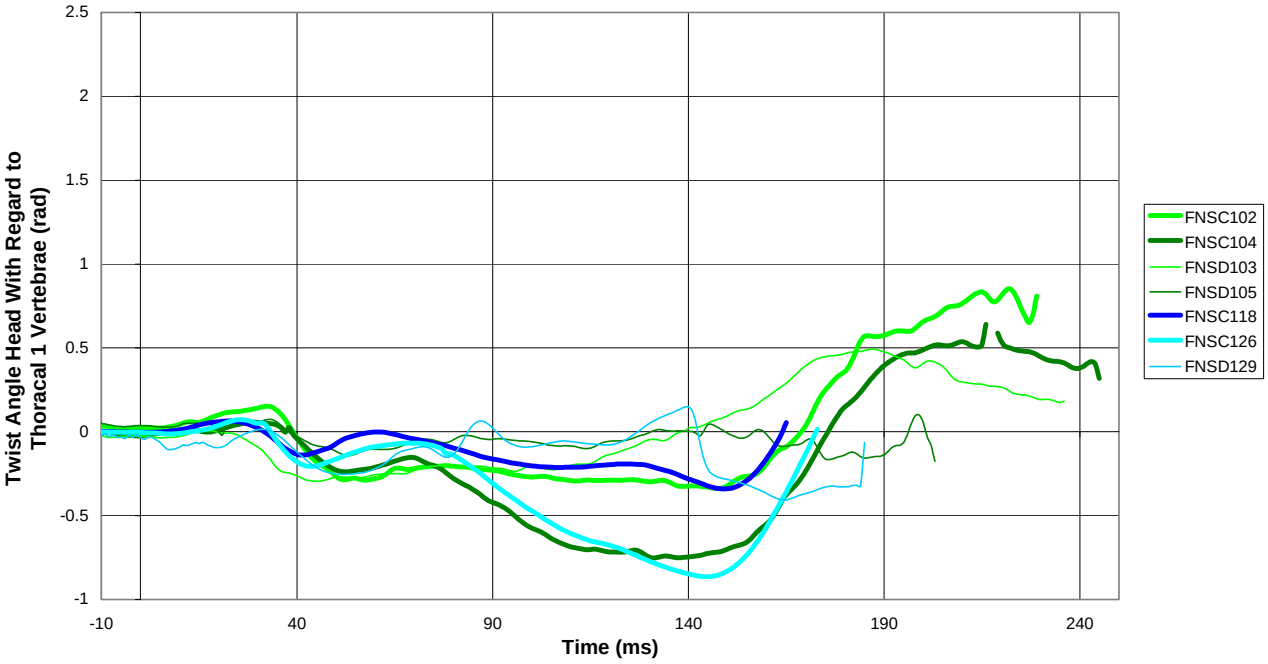

Figure C-31. Head Twist Angle With Regard to Thoracal 1 Vertebrae

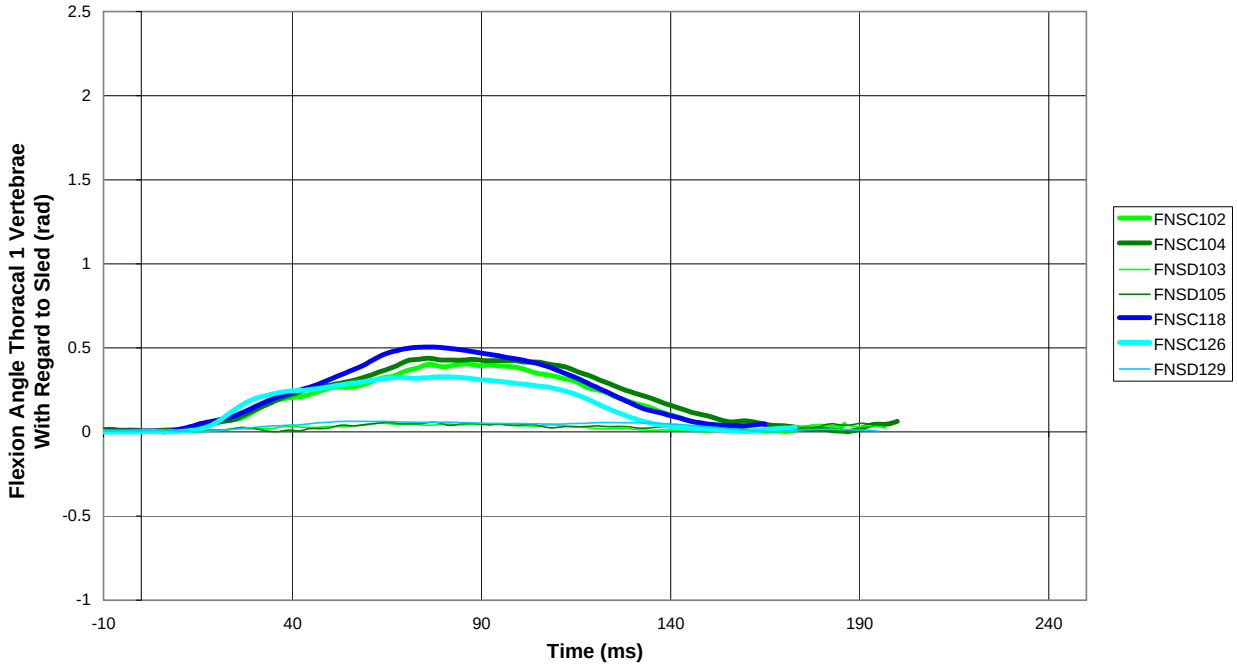

Figure C-32. Thoracal 1 Vertebrae Flexion Angle With Regard to Sled

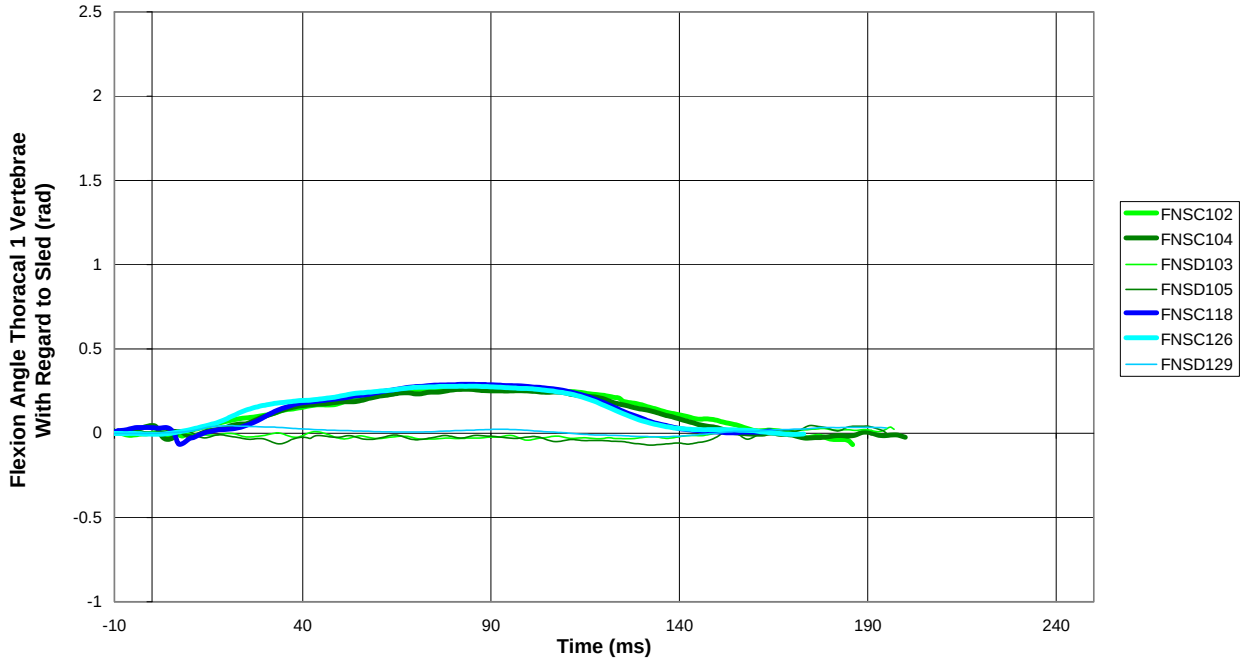

Figure C-33. Thoracal 1 Vertebrae Twist Angle With Regard to Sled

APPENDIX D—POSTMORTEM HUMAN SUBJECT AND EuroSID-2 RESPONSE TIME HISTORIES FOR THE AIRCRAFT SEAT CONFIGURATION

This appendix presents the response of the postmortem human subject (PMHS) and EuroSID-2 (ES-2) in the sled tests performed at the Medical College of Wisconsin. Time histories of various parameters are presented in figures D-1 to D-33. Note that the load parameters for the PMHS are only valid for the initial phase where the head has no contact with any surrounding structure. The contact times are listed in table D-1.

Table D-1. The PMHS Head Contact Times for the Aircraft Seat Test Configuration

Test	FNSC 109	FNSC 110	FNSC 115	FNSC 116
Contact time (ms)	104	102	112	113

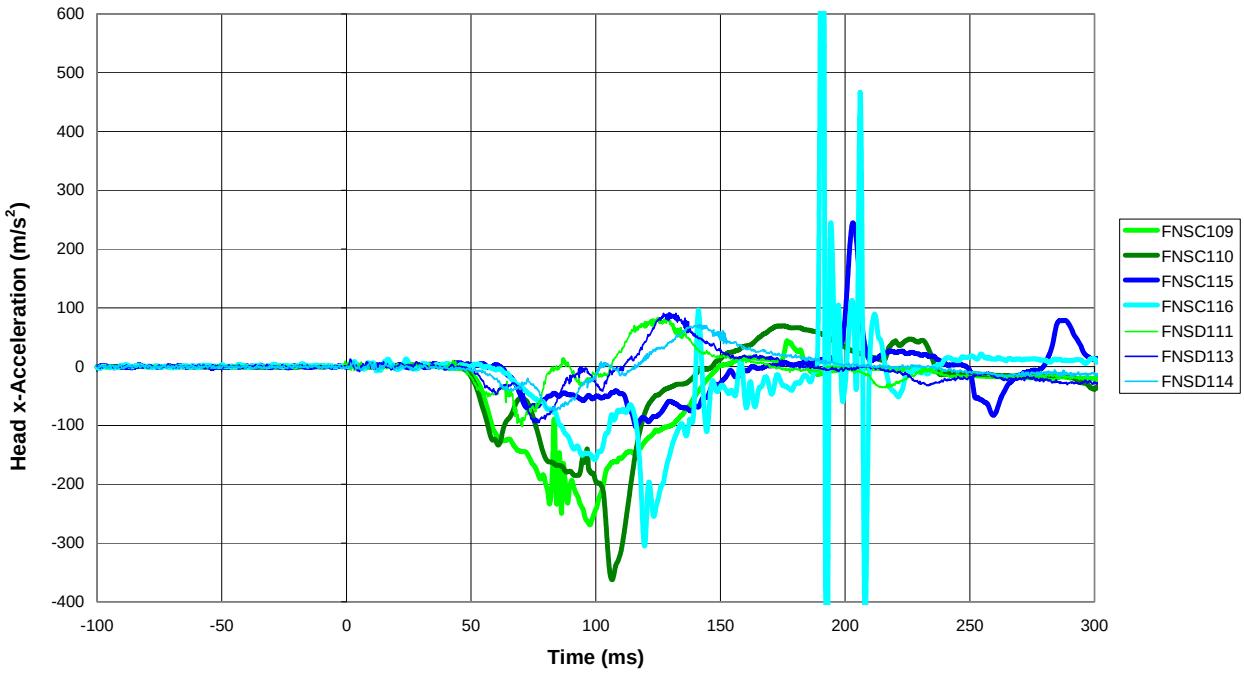

Figure D-1. Head Linear x-Acceleration

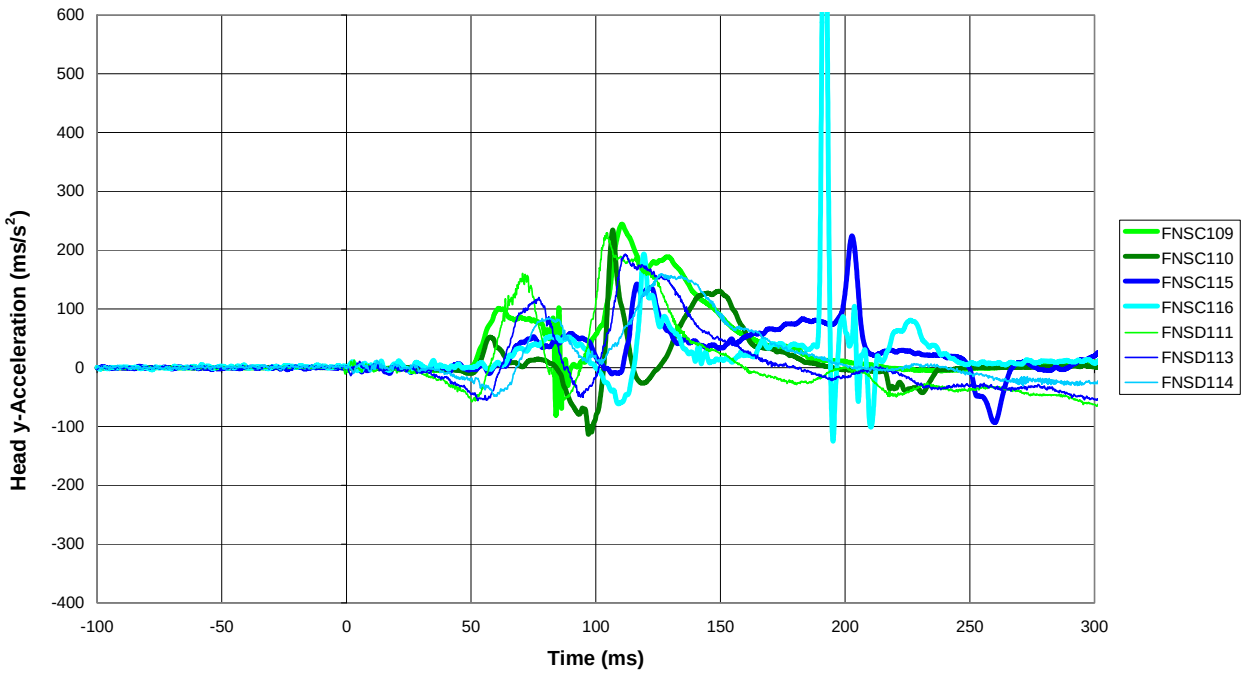

Figure D-2. Head Linear y-Acceleration

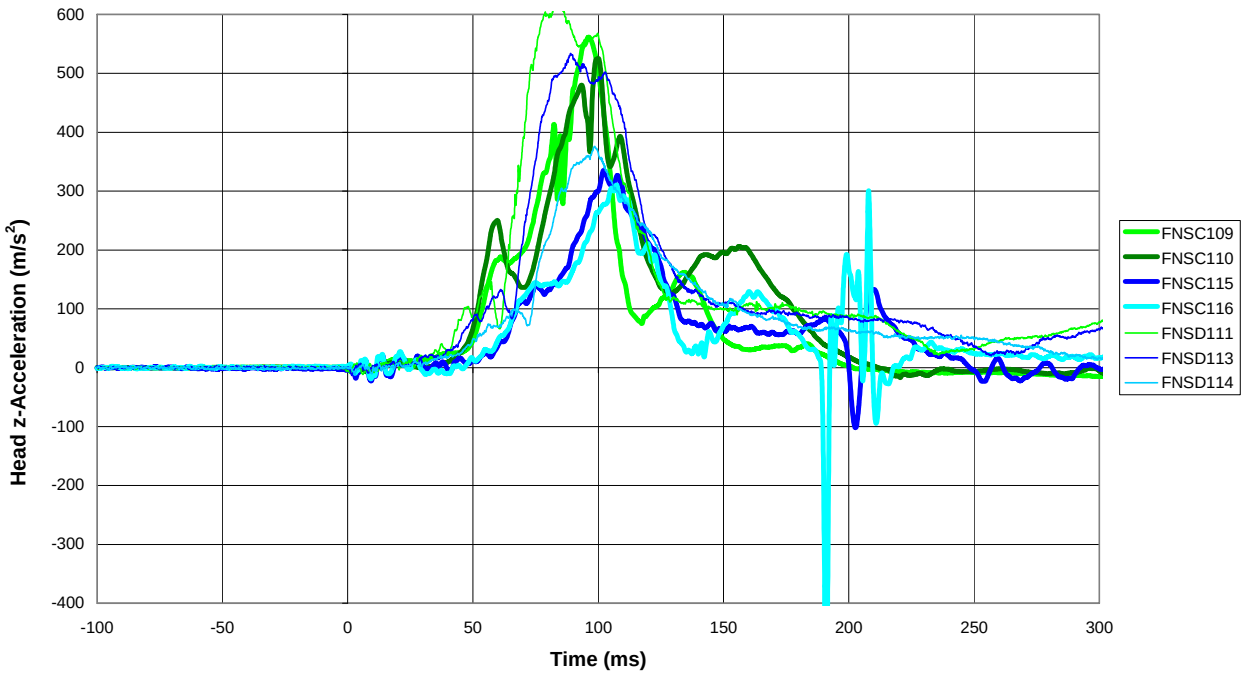

Figure D-3. Head Linear z-Acceleration

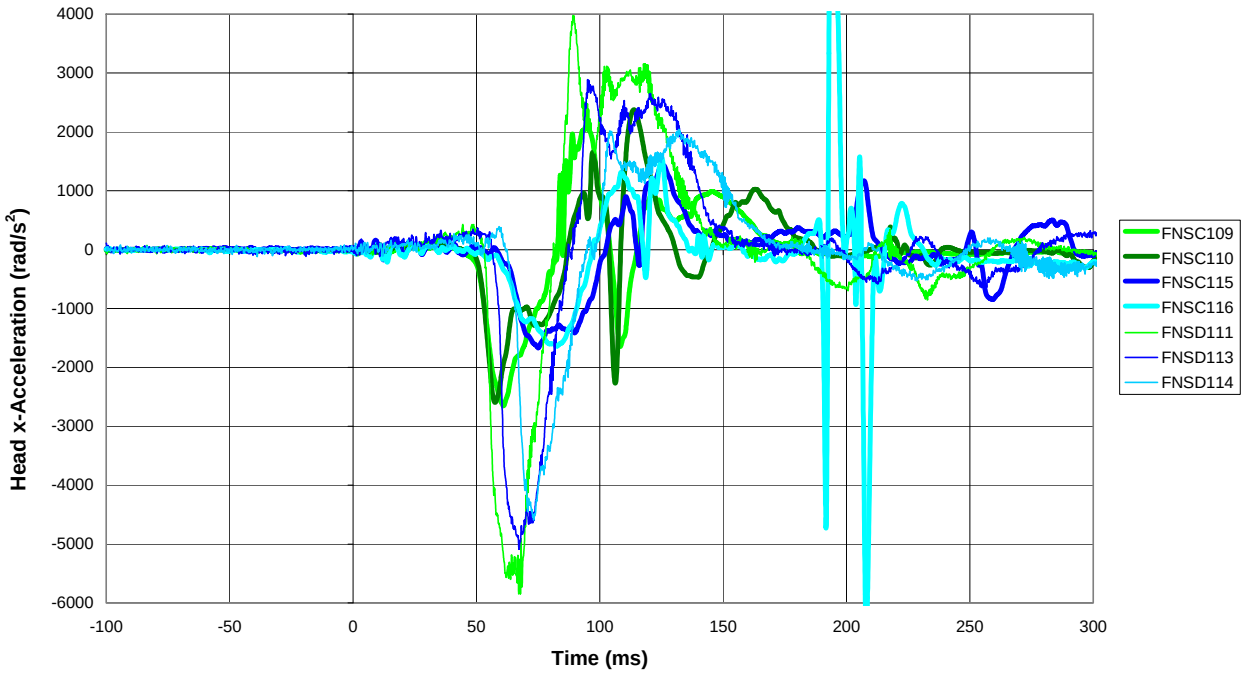

Figure D-4. Head Angular x-Acceleration

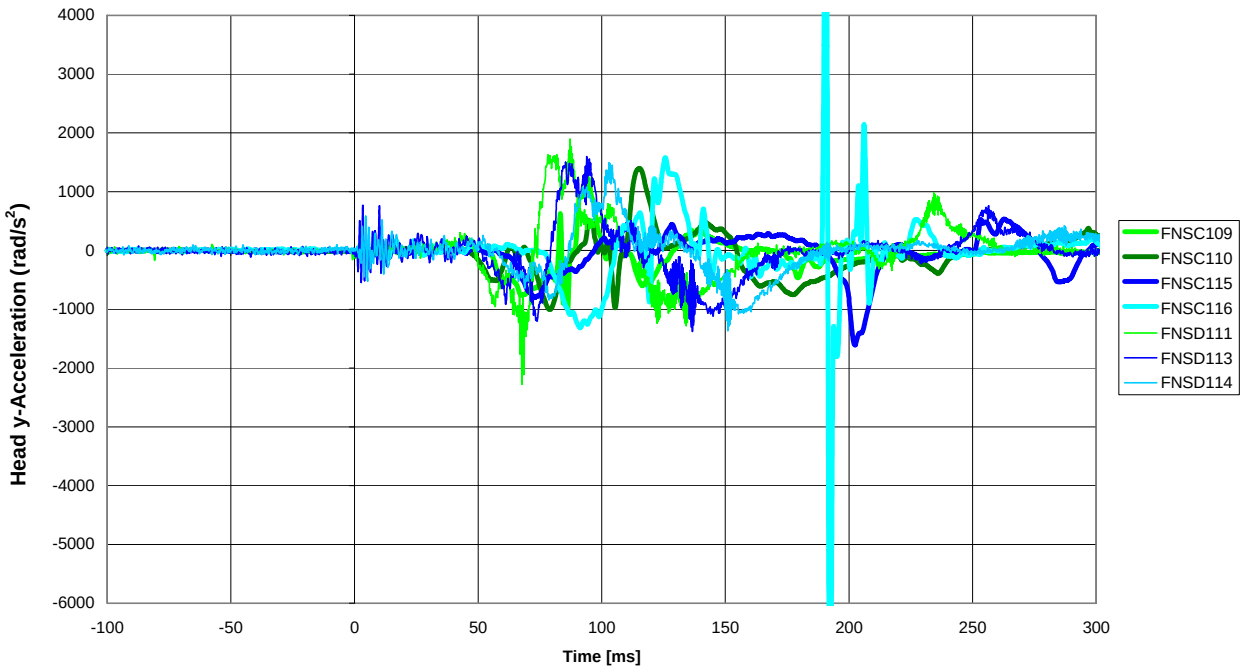

Figure D-5. Head Angular y-Acceleration

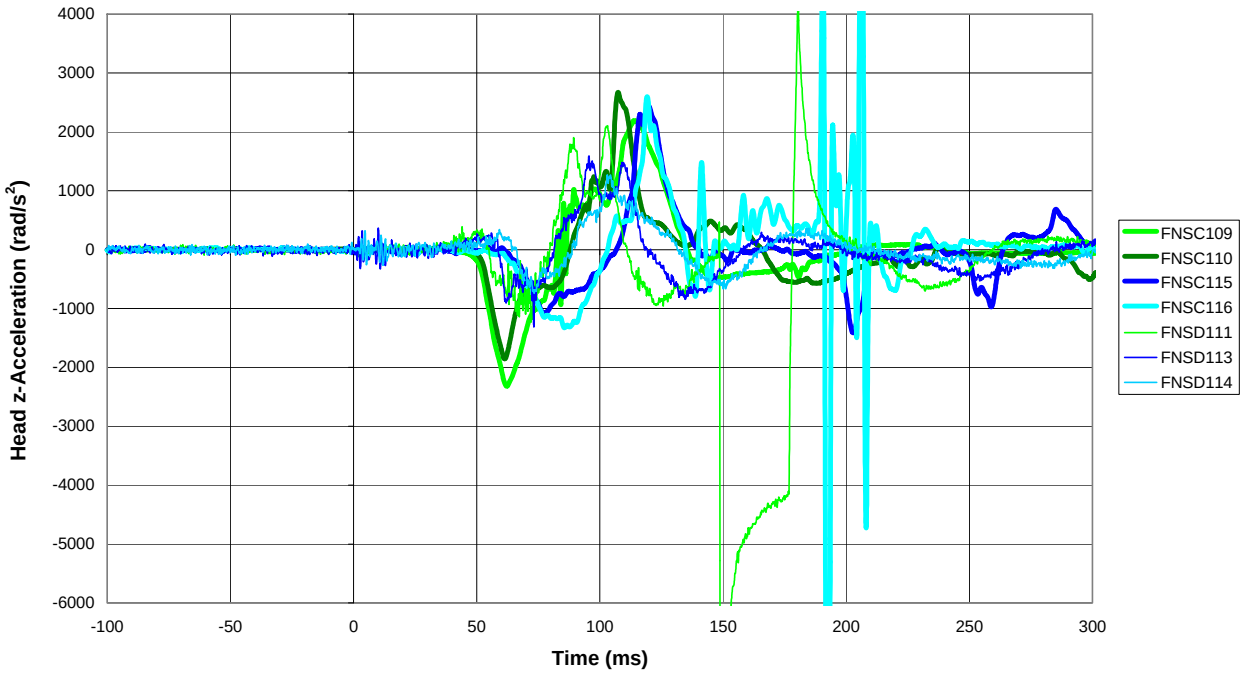

Figure D-6. Head Angular z-Acceleration

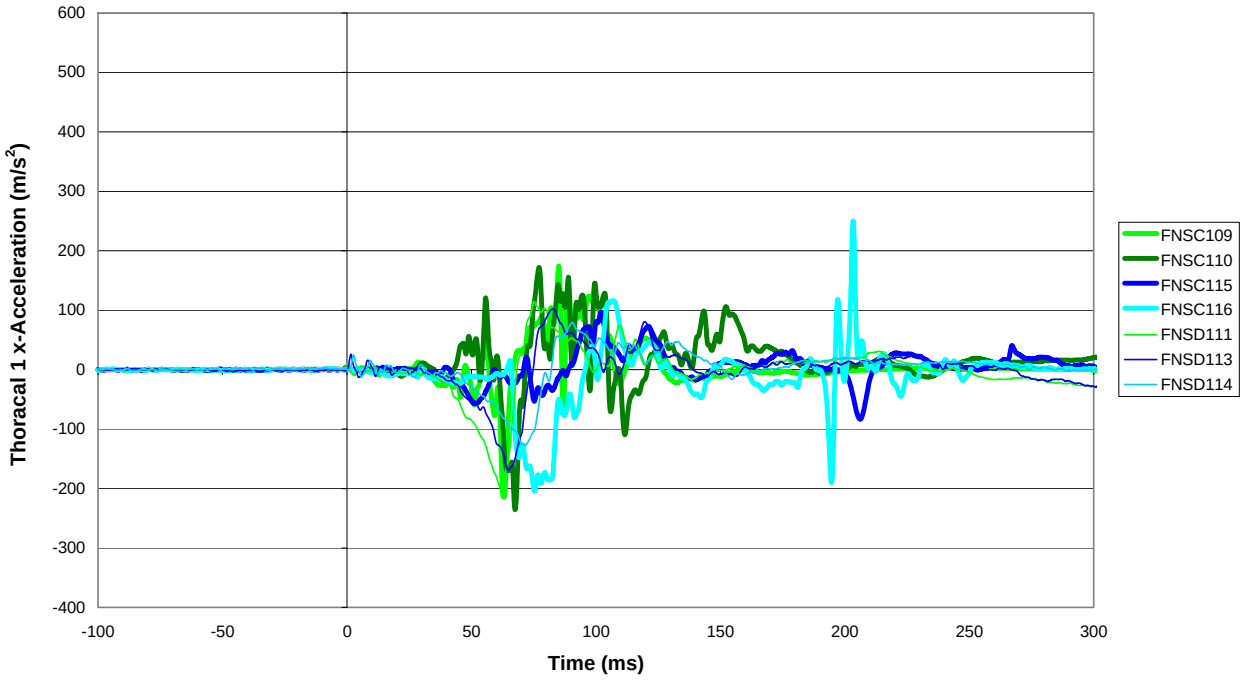

Figure D-7. Thoracal 1 Vertebrae Linear x-Acceleration

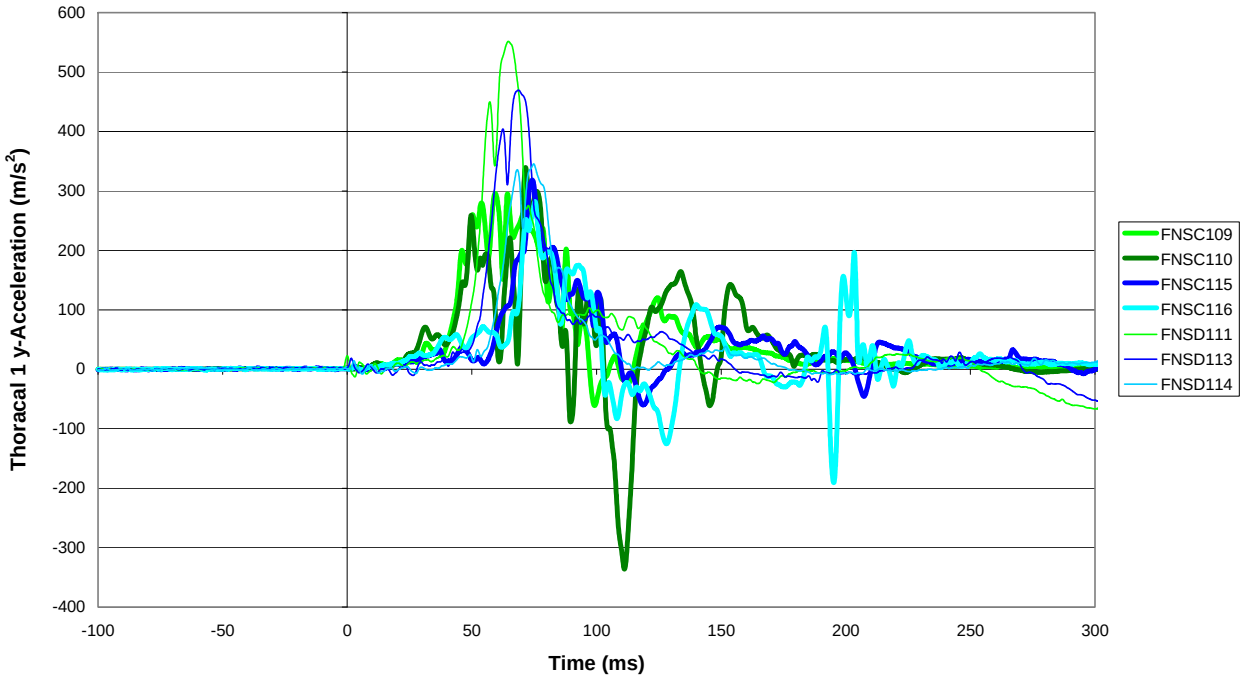

Figure D-8. Thoracal 1 Vertebrae Linear y-Acceleration

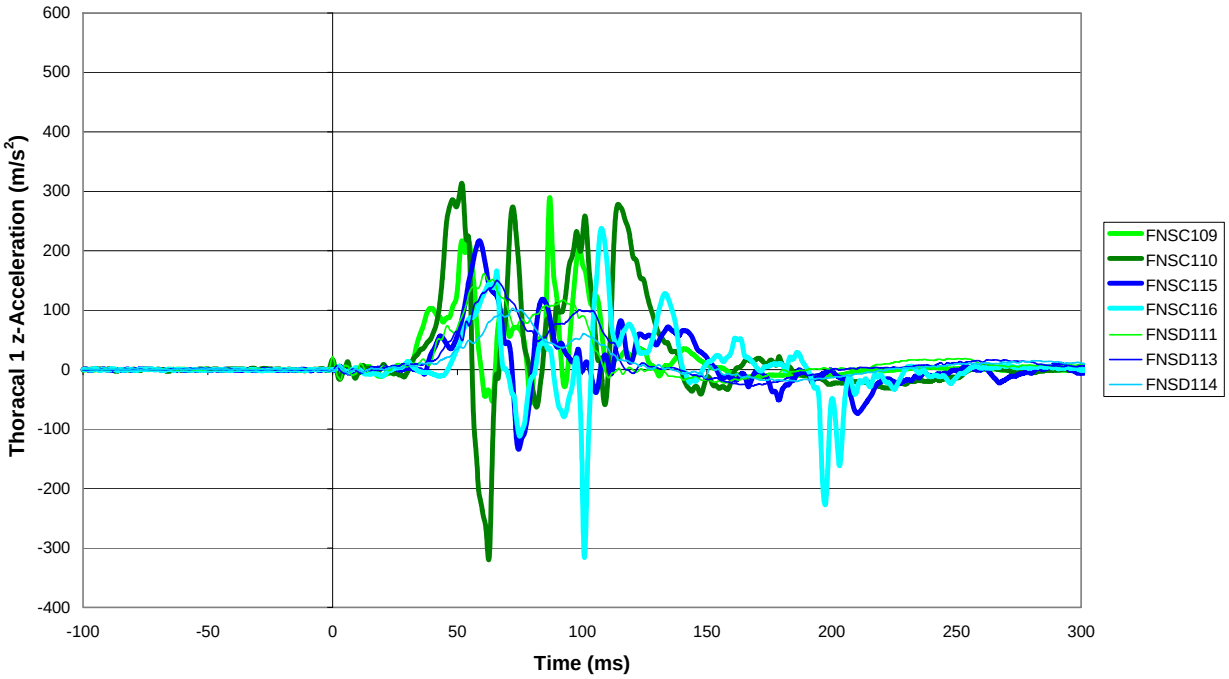

Figure D-9. Thoracal 1 Vertebrae Linear z-Acceleration

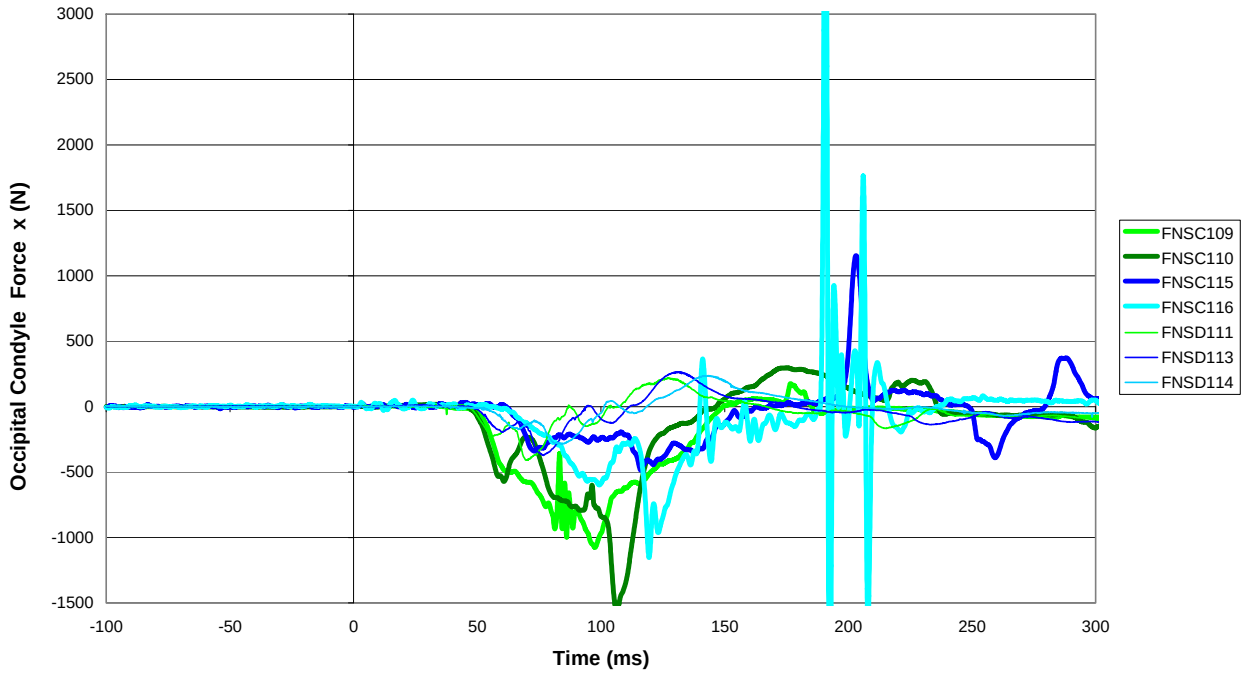

Figure D-10. The Occipital Condyle x-Force

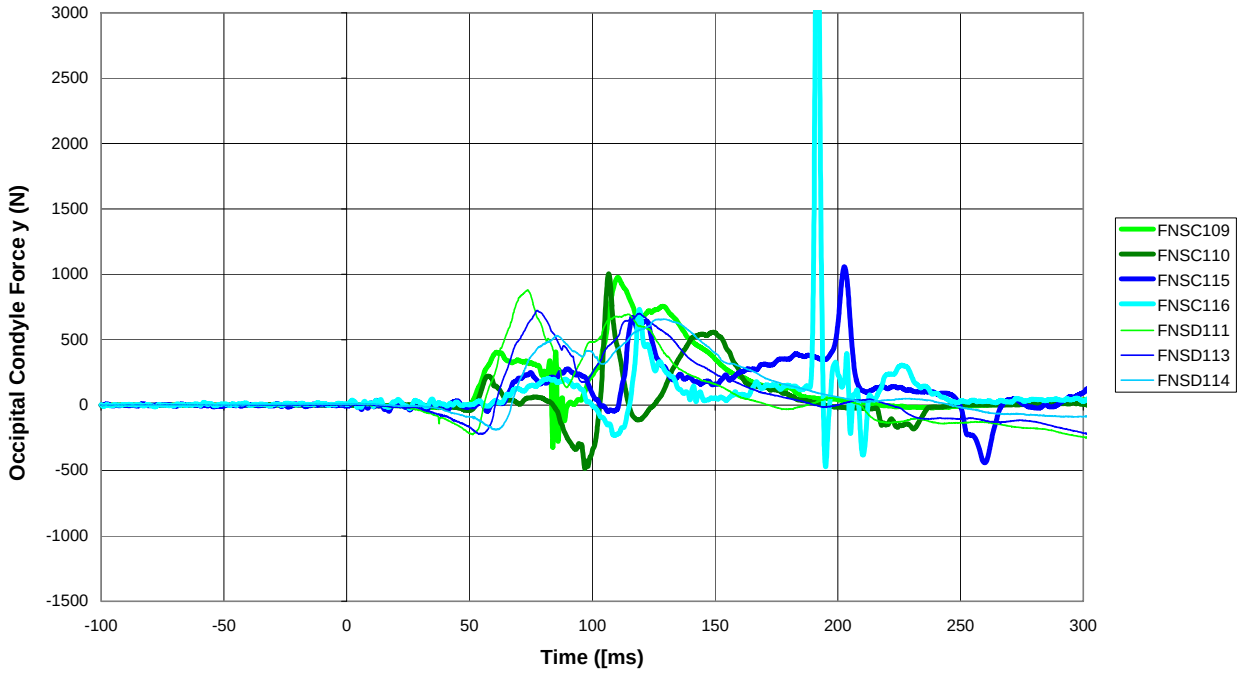

Figure D-11. The Occipital Condyle y-Force

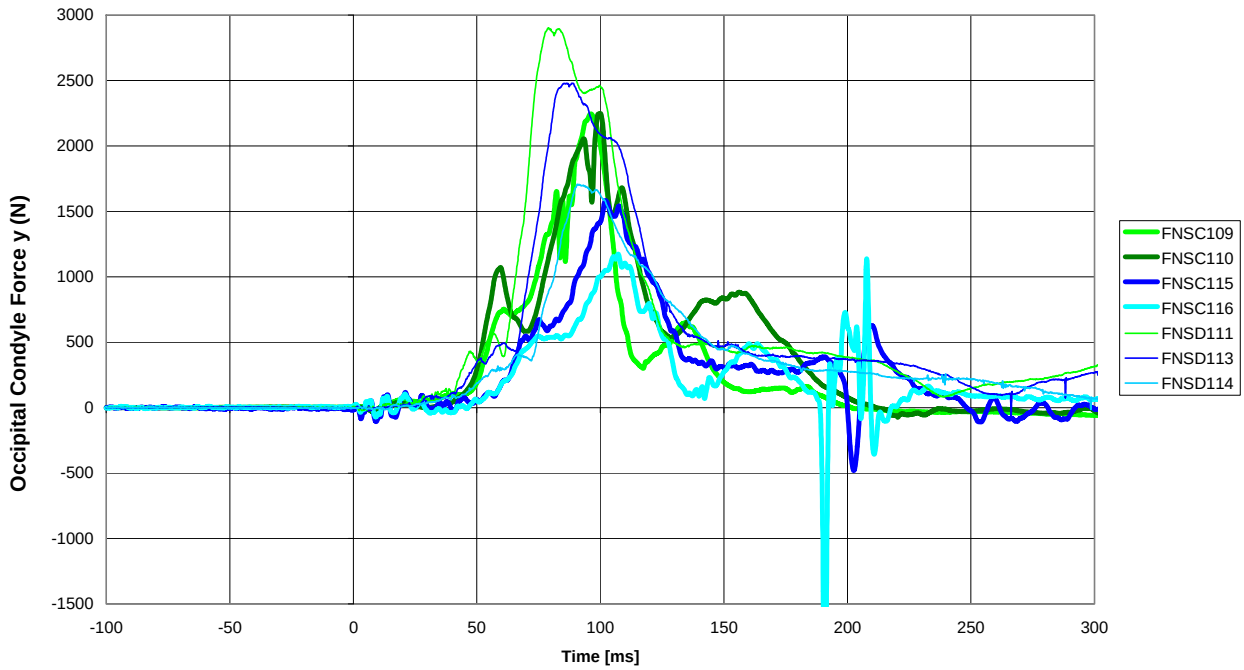

Figure D-12. The Occipital Condyle z-Force

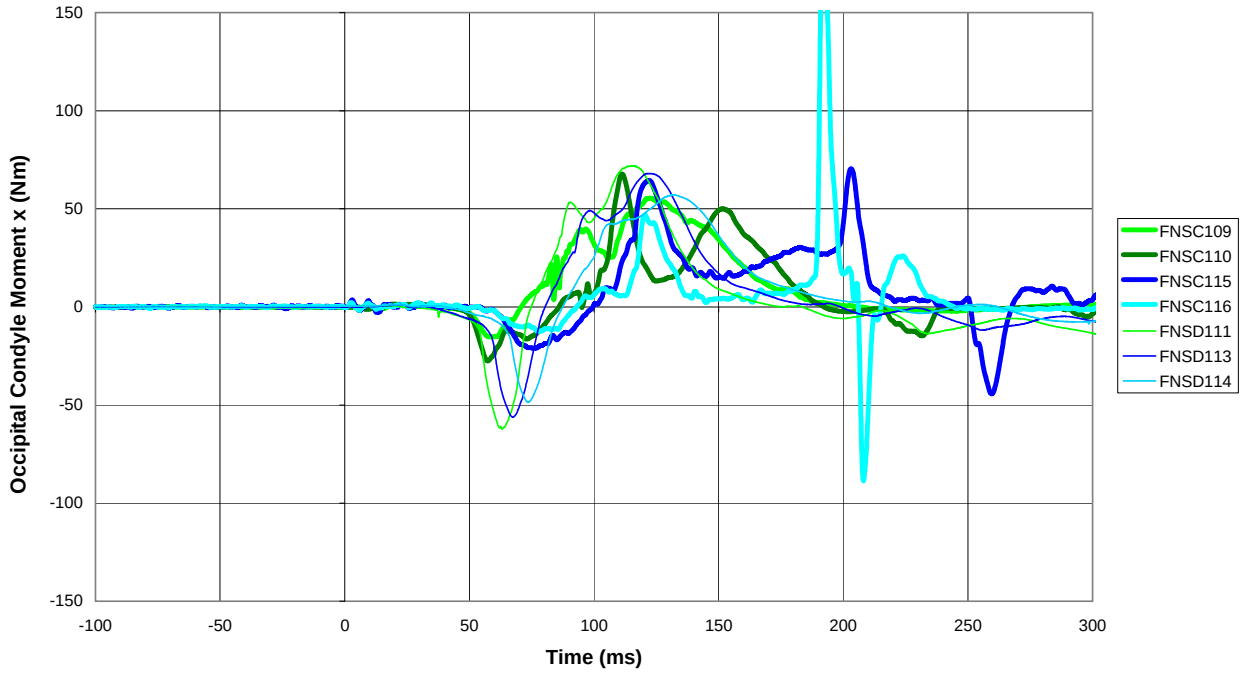

Figure D-13. The Occipital Condyle x-Moment

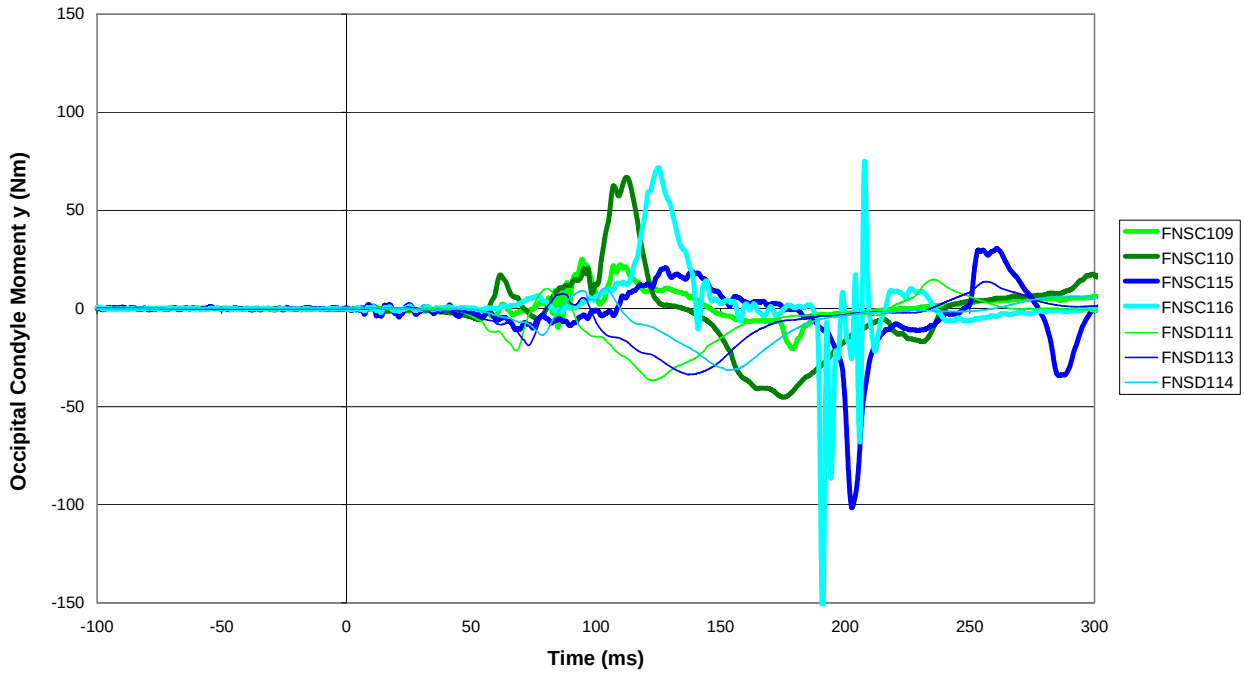

Figure D-14. The Occipital Condyle y-Moment

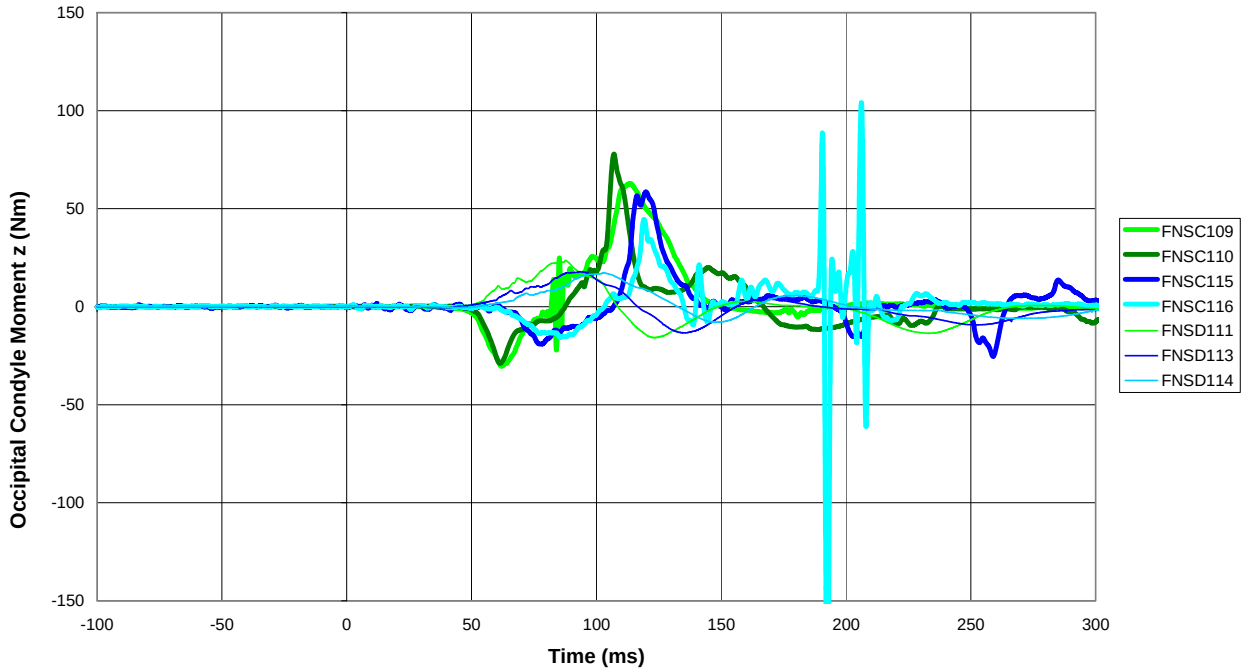

Figure D-15. The Occipital Condyle z-Moment

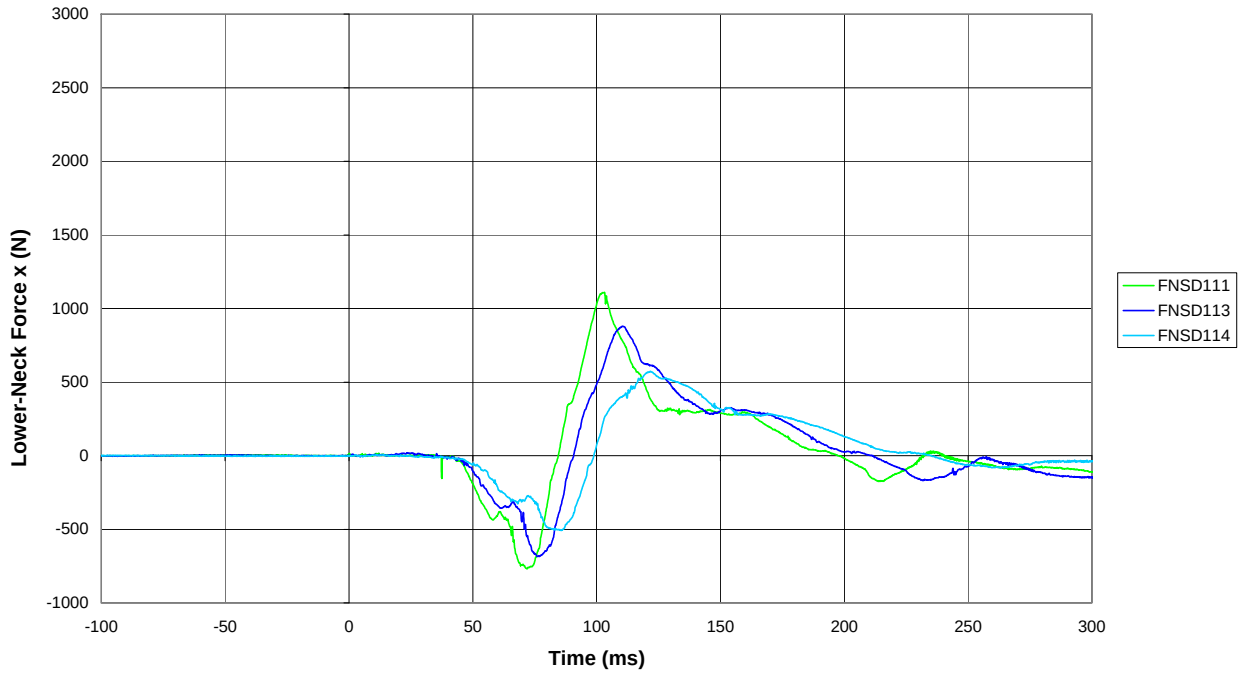

Figure D-16. Lower-Neck x-Force

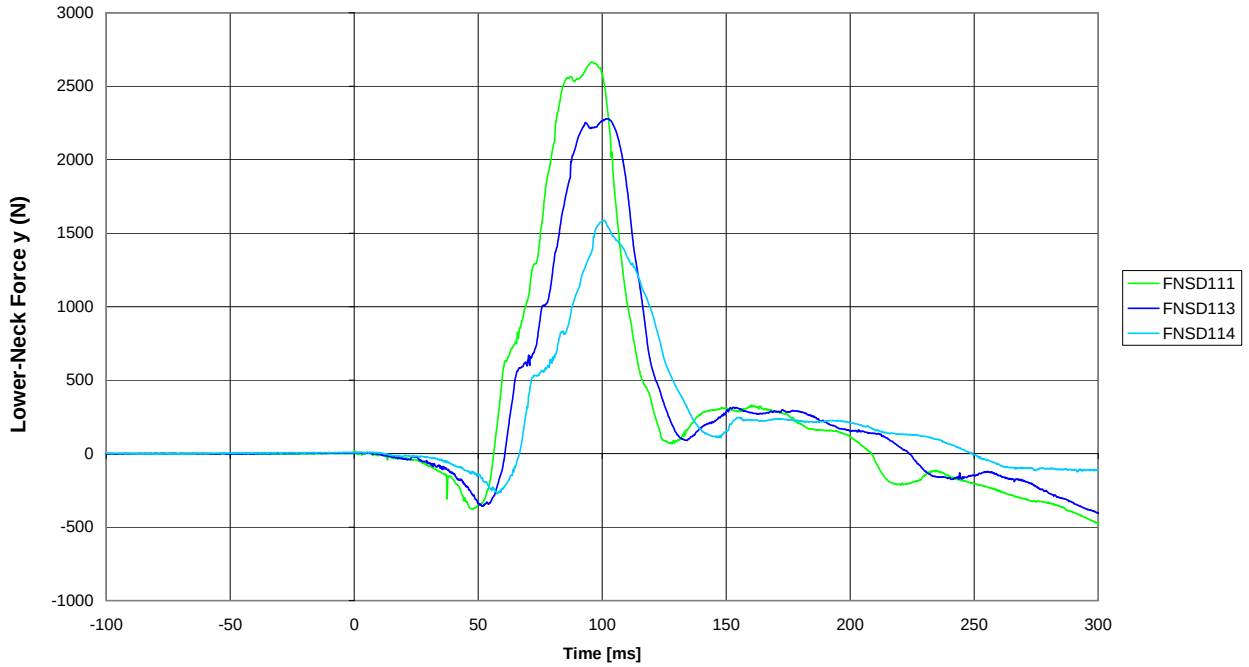

Figure D-17. Lower-Neck y-Force

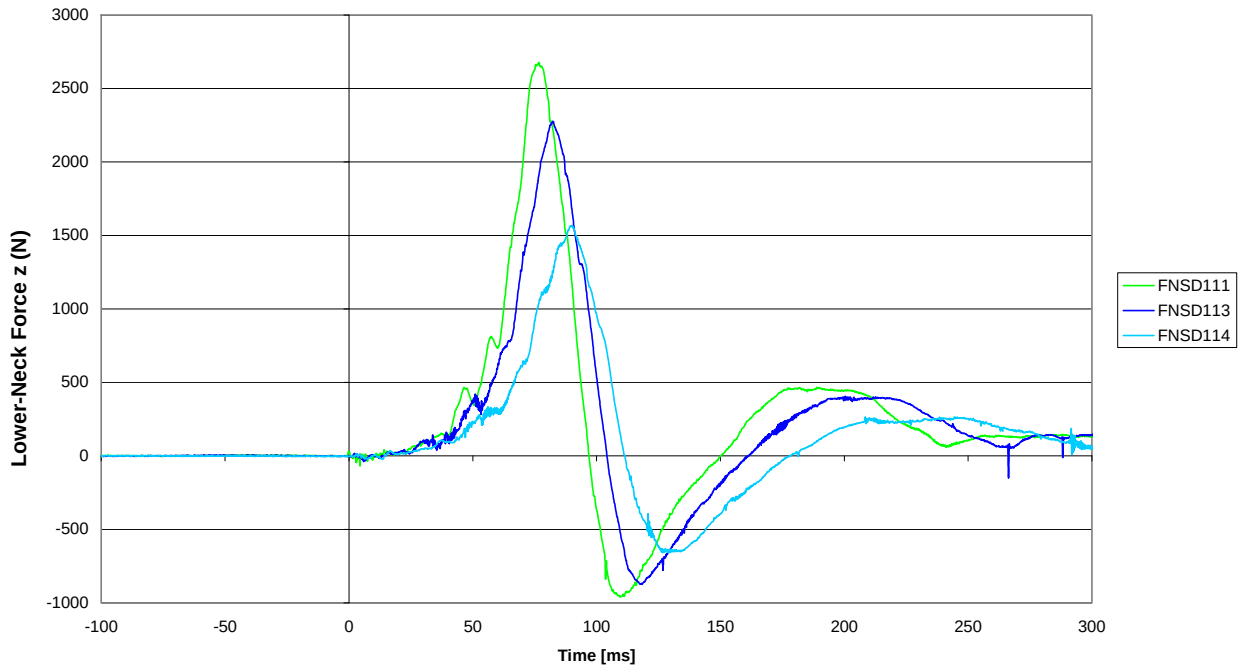

Figure D-18. Lower-Neck z-Force

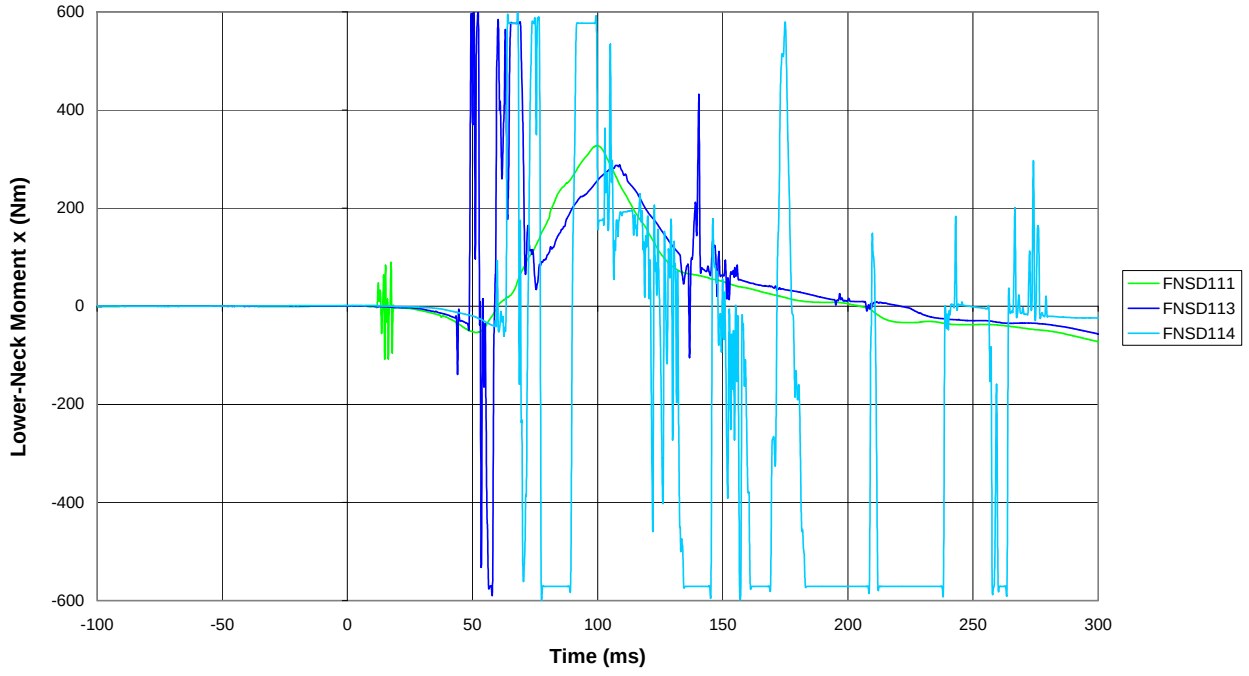

Figure D-19. Lower-Neck x-Moment

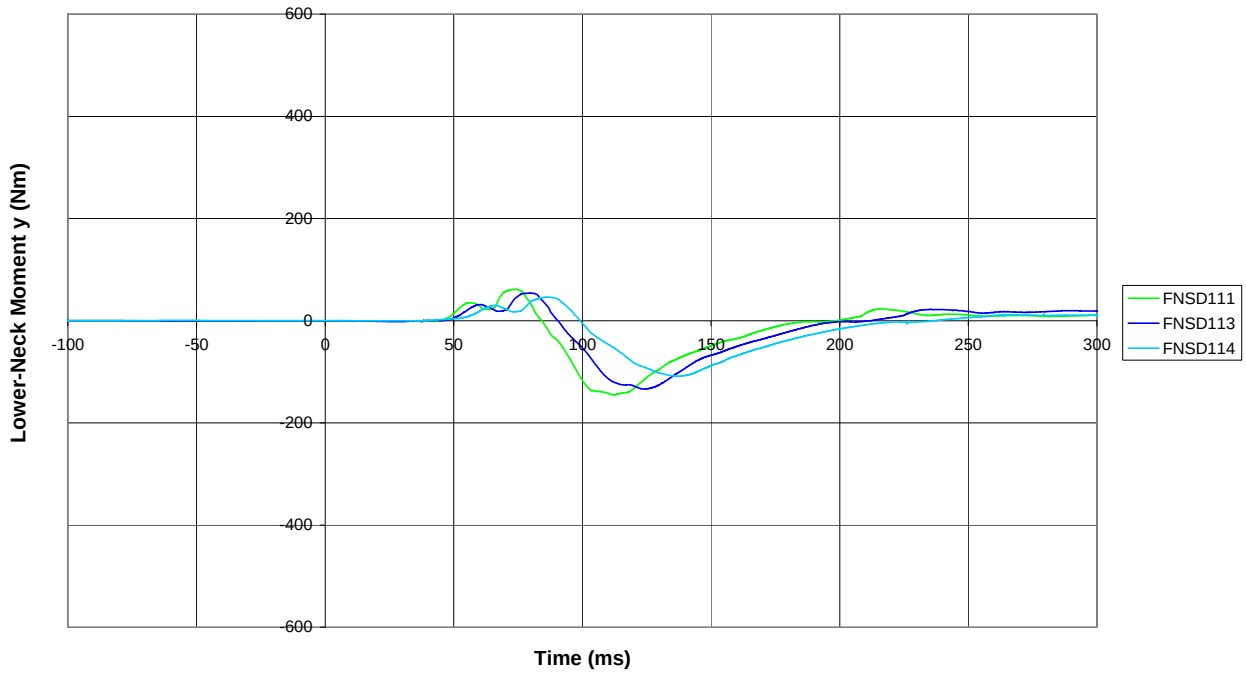

Figure D-20. Lower-Neck y-Moment

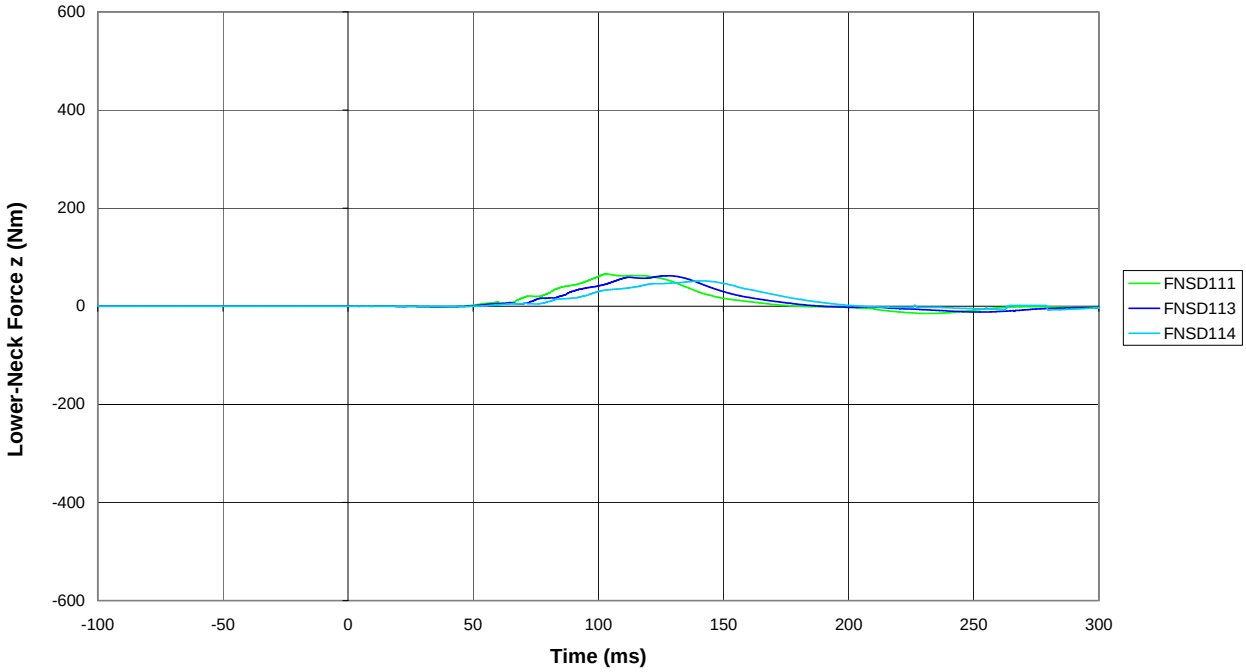

Figure D-21. Lower-Neck z-Moment

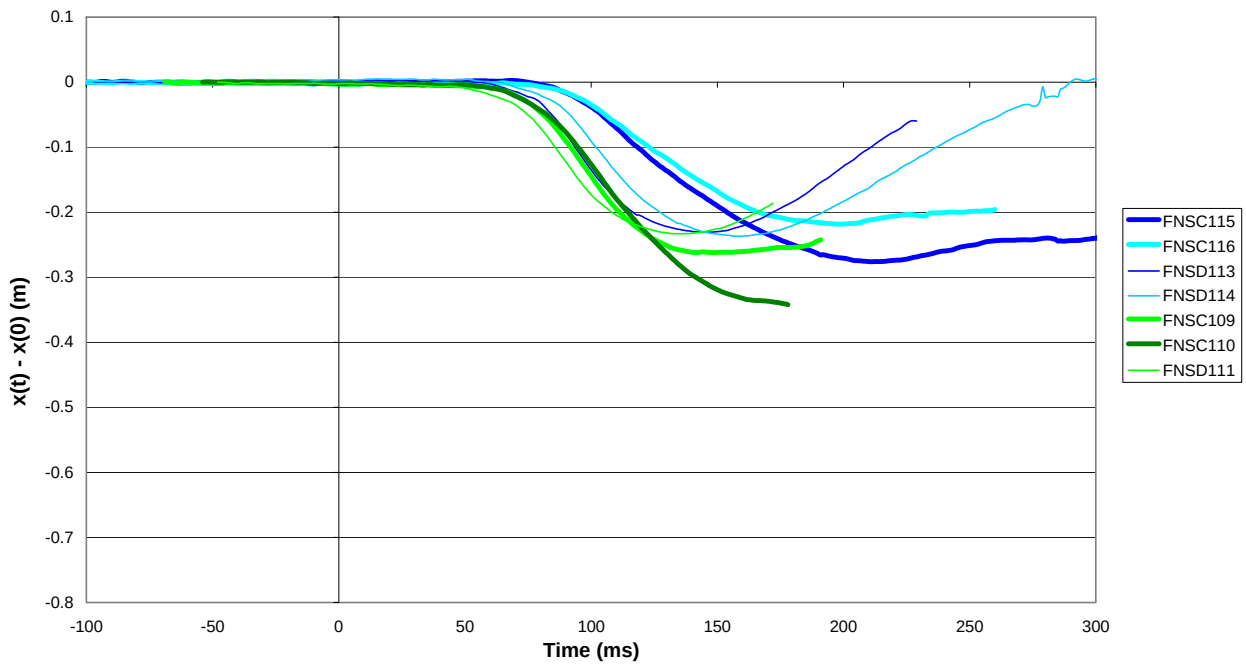

Figure D-22. Head c.g. x With Regard to Sled

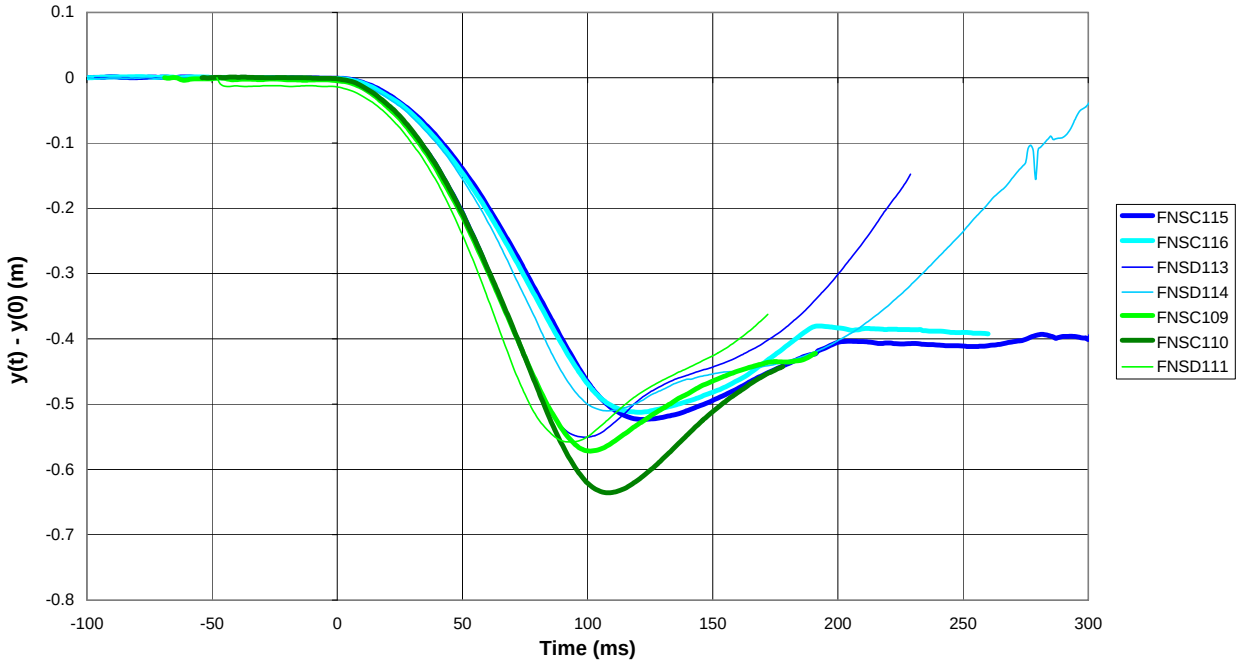

Figure D-23. Head c.g. y With Regard to Sled

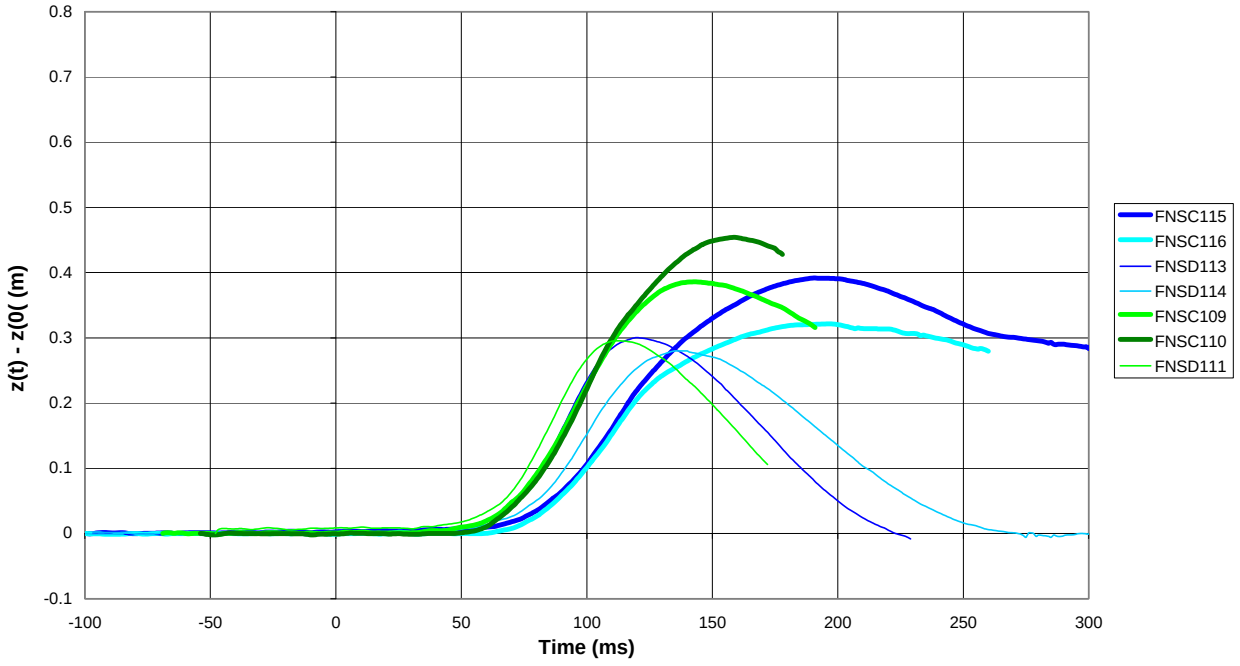

Figure D-24. Head c.g. z With Regard to Sled

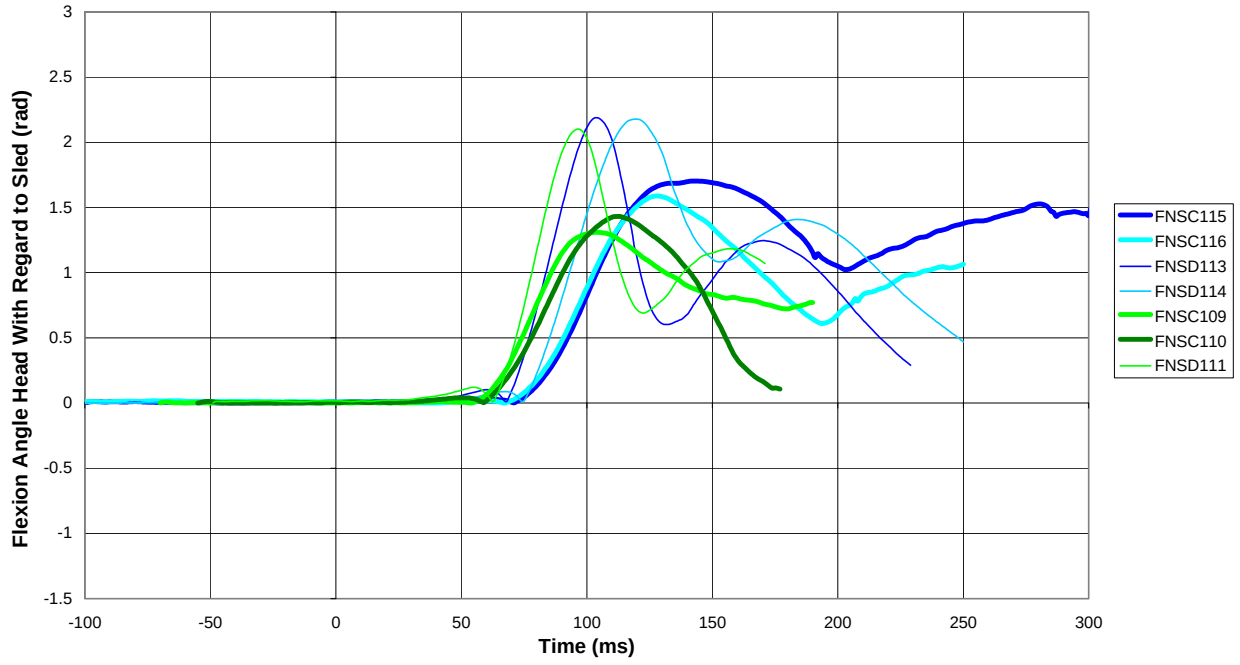

Figure D-25. Head Flexion Angle With Regard to Sled

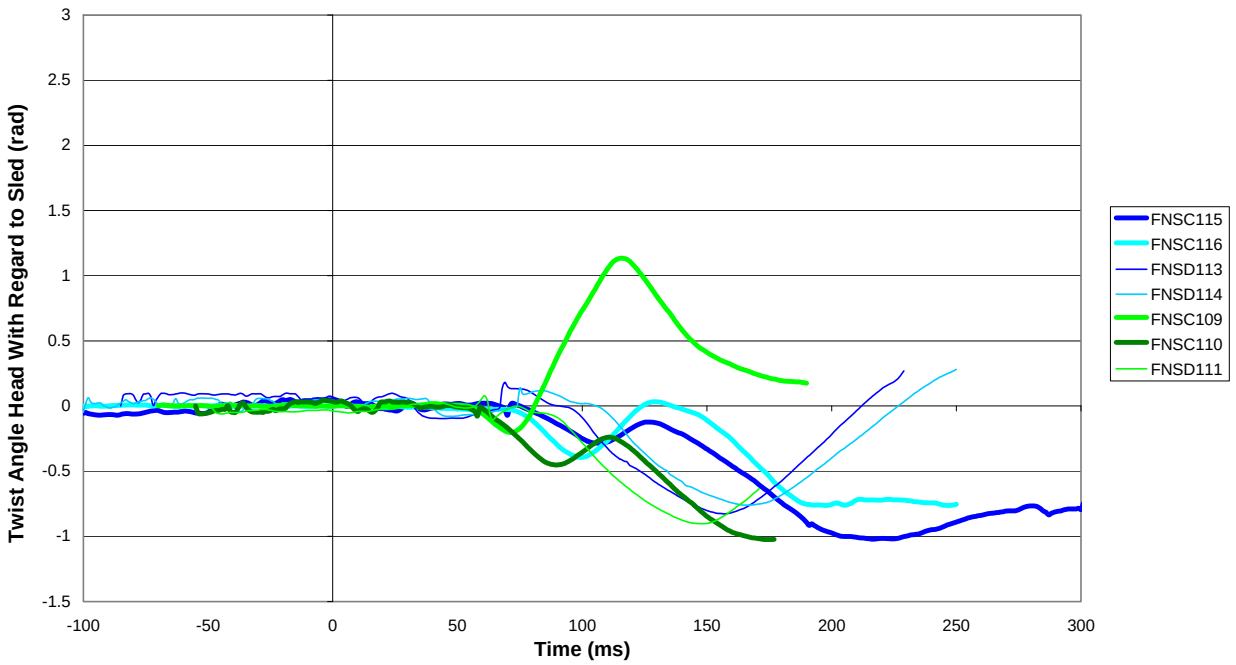

Figure D-26. Head Twist Angle With Regard to Sled

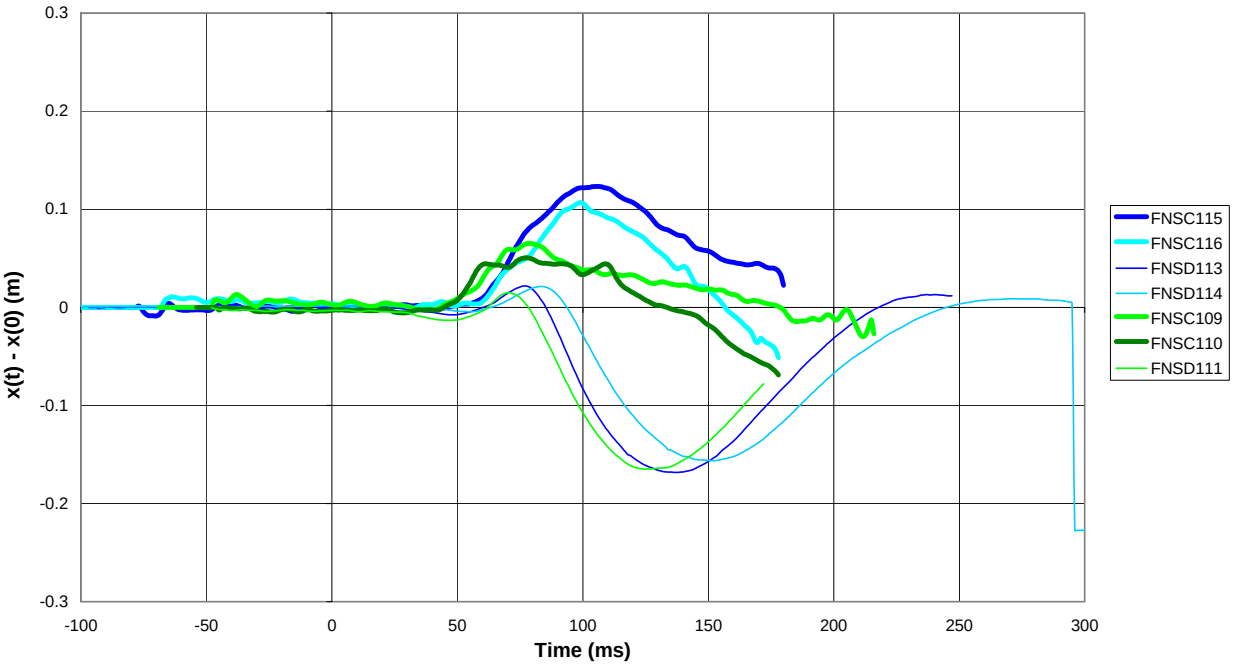

Figure D-27. Head c.g. x With Regard to Thoracal 1 Vertebrae

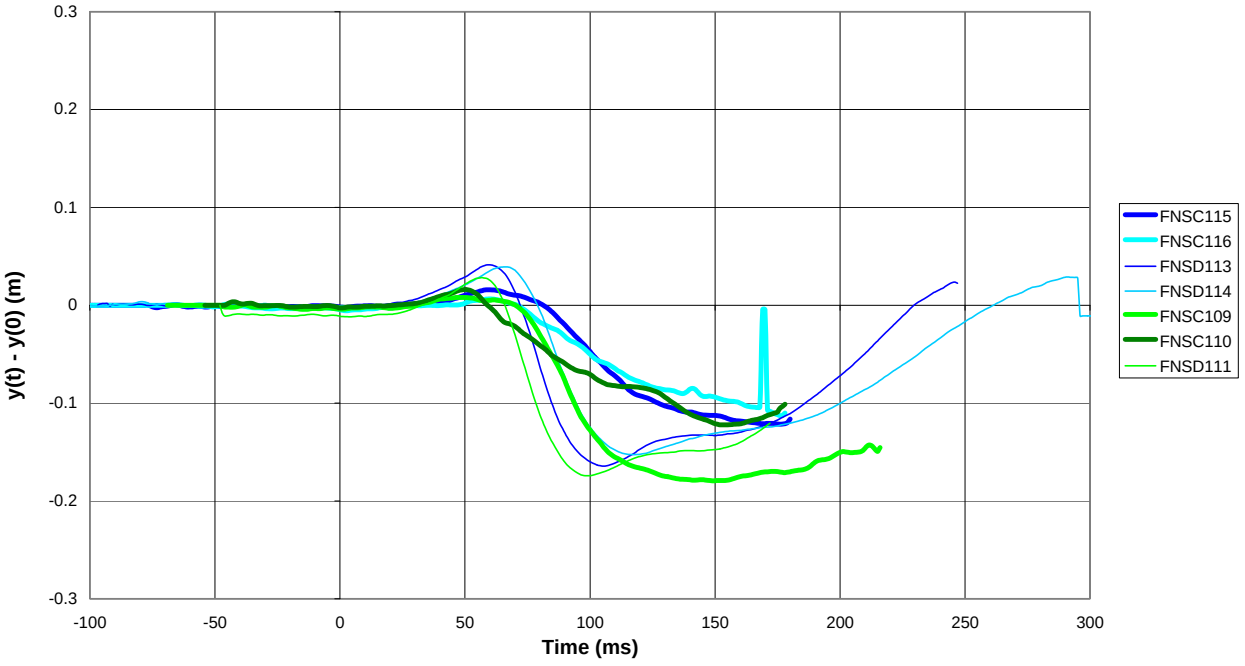

Figure D-28. Head c.g. y With Regard to Thoracal 1 Vertebrae

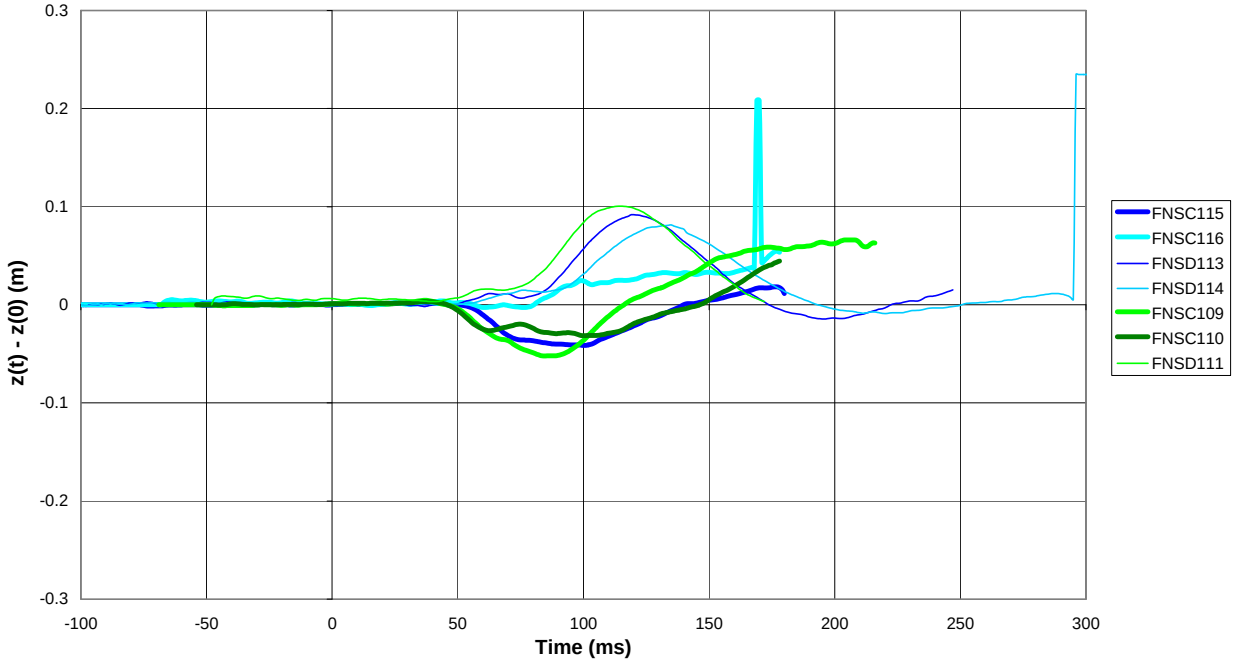

Figure D-29. Head c.g. z With Regard to Thoracal 1 Vertebrae

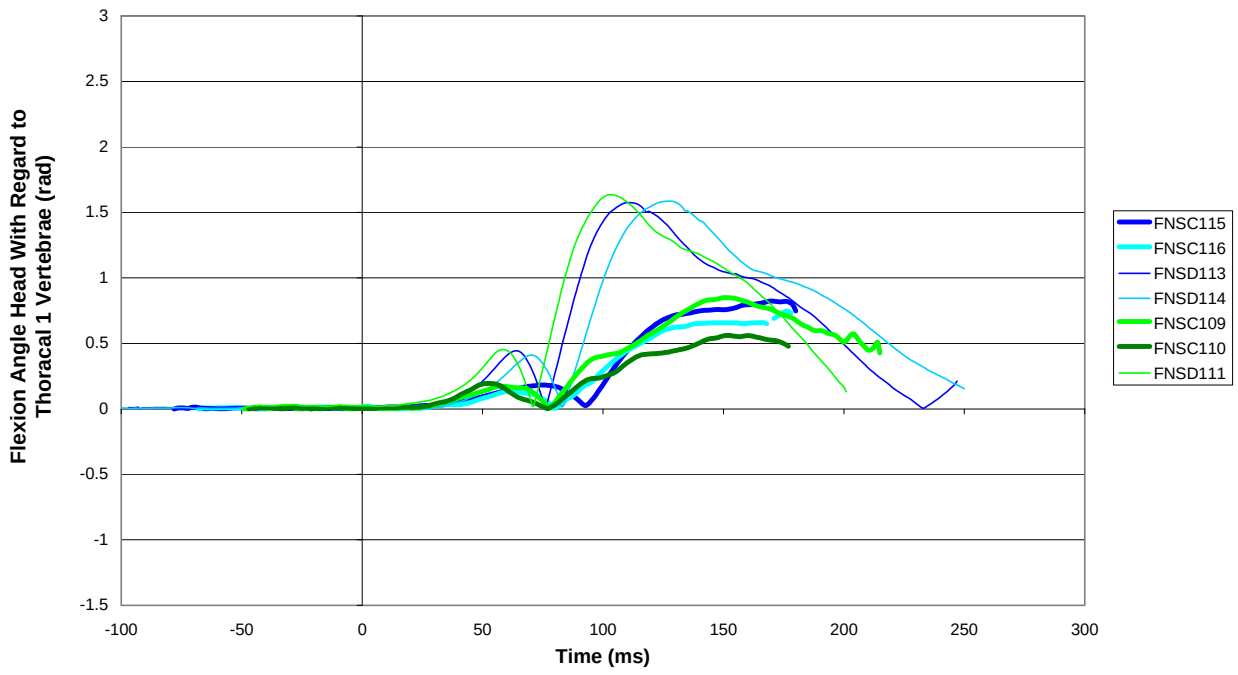

Figure D-30. Head Flexion With Regard to Thoracal 1 Vertebrae

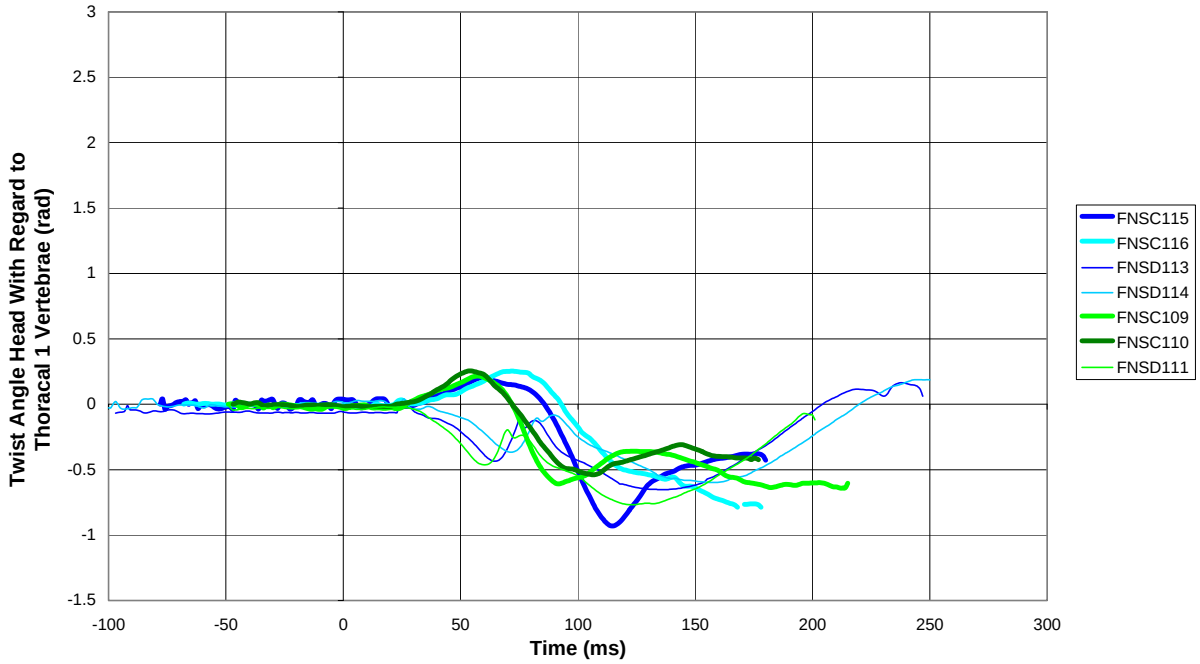

Figure D-31. Head Twist Angle With Regard to Thoracal 1 Vertebrae

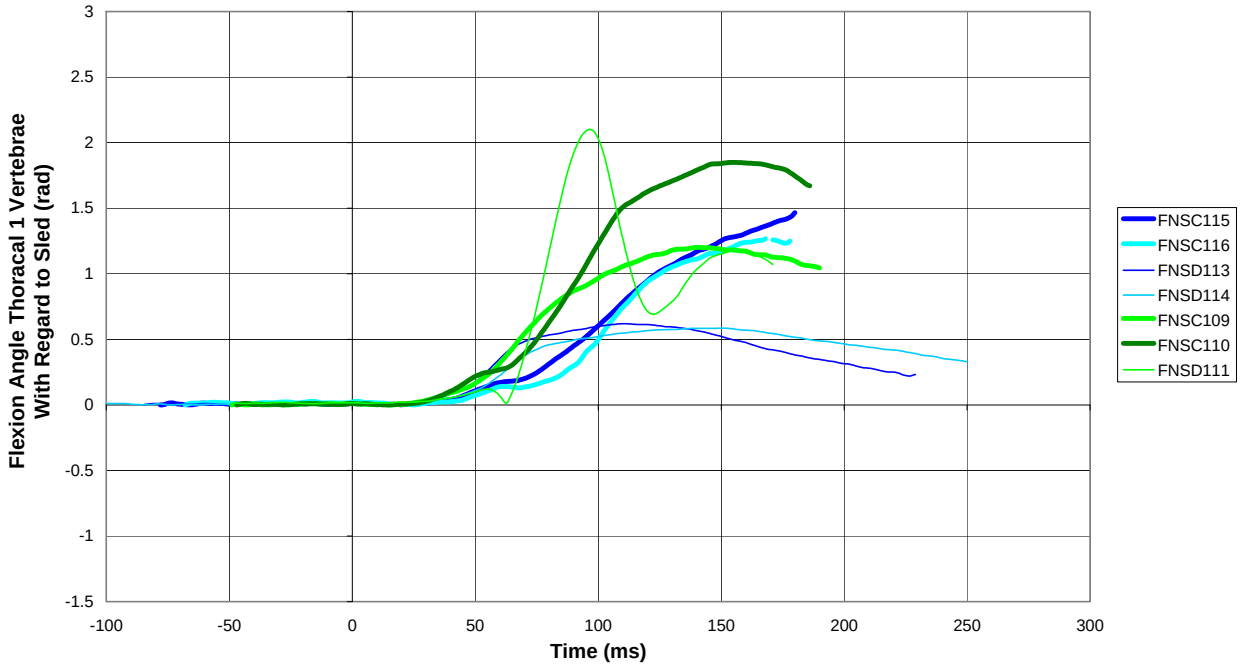

Figure D-32. Thoracal 1 Vertebrae Flexion Angle With Regard to Sled

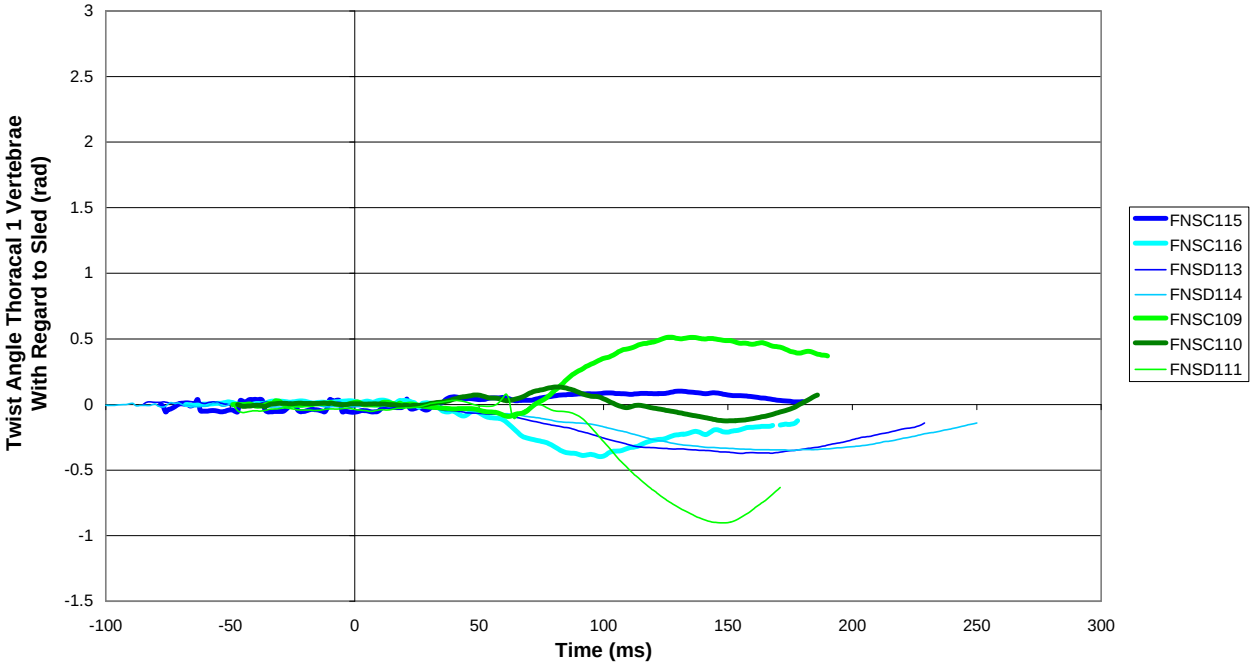

Figure D-33. Thoracal 1 Vertebrae Twist Angle With Regard to Sled